Quantifying the benefits from the spatial diversification of wind power in New Zealand

Dougal McQueen

A thesis presented for the degree of
Doctor of Philosophy
in
Electrical and Computer Engineering
at the
University of Canterbury,
Christchurch, New Zealand.

September 2016

ABSTRACT

Wind power is one of the least cost forms of electricity generation, which along with the need to reduce carbon emissions, means that wind power capacity will certainly increase. The turbulent nature of wind and the passive reaction of wind turbines ensures that wind power is variable. The variability in power increases the requirement for system reserves to ensure power quality is maintained. Integration studies are undertaken to determine what impact wind power development will have on the power system and an often reached conclusion is that spatial diversification can alleviate some of the impacts. However, many of these studies fall short of quantifying the benefit of spatial diversification. To quantify that benefit requires models of wind power that are spatially and temporally consistent and congruent with other forms of generation and demand. In this thesis a wind power model is formed, starting with wind speed time-series from the European Centre for Medium-range Weather Forecasting reanalysis which are interpolated, scaled and imputed. The imputation requires a model of turbulence and a Wavelet Multi-resolution Analysis model is developed that accounts for the heteroskedasticity of wind while enforcing the correct temporal and spatial correlations. The wind speed time-series are transformed to power using wind power plant power curves. A Low Pass Filter is developed that accounts for the effect of spatial integration performed by Wind Power Plants. To demonstrate the benefit of spatial diversification in the New Zealand power system four scenarios are developed representing 2 GW wind power portfolios. The scenarios are Compact, Disperse, Diverse, and Business As Usual (BAU). Metrics for reliability, variability, and predictability are defined that reflect the structure of the New Zealand Electricity Market. Reliability is assessed using the standard deviation of power. Variability is assessed using ramp rates over a 5 minute period which equates with the window used for reserves scheduling. Predictability is assessed using persistence forecast errors over 2 hour horizons which equates with the gate closure in the New Zealand Electricity Market. The conclusion is that a compact wind generation portfolio will exhibit lower reliability, a diverse portfolio will exhibit less variability, and a disperse portfolio will exhibit greater predictability. The BAU scenario shows that the existing portfolio of Wind Power Plants in New Zealand achieves some of the benefits of spatial diversification, however greater benefit could be achieved through careful planning. This thesis forms part of Research Aim 1.1.1 of the GREEN Grid project.

ACKNOWLEDGEMENTS

The integration of wind energy has attracted attention since the early 1990s when advances in wind turbine technology allowed Wind Power Plants (WPP) of significant size to be connected to the transmission network. The need for detailed analyses to determine the impact on the electricity transmission network of large WPPs reached a critical point in New Zealand with plans to construct very large WPPs (Project Hayes - Meridian Energy 633 MW, and Mahinerangi - Trustpower 200 MW).

While at Garrad Hassan Pacific Pty I was assigned to the Wind Generation Integration Project (WGIP) [1]. The aim of the WGIP was to estimate the impact on the New Zealand power system under various scenarios of WPP development. The methods employed for simulating power time-series used an empirical approach; I felt the methods lacked in rigour but commercial pressures forced a pragmatic approach. At the same time as working on the WGIP I also helped Meridian to design Project Hayes. I am still working to develop wind power in New Zealand, most recently designing the Flat Hill Wind Farm (commissioned in April 2015).

Figure 1 A wind turbine at Flat Hill

After building our home I had the opportunity to undertake my PhD. I sent a proposal to Prof. Pat Bodger, co-supervisor of my Masters in Applied Science, he forwarded this to Dr Alan Wood and Dr Allan Miller. They recognised the proposal would fit Research Aim 1.1.1 of the GREEN (Gathering Renewable Energies in Electricity Networks) Grid project [2].

Many thanks to the providers of data and support (in particular Pioneer Energy), and to Centre for Sustainability (CSAFE), University of Otago, for providing a work home.

My family have supported me to the end and I thank them greatly (Glenda, Finlay, Isla, Mum, Bugs, Meals, Marchell, and Lynx. In memory of Gana and Pa).

Abbreviation	Definition
ADMD	After Diversity Maximum Demand
AIC	Akaike Information Criteria
AR	Auto-Regressive
ARMA	Auto-Regressive Moving-Average
AUFLS	Automatic Under-Frequency Load Shedding
BAU	Business As Usual
BIC	Bayesian Information Criteria
CDF	Cumulative Distribution function
CIM	Correlated Innovation Matrix
CvM	Cramer von Mises statistic
EA	Electricity Authority
ENSO	El Nino Southern Oscillation
FFT	Fast Fourier Transform
FIR	Fast Instantaneous Reserves
FSIG	Fixed Speed Induction Generators
FWT	Fast Wavelet Transform
GH	Garrad Hassan
GIP	Grid Injection Point
GXP	Grid eXit Point
HAWT	Horizontal Axis Wind Turbine
HV	High Voltage
HVdc	High Voltage direct current
LPF	Low Pass Filter
MC	Markov Chain
MCP	Measure-Correlate-Predict
MOS	Model Output Statistics
MRA	Multi-Resolution Analysis
MV	Medium Voltage
NEM	Australian National Electricity Market
NWP	Numerical Weather Prediction
NZ	New Zealand
NZEM	New Zealand electricity Market
PCE	Parliamentary Commissioner for the Environment
PDF	Probability Density function
PSD	Power Spectral Density
QQ	Quantile-Quantile
RMS	Root Mean Square
RMT	Reserves Management Tool
SCADA	Supervisory Control And Data Acquisition
SIR	Sustained Instantaneous Reserves
SPD	Scheduling Pricing and Dispatch
STATCOM	STATic synchronous COMpensator
SMC	Stochastic Market Clearing
TER	Transmission to Enable Renewables
TKE	Turbulent Kinetic Energy
TP	Trading Period
UCED	Unit Commitment and Economic Dispatch
vAR	vector Auto-Regressive
WGIP	Wind Generation Investigation Project

WMA	Wavelet Multi-resolution Analysis
WPP	Wind Power Plant
WSTS	Wind Speed Time-Series
WT	Wind Turbine

Symbol	**Definition**
a	Taylor's exponent
A	A vector of coefficients
aero	Aerodynamic
b	Blade length
B	Moving average coefficient
C	Correlation matrix
Cf	Capacity factor
Cp	Capacity
γ	Cholesky decomposed correlation matrix
CvM	Cramer von Mises statistic
c	A constant
d	Wind direction
D	Total wind direction sectors
e	Ffficiency
E	Energy
elec	Electrical
ϵ	Rate of energy dissipation
ε	Innovation coefficient
FE	Forecast error
f	Frequency
$\mathcal{F}$	Fourier transform
$\mathcal{F}'$	Inverse Fourier transform
G	Gaussian probability distribution
h	Hour
H	Total hours
ι	Small increment of time
j	Scale
J	Total scales
k	Translation
K	Total translations
κ	Von-Karmann constant
L	AR model order
λ	Ramp rate
Λ	Lag operator
M	Low pass filter time constant
manage	Pertaining to management
mech	Mechanical
MO	Monin-Obukhov length
$\mu()$	Mean
n	A sample
N	Total samples
ν	Energy dissipation
o	Moving Average model order
ω	Frequency

Ω	Total frequency spectra
p	Auto-regressive model order
P	Power
PC	Power curve
PS	Power spectral density
ϕ	Atmospheric stability term
Ψ	Probability distribution function
ψ	Wavelet
q	A probability or Quantile
r	An alternate site or measurement
R	Pearsons correlation coefficient
RSQ	R-squared
ρ	Density of air
s	A site or measurement
S	Speed up
$\sigma(P)$	Standard deviation
$\sigma(P, P)$	Variance
ς	Standard error
t	Instant of time
T	Total time
Θ	Moving average coefficient
u^*	Friction velocity
v	Wind speed
v'	Turbulent component of wind speed
V	Wind speed bin center
φ	Phase
ε	Random innovation
WT	Of a wind turbine
x	Separation distance
y	Decay constant
z	Height above ground
$z0$	Surface roughness
Z	Randomly generated number
$\mathbb{Z}$	Set of integers

PREFACE

This thesis introduces the reader to the New Zealand power system and the place of wind power within it, develops scenarios for demonstrating the effect of spatial diversification, and develops models that enable the benefit of diversification to be quantified. The thesis is organised into eight chapters.

The first chapter (Power) introduces the power system; in particular the development and operation of New Zealand power system. If further information on the New Zealand power system is desired the reader is directed to the book *Alternating currents or counter revolution? Contemporary electricity reform in New Zealand* by L Evans and R Meade[3].

The second chapter (Wind Power) outlines the characteristics of wind power detailing how the technology associated with wind turbines and wind power plants affects power quality. For greater information concerning wind power the reader is directed to *Wind Power* by Paul Gipe [4].

The third chapter (Wind Power in New Zealand) identifies how wind power has developed and outlines the wind resource in New Zealand. Much of the information has been sourced from media releases, for further information specific to New Zealand the reader is directed to the website of the New Zealand Wind Energy Association (`www.windenergy.org.nz`). Using the information scenarios for testing the benefit of diversification of wind power are developed.

The fourth chapter (Wind Power Statistics) introduces the numerical analysis necessary for examining wind power time-series and uses measurements from New Zealand wind power plants to illustrate these concepts. A basic statistical text such as *A First Course in Applied Statistics* by M Clark and J Randal would help the reader gain a thorough understanding of the statistical analysis [5].

The fifth chapter (Wind) outlines the nature of wind, the measurements of wind, and the data sources available for simulation of wind speed time-series. The topic of turbulence is introduced and the need for accurate models discussed. For further information on wind the reader is invited to consult *An introduction to boundary layer meteorology* by R Stull [6].

The sixth chapter (Time-Series Simulation) introduces the tools necessary for simulating wind speed time-series. Data are used for development of a turbulence model that uses Auto-Regressive Moving Average models. For in depth discussion on simulating multiple time series the reader is directed to *New introduction to multiple time series analysis* by H Lutkepohl [7]. The importance of replicating scaled correlations is shown and a novel model that uses Wavelet multi-resolution analysis is developed. For in depth discussion on wavelet analysis the reader is directed to *A wavelet tour of signal processing* by S Mallat [8].

The seventh chapter (Wind power simulation) details the transformation of wind speed time-series to power time-series. Wind power time-series are simulated for specific wind power plants using the wavelet multi-resolution analysis approach and validated using measured wind power time-series. A generic model is then developed and used to simulate power time-series for each of the wind power plants in the scenarios developed for illustrating the benefits of diversification and quantities relating to dependability, variability, and predictability.

The last chapter (Conclusion) summarises the thesis, details limitations, and makes recommendations for further work.

LIST OF FIGURES

LIST OF TABLES

CONTENTS

Chapter 1

POWER

1.1 GENERATION

In the 1880's New Zealand (NZ) was in the grips of Gold Fever. The progressive exploitation of gold deposits in Otago led miners to the Shotover River where gold rich schistose rock was crushed using stamp batteries. While water played an integral part in allowing the extraction of gold deposits, through sluicing and driving stamp batteries, it was the lack of water at Bullendale (The Reefs) that drove the need for alternative means of powering the stamp battery. A hydro power plant, using water from the left branch of Skippers Creek, and a two mile transmission line were constructed in 1886 to supply power to the Bullendale battery located in the right branch of Skippers Creek. This was the first electricity used industrially in NZ. Soon after, in 1888, electricity was reticulated in Reefton making it the first town in the southern hemisphere to be wired [10].

The abundant hydro resources in NZ were exploited to provide electricity to individual towns, such as the Okere Falls scheme supplying Rotorua (constructed in 1901), and the Waipori scheme built for Dunedin. The Waipori scheme formed Lake Mahinerangi which is now overlooked by the Mahinerangi Wind Farm. The lake is the result of the Waipori hydro power scheme, which flooded the township of Waipori. The township was established in 1861, after gold was discovered in Lammerlaw Creek. By 1896 it was proposed that a dredge at Waipori should be powered by electricity generated at Waipori Falls [11]. The Waipori Electric Power Co tendered for the supply and erection of a sawmill in 1902 [12]), to clear the way, for providing electricity to gold dredges. However even before this it was realised, in a letter to the Otago Daily Times, that power was required further afield [13]. The Dunedin City Council bought the Waipori Electric Power Co in 1904, supplying electricity to Dunedin by 1907, and sealing the fate of the village by the 1930's as the scheme was extended.

The Waipori scheme initially supplied electricity to Dunedin, as did the Lake Colleridge scheme which was built in 1914 to supply Christchurch. These local networks have since been incorporated into the national electricity network. However the first regional transmission networks were established in the 1930's. The lower North Island was supplied by the Mangahao-Waikaremoana scheme, the upper North Island served by the Arapuni system, and in the South Island the Coleridge scheme was linked to Waipori and Monowai. Linking the hydro-schemes and establishing regional transmission network ensured security of supply and economic efficiency.

The distance between the large hydro resources of the Waikato, Clutha, and Waitaki Rivers and the major cities ensured the need for transmission of electricity over greater distances. The electricity network was progressively constructed using a backbone of 110 kV transmission lines started after World War 1 with the construction of transmission lines from the Waitaki Dam (1934). Post World War 2 220 kV transmission lines were built starting with the linking of Wellington to Auckland (1952) and Christchurch to the Roxburgh Dam (1956). The National

Figure 1.1 The Mahinerangi Wind Farm above Lake Mahinerangi. Ten of thirteen turbines are visible. Stage 2 could add a further 87 turbines.

Grid was established in 1965 with the commissioning of the High Voltage Direct Current (HVdc) link between Benmore and the Haywards substation near Wellington.

The construction of the National Grid and the majority of the large hydro and thermal generation stations was conducted by government departments; the State Hydro-electric department until 1958 and then the New Zealand Electricity Department (NZED). The modus operandi of NZED was to construct large power stations and reticulate the electricity to consumers; culminating in the Think Big schemes of the Muldoon government, such as the Clyde Dam (started 1982 but not completed until 1993) on the Clutha. Control of the electricity industry was enacted through the Electricity Act ensuring centralised generation and distributed demand. The effect of this policy can be seen in Figure 1.2, based on data as of the year end 2013, where the majority of the total generation capacity is held in stations with capacities greater than 100 MW.

The precarious financial state of NZ in 1984 led to large scale economic reformation of the country (Rogernomics). Reform of the electricity sector has been comprehensive. In 1987 the Electricity Corporation of New Zealand (ECNZ) was established, with its subsidiary Transpower New Zealand responsible for transmission assets. Transpower was converted into stand alone State Owned Enterprises in 1994, in 1996 Contact Energy was split from ECNZ, and on 1 October 1996 the whole sale market was established. Deregulation was further progressed through reforms implemented by Max Bradford in 1999 which privatized Contact Energy, and separated generation and distribution businesses. Reforms continue today with the partial privatization of the state owned electricity generation companies in 2014.

These reforms changed the capacity of newly commissioned generation stations, as shown using a 5 year rolling average in the lower pane of Figure 1.2. A peak mean commissioned capacity occurred during the 1970's with the commissioning of large power stations in the Waitaki and Manapouri.

1.2 DEMAND

The electricity network has been largely operated to ensure demand is met without restriction. While there are a few instances of demand side management, such as ripple control of hot water cylinders, by and large consumers are passive in their interaction with the electricity network. The electricity market may help shed some demand from peak times, however direct participation in the market is limited to very large consumers. While time of use metering is used by many commercial and industrial consumers it is not particularly evident that the price signals transfer

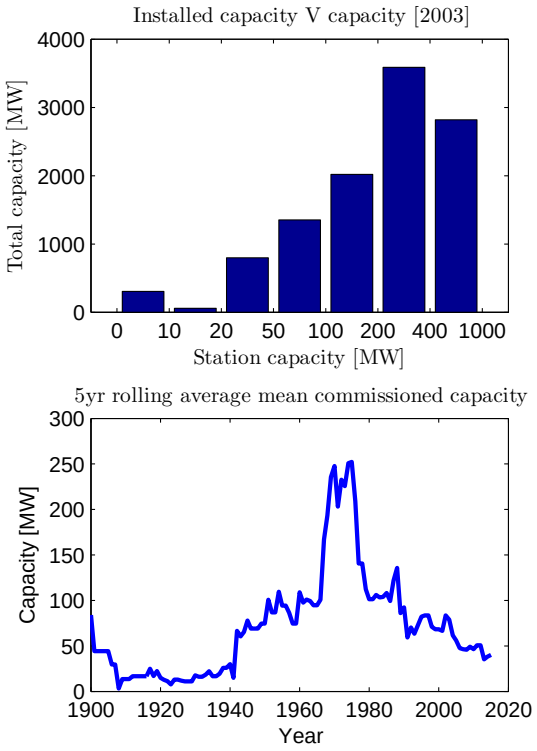

Figure 1.2 Total capacity versus station capacity

to significant changes in demand patterns [14]. Thus the total demand is largely the result of customers acting independently and hence is stochastic or random in its nature.

While consumer action is independent and hence demand is stochastic, consumers respond to common circumstances. Demand follows predictable patterns relating to the time of the day, day of the week, and month of the year. Daylight hours, weather, and even sports events mean that customers have similar usage patterns and hence aggregate demand follows predictable patterns. Demand patterns also reflect the type of consumer; residential consumers typically have peak usage in the evening hours when cooking, whereas industrial and commercial consumers have daytime peaks when employees are working.

Demand placed by an individual consumer may be very erratic reflecting relatively large changes as appliances are turned on and off. However, the aggregate demand from many consumers is less variable as the changes in demand resulting from individual consumers are small relative to the total demand. The actions of those individuals are independent, thus as greater numbers of consumers are aggregated the relative variability of demand reduces. Although the aggregation of consumer demand means the total demand is less variable it is still varies significantly and being stochastic there will always be some degree of unpredictability.

1.3 TRANSMISSION

The transmission network is essential for delivering power from power stations to consumers. Further, the transmission network allows the aggregation of generators and loads into a single system. This aggregation means that each generator or load in the system both supports and is supported by other generators and loads in the system. This aggregation is crucial for maintaining power quality. If a single generator in a small system fails then the relative effect on the system stability is very large. However, if an equivalent failure occurs in a large co-operative system then the effect on stability will be relatively small.

The transmission network in NZ has been constructed primarily to transport power from the large hydro resources to the major load centers. This has resulted in a transmission network that stretches the entire length of the country using a backbone of 220 kV and 110 kV lines. The network is enhanced by the Cook Strait Cable; a HVdc link between the Waitaki and the Haywards Substations (just north of Wellington). Substations where generation is connected to the network are termed Grid Injection Points (GIP) and those where load is taken from the network Grid eXit Points (GXP).

Figure 1.3 The centre of New Zealand's power system, Benmore (540 MW) on the right, and the southern terminus of the Cook Strait Cable on the left.

The development of the transmission network continues with particular focus on upgrading to enable possible growth in renewable generation. Significant projects conducted recently include construction of Pole 3 and other upgrades to the HVdc link; increasing the capacity of the link to 1200 MW, the Wairakei ring project involving the construction of a network of 220 kV lines in the center North Island to support growth in geothermal generation, and a 400 kV transmission line from Whakamaru to Pakuranga to enable transmission of power into Auckland. Other upgrades to the transmission network are planned in the lower South Island.

While the transmission network upgrade projects may help with the integration of more renewable generation there can be no doubt they are also intended to alleviate the impact of the foreseen closure of the Tiwai Point aluminum smelter [15]. The Tiwai Point smelter sits at the southern end of the South Island near Bluff and has a peak demand of over 600 MW. The Manapouri hydro power station was constructed specifically to supply electricity to the smelter and is connected directly using two double circuit 220 kV transmission lines. If the smelter were to close then the generation from Manapouri would be stranded as there are few other large loads in the southern South Island. Thus efforts have been made to ensure the power from Manapouri can be transmitted north if the smelter were to close.

1.4 DISTRIBUTION

The transmission network in NZ, operated by Transpower, delivers power from large generators to major substations. There are a few consumers directly connected to the transmission network (such as the Tiwai point aluminum smelter), but the majority of consumers are connected through distribution networks. The transmission network delivers power to large substations, and from these distribution or lines companies deliver power to consumers, typically at 230 V. A typical lines company will operate a network of Medium Voltage (33 kV and 11 kV) lines to

distribute electricity from the large Transpower substations to transformers which step down the voltage to 400 V (phase to phase) to which consumers are connected.

There are presently 26 lines companies in NZ, each operating its own geographic region, thus there is no direct competition between lines companies.

While the primary purpose of the lines companies is to deliver power from the transmission network to consumers they also allow connection of generators. Generation connected within the distribution network is termed embedded. The cost of connecting a power plant to the electricity system is dependent on the voltage at the point of connection. Higher voltages mean the electrical insulation of switch gear and transformers has to be increased, leading to more costly components. Thus it may not be economic for a small power plant to be connected to high voltage transmission lines. Further, power plants that are connected to the transmission network may have onerous requirements placed on generator capability, such as low voltage ride through and harmonic content, so that power quality can be maintained. Generators directly connected to the transmission network may also be required to participate in the electricity and ancillary services markets and thus incur associated costs such as generation forecasting. Thus embedded generation enables exploitation of smaller distributed resources such as wind power plants.

1.5 POWER QUALITY

To ensure that appliances connected to the network operate without fault it is necessary that the power quality of the electricity supply is maintained. The NZ electricity network is primarily designed such that consumers are supplied with single phase 230 V alternating current (AC), at a frequency of 50 Hz, with a sinusoidal waveform. Customers with high demand, welding equipment, or motors may also be connected using three phase connection or connected to the medium voltage network.

Power quality standards specify the acceptable range of power quality components. Power quality components as detailed in Power Quality Guidelines 2012 are: steady state voltage, voltage unbalance, harmonics, inter-harmonics, voltage fluctuation and flicker, voltage dips/sag, transients, voltage swells, frequency deviations, and interference. Each component must be maintained at points of supply [16] and can be classified as a variation or an event dependent on the cause and duration.

Each power quality component is propagated by typical mechanisms, is associated with a temporal span, and has certain effects on the electricity network. A summary of power quality components is provided in Table 1.1. The acceptable limits for some power quality components vary according to the voltage, thus limits for the medium voltage network may differ.

Component	Description	Mechanism of disturbance	Temporal span	Example effect on network	Target value	Allowed range
Stead State Voltage	The phase to ground or phase to phase root mean square of the sinusoidal wave form.	Load and impedance losses greater than generation,	Steady state	High voltages cause reduction in lifetime of resistors, low voltages may cause motors to stall	230 V	±6.00%
Voltage unbalance	Inter-phase angle or differences in the voltage magnitude of phases	Unbalanced loads, uneven system impedance	Steady state	Heating of rotor in three phase induction motors	120 degree	1.00%
Harmonics	Presence of waveforms in a power system that are integrals of the fundamental frequency	Non-linear power electronics, saturation of iron cores in transformers	Steady state and short term	Heating of capacitors, transformers, motors	0 V	Depends on harmonic
Interharmonics	Presence of waveforms in a power system that are not multiples of the fundamental frequency	Electric arc furnaces, arc welding machines, ripple control	Steady state and short term	Unwanted torque in induction motors	0 V	Depends on frequency
Voltage Fluctuation and Flicker	Repetitive or random fluctuations of the supply voltage	Electric arc furnaces, electric motor starts, intermittent generation	Steady state and short term	Physiological effects	0 V	See Figure 1.4
Voltage dips and sags	Voltage falls to less than 90 % of rated for period 1 min or less	Network faults or connection of large loads	0 - 60s	Electronic component malfunction	230 V	See Figure 1.4
Transients	Temporary spike in voltage	Switching of network components	0 - 60s	Component and insulation stress	230 V	See Figure 1.4
Voltage swells	Voltage rises to 110 % of nominal for 1 minute or less	Loss of load, unbalanced fault	0 - 60s	Over heating of components	230 V	See Figure 1.4
Frequency deviations	Periodicity of waveform changes	Mismatch between load and generation causes generator speed to change and hence frequency		Deviation in clock based equipment	50 Hz	1.50%

Table 1.1 Power quality components and characteristics

As detailed in the power quality components table, the type of component is defined by its duration, the deviation of voltage from its nominal value, and the duration. The acceptable range of voltage as a function of time is presented in Figure 1.4.

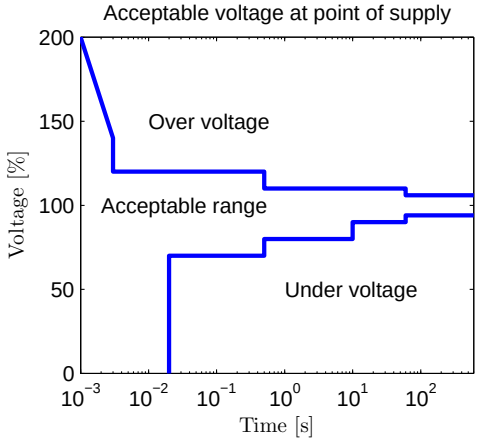

Figure 1.4 Acceptable range of voltage at point of supply

The power system frequency is managed centrally by the system operator; in NZ Transpower is both the system operator and owner of the transmission network. The range of acceptable frequencies is dependent on the duration of excursion. Nominally the frequency keeping band is 50 ± 0.2Hz. It is inevitable that frequency will depart from the nominal band; it is deemed acceptable for the frequency to range between 47 and 52 Hz in the North Island (45 and 55 Hz in the South Island) during momentary fluctuations. The onus is on the system operator to manage system frequency such that the magnitude and occurrence of fluctuations is limited.

The power quality guidelines specify limits for acceptable power quality at the point of supply. They do not specify how the lines company should operate the network efficiently or what actions to take to ensure these factors are met. To ensure efficient supply of electricity it is important that the power factor is kept near unity. The power factor is the angle between current and voltage waveforms and describes the ratio of real to apparent power. The highest efficiency of power delivery occurs when the voltage and current wave forms are coincident, resulting in a power factor of one. In inductive circuits, such as those with motors, the current will lag the voltage, resulting in mismatch between current and voltage waveforms, hence there will be reactive power flow and a power factor less than unity. The reactive power must be generated, and transmitted, but contributes no work, thus there is a reduction in efficiency. Power factor can be corrected by placing capacitance into networks. Lines companies may achieve power quality compliance by either placing restrictions on loads, i.e. enforcing limits on harmonic content produced by inverters and welders, or by adding power conditioning components into vulnerable circuits.

While the power quality guidelines are written with absolute limits; power quality standards are written in a manner that allows for infrequent excursions. This is to acknowledge that is it neither possible or practicable to ensure the supply of electricity is without fault, or that demand will always be less than the capacity of the network. The EN50160 standard states that "during each period of one week 95% of the 10-minute rms values of the supply voltage shall be within $U_n \pm 10\%$.", where U_n is the nominal voltage [17].

1.6 NETWORK OPERATION

At the farthest reaches of the distribution network power quality is maintained by ensuring that the voltage drop along the distribution network is kept within acceptable margins (through appropriate conductor sizing and design), that equipment connected to the network does not cause undue power quality issues, and that the voltage supply at the distribution transformer is maintained. In the Medium Voltage (MV) network voltage is kept within target ranges by automatic tap changes at GXP transformers and again by suitable design. At the High Voltage (HV) level voltage is maintained within tight limits and changes in power delivery managed by variations in frequency.

System frequency is governed using mechanisms that have various response times and magnitudes. These mechanisms are commonly grouped by response time into primary and secondary controls. Primary control relates to the balancing of the system on a sub-minute time-scale and is largely automatic. Secondary control mechanisms are those that allow the power system to operate within its scheduled plant commitment range [18]. A third mechanism, tertiary control, is added here describing the mechanisms used to allow the bulk scheduling of plant and longer term planning and resource management functions. Primary control reflects the physical operation of the network with secondary and tertiary control reflecting management functions.

Extending the ordinal control concept; basic control can be added reflecting static components in the power system. Basic control measures include: network design to ensure sufficient generation and transmission capacity, sizing conductors to ensure voltage drops are not excessive, addition of capacitance to provide reactive power, and damping to ensure oscillatory modes are reduced. These measures are largely passive. Oscillatory modes in power systems can be caused by: the interaction of pairs of generators (intraplant modes), the interaction of individual generators with the power system (local plant modes), interactions between coherent sets of generators (interarea modes), interaction of poorly tuned governors and transformer tap changers among other mechanisms (control modes), and the interaction of turbine generator shaft systems (torsional modes). Oscillatory modes have frequencies less than 3 Hz.

Basic control includes system inertia comprising the large amount of rotational inertia embodied within all the synchronous generators and motors. Imbalance between load and generation in the power system results in changes to system frequency. However, it takes considerable energy to change the rotational speed of all the generators hence the rate of change of frequency is limited. The response is an intrinsic capability of synchronous machines. System inertia, in NZ's power system, limits the rate of frequency change for times up to 5 second, when other responses such as generator mechanical governor systems become effective.

1.6.1 Primary control

Primary control mechanisms include governor response, automatic generation control, instantaneous reserves, over-frequency reserves, and load shedding. Reserves and load shedding are grouped together along with voltage support, and the provision of reactive power or power factor correction, into ancillary services. Ancillary services in NZ are presently procured through contracts with market participants via a closed tender process.

The majority of synchronous machines connected to the electricity network are operated to produce a set amount of power. To achieve regulation of the power the machines use a governor that attempts adjustment of the rotational speed using slope control. If system frequency is too low the governor tries to accelerate the machine, thus attempting to increase system frequency. Governor response times are generally in the order of 1 second to 1 minute.

Most generation connected to the system has passive control at short time scales, however demand and network states change rapidly. To control the system frequency over temporal spans

greater than that capable of being absorbed by system inertia, some designated generators are operated to provide frequency control. These generators are kept in a state where they are ready to provide rapid response to variations in system frequency. The generators are kept spinning with head room, so that if frequency drops they automatically increase power, and if frequency rises they can quickly reduce power.

As it is not economic to commit sufficient generation to frequency control, to accommodate all changes in demand and system state, instantaneous reserves and load shedding are used to help alleviate larger frequency excursions. Instantaneous reserves can be classified according to their response time and magnitude of reserved power as Fast Instantaneous Reserves (FIR) and Sustained Instantaneous Reserves (SIR). FIR must be capable of being activated within 1 s and be capable of being sustained for 60 s, SIR must be capable of being activated within 60 s and of being sustained until the time at which the system operator indicates a return to normal operation [19].

FIR and SIR can be provided through either generation or through load shedding. Generation of varying types can provide FIR and SIR through schemes such as keeping plant online in an operational state (often referred to as spinning reserves), or operating plant such that a fast response in power output can be achieved (such as tail-race water depression for hydro generators). The capability for FIR and SIR provision is dependent on the plant. Over-frequency reserves are provided through generation plant that can be rapidly disconnected; rapidly disconnecting some plant can lead to over-speeding and thus result in damage to the machine.

Load shedding is managed using either Automatic Under-Frequency Load Shedding (AUFLS), where loads are automatically disconnected if the frequency drops below a specified limit, or Interruptible Load, where the system operator sends a signal to the customer to disconnect. AUFLS comprise blocks of demand at Grid Exit Points, each block totaling 16% of GXP demand prior to engagement. At present there are two blocks at each GXP, the first block is disconnected if the frequency drops below 47.8 Hz for 0.4 s in the NI or 47.5 Hz in the SI, the second block disconnected if frequency remains below the same levels for 15 seconds [20].

The quantity of reserves that is procured by the system operator is sufficient to maintain frequency during a contingent event. A contingent event is a disruption on the power system caused by the loss of generation or outage of a transmission line. Contingent events are dependent on the structure of the power system at a particular time, depending on what generation is on-line and what transmission lines are open. For example in 2003 the largest contingent event for the North Island was the loss of the largest thermal unit 400 MW or the loss of Pole 3 (HVdc link) up to 700 MW [21]. Further, strategies are also used to ensure power system stability during extended contingent events, in NZ being the complete loss of the HVdc link for the North Island (equal to 1200 MW).

Black start capabilities are also procured as part of the reserves measures in NZ. It is crucial that after large interruptions in power due to weather or other circumstances that the electricity supply can be restored. There are large economic costs that are incurred through prolonged outages [22]. If a large fault occurs in the power system (or many coincident faults) then generators may be forced to disconnect due to not being able to “ride through” the fault. If generators disconnect, or further transmission lines are tripped, the network may suffer cascading failures and a black out result. Once the power system has collapsed it may be very difficult to restart it, as most generators require excitation to produce power, and there are large inrush currents when transformers and transmission lines are excited. Thus, the power system must have security provisions for black start, requiring the availability of specific generators, and these can be costly to maintain for an event that is very unlikely.

1.6.2 Secondary control

As the demand, availability of generators, and availability of lines changes, power stations must be scheduled so that generation is balanced with demand, and power quality is maintained. It is desirable that the scheduling of generation is done such that the demand is met in the most cost effective manner. Since 1987 NZ has gradually implemented the New Zealand Electricity Market (NZEM) to enable competitive scheduling of generation and thus find a quasi-optimal dispatch.

The NZEM wholesale spot market uses a 30 min window, each window known as a trading period (TP), and is administered by the Electricity Authority (EA). The electricity market operates on a nodal pricing basis. Each point in the transmission network where generators, large loads, and substations (feeding distribution networks) are connected constitutes a node. There are a total of 285 nodes in the transmission network, generators make offers at 59 nodes (GIPs) and retailers purchase electricity at 226 nodes or GXPs.

For each TP retailers place bids for supply at GXPs and generators offer tranches of generation at each GIP. The dispatch is then resolved using a market model. To aid with bids centralised load forecasts are produced by the system operator using methods outlined in GL-SD-204 Load Forecast Methodology and Processes [20]. Bids and offers open 48 hours before the TP. Generators (including intermittent generators) must provide a forecast to the system operator, for all generation not embedded, at least 71 TPs before the TP to which the offer applies [23]. There is no central forecasting of generation and responsibility for the preparation of offers lies with the generators and there is no mandated forecasting methodology. From 4 hours prior to the TP prices are resolved enabling participants to update offers and bids until 2 hours prior to the TP when the auction is nominally closed. Intermittent generators are required to provide persistence forecast offers for TPs with a horizon of less than 2 hours. A persistence forecast uses the present actual generation as a forecast for the future TPs with the appropriate horizon.

While the physical transmission of electricity ultimately resolves the network's power flows, to enable the operation of the NZEM, the transmission network is modeled using SPD (Schedule, Pricing, and Dispatch) market clearing engine [24]. The SPD model optimises generation and transmission (applying assumed line impedance, transformer performance etc) such that the tranche of generation with the lowest offered price is dispatched. Generators may bid in a manner than ensures dispatch (wind is typically offered at \$0/kWh to ensure dispatch), to reflect the marginal cost of generation, or to ensure maximum profit is gained. The market clearing price is based on the highest offer at each GIP that is dispatched. The price at GXPs reflects the highest bid at GIPs plus the marginal cost of transmission losses.

The NZEM uses a trading period of 30 minutes, however this temporal resolution is not sufficient to allow efficient scheduling of generation to adapt to changes in demand. Hence, the system operator resolves pricing and scheduling of generation every 5 minutes using the bids and offers placed in that TP [25]. While the market clearing process is performed at the time of the market window close based on vSPD modelling, this may not accurately reflect the physical dispatch that occurs during the TP. Thus, a confirmation process occurs that may take 24 hours is applied to ensure reconciliation reflects the physical dispatch.

All generation greater than 10 MW must participate in the spot market, however it is possible for retailers to hedge and or contract generation. While generation contracts fix prices and thus bypass the spot market process, the power flow must still pass through the NZEM, as physically the power flow passes through the transmission network and hence affects loading and market clearing.

To enable the NZEM to operate efficiently generators require good forecasts of load and generation capability. As stated Transpower provides load forecasts, however generators individually produce proprietary forecasts of their own and other generation capabilities. While this means

that some market participants may hold commercial advantage, it also means that coordinated response to adverse events may not be possible. Generators require forecasts with horizons 2 hours and greater, while the system operator requires forecasts with horizons as short as 5 minutes to enable the re-dispatch processes.

1.6.3 Tertiary control

In NZ there is no explicit form of tertiary control; all scheduling of generation is performed using the NZEM and the reserves markets. Generators perform long range forecasts of supply and demand and offer generation tranches according to their future forecast prices. Offering practice reflects the type of generation and whether it has the ability to store energy (reservoirs, coal stockpiles, or gas left in the ground) or must run (wind and run of river hydro). For instance coal fired power plants typically can hold large stores of coal enabling the balancing of seasonal changes in demand, however they have high thermal mass and tight efficiency curves thus it is not economic to change their output rapidly, hence they are used as base load and do not participate effectively in the reserves markets. Geothermal plant have consistent availability of steam and high capital costs hence also operate as base load. Hydro power plant such as in the Waitaki have large reservoirs enabling seasonal generation, and the Francis turbines are fast reacting allowing participation in the reserves markets. Other hydro plants have very little storage and operate on a principal of generating when water is available, so called run of river, and are effectively passive in their market participation.

While the actions of generators through the NZEM offering process ensures some efficiency in the use of resources it is not infallible. This is particularly the case in NZ where the small scale of the power system can lead to anomalous practices during outages of major plant. One example is the outage of the Otahuhu-Whakamaru transmission line on 26 March 2011. This outage ensured that the Huntly power station was placed in a must-run situation to ensure demand was met hence prices in the market escalated to $ 20000/MWh [26].

Further, the NZEM process may not handle dry year risk particularly well. The majority of NZ's electricity generation comes from hydro resources, and the majority of the storage capacity of the hydro generators is held in the lakes of the Waitaki scheme in the South Island. If there are low inflows to these lakes during the spring and summer preceding a winter, then by the middle of winter much of the storage capacity will have been used and a lack of generation capacity will result. Market participants may exacerbate problems by gaming the market; using too much water early in the winter to ensure higher prices later. This situation was particularly problematic as the entirety of the Waitaki scheme was operated by Meridian creating a partial monopoly on stored energy, hence the government intervened and transferred Tekapo to Genesis.

The NZEM also does not necessarily incentivise generators to hold capacity to meet peak demand. In NZ peak demand occurs during winter evenings and causes particular problems for distribution networks. Some distribution networks alleviate the peaks through load shifting, using ripple control to turn off hot water cylinders in the evening and reconnecting them at night. To date peak demands have not exceeded online generation capacity. However, for many years the Whirinaki station was designated in a reserve energy scheme and allowed a bid price of $ 5000/MWh [26]. This scheme has been suspended and the Electricity Authority now operates a Standing Reserve Supply Determination which allows the level of Lake Hawea and Lake Tekapo to be lowered below their normal operating range in times of of heightened supply risk [23]. Peak capacity problems are to some extent addressed by primary control measures but constitute a tertiary control issue as their recurrence is infrequent and time frames are long.

Tertiary control measures to meet peak demand using thermal stations are referred to as cold reserves. Cold reserves may need considerable time to warm up before power is able to be

produced and are often expensive to run, such as the oil fired plant that was operated at Marsden Point.

Likewise for secondary control, efficient tertiary control requires accurate forecasts of demand and generation capacity. Forecast horizons for tertiary control extend from seasonal to decadal. Seasonal forecasts for hydro inflows are necessary as the hydro lakes are cycled annually with the storage capacity being refreshed each spring, while peak demand occurs in winter. Decadal forecasts are required as events such as "dry years" occur infrequently, and maybe linked to climate patterns such as the El Nino Southern Oscillation (ENSO).

1.7 RELIABILITY AND RESILIENCE

Power system control measures are used to ensure that demand is met and power quality is maintained. However, the degree of control must be balanced against the costs of providing the control. It is not economically effective to design and operate a power system such that it will never fail, as such the system is designed to achieve some acceptable level of reliability. As the costs of non-supply can be very high (for instance if power were lost to a pot line at the Tiwai Point aluminum smelter the result could be terminal for the smelter as the aluminum would solidify in the pots, or worse people in Ponsonby might not get their latte!) there are strict policies to ensure reliability. Guidelines for the design and operation of the transmission system are provided by Transpower [27]. Reliability conditions in NZ are ensured through the security of supply N-1 criterion; the power system is designed such that under any contingent event (such as a transmission line fault) the power system can be restored to a stable state without loss of load. The guidelines also provide steady state performance and stability criteria.

While the reliability of the system can be improved through network design and be ensured by providing guidelines, reliability is intrinsically linked to the size of the network. The system inertia equals the sum of all rotating masses connected to the system; thus is proportional to the number of connected generators. The larger the system the greater the system inertia. Further, if more loads are added to the system and these loads are independent, then the aggregate load will be smoothed. A network that has a larger spatial extent also allows more resources to be exploited increasing the diversity of generators and thus reducing variability. Also, as more generators and loads are connected to the system, the proportional size of each generator / load becomes smaller and risks associated with disconnection become smaller. The result is that as the electricity network becomes larger and more diverse it becomes stronger and has greater reliability.

Most networks, particularly in Europe and North America, have strong ties to other networks allowing import and export of power, thus providing greater reliability. Interconnection increases the spatial extent of the network allowing aggregation of more loads, and more resources to be exploited. NZ is a very long distance from its nearest neighbour, Australia, hence it is not practical to inter-connect. Thus the power system operator in NZ must maintain good control as it must maintain system security without aid.

While maintaining the power quality and reliability of the electricity network, it is also necessary to ensure the network is resilient. That is, the network must be able to cope with extremes in demand, generation patterns, and fault conditions. Resilience can be achieved through either robust design or through diversity. Robust design entails engineering components such that they will only fail in extreme conditions, and this also entails greater cost. Diversity of generation sources can reduce the risks associated with failure of a particular resource (such as dry years impacting on hydro generation), and diversity of transmission routes lowers exposure to localised extreme events (such as wind storms). Although resilience of the power system may be increased by diversification of generation sources, this is only true if the resources are independent. For instance, there has been concern that wind and hydro resources may be correlated in which case

diversification of resources through investment in Wind Power Plants (WPP) would not reduce dry year risks [28].

1.8 EFFICIENCY

While it is desirable for the power system to be very reliable and resilient, this comes with added costs due to increased capital required to make the network robust or exploit more diverse resources. Hence, there is motivation to ensure the network achieves the reliability and resilience while incurring the least costs, thus obtaining the greatest economic efficiency.

Economic efficiency is also dependent on the energy efficiency. In the generating, transmitting, and distributing electricity there are energy losses due to the resistance in components. The ratio of energy delivered to the total used defines the energy efficiency. The energy efficiency of the network can be increased, for instance by increasing conductor sizes, but this has increased capital costs. Energy efficiency does not directly translate into an economic efficiency as the cost of various resources differ. The cost of wind for instance is negligible (although the energy losses must be made up by increases in generation capacity), whereas the cost of thermal generation is related to its capital costs as well as its fuel and environmental costs.

1.9 FUTURE NETWORK EVOLUTION

The electricity network has been static in its technological paradigm since its inception. Large power plants provide the frequency control and electricity is distributed radially. While integration of distributed generation has challenged the operation of the network new technologies such energy management systems, information technology, electric vehicles, and local storage pose even greater challenges. The evolution of the smart grid is central to policies aiming at ending dependence on fossil fuels, reducing carbon emissions, and combating anthropogenically induced climate change. The way in which the grid operates and electricity is supplied may therefore have to change. In order that this challenge can be overcome and that the best advantage is made of the technology, it is crucial that research and development is undertaken directed towards solving these problems. Accurate models of wind power are required to support analyses of future grid evolution.

The Gathering Renewable Energies in Electricity Networks (GREEN) Grid project seeks to determine what changes to the power system may occur, to develop methods and models to quantify the potential impacts, and find measures that may be used to smooth the path to a new power system paradigm [2]. This thesis constitutes part of Research Aim 1.1.1 of the GREEN Grid project.

1.10 PLANNING AND DEVELOPMENT

Generation in NZ has grown to ensure consumer demand is met, and that power quality and reliability are maintained. Power system infrastructure investments often require very large quantities of capital and significant lead times, due to design and construction. Prior to deregulation all the large power system projects (generation and transmission) have been led by departments of the government. While there has been deregulation and introduction of competition to the generation sector, the transmission of electricity is presently controlled by Transpower and regulated by the Commerce Commission. It is vital to the efficient operation of the electricity market that Transpower maintains good power system security in both in the short term (through power quality management) and in the long term (by ensuring the electricity network is appropriately designed and constructed to cope with future changes in supply and demand).

While in recent years the construction of new generation plant in NZ has tapered back there has been significant investment focused on reinforcing the transmission network. Projects have included the North Island Grid Upgrade Project (NIGUP), and upgrading lines in the South Island to enable investment in renewable energy resources; Transmission to Enable Renewable investments (TER) [29]. This project entailed costs of up to $170 million to upgrade five sections of transmission line from Roxburgh through to Benmore. As the transmission network is a regulated monopoly investment in large projects must presently pass through the Commerce Commission; Transpower submits Grid Upgrade Proposals (GUP) for approval by the Commerce Commission (formerly proposals were submitted to the Electricity Commission) [30]. As indicated in the name of the TER project the purpose was to ensure that the electricity from foreseen renewable generation projects in the lower South Island could be transferred north to the HVdc link. The foreseen projects included many notified and consented WPPs in Otago and Southland. The project would also help solve the potential glut of electricity in the lower South Island should the Tiwai Point Aluminum Smelter cease operations and thus effectively strand the generation capacity of Manapouri.

To support decision making in centralised or deregulated environments it is necessary to forecast changes in demand and generation. Hence it is important that accurate models of demand growth and generation are available to ensure that supporting transmission infrastructure can be constructed, so it is available to accommodate new generation and changes in load. Various models are required to support studies of different power system components and dynamics. The complexity of the models differs according to the part of the network being studied.

Some planning studies such as those used for designing distribution lines require very basic models such as After Diversity Maximum Demand (ADMD). The primary requirement for distribution lines is to be have sufficient capacity to meet the maximum annual demand, other design variables that may affect power quality are not important as standardised designs and mechanical requirements provide sufficient headroom. However, planning for major transmission network components, such as a 400 kV line requires a suite of studies. Such studies may include analysis of transient stability, short circuits, reactive power, insulation co-ordination, and harmonic analysis. Planning for entire transmission networks and power systems requires an even greater complexity as power flows, faults, and the entire gamut of power quality requirements must be studied.

1.11 SUMMARY

The electricity network in NZ has been constructed incrementally to satisfy growing demand and to adapt to changes in technology. A transmission network and a power generation portfolio has been constructed that allows exploitation of the large energy resources in rivers and gas fields and the transfer of this energy to load centers. To ensure that the electricity network operates with a high degree of reliability, as there are very high costs involved with non-supply and poor power quality, standards and guidelines have been developed. The power network continues to evolve with changes in technology and demand patterns, and as the projects involved are capital intensive and require significant planning and development lead times, there is a need for accurate models of generation.

This thesis seeks to develop models that can be used to support power systems studies specifically seeking to determine the effects on the transmission network from increases in wind generation. More specifically this thesis aims to provide models that can be used to determine primary, secondary and tertiary control requirements. The purpose of the models drives the desired temporal resolution; in the case here the requirement with the highest resolution being the effect of wind power on the reserves market, thus a temporal resolution of 5 minutes is desirable. The models must also cover a large temporal span as events that place stress on the power system

occur infrequently, and be spatially and temporally congruent with other sources of generation and demand.

Chapter 2

WIND POWER

2.1 WIND TURBINES

Wind energy is easy to harvest, is found everywhere, and with basic materials some device which captures the wind can be built. For at least 5500 years wind has been harnessed to power boats, provide ventilation, grind grain, and pump water. The first use of wind for generating electricity, and hence the invention of the wind turbine, was made in 1887 by Prof James Blyth in Scotland, who constructed a 10 meter high turbine for providing power for domestic lighting. The ease of harvesting wind resources has ensured a continual stream of inventions to convert wind into electricity. However, the basic architecture of the wind turbine has converged to the Horizontal Axis Wind Turbine (HAWT).

The HAWT can be described as a propellor on a stick. HAWTs capture wind using blades to generate lift, like an aeroplane wing (as opposed to drag). The blades are long and slender to enable the rotor area to be as large as possible and thus capture the maximum amount of wind. The blades are attached centrally to the hub which is connected to the low speed shaft which rotates in reaction to the lift applied to the blades. The shaft is connected through a gearbox to a generator from which power is produced. The generator, gearbox, radiators and other components are contained within the nacelle which is mounted on top of the tower. The nacelle is yawed so that the rotor faces into the wind and blades pitched to alter their angle of attack and thus the amount of lift generated. The power may be fed through power electronics to improve performance. There are many variations on the HAWT archetype, such as removing the gearbox and using a multi-pole permanent magnet generator, each variant having its own electrical and energetic characteristics. However, the power produced by HAWTs is subject to most of the same physics, independent of the exact machine design.

The technological development of HAWTs saw a steady increase in machine size from the 1980's allowing economies of scale to be achieved. In 1985, wind turbines had a capacity of approximately 0.5 MW with blade length (b) of approximately 7.5 m, by 2001 the largest machines had a capacity of 4.5 MW (b = 66 m), and in 2015 machines with a capacity of 7.5 MW (b = 60 m) were commonly installed [31]. While the pricing of turbines is complex, reflecting the fluctuating prices of raw materials, generally the costs per MW have decreased as the technology has improved. Further the capacity of wind turbines installed worldwide increased in an exponential manner from 1 GW in 1996 to 38 GW by 2009, and while still increasing the rate of increase has tapered off [31].

The increased length of wind turbine blades means that the rotor swept area has become much larger (a 7.5 meter blade will sweep 706 m^2 whereas the 66 m blade will sweep 39 408 m^2). This increase not only results in more energy but also results in greater spatial integration and hence smoother power delivery (as turbulence in small vortices is averaged out).

As the sizes of WTs have increased so too have the tower heights. Pragmatically this is to stop

the blades hitting the ground, but also to make use of higher wind speeds at greater heights. The wind speed at the ground is zero due to drag forces, and as height increases the mean wind speed will increase according to a wind shear profile (see section 5.3). However, as towers become taller so do loads exerted on foundations and lower tower sections, thus the height of the tower is a trade off between the increased energy due to increased wind speeds and increased costs due to materials. The tower height selected depends on the site.

2.2 WIND TURBINE POWER

The quantity of power produced by a wind turbine depends primarily on the wind speed incident over the rotor area. Note that the power is related to the wind speed and not wind velocity as wind turbines yaw into the wind. The amount of power available in the wind is proportional to the cube of the wind speed as presented in Equation 2.1.

$$P(t) = \frac{1}{2}\rho\pi b^2 v(t)^3 \tag{2.1}$$

Where P is power, t is time, ρ is the density of air, b is the blade length, and v is the wind speed.

Wind turbines are not 100 % efficient; there are physical limitations such as that described using the Betz limit. This is the limit at which no more energy can be extracted from the wind before the air diverts around the rotor disc, as air in front of the rotor is becalmed as its velocity is converted into power. The Betz limit places a theoretical maximum aerodynamic efficiency for a wind turbine, however it is unlikely even a well engineered wind turbine will attain an aerodynamic efficiency close to this. Experiments have shown the Betz limit to be approximately 0.6.

The aerodynamic efficiency is reduced by yaw errors (an error due to the turbine not facing directly into the wind), wind shear (the wind speed varies as a function of height and hence there is a velocity deficit below the hub height which may not be compensated by the velocity excess above hub height), and turbulence. Although the turbulence may mean there is more energy available in the wind than the mean wind speed would indicate it is unlikely the turbine can capture the rapid fluctuations in wind velocities and hence energy will be lost. Note that each of these factors, yaw error, wind shear, and turbulence are dynamic and thus the specific efficiency is a function of the wind speed, wind direction, atmospheric stability, and turbine operational state.

Wind turbines are limited in their mechanical design so that economic efficiency is maximised. Wind turbines have a “cut-in” wind speed, below which they will not produce electricity, as to do so would require more materials than the equivalent energy generated. Wind turbines typically also have a ”cut-out” wind speed above which the wind turbines shut down to avoid excessive loadings in storm conditions. Machines that shut down due to high wind speeds will not re-engage until the wind speed falls below a set level, usually lower than the limit at which it is forced to stop. The stopping and restarting generates a pattern of power production similar to a hysteresis loop, and losses in energy production are termed high wind hysteresis losses. High wind hysteresis losses are mitigated in some machines where the power produced is tapered as wind speeds rise; patented as storm control [32].

Besides the aerodynamic efficiency, the power produced by a wind turbine is affected by the efficiency of mechanical and electrical components. The mechanical efficiency describes energy losses due to friction in the gearbox and bearings. Electrical components that incur losses are the generator, transformers, and power conditioning equipment. In practice wind turbines have a maximum coefficient of performance of up to 0.5 [33], with most achieving a figure of 0.35. The efficiency of a wind turbine is presented in Equation 2.2.

$$P_{WT}(v) = e_{aero}(v) \cdot e_{mech}(v) \cdot e_{elec}(v) \cdot P(v) \tag{2.2}$$

Where WT denotes wind turbine, e_{aero} is the aerodynamic efficiency, e_{mech} is the mechanical efficiency, and e_{elec} is the electrical efficiency.

The power produced by a wind turbine, as a function of wind speed, is termed the power curve. Despite the range of turbine technologies all HAWTs have similar power curves. The power curve from a Vestas V80 2.0MW wind turbine is presented in Figure 2.1. At low wind speeds there is little energy available in the air, as the wind speed increases the availability of energy becomes greater, however at high wind speeds ($> 25\,\mathrm{m\,s^{-1}}$) the energy available is such that turbines can suffer damage. To achieve maximum economic efficiency turbines are equipped with components that make best use of the resource. Hence, turbine generators are sized such that they reach rated power at a wind speed which is regularly experienced and turbines decrease power or shut-down at high wind speeds to protect themselves.

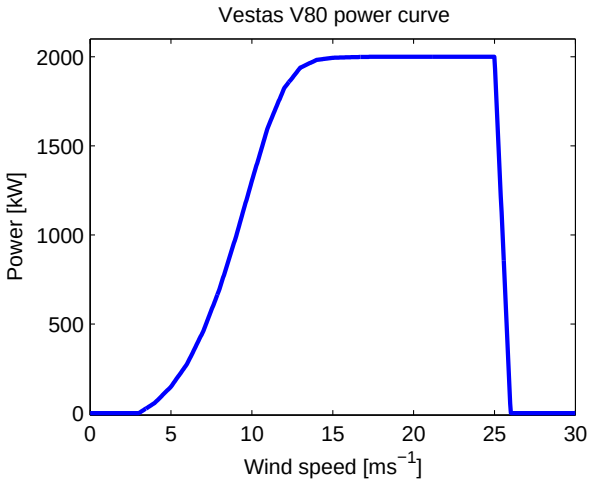

Figure 2.1 Vestas V80 wind turbine power curve

Figure 2.2 Vestas V80 wind turbines at White Hill

Wind turbine power curves are calculated with reference to a single point hub height wind speed

measurement. The procedure for determining the wind turbine power curve is standardised in Power Performance testing of wind turbines IEC 61400-12 [34]. The standard requires the installation of two meteorological masts, equipped with appropriate anemometry. Monitoring of these two masts is undertaken for a period such that the correlation in wind speeds is well defined. One of the masts is then removed and the wind turbine installed, and measurements from the turbine power and remaining mast made. The standard requires certain geographic conditions to be met including: that the turbine and mast are located such that the wind incident on the turbine and mast is free from interference from obstacles, that the surrounding topography is simple in relief so that wind shear and turbulence is not high, and meteorological conditions are neutral. Data are selected from the monitoring such that there is no interference to wind flow between the mast and turbine, i.e. data are selected only at times when the wind direction is within particular bounds according to the site layout. Using the selected data the power curve is then defined using the method of bins. Adjustments to the calculated power curve are made for air density, dependent on turbine type (pitch versus stall control), to arrive at the power curve for an air density of $1.225\,\mathrm{kg/m^3}$.

2.2.1 Wind turbine control

Early wind turbines relied on aerodynamic stall to regulate power output; that is at low wind speeds the rotor speed is likewise low. As the wind speed increases the rotor speed also increases until a point at which the rated power of the turbine is reached. Above the rated power the rotor speed does not increase but as the wind speed increases further the relative wind flow across the blades produces aerodynamic stall and hence the power output is decreased. Most stall machines have fixed blade angles and hence require few moving parts, further the blades may have a twist to ensure the stall region of the blade progressively increases as wind speeds increase above the rated power.

Most modern HAWTs use pitch control, whereby the angle of the blades is changed according to the wind speed. At low wind speeds the blades are angled such that the maximum amount of energy is extracted from the wind. As the wind speed increases the pitch remains constant and the rotor speed increases until the rated power is reached. As the wind speed increases further the pitch of the blade is controlled to keep the rotor speed constant and the output at rated power. Once the wind speed is very high the WT may pitch its blades to either decrease power or shut down.

The rotational speed that turbines adopt is optimised to extract the maximum energy from the wind. If the rotational speed is too great aerodynamic losses from turbulence at the tip of the blade (which may be moving at speeds of up to $80\,\mathrm{m\,s^{-1}}$) will impact on efficiency. Further, the blades will sweep into the wake left by the prior blade sweeping through the air. If the rotational speed is too slow then wind will be spilt between blade passes. High tip speeds cause increased noise emissions and hence rotor speeds may be lowered and power reduced to provide quieter operation.

Most early wind turbines were equipped with a gearbox and synchronous generator. This type of turbine is inflexible in terms of regulating power output, and any variation in the wind results in variation in exported power. As turbines have developed there has been a proliferation of generator configurations and types. Modern large machines may use multi-pole generators with full scale power converters or doubly fed induction generators; these machines allow great control over power export.

Of particular interest to NZ, the Windflow 500 kW machine uses a synchronous generator with teeter rotor and power smoothing is achieved using a torque limiting gearbox that uses a hydraulic pump connected to a second output from the gearbox.

2.2.2 Wind turbines and power quality

Wind turbines, particularly early examples, are passive in their reaction to the wind, and any variability in the wind is transferred to variability in power output. This variability of power output impacts power quality. As the technology used in wind turbines has developed so too has the ability to regulate power and control the quality of that power. The physical size of turbines has allowed increased spatial integration leading to greater power smoothing. Power quality is also improved in WTs through power electronic converters.

Because of the passive nature of wind turbines and the related poor power control, it has been necessary to develop standards for the power quality emitted by turbines. The International Electrotechnical Commission (IEC) has developed a set of standards designated IEC61400 that relate to the design, manufacture, and installation of wind turbines. Part 12 of these standards outlines methods for measuring and assessing the power quality from wind turbines [35], with the aim of providing manufacturers and network operators common ways of measuring power quality and defining acceptable limits.

Nowadays wind turbines may have many capabilities that allow the machines to actively regulate power quality and provide benefits to the electricity network. Strategies such as operating wind turbines at lower than the available power allows headroom which can be used to provide voltage or frequency support [36]. Power electronics, in some cases full scale power converters, allow turbines to actively manipulate wave-forms so that frequency and power factor can be managed. Active management of wind turbines can reduce the speed of power fluctuations and mitigate flicker. Thus distributing WPPs throughout the electricity network may provide support for power quality regulation.

The unit size of wind turbines (maximum 3 MW in NZ) is relatively small compared with conventional generators. Individual hydro turbines may be as large as the 121.5 MW generators installed at Manapouri (total station capacity 850 MW). Thermal generators may be even larger such as the 250 MW unit size at the Huntly power station. The small unit size means that if a fault impacts a wind turbine and causes it to suddenly disconnect the resulting change in generation is small compared with the loss of a large thermal plant. While a fault may occur that could cause the entire WPP to disconnect, such as a fault with the main transformer, the likelihood of this occurring is low and certainly not greater than for equivalent faults in other types of power plants. The small unit size results in WPPs not constituting part of the contingency allowance in power system scheduling.

2.3 WIND POWER PLANTS

A Wind Power Plant (WPP) comprises a grouping of wind turbines that are connected to the electrical grid through a common coupling. The reason for grouping turbines together is so that economies of scale can be obtained through sharing of electrical, civil, planning and development, and transportation costs. The turbines are spread over an area to maximise energy production while minimising turbine mechanical loading and keeping the benefits of grouping.

WPP design may be constrained by items in the following list:

- Topography; turbines should be placed in positions that maximise energy production, and minimise turbulence. Turbines should be placed so that the incident wind is smooth, if there is higher terrain upwind of the turbine then turbulent vortices may impact the turbine and cause excessive loads. The topography must allow for construction of turbine foundations, turbine set down areas, and roads for transportation of turbine components.
- Geomorphology; the geology must be suitable to support a wind turbine (WTs are often heavy). Rivers, bogs, and aquifers may require consideration.

- Forestry and obstacles: trees and obstacles slow the wind and induce turbulence.
- Land boundaries; turbines must be placed on property that is owned by project stakeholders. The blades of the turbines should not overhang neighbouring properties and depending on planning regulations further set-backs may be required.
- Planning regulations; local authorities and governments may place restrictions on development to protect cultural, scenic, and amenity values in certain areas.
- Electrical infrastructure; the point of connection must be within an economic distance of the WPP, and have capacity to connect the WPP. If new transmission is needed planning permissions for this may be required.
- Noise; in NZ WPP noise emissions must comply with NZS 6808:2010 [37], for turbines with rotor areas greater than $200\,\mathrm{m}^2$. The noise wind turbines emit is characterised by the sound power curve which is dependent on the wind speed. The acceptable noise depends on the background noise (due to wind rustling leaves etc) which is also dependent on wind speed. The noise emitted from the WPP must be calculated across a range of wind speeds and not exceed either 40 dB or the background noise level +5 dB at neighbouring dwellings.
- Visual impact; wind turbines are by necessity visible from a large area. The acceptability of the wind farm will depend on local attitudes and the relative impact of the WPP on the visual amenity.
- Radio, television, microwave, and radar interference; wind turbines may interfere with the transmission of electromagnetic waves and thus impact on a variety of communications technologies. This is particularly important near airports where turbines may interfere with air traffic controls.

The constraints placed on WPPs generally have the impact of spacing turbines further apart than an ideal layout (based solely on optimising energy production). The constraints also limit the turbine type that may be selected for a WPP, offshore projects are typically have fewer constraints and economies of scale can be obtained using very large turbines ($> 5\,\mathrm{MW}$).

As the wind passes through a wind turbine it slows, energy is extracted and velocity decreases, and turbulence is increased as separation of the wind flow occurs around the blades. The propagation of this velocity deficit and turbulence downwind of the turbine is the turbine wake [38]. The wake causes energy losses for turbines sited downwind. The wake also causes increased mechanical loadings on turbines downwind due to turbulence. As the wake propagates it decays as turbulent mixing of the air ameliorates the velocity deficit, and as the viscosity of the air causes the turbulence to dissipate. To reduce the wake losses and turbine loadings it is common practice for wind farms to be designed such that a minimum spacing between turbine is maintained. The exact spacing depends on the turbine manufacturer and developer's balance between energy production, and turbine loss of life and maintenance requirements.

The inter-turbine spacing is also dependent on the wind resource at the WPP site. If the wind resource is highly directional (that it there is a dominant wind direction), then it may be acceptable to apply small inter-turbine separation distances perpendicular to the wind direction. However, the spacing parallel to the prevailing wind direction will remain large. Typically an oval shaped separation distance is applied in designing the WPP. Typical distances may be 4 rotor diameters perpendicular to the prevailing direction and 6 rotor diameters parallel [39].

As wind turbines are spatially distributed the wind incident on each wind turbine in a WPP is unique. This is because the topography upwind of each wind turbine, especially in hilly terrain, is different; thus there is a unique topographic speed-up for each wind turbine in each wind direction. The topographic speed-up is defined as the ratio of the wind speed at the turbine

rotor center to the wind speed at some reference point (usually the meteorological mast). As the speed-ups are dependent on the wind direction, ignoring second order factors such as atmospheric stability, it is usual to characterise the power production using a power performance matrix where rows are defined by wind speed bins and columns by wind direction bins or sectors (as shown in Equation 2.3). It is possible to average across the columns of the matrix to find a WPP power curve as shown in Equation 2.4.

$$P_{WPP}(v,d) = \sum_{n=1}^{N} P_n(v,d) \tag{2.3}$$

Where WPP denotes Wind Power Plant, n is the wind turbine index, N is the number of wind turbines in the WPP, and d is wind direction.

$$P_{WPP}(v) = \sum_{d=1}^{D} q(d) \cdot \sum_{n=1}^{N} P_n(v,d) \tag{2.4}$$

Where $q(d)$ is the probability of wind in direction sector d, and D is the total number of wind direction sectors.

The topographic speed-ups are static, that is they are time-invariant with respect to the wind speed and wind direction. However, the power produced by the WPP is dynamic due to turbulence. The wind speed incident at each wind turbine is different, as vortices entrained in the wind impact on turbines with varying force dependent on their time of arrival and spatial extent. The correlation in the magnitude of wind speeds at neighbouring turbines is related to the coherence of the wind field; the effect of which is spatial diversity. The spatial diversity has the effect of smoothing out some of the variations in power from a WPP compared with that which would occur if all turbines were placed at a single point.

2.3.1 Wind power plant efficiency

The power from a WPP is a product of the sum of power from individual wind turbines and the WPP efficiency as shown in Equation 2.5. The WPP efficiency is affected by the electrical and operational losses. The electrical efficiency of the WPP is reduced due to losses incurred by reticulation within the WPP, transformers, power conditioning equipment, and transmission lines. The operational efficiency, often referred to as availability or technical availability, reflects losses in production due to faults, maintenance, and power control.

$$P_{WPP}(t) = e_{elec}(t) \cdot e_{oper}(t) \cdot P_{WPP}(v(t)) \tag{2.5}$$

Where e_{oper} is the operational efficiency.

The operational efficiency of WPPs has gradually increased as wind turbine technologies have been refined. In 2008 the measured operational efficiencies for 14 GW of WPPs worldwide had a mean value of 0.96 and a median of 0.97 [40]. Further it was shown that the operational efficiency was lower for larger wind turbines, possibly reflecting lower operational time and hence less time for technical issues arising, and the operational efficiency was higher for WPPs with a greater number of wind turbines.

The operational efficiency is the ratio of the exported power to possible power given no restrictions to operation of the WPP (excluding the electrical losses). The power from the WPP is reduced due to faults, wind farm management, and curtailment. The term availability is avoided as varying definitions are applied (such as the percentage of time the wind farm is available to produce full power, or the ratio of the quantity of power produced to the quantity that theoretically could be produced during a period of time) which can result in conflicting statistics.

While the total energy lost due to operational efficiency is small the influence on variability can be significant, as the change in power due to a fault or switching operation is instantaneous and may equal the WPP capacity. Hence, accurate simulation of the operational efficiency is important for determining the effects of the WPP on the electricity network.

Faults in wind farms can arise from mechanical and electrical failure. Wind turbines have many moving parts and hence there is a multitude of possible of mechanical failure modes. Gearboxes and main bearings are common causes of mechanical faults and these may take days or even months to repair, especially in NZ as the number of turbines is small and spare part availability is limited. The logistics of repair can be complex with cranes and other specialist equipment needed to make repairs.

Electrical faults vary from isolated short circuits that may require re-closure of automated fault protection, taking less than a second to clear, through to transformer failure which could take up to a year for a replacement transformer to be procured.

Turbulence can cause excessive vibration in wind turbines causing them to shut down or reduce power output for self preservation. Turbulence and gusts maybe related to weather events such as the sudden arrival of a front or storm, the influence of terrain, or turbine wakes. The wind turbine may restart after once the turbulent conditions have passed or a manual restart may be required once the turbine has been inspected for damage. Wind turbines may also use "sector control" whereby the wind turbine may shut down or reduce power in certain wind directions (where there maybe many turbines or bad terrain features upwind).

The management of a WPP can cause a loss in power for many reasons, typically wind turbines are shut down to allow for maintenance and servicing. Servicing is likely to occur at specified times to accommodate the availability of labour during work hours. Often a sequential pattern of servicing is undertaken as all turbines in the WPP are serviced during a single period. Certain periods during the lifetime of the WPP may require additional servicing to be undertaken such as during commissioning.

The management of the WPP also includes wind turbine control strategies such as turbine unwind. As wind turbines yaw into the wind they twist the power cables in the tower, if the turbine yaw continuously in one direction through several turns the cables will wind up all their slack and the turbine must yaw in the opposite direction to unwind the cables.

The operational state for turbines is often correlated with neighbouring turbines, as turbines are electrically connected in WPPs in "strings" of turbines, and a string of turbines maybe disconnected for common maintenance.

WPPs maybe curtailed due to grid congestion (so called run-backs), and maintenance and faults (in the electricity network). Run-backs are timed when the variability of wind power causes excessive risk to power quality. Thus run-backs are likely to occur at times when either the network is highly stressed or at times when the percentage of variable generation is very high. Maintenance of the network, as for turbine servicing, is likely to occur at times when there is available labour. Network faults are similar to electrical faults in that they may be short (e.g. possums on the power lines [41]) or long in duration (e.g. line outages associated with extreme weather events).

2.3.2 Wind power plant control

Wind turbines are manufactured as stand alone units, and power control is possible at each wind turbine. The wind turbines are linked together electrically to form a WPP and have a single point of connection to the electrical network. Most modern WPPs connect the wind turbines using a Supervisory Control And Data Acquisition (SCADA) to provide centralised control and monitoring of the wind turbines. This has many advantages for managing the WPP and also benefits power control and power quality. Centralised control may be particularly advantageous

at times when the WPP is sent instructions from the network operator to control power output, as either individual turbines can be shut down (so as to not accumulate run-hours), or power may be reduced from all turbines to allow headroom and thus accommodate power smoothing.

2.3.3 Wind power plants and power quality

The power quality from a WPP not only depends on the characteristics of individual wind turbines but also on the aggregate power from turbines. To assess the power quality from a WPP it is necessary to account for the aggregate impact from all wind turbines in the WPP. Further, as the wind speed incident on one wind turbine is closely related to the wind speed incident on neighbouring wind turbines the power output from neighbouring wind turbines will be highly correlated. To estimate, for example, the magnitude of flicker created by a WPP it is necessary to simulate the coherence in wind speeds incident on the wind turbines in the WPP, which in turn affects the covariance of turbine power output [42]. While all wind turbines in a WPP fetch a similar wind speed, the spacing of the turbines ensures that there is some degree of diversity in wind speeds, and the power output will be smoothed.

To avoid power quality issues propagating from WPPs additional regulating equipment such as switched capacitors or STATCOMs (STATic synchronous COMpensator) may be installed. STATCOMs are used to provide sinks or sources of reactive power, and are used for power factor correction. These devices can be considered part of the WPP and benefits to the power network attributable to the WPP.

While WPPs may be the source of power quality issues on the electricity network they are equally vulnerable to departures from normal operating conditions. This vulnerability may lead to the WPP being damaged or activating protection measures to limit damage. The actions taken for protection may lead to exacerbation of the network problems. For example a fault may occur on a transmission line induced by a lightning strike, the WPP may then trip or disconnect from the network and subsequently there may be a voltage sag until the WPP can be re-connected.

2.4 INTEGRATION OF WIND POWER

To ensure the connection of a WPP to the electricity network does not result in excursions of power quality outside of acceptable operating conditions it is necessary to simulate the actions of the WPP and network prior to construction. Studies may look at power flow, low voltage ride through capability (to avoid prolonged voltage sags), power factor, performance of the WPP under transients and fault conditions, etc.

Integration studies may investigate the effect of individual WPPs on the network prior to construction, or may investigate the effects of fleets of WPPs. Studies that assess individual WPPs are likely to focus on assessing effects on the power network local to the WPP, whereas studies that assess fleets of WPPs will focus issues that effect the broader operation of the power system.

2.4.1 Integration studies

The potential for the integration of large amounts of wind power into power systems has attracted significant attention internationally. Many system operators have conducted studies; replicating work that has been completed many times before. To aid system operators in completing wind integration studies efficiently and to ensure studies are comparable the International Energy Agency (IEA) commissioned *Task 25: Design and Operation of Power Systems with Large Amounts of Wind Power* with Part 16 of the expert group report focusing on wind integration studies [43]. The Task 25 report details the various elements to be considered in integration studies. These elements are:

- Contents of a wind integration study,
- data requirements,
- portfolio development and system requirements,
- capacity value,
- production cost simulation and flexibility assessment,
- transmission grid simulations: load flow and dynamics,
- analysing and presenting the results.

The IEA Task 25 report identifies two main objectives for wind integration studies. The first study type focuses on capacity value. That is the value to which wind energy can play in the provision of power. The second type of study focuses on Unit Commitment and Economic Dispatch (UCED) which requires calculation of reserves requirements. Many studies may address both aspects simultaneously.

Capacity studies require a lower temporal resolution than UCED studies. A temporal resolution of 1 hour is generally sufficient for capacity studies whereas UCED studies require a temporal resolution of minutes.

Further studies, not covered by IEA Task 25, may also be conducted assessing the behaviour of WPPs in response to transient or steady state grid conditions (e.g. faults, swells, sags, and harmonics). Studies to assess faults, sags, and swells require electromagnetic transient simulations and can be classified as dynamic studies. Dynamic studies require temporal resolutions of milli-seconds to seconds and temporal spans in the order of minutes. Dynamic studies are generally used to assess the reaction and impacts of individual WPPs to grid conditions. Integration studies conducted to assess power quality phenomena such as harmonic emissions can be classified as Power Quality (PQ) studies, and although the phenomena may be steady state, the resolution for simulations is milli-seconds and requires a temporal span of minutes. Dynamic and PQ studies usually assess impacts that are localised to individual WPPs and thus not characteristic of the integration of fleets of WPPs.

The temporal span necessary to support capacity studies is relatively long, 6 years is recommended in IEA Task 25. Indeed even this length may be insufficient to address climatic variations that may impact the power system, such as El Nino Southern Oscillation (ENSO). For UCED studies a temporal span of one year may be sufficient.

The effect of wind generation on the power system is dependent on the capacity of wind power installed compared with the total system generation capacity. The ratio of the total installed wind generation to total generation capacity is termed the penetration. If the wind power penetration is less than 5% to 10% then the impact of the installed wind power on the power system will be relatively minor. That is the wind power will not significantly affect the generation mix dispatched in the system. Hence, capacity and UCED studies can be performed by adding the assumed wind power to the existing or foreseen power system. If the penetration is greater than 10 percent then the installed wind power will significantly affect the generation mix and changes to other generation must be incorporated into the integration studies.

The IEA Task 25 report notes that the impact of the variability of wind power is relative to the total system variability. The total system variability is equal to the load variability; thus it is important to assess wind and load variability together in a time coincident manner. A useful abstraction sometimes applied is to treat wind power as negative load.

IEA Task 25 also states the need for accurate models for forecasting wind power, and the importance of using state-of-the-art wind power forecasts. Even small improvements in wind

power forecasts can have a marked reduction in the quantity of reserves procured, so costs associated with wind integration are very sensitive to forecast error. Ensuring that the forecasts used for integration studies are as realistic as possible, or are representative of future forecast accuracy, is highly important. Further, IEA Task 25 highlights that to ensure that estimates of variability and aggregate forecast performance are accurate it is important to ensure the smoothing effects of spatial diversity on wind power are well characterised.

There have been a multitude of integration studies, as the effects of integration of wind power are network specific. Each network has its own characteristic loads, generation, wind resources, and transmission topologies, hence the impacts of wind integration differ significantly. A detailed review of integration studies is not conducted here rather results from a few selected reviews and studies are presented.

Wind integration has been a particular focus for network operators in the United States of America and there are many integration studies, from which a summary of twelve studies is provided by Johnathon Dowds et al. [44]. The review focuses on studies that address short term balancing reserves i.e. UCED studies mainly in the USA. The studies reviewed include:

- New York (NYSERDA) 2005,
- Minnesota 2006,
- Texas (ERCOT) 2008,
- United States 20% wind (NREL) 2008,
- Europe (EWEA) 2009,
- California (CEC) 2010,
- Nebraska 2010,
- New York (NYISO) 2010,
- Southwest Power Pool (SPP) 2010,
- Western United States (WWSIS) 2010,
- Eastern United States (EWITS) 2011,
- United States 80% renewables (NREL) 2012.

Dowds et al. note differences in the magnitude of reserve requirements calculated using different methodologies. Studies that assumed probability distributions, in particular Gaussian distributions, to characterise step changes in wind power tended to under-estimate the frequency of large changes in wind power compared with wind power measurements. The studies assuming Gaussian wind speed step changes tended to under-estimate the reliability and operating costs. Dowds also notes that studies making use of wind speed time-series derived from Numerical Weather Prediction (NWP) models (see Section 5.6) tended to underestimate the Power Spectral Density (PSD)(see Section 4.2.2), of wind speed compared with the PSD of empirical wind data. Note that many of the studies utilise the same NWP model data sets (the AWS truepower 2km meteorological model used in four studies and AWS truepower providing other NWP products for a further four studies). However, the underestimation of PSD is not likely a result of the particular numerical model but rather that NWP models do not accurately characterise turbulence. The underestimation of wind speed PSD leads to underestimation of the variability of wind power. It is noted that the degree to which the variability is underestimated is uncertain

as WPPs have smoothed power output compared with a power time series inferred from a single point wind speed measurement.

A recurring conclusion of the integration studies, identified by Dowds, is the benefit of the spatial diversification of WPPs and the potential to reduce the impacts of wind power integration. Many of the conclusions from the Dowds study, including the benefit of spatial diversification, are repeated in the review of wind integration and transmission in the United States undertaken by Milligan et al. [45]. This review assessed impacts of wind energy on the power system given the Department of Energy's vision of 20% wind penetration by 2030 and 35% penetration by 2050.

The NZ electricity grid is relatively small and is isolated. The spread of WPPs in small isolated networks is not as great as in large inter-connected networks as there is not the geographic span over which WPPs can be placed. Thus it is likely that there will not be as great a spatial extent of WPPs and hence there will be lower spatial diversity. Lower spatial diversity means greater coherence in wind resources, and WPP outputs will have higher correlation. For small networks it is more pressing to accurately characterise coherence. It is useful to present integration studies that have been conducted for networks that are small with no inter-connection (i.e. similar to NZ's).

Hawaii has many similarities to NZ; the Hawaiian Islands are situated in the middle of the Pacific Ocean and are not influenced by continental climate cycles, and a similar percentage of electricity is generated by wind power in Hawaii (5.1%) as NZ (7%), although the Island's demand is approximately one third of NZ's. Like NZ, Hawaii consists of several islands, and these are linked together with sub sea cables. It is projected that wind power penetration in Hawaii could reach 25%, which is further complicated by the potential for 5% of supply to come from solar power [46]. The potential impact on the Hawaiian power network spurred a number of integration studies, lead by the Hawaiian Clean Energy Initiative (HCEI), a summary of which has been produced by NREL [47]. From this set of studies the report of particular relevance here is *Development of a Regional Wind Resource and Wind Plant Output Datasets for the Hawaiian Islands* [48]. This study uses "state of the art" methodologies for generating time-series of power output from WPP and is detailed in the following section.

Oahu integration study

The Oahu integration study was conducted by AWS Truepower and hence the methods are similar to many of the other integration studies reviewed by Dowds and Milligan. The method uses reanalysis taken from a Numerical Weather Prediction model, a meso-scale model to increase resolution, WPP curves to transform wind speed to power, and smoothing of the power output using a time-series filter. As the numerical procedures are complex there are many choices at each step in the model development, and at each step there is potential for the introduction of errors. The Oahu study method is presented in detail to illustrate techniques adopted to ensure the results are useful.

Wind speed time-series are taken from the NCEP/NCAR Global reanalyses (Numerical Weather Prediction model hindcasts), these have a relatively coarse temporal (6 h) and spatial resolution (1.9 degrees or approximately 210 km between grid points). The spatial resolution of the reanalysis is enhanced using a meso-scale model, in this case the Mesoscale Atmospheric Simulation System (MASS). MASS is run using nested grids with resolutions of 30, 12, 4, and 1 km. The MASS model is initiated using Model Outputs from the NWP model and additional data is assimilated into MASS including satellite based sea surface temperatures, rawinsonde and surface meteorological station measurements (temperature, humidity, wind speed and direction). Using the results of MASS time-series of surface pressure, temperature, turbulent kinetic energy at 60 meters, and wind speed and direction at 60 meters and 80 meters are obtained for each grid

point. The grid point time-series have a temporal resolution of 10 minutes and span a period of 2 years. The results of the meso-scale modeling are then adjusted using measurements made at meteorological (validation) towers to remove model biases.

Time-series representative of each WPP are found by taking the set of time-series from grid points spanned by the WPP (note that the WPPs span many kilometers and are represented by many grid points). The time-series are scaled to a mean wind-speed derived from wind resource mapping undertaken by AWS Truepower [49]. The wind speed time-series are modified to account for wake losses (assuming the wake loss is dependent on the wind direction, being lower in the prevailing wind direction), and for turbulence. The turbulence modification is applied by adding a random value with a mean of zero and standard deviation equal to the Turbulent Kinetic Energy (TKE) to each time-series element. The TKE varies according to the time of day reflecting diurnal changes in boundary layer stability.

The wind-speed time-series of each grid cell are then converted to power by applying a wind turbine power curve. The power curves are either taken from the power curve for the machine installed at the WPPs or from representative curves formed from the power curves of commonly installed turbines. The power curves are adjusted to the air density calculated from MASS outputs. A filter is then applied to the power time-series to account for the spatial averaging of wind turbines within the area represented by each grid point. The filter applies a weighting of 90% to the present value of predicted output and 10% equally applied across the 17 preceding values. The total power from the WPP is then calculated as a weighted average applied according to how much of the WPP is covered by each grid point. Finally, allowances are made for operational and electrical efficiencies.

Validation of the power time-series predicted for three WPPs is carried out using data at a temporal resolution of 10 minutes for one of the WPPs and 30 minutes for the remaining two. The validation shows that the model accurately simulates diurnal variations, precisely replicates ramp-rates for two of the WPPs, but over estimates ramp-rates for the third. It is noted that there were some irregularities in the results due to model restart and assimilation of updated data causing discontinuities in the modeling.

As part of the Oahu integration study simulations of power forecasts were produced. AWS Truepower used its proprietry forecast system *eWind* to produce hindcasts. For each WPP at each time-interval, Model Output Statistics (MOS) were extracted from the MASS 4 km model and the 30 days of prior operational data were used to initiate the forecast model. The 30 days of operational data were used to form a non-linear transfer function between MOS and power. The forecast model was run to produce forecasts with horizons of 1, 4, 6, and 24 hours and these forecasts compared with the measured data. It was found that forecast accuracy decreases with increasing horizon, such that the Pearsons correlation coefficient equals approximately 0.93, 0.75, 0.69, and 0.54 for the 1, 2, 6, and 24 hour horizons respectively. Further the study investigated the auto-correlation of forecast errors finding high persistence in the errors.

The Oahu integration study also provided data to support UCED studies by simulating power output for WPPs with a temporal resolution of 2 s and 1 min. The high frequency power output was simulated by combining measured high frequency power output that was de-trended using a bicubic fitting procedure (effectively removing the 10 min mean values), and adding these using a boot strap type algorithm to the simulated wind power data (resolution of 10 min). Although much care was taken, by removing periods with curtailment and other operational restrictions from the sampled high frequency data, problems were noted due to the binning method used to discount seasonality. The simulated high frequency data were then compared to the measured value by comparing Power Spectral Densities (see Section 4.2.2). It was observed that the simulated PSD were lower at frequencies with a period less than 1 min, although this did not significantly challenge the accuracy of the predicted ramp rates over either 2 s or 1 min.

AEMO integration study

Although much larger than NZ, Australia is of local interest. The Australian Energy Market Operator completed a report on the integration of wind power into the Australian National Electricity Market (NEM) in 2012[50]. The study used simulated wind speed time series obtained from the CSIRO meso-scale atmospheric wind model for 148 points across the NEM area. The wind speed time-series were converted to power using wind turbine power curves scaled to the capacity of the indicative WPP; there was no smoothing of the wind turbine power curve to allow for diversity within the WPP. The study did not constrain WPP output due to transmission requirements or availability. The study used a 1 year period for analysis with an hourly temporal resolution. The AEMO study assessed the total wind power output for regions or "NEM wind bubbles" as a method of examining the diversity in wind power output between geographic regions.

The AEMO study investigated the correlation of wind power with demand, concluding that there was no significant correlation between wind and demand patterns. The study also highlighted the correlation of power output between Victoria and Tasmania and Victoria and New South Wales. However, there was observed a near anti-correlation between simulated power output in New South Wales and Queensland. This indicates that diversity in power output is due not only to spatial separation but also to meteorological patterns.

The AEMO study was used to support an analysis of the actions of the NEM in response to increased wind penetration [51]. The analysis of market impacts concluded that in most cases wind generation would not be constrained by network limitations. However, in certain areas such as the Eyre peninsular the local transmission network would become congested and this could lead to price collapse events at market nodes near to the congestion. And, as the value of the wind generation at the times of price collapse is low it would be difficult to economically justify network upgrades.

2.4.2 Managing the integration of wind power

While WPPs are largely passive in their reaction to the wind, some of the issues arising from integration can be managed. Primary control, or UCED, issues can be addressed by ensuring WPPs meet standards for connection (Grid Codes), through limited power control measures, and ensuring connection to "strong" parts of the power network. Secondary and tertiary control issues can to some extent be managed by ensuring that the fleet of WPPs is constructed to maximise the benefit of spatial diversification, and through improved forecasting of power output.

The integration of WPPs is not only addressed by managing the WPPs but also by ensuring the power system has the capability to absorb the generated power. Thus the power system is designed to ensure adequate reserve generation and transmission capacities are available to manage the variability of wind power. Much of the necessary reserves capacity usually exists prior to WPP construction as power systems are designed to manage the variability of load. The addition of wind power to a power system can be reconciled as addition of negative load rather than wind power constituting some novel dynamic in the power system.

Grid codes

As the number of WPP connections in some networks can become very large, the number of power system studies required can become onerous. To avoid some of the work necessary to ensure that WPP connections do not threaten power quality, it is common for network operators to specify operating parameters that WPPs must meet. The collection of operating parameters is grouped into a grid code which is typically specific to a network operator. However, turbine manufacturers supply turbines installed in many different networks. Each network requires

compliance with its grid code, and the grid codes may differ between networks. Thus it may become onerous on turbine manufacturers to prove that WPPs will comply with the many grid codes that are instituted by many different networks. In Europe there is presently work under way by the European Network of Transmission System Operators for Electricity (ENTSO-E) to unify grid codes such that turbine manufacturers can utilise a single turbine design in many electricity networks [52].

Power control

The variability of wind power can be alleviated to some extent by managing WPP power output. Wind power plants may be restricted in their output, often referred to as being curtailed or run-back. Run-backs are often used if there is local congestion on the network so that lines are not overloaded. Run-backs may also be placed to reduce the risk of power loss at times when networks may be vulnerable to rapid changes in power (e.g. if plant that supply rapid response reserves are offline and replaced by more cumbersome plant it may be necessary to reduce the variability of power supplied to the network). Curtailing WPPs also creates "head room" which can be used to provide voltage or frequency support.

WPPs may also have ramp rate controls (controls to the rate of change of power output) imposed by the network operator. For WPPs it is easy to control the rate of increase of power output, as this simply requires turbines to not produce power to their maximum ability. However, as wind turbines do not store power and their inertia is limited, it is more problematic to place limitation on negative ramp rates. Very large negative ramps may occur during storm events that cause high wind speed shut-downs. This may be particularly problematic when a storm front moves across a WPP or even an entire country as wind turbines progressively shut down.

Forecasting

To enable active participation in energy markets and for system operators to ensure optimal generation scheduling it is necessary that the energy production of WPPs is predicted. Much effort has been taken to increase the accuracy of wind power forecasts and the methods apply depend on the forecast horizon.

For short horizons, out to 2 h, the persistence of wind power naturally provides a high degree of certainty and is regarded as the method of choice for NZ [53]. Persistence forecasts may be improved through use of time-series tools such as ARMA (see Section 6.1), neural networks, and wavelet decomposition (see Section 6.3.1). For horizons greater than 6 h Numerical Weather Prediction models prove useful. A great deal of focus has been applied to developing forecasting tools and to creating forecasts that use ensembles of NWP models [54].

2.5 SUMMARY

Wind power is relatively recent addition to the mix of generation in the power system. Technological development of HAWTs since the 1980's has ensured that WPPs now make up a significant proportion of generation capacity. The largely passive reaction of WTs to the wind coupled with the variability of wind ensure that power from WPPs has some degree of variability and unpredictability. To ensure integration of WPPs into the power system does not undermine reliability or have excessive reserves costs integration studies are undertaken. As many integration studies are undertaken by system operators it has been necessary to provide guidelines for conducting studies. These studies can be classified as steady state, dynamic, UCED, or capacity studies with each type of study having differing requirements. Many UCED and capacity studies have shown that some of the impact of wind power integration can be reduced through

spatial diversification, and to assess the benefit of spatial diversification requires accurate models of wind power. State of the art methodologies rely on data from NWP models coupled with transfer functions to convert MOS to power time-series.

Chapter 3

WIND POWER IN NEW ZEALAND

3.1 NEW ZEALAND'S WIND RESOURCES

New Zealand lies in the familiarly named roaring forties. The term, while derived from nautical roots, is highly applicable to NZ's terrestrial wind resources. Dominated by the westerly flow and passage of cyclones across the Southern Ocean, NZ is very exposed to wind. Further, NZ is comprised of two islands that are long north to south with high mountain ranges extending along their lengths. Air masses are blocked from progressing through the centres of both islands by the mountain chains (the Southern Alps, and the Volcanic Plateau). The air masses seek, like water in a river, to flow around the ends of the mountain chains and through major passes. Hence the principal wind resources are located at the southern end of the South Island, the northern end of the South Island and southern end of the North Island adjacent to Cook Strait, in the Manawatu (specifically the saddle between the Tararua Mountains and the Ruahine Ranges which is the southern limit of the ranges to the east of the Volcanic Plateau), and along the isthmus projecting north east from the Volcanic plateau to Cape Reinga. Although these are the principal areas, there are few regions in NZ without an exposed hill on which the wind resource will be sufficient for power production.

NZ does not have a particularly large land area and is not sufficient in size to dominate weather patterns in the manner that continents do. This lack of continental area results in few areas with significant sea breezes. Sea breezes do occur in areas such as the edges of the Canterbury Plains, often noticeable in Christchurch, however unlike in places such as Australia these winds do not comprise an economic resource.

The complex geography and abundance of hills in NZ ensures that WPPs are constructed on top of hills where wind resources are greater. No WPPs have been constructed offshore and it is unlikely that any will in the near future. Because sea breeze winds do not comprise an economic resource it is likely that WPPs in NZ will not be greatly influenced by diurnal patterns of wind forcing, and atmospheric stability, and rather more influenced by the terrain and progression of cyclonic systems.

A well known wind in NZ is the Nor'wester. The westerly flow drives moist air over the Southern Alps and Volcanic plateau, as the air rises it loses capacity to hold moisture and precipitation occurs on the western side of the mountains. As the air passes over the mountains it loses altitude and accelerates producing a hot dry wind (or a Foehn wind). This hot dry wind in the lee of the mountains can often be very energetic. The Nor'wester is characterised by very high extreme gust velocities making many locations exposed to this resource unsuitable for wind turbines, such as inland Canterbury.

Although NZers were aware from an early date that its wind resources were excellent, it wasn't until the 1970's, inspired by oil price shocks that spurred wind energy development in Europe, that an extensive survey of NZ's wind resources was undertaken. Using wind speed measure-

ments made by the Meteorological Service, Cherry identified regions where wind resources may be suitable for WPP development [55]. The resource evaluation of Cherry was reaffirmed by Edwards in 1990 who also made a case for the economics of wind energy development in NZ[56] . The resource monitoring programs were not only conducted for wind energy development but also supported calculations for determining maximum wind loadings on structures [57].

Further research of note undertaken in NZ was by Edwards and Dawber[58]. Their investigations examined the wind resource in Central Otago (at sites close to the site of the withdrawn Project Hayes WPP). Analyses included deriving the altitude dependence of the wind resource, the shape of the wind speed frequency distribution, the temporal dependence of turbulence, wind shear, turbulence intensity, and some approximations toward calculating the power density of the site.

Since the 1990's resource evaluation has been undertaken by most of the generators, a large percentage of the lines companies, and some independent wind development enterprises. A network of wind monitoring masts was spurred in the 1990's as a wind rush took hold of NZ and companies prospected vigorously. Most of the data is held privately and data provided for academic research is often normalised to protect commercial interests. However, NIWA has been able to published maps of the mean wind resources using a conglomeration of methods and data [59] which clearly show the regions surrounding Cook and Foveaux Straits as having particularly good resources. The mean wind speed alone is not on its own indicative of where WPPs should be constructed and NIWA [59] also provide a map of realisable wind power density for both onshore and offshore resources.

3.2 DEVELOPMENT OF WIND POWER IN NEW ZEALAND

A pedant may point out that wind power was used to provide the motive power for the first people of both Pacific and European descents to arrive in NZ. And, that wind power has been used for providing mechanical power in NZ since 1927, due to the efforts of Ernest Hayes [60]. However, NZ has been relatively slow to embrace wind power for generating electricity.

The Brooklyn wind turbine, in Wellington, was installed by the Electricity Corporation of New Zealand (ECNZ) in 1993 to assess the feasibility of using wind power for electricity generation. The Vestas V27 machine was part of the Wellington skyline but reached the end of its economic life and was replaced with an Enercon E-44 wind turbine, due to popular demand, in April 2016. The Brooklyn turbine has helped cement Wellington's reputation as the windy city. Even though the Brooklyn turbine achieved a capacity factor of 50% [61], it was not until 1996 that seven Enercon E-40 turbines (total 3.85 MW) were installed at the Hau Nui Wind Farm in the Wairarapa. However, wind power capacity began to increase to significant levels with the installation of Stage 1 of the Tararua Wind Farm in 1999. Stage 1 consisted of 48 Vestas V47 turbines with a total capacity of 31.7 MW, and was quickly added to with stage 2 comprising a further 55 Vestas 47 machines. The fleet of power plants in the Manawatu has increased further with the installation of Te Apiti, Te Rere Hau, and the 3rd stage of the Tararua Wind Farm bringing the installed capacity to nearly 300 MW or 30% of NZ's total presently installed capacity.

The exceptional nature of the wind resource next to Cook Strait was demonstrated in the construction of NZ's largest WPP, West Wind, adjacent to Wellington. The wind turbines were shipped to Picton, placed on barges and ferried across to a purpose built wharf in Oteranga Bay, unloaded and carted on specially built roads to be placed high on exposed ridges. With the Mill Creek Wind Farm constructed on hills directly to the north of West Wind the total capacity in the Wellington region has grown to over 200 MW. Nearly 75% of NZ's wind capacity is located within an ellipse with a major axis less than 160 kilometers in the lower North Island.

Figure 3.1 WPPs in the Manawatu. Looking south across Te Apiti, to Tararua 1,2, & 3, & Te Rere Hau beyond.

NZ's WPPs are dominated by wind turbines produced by European manufacturers Vestas and Siemens, which have deployed "state of the art" technologies with respect to power conditioning. This is exemplified by Te Uku being the first WPP with a governor allowing frequency control [62]. However, a wide spread of wind turbine technologies has been installed in NZ with second hand turbines being imported and reconditioned for use at Horseshoe Bend, Weld Cone, and Lulworth hence some localised power quality issues may be apparent. Grid connected wind turbines range in capacity from the 100 kW Tellus wind turbine at Southbridge to the 3 MW Vestas V90 machines installed at Mahinerangi.

Of note in NZ's wind energy history is the Windflow 500 turbine. This turbine was manufactured in Christchurch, using a two bladed teeter rotor design coupled to a hydraulic torque limiting gear box. A prototype turbine was installed at Gebbies Pass in 2003 and a further 97 of these innovative machines were installed at Te Rere Hau from 2006 through 2011 providing 49 MW of capacity into the grid.

The development of NZ's wind resources has been gradual as demonstrated in Figure 3.2. Presently there is some 690 MW of installed capacity, representing approximately 7% of generation capacity and contributing approximately 5% of electricity generated in 2014 [63]. The top left pane of Figure 3.2 presents the number of WPP projects presently either notified (green), consented (blue), operational (red), or withdrawn (black). Notified projects are dated from the earliest press or company release that has been found via searches of the internet, likewise for consents being granted, and projects being withdrawn. Project operational dates are based on the date press releases or other sources have stated projects have been fully commissioned.

The top right pane presents the capacity of the projects. While there are a large number of small projects that have been consented these will not add much capacity to the power system. While there have only been a couple of large projects withdrawn (Project Hayes and Hauauru ma raki) these represent the removal of a large fraction of the potential capacity. The lower left pane presents the number of projects at the various stages of development from 1994 through 2016, and the lower right pane presents the capacity of wind power projects at various stages of development. There is a large capacity of notified and consented projects despite withdrawals. There was large increase in the number of projects from 2002 through 2012 and subsequently a lack of growth.

A list of operational wind power plants is presented in Table 3.1, and a list of proposed wind power plants in Table 3.2. Each of the proposed WPPs has an associated reference and these are detailed in Table 3.3. The spread of proposed wind power projects (notified, consented,

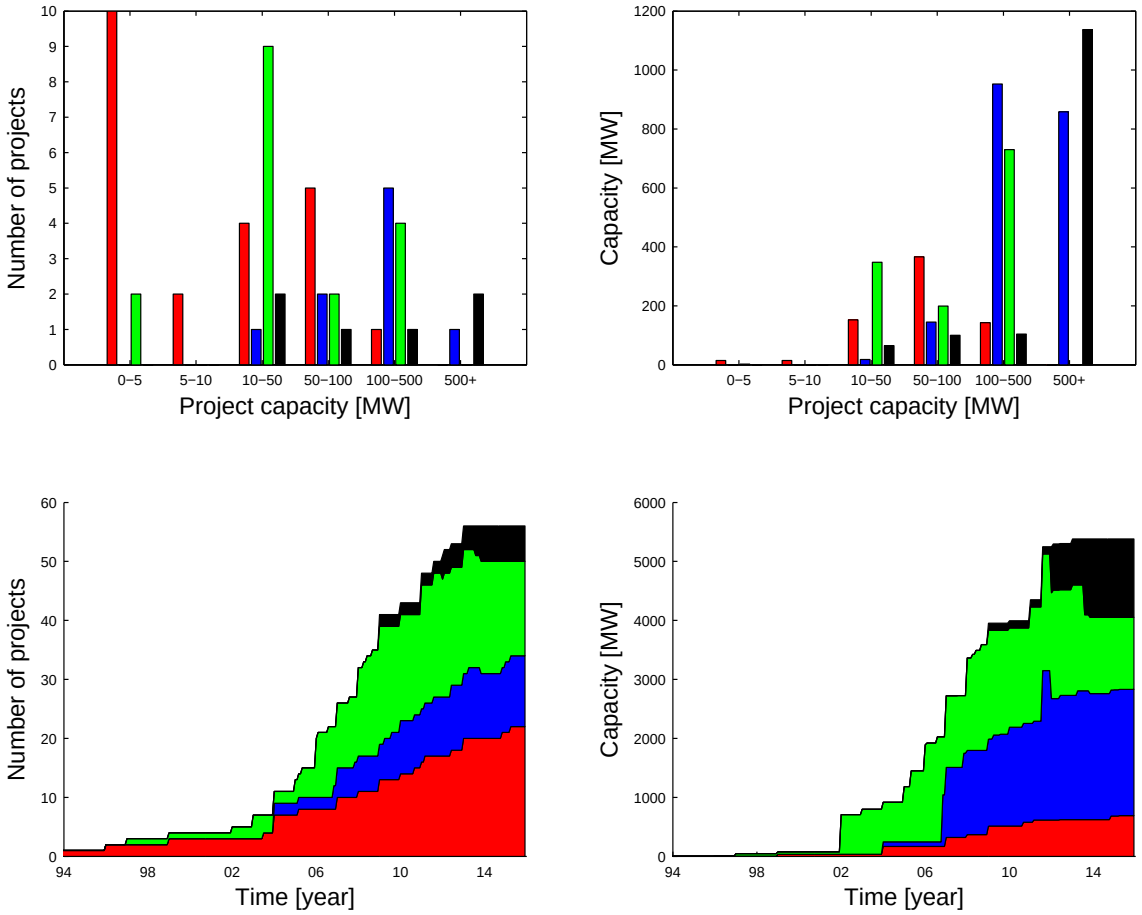

Figure 3.2 New Zealand WPP development: operational (red), consented (blue), notified (green), withdrawn (black).

withdrawn) is presented in Figure 3.3 as purple dots, and the spread of operational wind power plants as blue dots.

Wind farm	Operator	Region	No. turbines	Capacity [MW]	Year comm.
Brooklyn	Meridian	Wellington	1	0.23	1993
Gebbies Pass	Windflow	Canterbury	1	0.5	2003
Hau Nui (Stage 1)	Genesis	Wairarapa	7	3.9	1996
Hau Nui (Stage 2)	Genesis	Wairarapa	8	4.8	2004
Southbridge	Energy3	Canterbury	1	0.1	2005
Tararua (Stage 1)	TrustPower	Manawatu	48	31.7	1999
Tararua (Stage 2)	TrustPower	Manawatu	55	36.3	2004
Tararua (Stage 3)	TrustPower	Manawatu	31	93	2007
Te Apiti	Meridian	Manawatu	55	90.8	2004
Te Rere Hau	NZ Windfarms	Manawatu	97	48.5	2006-2011
White Hill	Meridian	Southland	29	58	2007
West Wind	Meridian	Wellington	62	142.6	2009
Horseshoe Bend	Pioneer Generation	Central Otago	3	2.25	2009
Weld Cone	Energy3	Marlborough	3	0.75	2010
Chatham Islands	CBD Energy	Chatham Islands	2	0.46	2010
Lulworth	Energy3	Marlborough	4	1	2011
Te Uku	Meridian	Waikato	28	64.4	2011
Mahinerangi	TrustPower	Clutha	12	36	2011
Mt Stuart	Pioneer Generation	Clutha	9	7.65	2011
Mill Creek	Meridian	Wellington	26	59.8	2014
Lake Grassmere	Energy3	Marlborough	1	0.66	2014
Flat Hill	Southern Generation Limited Partnership	Southland	8	6.8	2015
Total			491	690.2	

Table 3.1: Operational WPPs in New Zealand

Name	Owner	Cap. [MW]	Region	Status	As of	Ref.
Awakino	Ventus Energy	32	Taranaki	Investigation	Jul-14	3
Awhitu	TrustPower	18	Franklin	Consented	Apr-04	2
Baylys Beach	Northpower	N/A		Investigation		4
Belmont	Welington Regional Council	100	Wellington	Withdrawn	Sep-08	5
Blueskin Bay	Community project	2.55	Otago	Investigation	Jul-14	7
Cape Campbell	Mighty River Power	150	Marlborough	Investigation	Jan-11	8
Castle Hill	Genesis Energy	858	Wairarapa	Consented	Jul-14	9

Central Wind	Meridian Energy	119.6	Rangiteki	Consented	Jul-14	10
Doctors Hill	Mainpower	N/A	North Canterbury	Investigation	Jul-14	11
Flat Hill	Energy3	6.8	Southland	Consented	Oct-11	12
Glinks Gully	Northpower	30	Northland	Investigation	Jul-14	13
Gumfields	Meridian Energy	99	Northland	Investigation	Jul-14	2
Hauauru ma raki	Contact Energy	504	Waikato	Withdrawn	Sep-08	14
Hawkes Bay	Meridian Energy	270	Hastings	Consented	Jul-14	15
Hodson Hill	Aurora Energy	N/A	Otago	Withdrawn	Dec-97	16
Hurunui	Meridian Energy	75.9	Hurunui	Consented	Jul-14	17
Jericho Station	Pioneer Generation Limited	N/A	Southland	Investigation	Jul-14	18
Kaiwera Downs	TrustPower	240	Gore	Consented	Nov-07	19
Long Gully	Windflow	12.5	Wellington	Consented	May-09	2
Somes Island	Department of Conservation	0.01	Wellington	Investigation	May-12	6
Mahinerangi	Trustpower	164	Otago	Consented	Jul-14	20
Maungatua	Windpower Maungatua	20	Otago	Abandonded	Jul-14	1
Motorimu	Mighty River Power	104.06	Manuwatu	Withdrawn	Jul-14	21
Mt Cass	MainPower	69	Hurunui	Consented	Jul-14	22
Mt Munro	Meridian Energy	46	Wairarapa	Investigation	Jan-12	23
Mt Stalker	Waitaki Wind	N/A	Otago	Investigation	Jul-14	1
Omamari	Meridian Energy	100	Northland	Investigation	Dec-06	24
Pouto Forest	Meridian Energy	300	Northland	Investigation	Jul-14	1
Project Hayes	Meridian Energy	633	Otago	Withdrawn	Jul-14	25
Puketiro	RES	130	Wellington	Investigation	Jul-14	26
Puketoi	Mighty River Power	159	Wairarapa	Consented	Jun-13	27
Rock and Pillar	NZ wind farms	25	Otago	Withdrawn	Jul-14	28
Roundtop	Uncertain	40	Canterbury	Investigation	Oct-10	29
Slopedown	Genesis Energy	150	Southland	Investigation	Jul-14	1,30
Taharoa	Taharoa C and PowerCoast	100	Kawhia	Consented	Dec-05	3
Taumatatotara	Ventus	27	Waikato	Consented		2
Te Anga	Ventus Energy	25	Waikato	Investigation	Feb-06	3
Te Waka	Unison	111	Hawkes Bay	Withdrawn	Jul-14	1
Tiwai	Meridian Energy	79	Southland	Investigation	Jul-14	31

Turitea	Mighty River Power	180	Manawatu	Consented	Jul-14	1
Waitahora	Contact Energy	156	Southern Hawkes Bay	Consented	Jul-14	32
Waverly	TrustPower	130	Taranaki	Investigation	Jul-14	1
Windy Peak	Meridian Energy	60	Wairarapa	Investigation	Jul-14	2
Total		5326.42				

Table 3.2: Proposed WPPs in New Zealand

Reference	Title	Author	URL	Accessed
1	Proposed Wind Farms	New Zealand Wind Energy Association	http://windenergy.org.nz/nz-wind-farms/proposed-wind-farms	17-07-14
2	Proposed wind farms	New Zealand Wind Energy Association	http://archive.today/EZ4F#selection-2957.0-2184.4	17-07-14
3	Three wind farms planned for Waikato	New Zealand Herald	http://www.nzherald.co.nz/nz/news/article.cfm?c_id=1&objectid=10366533	02-02-06
4	Infrastructure	Northland Inc.	www.northlandinc.co.nz/about-your-place/infrastructure	17-07-14
5	Council calls halt to Belmont wind farm	stuff.co.nz	http://www.stuff.co.nz/national/650812/Council-calls-halt-to-Belmont-wind-farm	30-09-08
6	Somes Is to get three-storey wind turbine	stuff.co.nz	http://www.stuff.co.nz/dominion-post/news/local-papers/hutt-news/6877321/Somes-Is-to-get-three-storey-wind-turbine	08-05-12
7	Blueski energy project	Blueskin Power	http://www.blueskinpower.co.nz/info.php?page=11	17-07-14
8	Major wind farm planned	PENNY WARDLE	http://www.stuff.co.nz/marlborough-express/news/4548295/Major-wind-farm-planned	17-01-11
9	Castle Hill Wind Farm	Genesis Energy	https://www.genesisenergy.co.nz/generation/our-projects/castle-hill	17-07-14
10	Central wind project	Meridian	http://www.meridianenergy.co.nz/about-us/generating-energy/our-generation-projects/central-wind-project/	17-07-14

11	Statement of Corporate Intent 2012-2013	Mainpower	http://www.mainpower.co.nz/index.cfm/3,433,595/sci1213.pdf	17-07-14
12	Flat Hill wind farm medie release	Pioneer Generation Limited	http://www.pioneergen.co.nz/about-us/new-current-projects/new-standard-page/	17-07-14
13	Energy Resources - Sustainable futures 30/50	Annejo Liang	http://www.wdc.govt.nz/PlansPoliciesandBylaws/Plans/SustainableFutures/Documents/Sustainable%20Economy/30-50-Energy-Report.pdf	01-03-10
14	Hauauru Ma Raki	New Zealand Wind Energy Association	http://www.windenergy.org.nz/haururu-ma-raki	17-07-14
15	Titiokura and Hawkes Bay	New Zealand Wind Energy Association	http://www.windenergy.org.nz/tikiokura-and-hawkes-bay	17-07-14
16	1997 NEWS ARCHIVE	DUNEDIN ELECTRICITY	http://www.auroraenergy.co.nz/pdf/news/1997NewsArchive.pdf	17-07-14
17	Hurunui wind project	Meridian Energy	http://www.meridianenergy.co.nz/about-us/generating-energy/our-generation-projects/hurunui-wind-project/	17-07-14
18	Energy3 Capabilities	Energy3	http://energy3.co.nz/services/capability/	17-07-14
19	Kaiwera Wind Farm	Trustpower	https://www.trustpower.co.nz/our-assets-and-capability/power-generation/kaiwera-downs	17-07-14
20	Mahinerangi Wind Farm	Trustpower	https://www.trustpower.co.nz/our-assets-and-capability/power-generation/mahinerangi	17-07-14
21	Motorimu wind farm seen as key	stuff.co.nz	http://www.stuff.co.nz/manawatu-standard/news/2570790/Motorimu-wind-farm-seen-as-key	07-07-09
22	Mt Cass Wind Farm - MainPower's Proposal	Mainpower	http://www.mainpower.co.nz/index.cfm/1,508,html/Mt-Cass-Wind-Farm-MainPower-s-Proposal	17-07-14

23	Mt Munro wind project	Meridian Energy	http://www.meridianenergy.co.nz/about-us/generating-energy/our-generation-projects/mt-munro-wind-project/	17-07-14
24	SOEs exploring wind development together	Landcorp	http://www.scoop.co.nz/stories/BU0612/S00245.htm	17-07-14
25	Project Hayes a lesson for wind-farm industry	SAM SACHDEVA	http://www.stuff.co.nz/business/6286915/Project-Hayes-a-lesson-for-wind-farm-industr	20-01-12
26	PUKETIRO WIND FARM	Renewable Energy Systems Ltd	http://www.res-australia.com/wind-farms/puketiro-wind-farm/introduction	17-07-14
27	Puketoi wind farm gets final go-ahead	JANINE RANKIN	http://www.stuff.co.nz/manawatu-standard/news/8758084/Puketoi-wind-farm-gets-final-go-ahead	05-06-13
28	Impacts of wind farms on birds: a review	Ralph G. Powlesland	http://www.doc.govt.nz/Documents/science-and-technical/sfc289entire.pdf	17-07-14
29	Reviewing Smart Grid Opportunities Around The World	Dinesh Chand	http://neptune.solnetsolutions.co.nz/emanz-test/images/stories/Presentations/AdvancedMetering/advmet20oct10_chand.pdf	17-07-14
30	FACTS & FIGURES: SLOPE-DOWN WIND FARM	Wind Prospect	http://www.windprospect.com/docs/news_pdf_41.pdf	17-07-14
31	Neighbouring wind farm could feed Tiwai smelter	stuff.co.nz	http://www.stuff.co.nz/southland-times/news/230101/Neighbouring-wind-farm-could-feed-Tiwai-smel	22-01-08
32	Waitahora wind farm	Contact	http://www.contactenergy.co.nz/web/ourprojects/waitohorawindfarm	17-07-14

Table 3.3: References for proposed WPPs

It should be noted that a project may not progress from notification, to obtaining consent, and finally being constructed in an orderly fashion. For instance projects may be only notified when consent is lodged, or projects that are consented may be withdrawn. Further, the design of the consented / constructed wind project may differ significantly from that notified; indeed it is probable that many notified / consented projects may never be constructed due to difficulties

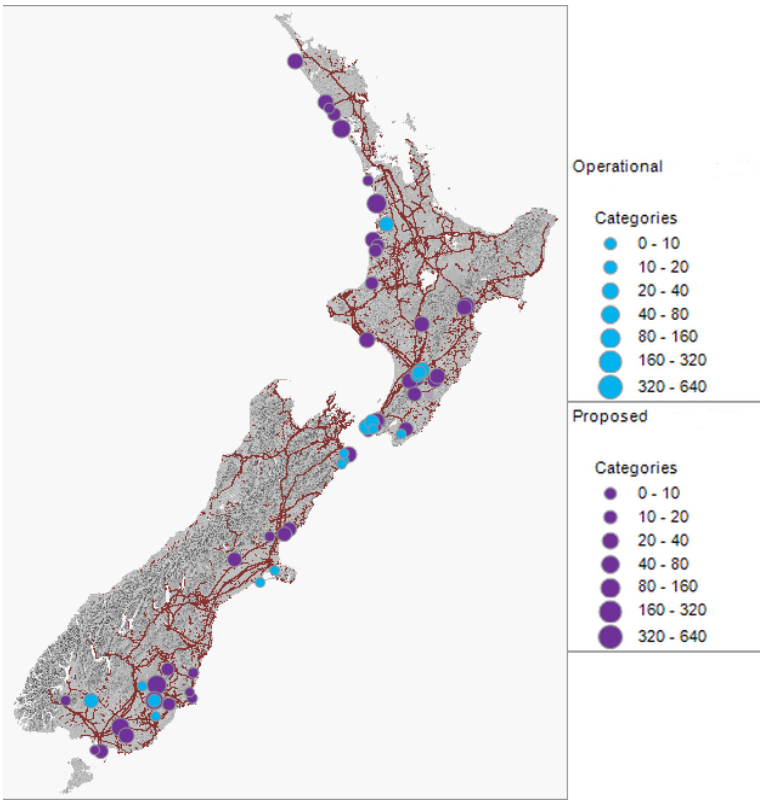

Figure 3.3 New Zealand WPP development: operational (blue), proposed (purple: notified, consented, and withdrawn).

in development not foreseen at the time of seeking consent.

The exceptional nature of NZ's wind resource is revealed if the capacity factors for WPPs are examined. The capacity factor is a commonly applied metric for measuring WPP efficiency; being the ratio of actual annual electricity production to possible annual production if the wind turbines were to operate at full capacity for the entire year. The capacity factor is presented in Equation 3.1, where E is the annual energy output from a WPP measured in units of MWh/annum, C is the rated capacity of the WPP measured in units of MW, and h is the number of hours per year. While the capacity factor reflects availability, electrical and other losses it is most closely related to the mean wind speed. The capacity factor for WPPs in NZ may be anywhere from 33 % [64] to 50 % [61], and is commonly above 40 % [65], compared with capacity factors for WPPs in Europe averaging 21 % [66].

$$Cf = \frac{E}{H_{annum} \cdot Cp} \tag{3.1}$$

Where Cf is the capacity factor, E is the energy production, H_{annum} is the number of hours per year, and Cp is the WPP capacity.

3.3 WIND INTEGRATION IN NEW ZEALAND

While WPP development was initiated prior to deregulation by the government controlled generator ECNZ, the majority of wind development has occurred in a competitive electricity market. Thus WPP development has not resulted from a centralised planning environment. This has led to a fleet of WPPs that is reflective of a diversified planning approach and diversity in WPP siting has resulted.

All but a few WPPs in NZ are embedded (Tararua Stage 3 being one exception) . That is the WPP points of connection are within distribution networks and not directly connected to the transmission network. However, this embedding is largely immaterial to power system operation as the system operator simply sees WPPs as connected at GXPs.

As WPPs lack storage and must use their fuel (wind), they are typically offered into the electricity market at zero price, they may offer at a marginal cost to reflect operational costs however the cost of fuel (wind) is zero. This does not mean that the WPPs will necessarily be dispatched. At times of high grid congestion, low demand, or when security of supply is threatened the system operator may not dispatch wind generation.

The particularly good wind resources, economic electrical connection, and suitable terrain for WPP construction ensured that by 2004 there was 150 MW of WPPs operational in the Manawatu. The variability of the recently connected WPPs caused the system operator, Transpower, to develop concerns regarding the effect on the power system. A detailed study was published in September 2005 illustrating several large ramp events and their impact on system frequency [27]. During two events, 15 November 2005 and 25 March 2005, the sudden change in wind generation output resulted in the frequency keepers going outside their dispatched MW frequency keeping band [27]. Further, the additional generation in the Manawatu, between the northern terminus of the HVdc link (Haywards) and Bunnythorpe (a major substation just north of Palmerston North), was identified as a risk for potentially exceeding line capacities. Note that the loading on lines between Bunnythorpe and Haywards are also affected by a significant quantity of wind generation capacity added in the Wellington region (which is reasonably well correlated with wind generation in the Manawatu [67]).

A further concern for the system operator was the impact of wind generation on the electricity market due to the potential inability to gain forecast accuracy comparable with pre-existing variable generation and load. Transpower also had concerns about the behaviour of wind offered into the electricity market, as it was offered at zero cost reflecting a “must-run” status, different to most pre-existing generation.

Transpower suggested the following methods for mitigating the impact of increased wind power:

- introducing ramp rate control,
- more frequent re-dispatch of frequency keeping reserves,
- changes to frequency keeping management,
- revision of transmission constraints,
- changes to the ”must-run” dispatch behaviour.

Transpower also highlighted the potential for greater impacts on the network, as it identified the potential for the total wind capacity in the North Island to increase to 1300 MW by 2010 (in actuality the total generation in the North Island increased to 451 MW). The concerns of the system operator were exacerbated by proposals for very large WPPs (Project Hayes, Mahinerangi, Kaiwera Downs, and Turitea) in what was described as a wind rush [68]. A large increase in the quantity of wind generation could have had a severe impact on the power system and the system operator responded by progressing the Wind Generation Investigation Project (WGIP) and the Transmission to Enable Renewables project (TER) [29].

3.3.1 Wind Generation Investigation Project

To begin the WGIP project an investigation into the correlation of wind resources and wind power was undertaken by Garrad Hassan (GH) [67]. This study showed that the correlation is

dependent on averaging period, the theoretical correlation of power output is generally lower than the correlation obtained using equivalent wind speed measurements, the correlation in theoretical ramp rates is low even for WPPs in close proximity, and that correlations between WPP sites outside of the Northland-Auckland-Waikato region is small. The study also predicted the generation and ramp rates for a wind power scenario comprising 1100 MW of generation made up of 100 MW WPPs.

To enable the GH study a dataset comprising measurements from 21 meteorological masts was collated. The measurements included wind speed and wind direction from the top level on masts ranging in height from 10 meters to 80 meters monitored using a 10 minute averaging period. The masts were located across NZ and a replica of this data set has been collated for use in analyses in this thesis, see Section . To transform the wind speed time series to power a WPP power curve was formed assuming a representative wind turbine power curve, a normal distribution of topographical speed ups (mean = 0, standard deviation = 5%), and normally distributed wake losses (mean = 5%, standard deviation 2%). Further discussion on the transformation of wind speed to power is presented in Section 7.

The GH study was extended upon, using the same data-set and similar methods, to determine the generation and power volatility for a set of four scenarios; the result of extensive stakeholder consultation also completed by GH [1]. The first scenario represented possible future WPP development achieving a medium capacity centralised portfolio, the second a medium capacity diversified portfolio, the third a high capacity portfolio, and lastly a low capacity portfolio.

The method applied in the GH study [67] included using wind speed data to predict wind power time-series representative of each WPP by transformation through a WPP power curve. However, it was recognised that this approach did not account for rapid changes in the WPP generation due to operational dynamics (turbine shut-downs due to high wind speeds, curtailment, maintenance, and faults). Hence, an empirical correction was found based on the difference between the measured power and predicted power for the Te Apiti Wind Farm. This empirical correction was extended to allow the prediction of ramp rates for periods of 10 s, 1 min, 5 min, and 10 min. The predicted ramp rates resulting from each of the wind scenarios was compared with those placed by demand.

The second GH study [1] predicted forecast errors for the four scenarios. The methods used were based on forecast data from the Te Apiti Wind Farm. Forecast errors for horizons of 2 hour, 3 hour, 6 hour, 12 hour, and 24 hour were predicted (reflecting the changing accuracy of forecasts with changes in forecast horizon). The errors in generation forecasts were compared with demand forecast errors.

Conclusions from the second GH study were that diversification of WPPs resulted in decreasing ramp rates by a factor of 2, that at a 5 minute temporal resolution the volatility due to load is greater than that predicted for any wind generation scenario, and that wind forecast errors will be significant with respect to combined wind and load forecast errors. The study recognised the limitations of the methods and resolved the need for better methods.

The simulation of wind generation time-series completed by Garrad Hassan was used in the WGIP to support the following investigations:

1. *Effect of unpredictability of wind generation output on pre-dispatch processes* [69],[70]. The review of processes and tools applied by the system operator identified that wind generation forecast errors would affect:

    - The security assessment used to determine whether any asset will be overloaded or grid voltages will be forced outside the target range following a contingency event.
    - The stand by reserves check which determines whether sufficient generation has been offered but not dispatched to ensure Sustained Instantaneous Reserves to be restored

within 30 minute following the loss of the largest generating unit.

- The Scheduling Pricing and Dispatch model (SPD) which is used to determine the most efficient dispatch of generation.
- The Reserves Management Tool (RMT) which determines the quantity of fast and instantaneous reserves required to meet power quality targets given the loss of the largest generating unit or the HVdc.

This investigation concluded that at the rate wind generation was forecast to expand in the North Island the error in wind power forecasts would be the main source of error in dispatch processes within 2-3 years of the report being issued. This would in turn affect the system operator's ability to identify and respond to security issues. The investigation recommended that the accuracy of wind generation forecasts be given priority, forecasts should be incorporated into security processes, and further investigation to determine the magnitude of forecast errors be undertaken.

This investigation also identified that large errors in wind generation forecasts typically arise from two sources:

- Errors in the timing of large changes in wind speed (that is if a change in wind speed is forecast due to the arrival of a weather system and the time the arrival is miscalculated then large errors in predicted wind generation will result).
- Errors in the magnitude of wind speeds arising from the failure to accurately predict weather systems.

2. *Effect of variability of wind generation output on dispatch of generation* [71]. This investigation found that:

   - Even for the high capacity scenario wind power will only have limited effect on the processes used by the system operator for generation dispatch, and that if processes and tools remain as the status quo then there may be a need for additional frequency keeping services to be procured (although these would not be great even for the high capacity scenario).
   - The variability of wind generation would lead to the need for re-dispatch of generation during trading periods, however this re-dispatch would not be outside the capability of the dispatch processes used at the time.
   - Dispatch considerations should be given medium priority for further investigations.

3. *Effect of variability of wind generation output on asset loading* [72]. This investigation focused on identifying parts of the transmission network that may be vulnerable to overloading as a result of the increase in wind generation. Circuits identified as being potentially affected included:

   - Invercargill - Roxburgh 220 kV,
   - Roxburgh - Clyde 220 kV,
   - Livingstone - Waitaki,
   - Naseby - Roxburgh,
   - Bunnythorpe - Haywards 220 kV,
   - Bunnythorpe - Tokaanu 220 kV,
   - Tokaanu - Whakamaru 220 kV,
   - Wairakei - Redclyffe 220 kV.

The investigation concluded that the wind generation variability for the high capacity scenario would not materially affect the loading on circuits in the core transmission network. However, it was acknowledged that the limitations of the models applied meant that the accuracy of the results and hence conclusions could not be guaranteed. Hence, the probability of large but infrequent changes in wind generation output could not be substantiated. It was recommended that appropriate wind generation data be collated and effects reviewed.

4. *Effect of wind generation capability on steady state voltage management* [73]. This investigation focused on determining what effect wind generation may have on the voltages in parts of the transmission system that had pre-existing issues with voltage stability. Analysis was performed to determine the exacerbating effect that wind generation may cause in the North Isthmus, Auckland/Waikato, Hawkes Bay, Nelson/Marlborough, and Southland/Otago regions. The investigation sought to test the worst possible outcome, and assumed:

   - That the wind generation technology had minimum capabilities (no ability for voltage support),
   - That wind generation capacity reflects the high capacity scenario,
   - That wind generation would displace other generation that would otherwise provide voltage support,
   - That wind generation has limited capacity to provide reactive power.

   The investigation concluded that some parts of the system may experience steady state voltage management issues but these are likely to be minor in extent, and that management of steady state voltages is unlikely to impede integration of large scale wind generation, although there may be steady state voltage management issues local to WPP connections.

5. *Effect of wind generation capability on management of frequency excursions* [74]. This investigation sought to determine the effect of wind generation on the ability of the system to maintain frequency within power quality targets given the increase in wind generation under the high capacity scenario. The investigation assumed wind generation to have minimum capability, i.e. no capability for frequency keeping, low-voltage ride through, or low-frequency ride through. The investigation found that:

   - there was a risk to system frequency management due to the disconnection of WPP as the result of low voltages caused by faults on the system and it was important to ensure wind generation connected to the system should have low-voltage ride through capability,
   - that the lack of low-frequency ride through capability from wind generation would require additional instantaneous reserves to be procured.
   - while wind generation provides some inertia to the system, the benefits of this are outweighed by the loss of conventional generation that is capable of providing frequency support when wind generation output is more than 40-50% of connected wind generation capacity. To alleviate the loss of frequency support from the displaced conventional generation additional instantaneous reserves would need to be procured.
   - that sudden large increases in wind generation will not result in frequency quality targets being exceeded.

   This investigation recommended that low voltage and low frequency ride through capability of WPPs is investigated, and the cost allocation for Instantaneous Reserves be considered.

6. *Effect of wind generation capability on voltage stability* [75]. This investigation sought to determine the effect on voltage stability given increased wind generation with minimum capability displacing conventional generation. In particular the investigation was concerned with changes in load or voltage at a bus. The investigation applied results from the high capacity scenario and concluded that voltage stability would only be of concern in the North Isthmus, Auckland, and Hawkes Bay regions. The investigation found that increased wind generation would not be problematic for voltage stability and that additional distributed wind generation provided benefits through lowering power transfer and hence reducing reactive power requirements, and reducing voltage drop.

7. *Effect of wind generation capability on power system transient stability* [76]. To assess the effects of wind generation on transient stability, oscillatory stability, and dynamic voltage stability the WGIP used DigSILENT to analyse system dynamics [77]. The focus of this investigation was to determine the ability of the system to maintain frequency following large disturbances and thus avoid cascade failures. It concluded that additional wind generation as proposed in the high capacity scenario would not materially affect transient stability.

8. *Effect of wind generation capability on oscillatory stability* [78]. This investigation sought to determine the effect of wind power on oscillations in the power system caused by the interaction of generators. It was acknowledged that wind generation would not lead to an increase in oscillations as most wind turbines have power electronics and WPPs are often connected using STATCOMS. However, the addition of wind generation would displace conventional generation that may have system damping capability. The investigation identified one case where oscillatory behaviour in the system may lead to excursions outside acceptable levels as a result of increased wind capacity. A large increase in wind generation south of Bunnythorpe could lead to degradation in the damping in the Taranaki region (when generation is high) and if accompanied by a fault on the Stratford - Taumaranui 220 kV transmission circuit the minimum acceptable limit may be approached. The investigation concluded that increased wind capacity would not significantly affect the oscillatory stability of the power system in NZ.

9. *Effect of wind generation capability on dynamic voltage stability* [79]. The final investigation in the WGIP focused on assessing changes in system short-circuit levels as a result of displacing synchronous generating units with wind generation. The investigation found that the technology used in wind turbines has a marked effect on the risk of voltage stability. The use of turbines with Fixed Speed Induction Generators (FSIG) could cause voltage collapse subsequent to a severe power system fault, however this could be mitigated by installing dynamic reactive support (STATCOM) or limiting generation from FSIGs. It was recommended that low-voltage ride through capability for WPPs and protection system performance be reviewed.

The WGIP concluded that increased wind generation could affect the electricity system by making energy balancing more difficult, increasing variability, increasing forecast error magnitudes, and causing some local network loading issues. Technological issues were also highlighted, particularly the need for low voltage/frequency ride through capability. The WGIP demonstrated the potential benefit for the power system through the spatial diversification of wind energy and highlighted the need for a greater temporal span of simulated power data and better models of wind generation.

3.3.2 Further integration studies

The potential impact from a very large increase in wind power capacity on the NZ power system, around the year 2005, was not a concern for the system operator alone. Many companies and government departments commissioned studies to investigate wind integration and the topic has been the focus of much academic attention. The academic interest in wind integration was sufficient to warrant the Australian and New Zealand Industrial and Applied Mathematics society (ANZIAM) posing the aggregation of power from multiple WPPs as its Mathematics and Statistics in Industry Study Group (MISG) problem in 2011. From this study group McDonald developed a regression method for predicting the probability distribution of power from a WPP, some minutes into the future, given its present output, and the aggregation of the probability distributions assuming independent variations in power [80].

Transpower collaborated with Ibel Moll Rasmussen, for her masters thesis (2008), to determine the impacts on the power network of four scenarios of potential wind power development [81]. The four scenarios of wind power development out to the year 2025 were assessed:

1. Reference: 9% of system capacity (1329 MW)
2. Compact: 16% of system capacity (2484 MW located in Otago/Southland (1160 MW), Wellington (323 MW), Manuwatu (695 MW), and Hawkes Bay (147 MW)),
3. Disperse: 16% of system capacity (2484 MW spread throughout New Zealand with Otago/Southland receiving (408 MW), and Manuwatu (242 MW)),
4. 25% wind: 25% of system capacity (4064 MW).

Rasmussen used the energy market modeling Plexos software package (analogous to SPD) to analyse the effect of the wind generation on the power system in the years 2010, 2015, 2020, and 2025. Rasmussen's study comprises a capacity study and hence reserve calculations are based on the uncertainty of power production rather than cover for variability. WPP power time-series were produced from wind speed time-series measured at 29 sites throughout NZ. Most of the sites are part of the NIWA network and have a measurement height of 10 m. Each mast is assumed representative of a region, scaled using a linear regression and multiplied by a WPP power curve to obtain a wind power time-series with a target capacity factor. The WPP power curve was formed by convolving a Gaussian function with a representative wind turbine power curve (being an average of the Siemens 2.3-82, Siemens 2.3-92, and Vestas V90 power curves).

Rasmussen found little difference between the compact and diverse scenario in terms of average load weighted prices in the North Island, however she found a slight reduction in price for the compact scenario in the South Island from 2020 onward. Rasmussen also found the reserves requirements of the disperse scenario, in 2025, are on average 17% lower than for the compact scenario, and 56% lower for the maximum reserves requirements. Transmission losses are assessed with the disperse scenario having 26% lower transmission losses and 23% fewer hours of network congestion than the compact scenario by 2025.

Rasmussen followed the technical assessment with economic costings finding that the Tararua 1 and 2 projects would net 36% greater income in 2025 in the disperse scenario than for the compact scenario (with the compact scenario requiring 14% spill of wind whereas the disperse scenario requires no spillage). For WPPs connected at Roxburgh; the disperse scenario nets 53% greater income, in 2025, than WPPs in the compact scenario.

The economic analysis was then used to support a socio-economic benefit assessment that finds positive benefits for the compact and disperse wind scenarios, above the reference, with the disperse scenario netting 9.5% greater benefit that the compact scenario. The cost of a proposed subsidy scheme to ensure wind power development, with costs met by the government thus

ultimately tax payers, is assessed and it is found that the additional price paid by customers to cover the subsidy scheme is 140% higher for the compact scenario than for the disperse scenario.

To calculate the reserves requirements Rasmussen assumed highly accurate wind forecasting methods would be developed by 2025. To assess the potential costs if forecasting accuracy does not improve Rasmussen assessed costs assuming persistence forecasting. The reserves costs balloon from $33M to $285M for the compact scenario showing the importance of forecast accuracy on the operation of the power system. The effect is even more detrimental for the disperse scenario with costs ballooning from $23M to $356M.

Of particular concern for the NZ power system is the "dry year" risk and Rasmussen found that under any of the scenarios there is no un-served energy. However, electricity costs do increase in dry years due to increased commitment of thermal plant. This theme was further analysed by Bull in 2010 who posited that if wind and hydro resources were highly correlated then the risks associated with "dry years" would be exacerbated; the degree of correlation was found to be weak and Bull concluded that the contribution of wind to energy production should be lowered by 10% from its forecast total contribution [28].

Rasmussen's work clearly showed the benefit of spatial diversification to the power system, however her work is limited by the methods used to simulate wind power time-series. The time-series are based on measurements from meteorological masts that may not be representative of WPPs (see Section 5.5), the time-series have a short temporal span, and the transformation of wind speed time-series to power time-series has not been explicitly simulated (rather regional conglomerates have been used).

The Electric Power Optimisation Centre at the University of Auckland has conducted a lot of work studying the operation of the NZEM and the effect of wind integration on it. As wind power is inherently variable and unpredictable there are costs when integrating wind power into the electricity market. These costs can to some extent be alleviated through market design; the benefit of a Stochastic Market Clearing (SMC) tool was assessed by Khazaei who weighed the benefits from SMC against the additional costs imposed by applying the more complex market mechanism when applied to the NZEM[82]. The analysis showed that the SMC proceedure did not reduce costs under the present penetration of wind power, however for a penetration of 20% the SMC mechanism would save $1.2M per year.

The potential for using residential demand response for balancing fluctuation in wind power was assessed, using data from West Wind in Wellington by Alzaanin, of Victoria University, in 2014 [83]. A model for residential electricity demand was constructed which included the possible response from controlling domestic loads such as refrigerators. The demand model was combined with data from West Wind in a regional load flow model to assess the ability of demand response to mitigate variations in active power flow due to the variability of the wind power. The DigSILENT Power Factory software was used to assess the response of the power system and this study can be classed as a dynamic study.

Energy Link and MWH

The Ministry for Economic Development and Energy Efficiency and Conservation Authority commissioned a study by Energy Link and MWH NZ (EL & MWH) in 2005 [84]. This report provides an outline of the wind energy integration problem, detailing technology, power systems, and power system operation. The report highlights potential benefits of small WPPs and the potential for power system benefits from the spatial diversification of WPPs. Further, the report details NZ's dry year security risk and how wind energy could help to mitigate this.

To assess the potential impact of wind energy EL & MWH developed a *Low Demand Case Study* [84] to assess Unit Commitment and Economic Dispatch (UCED). This case study sought to derived the maximum penetration of wind energy that the power system could accommodate

assuming demand equal to the lowest half hourly period during 2004 plus 2% (to allow for projected growth in demand); giving a total demand of 1550 MW in the North Island and 1180 MW in the South Island. Assumptions for the case study included that wind speeds at all WPPs sufficient to allow 100% power output, and that the North and South Islands should be assessed independently (as the provision of security measures are separate in each island), that WPPs would consist of wind turbines capable of fault ride through and providing synthetic inertia, that wind power would displace other base load plant, and that wind power plants would be distributed throughout the country. Applying these assumptions, key factors of power system security were assessed to find the maximum wind penetration. The key factors included:

- the provision of regulation,
- assessment of reserve risk and provision of instantaneous reserves,
- the need for a marginal station to be a load follower,
- how the system responds during a fault.
- grid stability maintenance and voltage support,
- how the system operator could manage security of supply out to the end of the pre-dispatch time.

The study concluded that in the North Island 1300 MW of wind could be integrated during times of lowest demand and an additional 930 MW could be added in the South Island. Thus a total wind power capacity of 2230 MW (a penetration of 34%), given generation capacity forecasts for the year 2005, could be added to the system while maintaining security of supply.

EL & MWH noted that the high level of wind power able to be absorbed into the grid was dependent on the geographic spread of WPPs. At the time of writing the report 97% of wind capacity was installed in the Manawatu; the report assumed that this would reduce to 61% by the end of 2008. Further analysis showed that if all wind power capacity were confined to the Manawatu then the amount of wind power that could be accommodated in the power system would fall to 15%, less than half of that calculated using the assumed geographic dispersion. However, applying the assumption that the HVdc could transmit 600 MW of power from WPPs in the Manawatu to the South Island, then a wind penetration of 23% could be accommodated (as in this scenario no WPP would be present in the South Island). However, the study also noted that wind capacity in the Manawatu would be limited not only by security of supply constraints but also due to loading on lines in the local area, notably the Bunnythorpe-Tokomaaru (BPE-TKU) line.

EL & MWH recommended establishing a wind data-set for integration studies; the analyses in the low demand case study were “single point” analyses and not supported by wind power time-series but instead assessed the power system state for a single half-hour period. Thus the study was not able to address concerns relating to the variability or predictability of wind power. Recommendations include the establishment of connection standards (grid codes), improving wind forecasts, constructing smaller WPPs, further analysing dry year security risks, assessing whether reserves should cover large wind events such as storms, review of power quality standards, introduction of rules concerning block bidding of wind-hydro or wind-thermal generation tranches, and changes to bidding behaviour to ensure all available generation is bid into the market.

Meridian

The electricity generator Meridian Limited commissioned a wind integration study to *quantify the additional system requirements and associated costs under various future wind development scenarios in New Zealand*, initial findings were published in 2006 with a comprehensive report detailing scenarios published in 2008 [85]. The Meridian study can be classed as a capacity study.

The Meridian study developed reference scenarios of generation and demand growth to establish the expected state of the power system in the years 2010, 2020, and 2030. Levels of generation and demand in the 2007 year are used as a basis from which to develop the scenarios along with assumed demand growth of 120 MW/annum, with additional generation coming from geothermal, thermal, and wind generation (it is assumed that there will be no growth in hydro generation). Two sets of scenarios are developed: one assuming growth in wind generation, and one with no wind generation. The difference in the commitment of thermal stations between the sets of scenarios is assessed and thus the costs associated with wind power determined.

The total wind generation in the scenarios totals 634 MW in 2010, 2.066 GW in 2020, and 3.4 GW in 2030. The wind capacity is progressively distributed throughout the country as the scenarios develop, so that in 2010 the wind capacity is concentrated in 5 regions, in 2020: 9 regions are used, and by 2030 wind power plants are located in 15 regions.

In addition to the reference scenarios the Meridian study proposed a *Southland* scenario. The Southland scenario differed from the reference scenarios by an additional 250 MW of wind capacity installed in Otago in 2010. For 2020 the Southland scenario allocates more wind development in Otago (940 MW) and less in the North Island, so that the total installed capacity remains unchanged. For 2030 the Southland scenario favours more wind installed in Otago than the reference case, yet the total wind capacity is nearly equal to the reference scenario.

To support the analyses wind power time-series are developed for 15 sites located throughout NZ. These sites are either operational WPPs or sites that have been investigated for WPP development. Wind speed measurements, with a temporal resolution of 10 minutes, are converted to wind power using the "Windfarmer" software package. These time-series are then averaged to obtain half hourly time-series that are used in further analyses. It is not stated how Windfarmer has been applied; thus it is not known whether the study has assumed smoothing of power curves or time-series to account for spatial distribution of wind turbines. It is stated that representative wind turbines have been used and that topographic, array, turbine outages, hysteresis, and local losses have been accounted for. Thus it may be assumed that smoothing of the power curves due to spatial distribution has been accounted for but temporal smoothing has not been applied. Wind speed time-series for the 2005 and 2006 years have been used, with the 2006 year resulting in an annual energy production from wind power 10% greater than 2005, thus allowing some assessment of the impact of windiness on power system.

The Meridian study used a generation optimisation model based on linear programming to simulate the power system. The model used a half-hourly temporal resolution and did not explicitly model the transmission network. The model incorporated various components to account for plant availability, and system constraints. Demand profiles were derived from one year of historic data and modified to suit the scenarios.

The Meridian study uses the notion of a capacity credit to assess the benefit of wind generation. The capacity credit of wind is defined as the difference between the capacity of thermal stations in a hydro-thermal power system, minus the capacity of thermal stations in a wind-hydro-thermal system, divided by the capacity of wind in a wind-hydro-thermal system. The capacity credit gives a measure of the degree to which wind is able to displace generation from thermal stations.

A summary of the findings from the Meridian study follows:

- NZ can accommodate up to a 20% penetration of wind power without major problems,
- increased reserves are required with integration of wind generation, and the reserves requirements increase significantly as the penetration of wind energy increases,
- system reliability would be enhanced through upgrade of the HVdc power transfer capability,
- the capacity credit of wind decreases as penetration increases, decreasing from 32% for a 5% penetration to 19% for an 18% penetration,
- the capacity credit of wind is limited by the large variations in power over small periods of time,
- the variability of wind energy will add capacity costs of between $2.4/MWh for a penetration of 5%, and $9.3/MWh for a penetration of 20%,
- additional operating reserves would be necessary to manage the uncertainty in wind generation output. The quantity of the reserves is dependent on the level of penetration, geographic diversity, load factor (capacity factor), and wind output profile,
- for a low penetration of wind power hydro is able to provide most of the operating reserves, however as wind penetration increases it is necessary to use reserves from other generation sources and interruptible loads,
- dry years lead to increased costs for procuring reserves as these have to be provided by thermal plant which are more expensive to operate,
- wet years also lead to higher reserves costs as the hydro stations are operated to provide base load and thus are less flexible in their operation,
- the cost of wind related reserves requirements is 44% lower for scenarios where large amounts of wind generation are installed in Otago compared with an equivalent scenario where wind capacity is concentrated in the North Island,
- reserve costs are relatively indifferent to windiness for low and medium penetrations but increase significantly in times when there is less wind if the penetration of wind energy is high.
- the results showed that allocation of reserves (spinning versus stand-by) has a profound influence on the costs of additional reserves attributable to wind power for high penetration scenarios.

The Meridian study quantifies the costs associated with additional wind energy generation and highlights the benefit of placing wind generation in the South Island. It must be noted that the study's design was directed toward assessing the impact of the proposed Project Hayes WPP on the power system and scenario development was based on Meridian's view of power system development at the time. The study also shows the impact of power system management on costs; i.e. the difference in costs between using spinning as opposed to stand-by reserves.

3.3.3 Managing the integration of wind power in New Zealand

The penetration of wind energy in NZ has not yet reached levels sufficient to require wide spread mitigation measures. There have been some measures put in place to mitigate the effects of concentrated wind power in the Manawatu with infrequent run-backs applied to the Te Apiti

Wind Farm, however these measures are to combat localized network over-loading. Arguably there have been some changes to the management of the power system due to the foreseen risks of increasing wind penetration, including design of frequency keeping markets, however these changes were likely to have occurred as part of the progressive improvement of the electricity industry.

Since the WGIP, EL & MWH, and Meridian investigations were undertaken a lot of experience has been gathered by the system operator and market participants in managing WPPs. Monitoring of these WPPs has provided data which could be used to support an empirically based integration study.

3.4 FUTURE WIND POWER DEVELOPMENT

As NZ has a demonstrably good wind resource, and if targets to aid in the reduction of carbon dioxide emissions (90 % of electricity generation from renewable resources by 2025) are to be met, it is expected that 2 GW of wind power will need to be installed [61]. Thus an additional 1.3 GW is likely to installed within the next 10 years. This target is relatively small compared with the number of WPP projects that have been proposed as presented in Table 3.2 which total 5.3 GW.

The development of wind power in NZ has stalled in recent years (due to many factors such as the Global Economic Crisis, Canterbury Earthquakes, increases in appliance efficiency and energy management, increases in geothermal capacity, and uncertainty over the future operation of the Tiwai Aluminium Smelter). However, the progressive closure of the Huntly coal fired power station, closure of the Otahuhu and Southdown power stations, and uptake of new technologies such as electric vehicles may require construction of new power stations. Wind power is one of the least cost sources of electricity, and importantly has low associated carbon emissions, thus it is likely new wind power plants will be constructed.

The size of some of the proposed projects could mean that all of the required capacity could be added using only a few wind power plants (i.e. Castle Hill) and these may be sited nearby to most of the presently installed capacity. This would result in highly correlated power output and thus pose greater risks and costs to the electricity grid. However, alternative development paths may ensure NZ makes the most of spatial diversity but they may reduce economies of scale and thus increase costs overall. Thus it is desirable to quantify the benefit of the spatial diversification of wind energy in NZ. To help test the benefit of spatial diversification scenarios must be developed that are inside the bounds of what could occur but are also near the extremes of development paradigms.

3.4.1 Scenarios

A useful basis for developing scenarios is in the Parliamentary Commissioner for the Environment's (PCE) 2006 report Wind Power, People and Place [86]. The PCE report indicated two development scenarios: the first representing development using small scale WPPs typically consisting of 20 wind turbines per WPP and each wind turbine having a capacity of 1.5 MW. This would result in 65 WPPs with a total wind energy capacity of 1.95 GW. The second scenario represents large scale WPPs with each WPP consisting of 100 wind turbine each having a capacity of 3 MW. Thus a total of seven WPPs would be used with a total capacity of 2.1 GW.

The scenarios presented in the PCE report have been extended here using the list of proposed and operational WPPs (see Table 3.1 and 3.2). The first scenario is titled compact and comprises seven WPPs located in the lower North Island, as detailed in Table 3.4, with a total capacity of 2 GW. The second is a disperse scenario with seven WPPs distributed across NZ. The third is a diverse scenario and applies a nominal capacity of 30 MW per WPP, and substitutes a WPP at

each of the conjectured or existing WPP locations in Table 3.1 and Table 3.2, this results in 64 WPPs some of which have been adjusted to a capacity of 40 MW such that the total capacity equals 2 GW.

A fourth scenario represents Business As Usual (BAU) development. The WPPs as listed in Table 3.1 are augmented with WPPs that have a similar make up to those presently operational. It is found that the capacity of WPPs in NZ is best characterised using a Weibull distribution with a shape parameter equal to 0.53 and a scale parameter 20. Using the Weibull distribution parameters a set of random WPP capacities is generated, these capacities are assigned such that the largest capacity is assigned to the largest of the proposed WPPs as detailed in Table 3.2 except for the Castle Hill WPP. The Castle Hill WPP is assigned a capacity such that the total capacity equals 2 GW. The scenarios are presented graphically in Figure 3.4.

The WPPs in the scenarios are assumed to consist of Vestas V80 2.0 MW turbines, spaced in approximate square arrays, with an inter-turbine spacing of four rotor diameters. A capacity factor of 40 % is assumed for the WPPs, close to an average capacity factor for WPPs in New Zealand.

WPP	**Compact**	**Disperse**	**Diverse**	**BAU**
Ahipara / Gumfields			30	8
Awakino			30	4
Awhitu			30	
Baylys Beach			30	
Belmont			30	10
Blueskin Bay			30	
Brooklyn			30	
Cape Campbell			30	32
Castle Hill	300	300	30	214
Central Wind	200		30	22
Doctors Hill			30	
Flat Hill			30	
Gebbies Pass			30	
Glinks Gully			30	2
Hau Nui 1			30	4
Hau Nui 2			30	4
Hauauru ma raki		300	30	166
Hawkes Bay			30	60
Haycocks Station			30	
Hodson Hill			30	2
Horseshoe Bend			30	2
Hurunui			30	6
Jericho Station			30	2
Kaiwera Downs		200	30	58
Lake Grassmere			30	
Long Gully			30	
Lulworth			30	2
Mahinerangi			40	56
Mahinerangi 2			30	36
Matui / Somes Island			30	
Maungatua			30	
Mill Creek			30	60

Motorimu			30	12
Mt Cass			30	6
Mt Munro			30	6
Mt Stalker			30	4
Mt Stuart			30	8
Omamari			30	12
Pouto Forest		300	30	118
Project Hayes		300	30	230
Puketiro			30	22
Puketoi			30	50
Rock and Pillar			30	
Roundtop			30	6
Slopedown			30	36
Southbridge			30	
Taharoa			30	12
Tararua 1	300	300	40	32
Tararua 2			40	36
Tararua 3			30	94
Taumatatotara			30	
Te Anga			30	
Te Apiti			40	92
Te Rere Hau			40	48
Te Uku			40	64
Te Waka			30	20
Tiwai			30	6
Turitea	300		30	56
Waitahora			30	50
Waverly	300		30	24
Weld Cone			30	
West Wind	300	300	40	142
White Hill			40	58
Windy Peak	300		30	6
Total	2000	2000	2000	2000

Table 3.4: Scenarios (WPP capacity [MW])

3.4.2 Integration study requirements

To determine the effect of the various scenarios it is necessary to define what aspects of system operation will potentially be affected. The 2 GW capacity of the scenarios equates to a penetration of approximately 20 percent. Such a large capacity will significantly change both the generation mix (types of generation available in the system) and have significant impact on the operation of system scheduling and balancing. To determine the effect of the increased wind penetration on Unit Commitment and Economic Dispatch (UCED) a temporal resolution at least equal to the re-dispatch window should be used. Thus a minimum temporal resolution of 5 minutes is desired.

The spatial resolution of the analyses should be sufficient that the diversity in power output from WPPs that are adjacent to one-another can be replicated. The minimum distance between adjacent WPPs in the scenarios adopted for this study is 2.8 km, hence the spatial resolution of the analyses must be in the order of kilometers. The wind power plants in the scenarios are

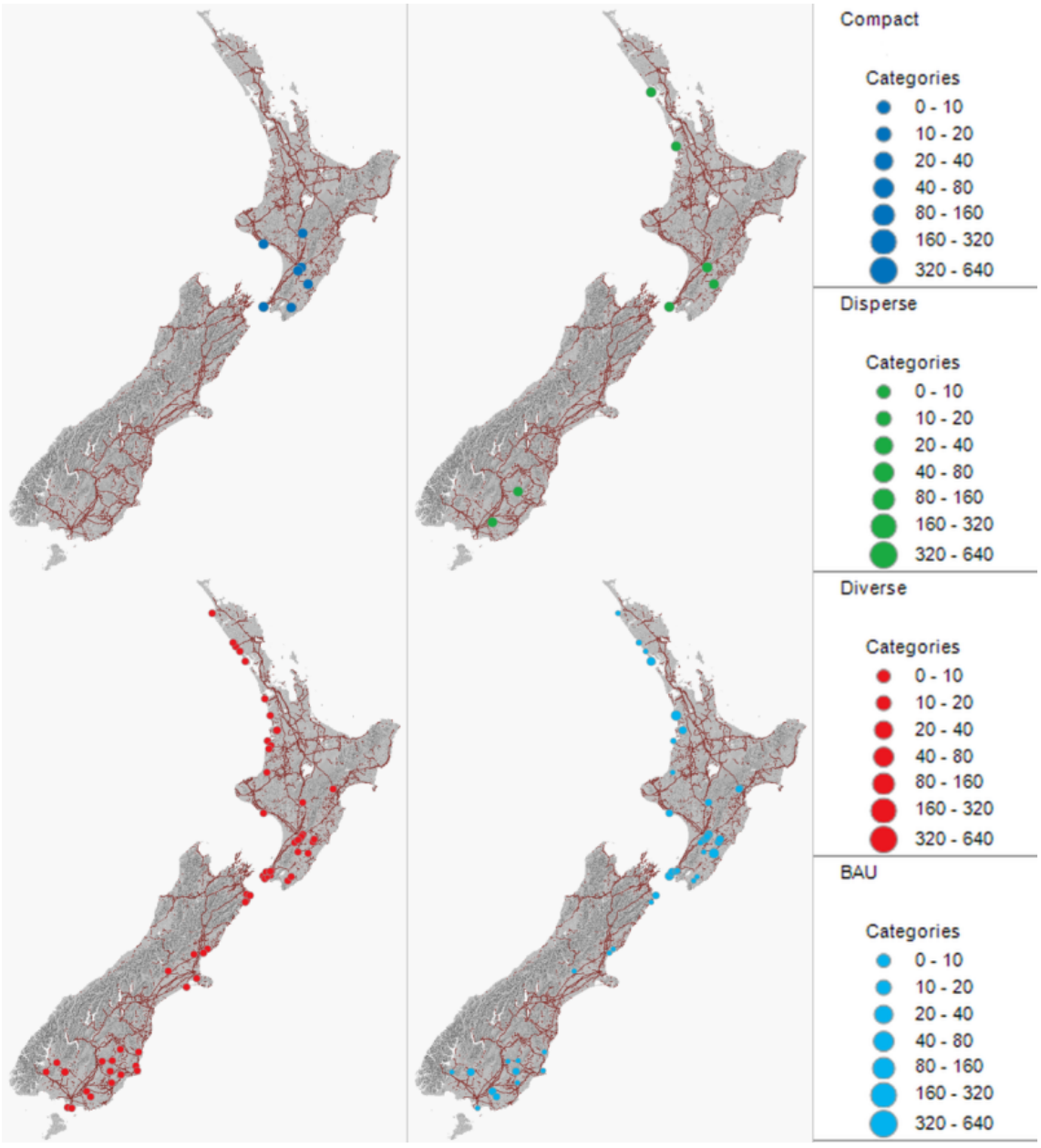

Figure 3.4 Scenarios assessed in this thesis (Top left: compact, top right: disperse, bottom left: diverse, bottom right: business as usual (BAU).

spread across the North and South Islands of NZ; hence the spatial extent of the models must likewise span the entirety of the two islands.

The IEA task force recommends a temporal span of at least 6 years should be used to assess capacity requirements [43]. However, the reliance of the NZ power system on hydro electric generation means that the system is susceptible to "dry year risk". The last dry year to severely impact the NZ power system was in 2004, hence the temporal span for the integration study must be at least 10 years and preferably longer, and include one or more dry years.

The purpose of the study here is to determine the benefit of the spatial diversification of wind energy. The scenarios represent an installed capacity of approximtely 20 percent and hence the wind generation would significantly impact the generation mix in the system. It is important that the resulting simulations are synchronous with other generation and load. The easiest way to ensure that data are synchronous is to produce simulations for a period over which measurements for other generation and load have been made or can themselves be simulated; thus simulations for a recent historic period are preferable.

As the level of wind power penetration included in the scenarios presented here is sufficient to impact UCED, it is necessary that wind power forecasting, for forecast horizons less than 6 hours, is assessed [43].

3.5 SUMMARY

The construction of WPPs in NZ was initiated under ECNZ, however all the large WPPs have been constructed subsequent to deregulation. There was a rapid growth in installed wind capacity up to 2005 at which time the system operator became concerned about large changes in power output from WPPs in the Manawatu. This was due to the excellent wind resource in the Manuwatu, competitive generation model, and the high degree of correlation in wind resources between the WPPs sited in close proximity. The rapid concentrated growth coupled with the notifications for connection of very large WPPs throughout NZ caused the system operator and other parties to initiate integration studies. These studies, to a large extent, alleviated concerns and enabled the system operator to focus on specific grid upgrade projects to enable renewable integration. However, the methodologies used to support the integration studies have not necessarily applied thorough methods (particularly in simulating the power output from WPPs).

It is expected that the wind portfolio in NZ will grow and hence the impacts of integration on the power system will increase. Some of the effects of integration can be reduced by the spatial diversification of WPPs, however this may increase costs due to reductions in economies of scale. It is therefore essential to quantify the benefits of spatial diversification and this requires accurate models of wind power. Several scenarios have been developed using projected wind projects that can be used to assess the benefit of spatial diversification using the developed models.

Chapter 4

WIND POWER STATISTICS

4.1 WIND POWER DATA

The benefits of spatial diversification of wind power in New Zealand can be explored by examining the power output from operational WPPs. WPP power time-series have been provided by the Electricity Authority for a select number of WPPs as presented in Table 4.1, and is referred to as the EA data-set. The data comprises power output at a 4 second sampling interval for a period of 6 months from 1st August 2012 through 31st January 2013.

WPP	**Cap. [MW]**	**No. WTs**	**Model**	**WT cap. [MW]**	**Proxy mast**
Te Apiti (TAP)	90.8	55	Neg-Micon NM72	1.65	Tararua 1
Tararua 1 (TWF1)	31.7	48	Vestas V47-660	0.66	Tararua 2
Tararua 2 (TWF2)	36.3	55	Vestas V47-660	0.66	Tararua 2
Tararua 3	93	31	Vestas V90	3	Tararua 3a
Te Rere Hau	48.5	97	Windflow WF500	0.5	Tararua 3b
West Wind A	71.3	31	Siemens SWT2.3-82	2.3	Wellington 1
West Wind B	71.3	31	Siemens SWT2.3-82	2.3	Wellington 1
White Hill	58	29	Vestas V80	2	Southland 2

Table 4.1 EA dataset metadata

The data are complicated as 5 of the wind turbines constructed at Te Rere Hau were initially connected to the power network through the Tararua Stage 3 WPP connection; in the EA dataset Te Rere Hau comprises 94 Windflow 500 turbines, and Tararua Stage 3 comprises 31 Vestas V90 turbines plus 5 Windflow 500 turbines.

To aid in the explanation of the power output from WPPs, data from Tararua Stage 1 WPP (TWF1) for the period of one week, from 22^{nd} August 2012 through 29^{th} August 2012, is presented in Figure 4.1. The top left graph presents a time-series of power, the data have been averaged to a temporal resolution of 10 min for presentation. The top right shows a histogram, with the probability distribution function (PDF) shown as a red line (referenced to the right axis) and the cumulative distribution function (CDF) shown as a green line. The lower left graph presents a correlogram formed from the data, and the lower right presents the periodogram.

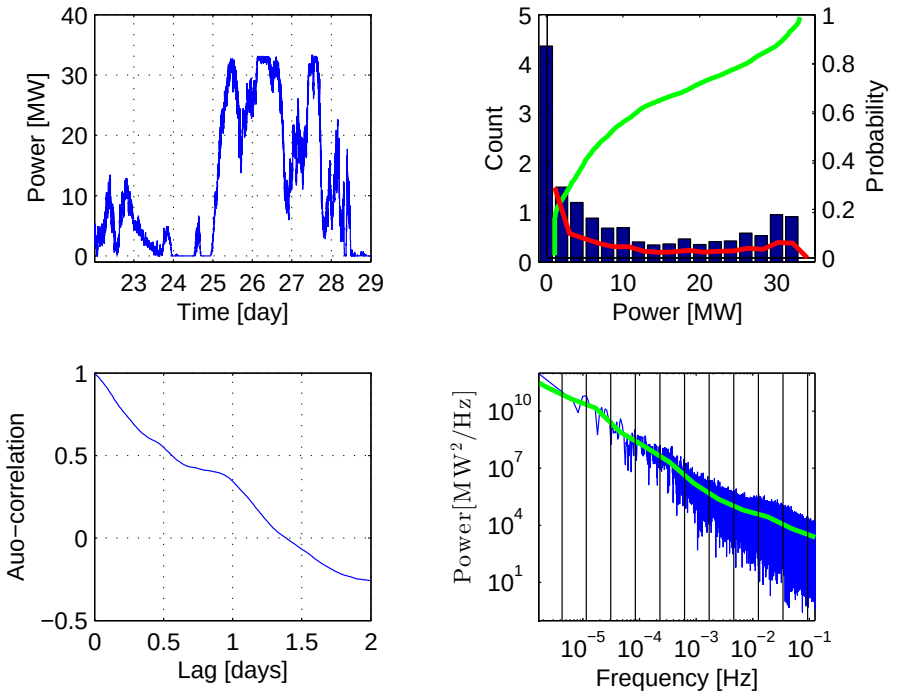

Figure 4.1 Statistics derived for Tararua WPP Stage 1. Top left: time series; top right: histogram, PDF (red) and, CDF (green); lower left: correlogram; lower right: periodogram.

The series of discrete measurements of the power at regular intervals form a time-series. A finite discrete time-series for power measured at a WPP is represented in Equation 4.1, where T is the length the the time-series.

$$P = \{P_1, P_2, P_3, \ldots, P_t, \ldots, P_T\} \tag{4.1}$$

Where P is power, t is time, and T is the total time.

4.2 PROBABILITY

The power from a WPP can be described using statistics derived from a measured time-series. The cumulative probability distribution describes the likelihood that the power will be less than a certain value and is presented in Equation 4.2.

$$Q(P) = Pr\left[P \leq q\right] \tag{4.2}$$

Where Q_P is the probability distribution function, q is a certain probability or quantile

The power output from TWF1 varies over the week from an output of near zero, to close to the rated capacity of the WPP (note electrical losses reduce the output from the total capacity). Over the week the WPP produces zero power for less than 20% of the time, and more than 10 MW for 50% of the time. The power output from the WPP has a "lumpy" histogram with a large number of counts for zero power output, a high chance of producing low power, and an increased chance of producing near full power as turbines regulate maximum power according to their power curve.

The complete description of a time-series using its probability distribution requires a set of T parameters, however it is often desirable to describe a time-series using a small set of numerics and assumptions. The mean is a numeric describing the central tendency of the time-series.

The mean is calculated as the sum of the time series divided by the number of samples and is presented in Equation 4.3. The mean power from TWF1 during the week assessed is 11.6 MW.

$$\mu(P) = \bar{P} = \frac{1}{T}\sum_{t=1}^{T} P(t) \tag{4.3}$$

Where μ is the mean, and the overbar represents the mean value of a variable.

The variance is a metric that describes the spread of values about the mean and is defined as the average squared difference from the mean. The variance is presented in Equation 4.4. The standard deviation is alternatively used to describe the spread of values and is defined as the square root of the variance and presented in Equation 4.5. The variance of power during the week assessed for TWF1 equals 133 MW^2 and the standard deviation equals 11.5 MW.

The mean and variance are commonly referred to as the first and second moments respectively. Further statistics that are commonly used to aid the description of a statistical distribution include the third and fourth moments. The third moment is the skewness, which is a measure of how anti-symmetric the probability distribution is. The fourth moment is the kurtosis which is a measure of how pinched the probability distribution is; a distribution with a tall and narrow shape has a higher kurtosis than a distribution with a squat and wide shape.

$$\sigma(P,P) = \frac{1}{T}\sum_{t=1}^{T}(P(t) - \overline{P})^2 \tag{4.4}$$

Where $\sigma(P,P)$ is the variance of P.

$$\begin{gathered}\sigma(P) = \sqrt{\sigma(P,P)} \\ \sigma(P,P) = \sigma^2(P)\end{gathered} \tag{4.5}$$

Where $\sigma(P)$ is the standard deviation of P.

Statistics, such as the mean and standard deviation, can be used in conjunction with an assumption that a time-series belongs to a particular family of probability distributions, such as the Gaussian distribution, to provide a complete description of the probability distribution. A commonly applied family of probability distributions is the normal or Gaussian distribution which is defined in Equation 4.6. The Gaussian distribution is particular in that it is the distribution formed when aggregating sufficient numbers of samples from continuous independent random processes; this being described as the central limit theorem [87].

$$Q_G(q,\mu,\sigma) = \frac{1}{\sigma\sqrt{2\pi}} e^{-\frac{(q-\mu)^2}{2\sigma^2}} \tag{4.6}$$

Where G denotes a Gaussian distribution.

There are many families of probability distributions that describe naturally occurring processes, such as the Beta and Weibull distribution. Probability distributions such as these can be useful for generalising statistics when matched to measurements comprising finite time-series. However, not all processes are well described using probability distributions with known functions.

To help describe distributions that are not well characterised using known probability distribution functions it is possible to use various tools such as piece-wise linear probability distributions, transformation functions, and mixture models. A piece-wise linear probability distribution can be defined by using quantiles from the measured distribution mapped to equivalent quantiles from a continuous probability distribution function. Between subsequent quantiles, linear interpolation is applied and a transform can be defined for values between the lowest and highest in the measured set.

Functions maybe used to transform measured probabilities to probabilities that more closely match well known probability distributions. Indeed many well known probability distributions

are themselves transformed from underlying distributions. An example is the log-normal distribution being obtained using the log transform of the normal or Gaussian distribution.

It is possible to use a combination of probability distributions by applying a mixture model. A mixture model, as the name suggests mixes several probability distributions together such that the complex shape of the measured probability distribution can be replicated. A mixture Beta model has been applied to the simulation of WPP in New Zealand by Nan [88].

4.2.1 Auto-covariance and auto correlation

The rate of change of power output from a WPP can be characterised by the auto-correlation. The auto-correlation is defined as the correlation of the time series with itself given a time shift or lag. It describes how well the time series matches itself after being time shifted. For a discrete time series of length T the auto correlation is defined in Equation 4.7.

$$R_{s,s}(l) = \frac{\sigma(P_s(t+l), P_s(t))}{\sigma(P_s(t+l)) \cdot \sigma(P_s(t))} \tag{4.7}$$

Where $R_{s,s}$ is the auto-correlation for lag l at site s.

The auto-correlation presented as a function of the lag is a correlogram. A correlogram for WPP power is presented in the bottom left graph of Figure 4.1. The graph shows that as the lag increases the auto-correlation decreases. The high auto-correlation for short lags implies that the power time-series has a high degree of persistence. The auto-correlation decreases at a fairly uniform rate and for lags greater than 1 day approaches zero, thus the power produced on a particular day is not well predicted using measurements of power produced during the preceding day. The auto-correlation function becomes negative at 1.5 days.

4.2.2 Power spectral density

The correlogram is a useful tool for describing the variation in a time-series. However, it is not especially useful for characterising processes that have time frames much greater than the sampling interval (so called long-memory processes), or processes that have oscillatory patterns. Further, it is often the case that time-series are the result of many processes, some of which may have oscillatory characteristics, and it is often advantageous to describe the influence of the individual processes on the time-series.

A wind power time-series is the result of the wind speed and its variance (or turbulence) and the transformation of that wind speed into power. The wind comprises an advected train of vortices, with vortices having magnitudes, spatial extents, and temporal duration described by the Kolmogorov spectrum and governed by the viscosity of air. A full description of turbulence and wind speed spectra is presented in Section 5.4. The transformation of the wind speed to power is made using wind turbines as part of a WPP. The turbines, individually and collectively, have a spatial extent which integrates the wind field and causes smoothing of the wind power time series compared with a point wind speed time-series. While this smoothing effect may be observable in the auto-correlation function, the magnitude of smoothing applied to vortices of different sizes is not readily deductible. Further, wind speed varies according to changes in atmospheric stability and weather patterns; exhibiting diurnal and annual patterns (see Section 5). In addition to this the operation of the WPP may exhibit regular curtailment or other operational patterns. In order that the effect of these different phenomena on the wind power time-series can be observed independently it is useful to examine a spectral representation of the time-series.

A time-series can be represented as a set of sinusoids using a Fourier series expansion as shown in Equation 4.9. A sinusoid is a function that describes a smooth repetitive oscillation and is

presented in Equation 4.8. The set of sinusoids is termed a spectrum. Each sinusoid is defined using its frequency and phase, the frequency being the inverse of its wavelength (or temporal span of one complete cycle or oscillation), and the phase describes the temporal offset. The components resulting from the Fourier series expansion range from the fundamental frequency, a frequency such that one complete cycle of the sinusoid is equal to the length of the time-series, to the the Nyquist frequency (being equal to half the sampling frequency of the time-series).

$$y(t) = Asin(2\pi ft + \varphi) \tag{4.8}$$

Where $y(t)$ is a circular oscillatory function, A is the function magnitude, f is the frequency, and φ is the phase.

$$f_\omega = \sum_{t=0}^{T-1} x_t \left[cos\left(-2\pi f \frac{t}{T}\right) + i \cdot sin\left(-2\pi f \frac{t}{T}\right)\right] \tag{4.9}$$

Where f_ω is the complex valued frequency component, T is the number of samples in the time-series, t is the current sample considered.

Each complex valued frequency component in the Fourier series expansion of a time-series can be described using an angle (or phase) and a magnitude. The power spectra which is presented in Equation 4.10 is the useful for detecting the contribution of particular frequencies to the time-series.

$$PS = |f_\omega|^2 \tag{4.10}$$

Where PS is the power spectra.

The power spectra for the time-series from TWF1 is presented in Figure 4.1 as the blue line in the lower right graph. As the time-series has a sampling period of 4 second and a duration of 1 week there is a total of 75600 frequency components in the spectrum, making inference of any underlying trend difficult. The green line shows the trend of the power spectrum derived using a histogram, also known as the method of bins, as shown in Equation 4.11, where the bin edges are marked by the vertical black lines. Note that the amplitude spectrum is near linear when plotted on the log-log scale.

$$PS(F) = \frac{dF}{df} \sum_{f=F-\frac{dF}{2}}^{F+\frac{dF}{2}} PS(f) \tag{4.11}$$

Where F are the bin center frequencies, dF is the bin width, and df is the difference between consecutive frequencies.

The bias for the power spectra, seen as the point at the far left, equals the integral of the square of the time series which in this case equals $3.04 \times 10^{12}\,\mathrm{MJ}^2$. Also note that the time-series is dominated by low frequency components.

4.3 MULTIPLE TIME-SERIES

It is obvious that the time-series from different WPPs should be different due to differences in WPP location, design, and wind resources. Further, the time-series from different WPPs will not be concomitant, or exhibit the same patterns of variability. However, different WPPs exhibit similarities in their power output due to similarities in technology, and particularly for WPP sited in close proximity, similarities in their wind resources. Thus it is necessary to identify statistics that quantify how closely related the power time-series are.

If the power output from two WPPs were of equal magnitude and concomitant then their power output at any time would be simply twice the power export of one of them. And, as Pythagoras found for right angled triangles, if the WPP's power output were entirely independent, or orthogonal, then the power export on average will equal the root sum of the squares of the power. In reality the cumulative power export from a pair of WPPs will be somewhere between these two extremes.

To illustrate the difference in WPP power output, statistics from the EA dataset are presented in Figure 4.2. Probability distributions for power from different WPPs are presented in the top left graph. The shapes of the measured probability distributions are particular, reflecting differences in wind resources, WPP design, and wind turbine types. Individually and collectively they are not well approximated by a single family of well known continuous probability distributions. Some WPPs achieve maximum output for a considerable amount of the time, such as TWF1, TWF2, and WHL. All the other WPPs have lower probabilities of achieving high output.

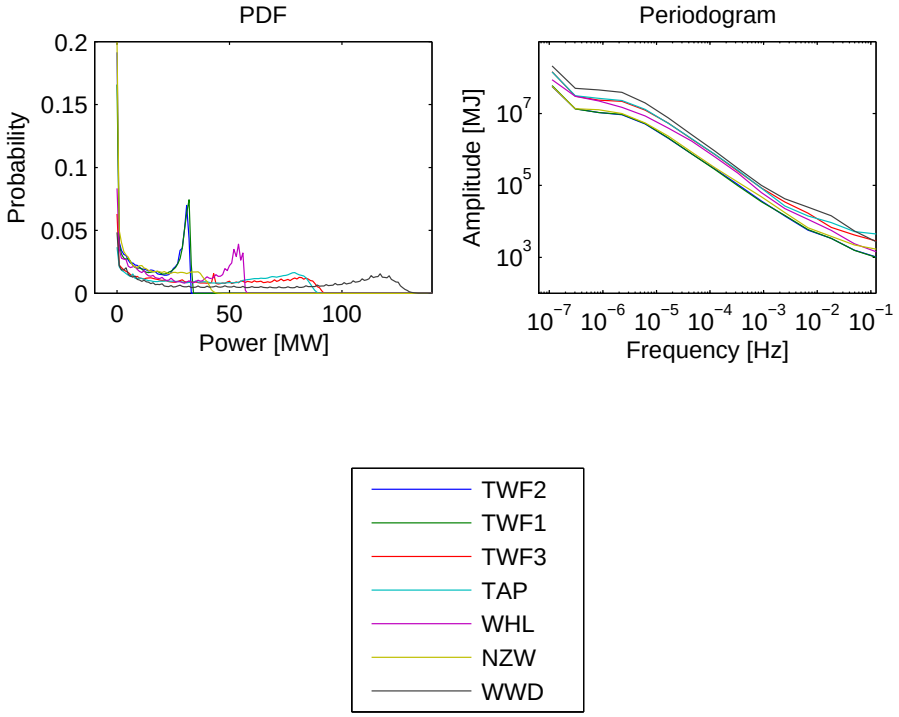

Figure 4.2 Measured WPP power statistics

The top right pane of Figure 4.2 presents periodograms for all the WPPs. All WPPs exhibit similar power spectral densities, with most of the energy contained in the low frequency components, and spectral densities decreasing in a manner described by the power law, which is shown as a linear function in a double log presentation.

4.3.1 Correlation and covariance

To measure how closely related two time series are, it is useful to define a numeric; the covariance. The covariance is defined as the sum product of the variation in values about the mean of their respective time-series and is presented in Equation 4.12.

$$\sigma(P_r, P_s) = \frac{1}{T}\sum_{t=1}^{T}(P_{t,r} - \bar{P}_r) \cdot (P_{t,s} - \bar{P}_s) \tag{4.12}$$

Where $\sigma(P_r, P_s)$ is the covariance between time series r and s.

As a metric the covariance is not particularly useful for describing the correlation between two time-series, as its magnitude is proportional to the variances of the two time-series. A useful statistic is the Pearson's correlation coefficient, which is defined as the ratio of the covariance to the product of the standard deviations of the time-series and is presented in 4.13. Pearsons's correlation coefficient, referred to as the correlation coefficient, can take values between -1 and 1. For time-series with infinite length a value of zero will result if the two time-series are independent, a value of one if the time-series are positive scalar products of each other, and -1 if the time-series are mirror scalar products of each other.

$$R(P_r, P_s) = \frac{\sigma(P_r, P_s)}{\sigma(P_r) \cdot \sigma(P_s)} \tag{4.13}$$

Where $R(P_r, P_s)$ is the Pearson's correlation coefficient between power time series from sites r and s.

A correlation coefficient of 1 results when two time-series have a perfect positive relationship. That is if two time-series are regressed, or compared in an orthogonal frame, all values will fall on a unique line (not necessarily a straight line). The correlation between pairs of WPPs as a function of the distance between WPPs is presented in the top right pane of Figure 4.4. As expected the correlation is much higher for WPPs that are located in close proximity. Some of the WPPs are co-located and would not appear on the graphic; the distance has been set to 1 m.

Often time-series that are closely related will exhibit linear dependence; the best fit regression is a straight line. The solution of the best linear approximation of a time-series given the values in another time-series, or a predictor time-series, is termed linear regression and is presented in Equation 4.14, where A and B are the regression coefficients and ϵ is the error or residual.

$$\widehat{P_s(t)} = A_{r,s} \cdot P_r(t) + C_{r,s} + \epsilon_{r,s}(t) \tag{4.14}$$

Where $\widehat{P_s(t)}$ is the predicted power at site s at time t given the linear regression, $A_{r,s}$ is the slope and $C_{r,s}$ the offset of the linear regression formed between power time-series from sites s and r, and $\epsilon(t)$ is the error in the regressed time-series at time t.

$P_{TAP} = 1.06 \cdot P_{TWF3} + 3.91$
$\sigma(P_{TAP}, P_{TWF3}) = 39.1$
$R(P_{TAP}, P_{TWF3}) = 0.84$
$RSQ(P_{TAP}, P_{TWF3}) = 0.7058$

Table 4.2 Parameters and statistics for regression example.

There are many methods for approximating the coefficients A and C, a common approach is ordinary least squares. The ordinary least squares method minimises the squared sum of the residuals as shown in Equation 4.15.

$$\overline{\epsilon_{r,s}} = \sum_{t=1}^{T} (\widehat{P_s(t)} - Pr(t))^2 \tag{4.15}$$

Where $\bar{\epsilon}$ is the mean residual

If the time-series are independent the regression coefficients may be found by solving the relationships presented in Equation 4.16.

$$\begin{aligned} A_{r,s} &= R(P_r, P_s) \cdot \tfrac{\sigma(P_r)}{\sigma(P_s)} \\ C_{r,s} &= \mu(P_r) - A_{r,s} \cdot \mu(P_s) \end{aligned} \tag{4.16}$$

An estimate of the error in the regression is given by one minus the ratio of the sum of squared residuals to the total sum of squares as shown in Equation 4.17, this error estimate is the coefficient of determination or r-squared.

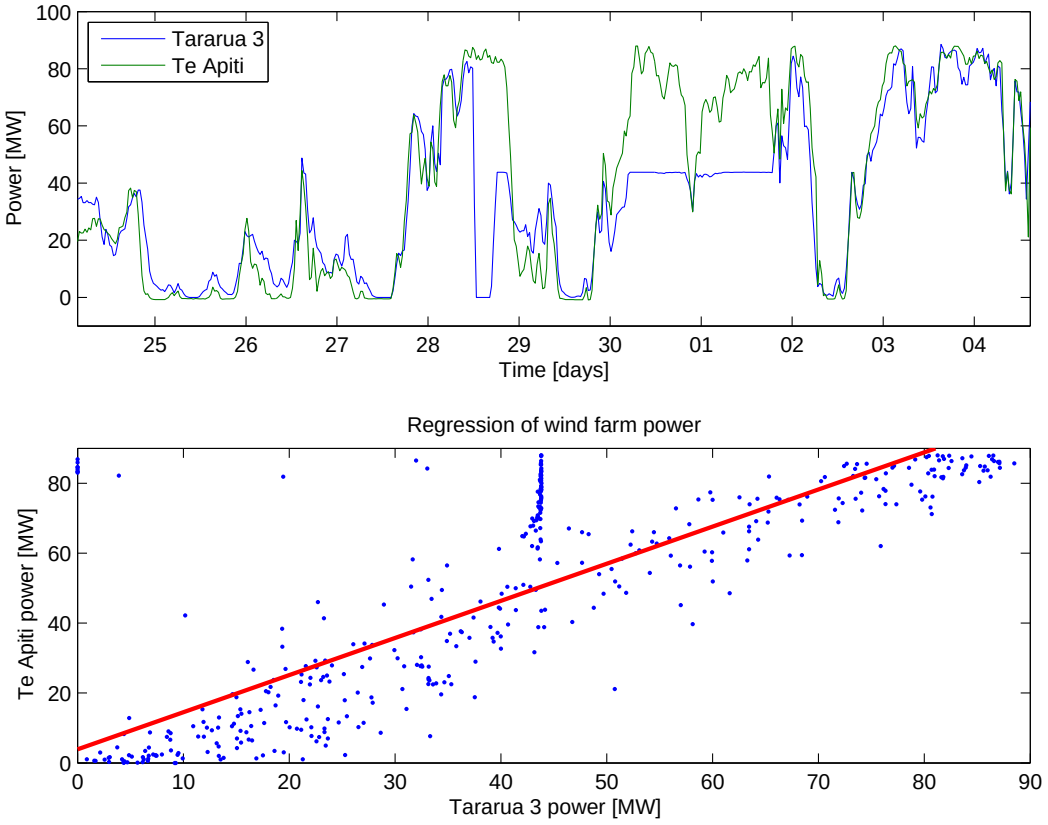

Figure 4.3 Linear regression example. Top graph shows a coincident sample of two time-series. The bottom graph shows the linear regression formed using the time-series. Parameters and statistics relating to the regression are presented in Table 4.2.

$$RSQ_{r,s} = 1 - \frac{\sum_{t=1}^{T} \epsilon_{r,s}(t)}{\sum_{t=1}^{T} (P_s(t) - \bar{P}_s)} \tag{4.17}$$

Where $RSQ_{r,s}$ is the root mean squared error.

An example linear regression between two time series is presented in Figure 4.3. The top graph shows the power from the Tararua 3 and Te Apiti WPPs for a period of 11 days. It can be seen that the power output between the two farms is closely matched. This is unsurprising considering they are situated on opposite sides of the Manawatu Gorge. The lower graph shows the best fit linear regression solved using least squares as a red line. The equation for the linear regression is shown in Table 4.2, along with the covariance, correlation coefficient, and R-squared.

The part of the Tararua 3 WPP time-series that is presented exhibits curtailment to zero output during day 28 and is subsequently curtailed to 45 MW during days 30 and 01. Note that the curtailment biases the regression and illustrates the difficulties in using raw power data to derive statistics.

A multiple-linear regression may be formed when more than one time-series is used as the regressor as shown in Equation 4.18. Here the coefficient $A_{R,s}$ is a vector with a length equal to the number of regressors.

$$P_s(t) = A_{s,r=[1,2,\ldots R]} \cdot [P_{s,r=1}(t), P_{s,r=2}(t), \ldots, P_{s,r=R}(t)] + B_{s,r=[1,2,\ldots R]} + \epsilon_{s,r=[1,2,\ldots R]} \tag{4.18}$$

The correlation coefficients for the wind power time-series in the EA data set are shown in the upper left graph of Figure 4.4 as a function of the distance between sites. The graph shows a strong relationship between the correlation and the distance between sites. Some of the sites have near zero distance between them as they roughly co-located, such as the Tararua 1, Tararua 2, and Tararua 3 WPPs. A minimum distance between WPPs of 1.5 km has been assumed so they are displayed using a log scale.

4.3.2 Scaled correlation

The correlogram and power spectra are useful for illustrating the variation of wind power time series at different temporal scales. The variations in wind power time-series are mostly in response to changes in wind speed reflecting the passage of weather systems over the WPP. If two WPPs are in close proximity then passing weather will simultaneously affect both WPPs and the power output time-series will exhibit similar patterns of variability. If the pair of WPPs are further apart their power output may still exhibit a degree of correlation, however the spatial extent of weather systems that affect both WPPs will be larger and hence the temporal span of the correlation longer. Thus it is expected that the correlation in power output will be a function of the temporal span or scale.

A measure of the correlation as a function of the temporal span is the Scaled Correlation. For a particular scale the time-series pairs are broken into segments of the corresponding length (as presented in Equation 4.19), the correlation coefficient for each pair of segments is derived, and the average of these correlation coefficients calculated as presented in Equation 4.21.

The scale is notionally the equivalent of the wave length, and is the inverse of the frequency. The terminology scale is used as frequency and wavelength are used in the description of periodic or oscillatory functions.

$$dk(j) = floor(\frac{T}{j}) \tag{4.19}$$

Where j is the scale, k is the translation, dk is the translation window length, and T is the total time in the time-series.

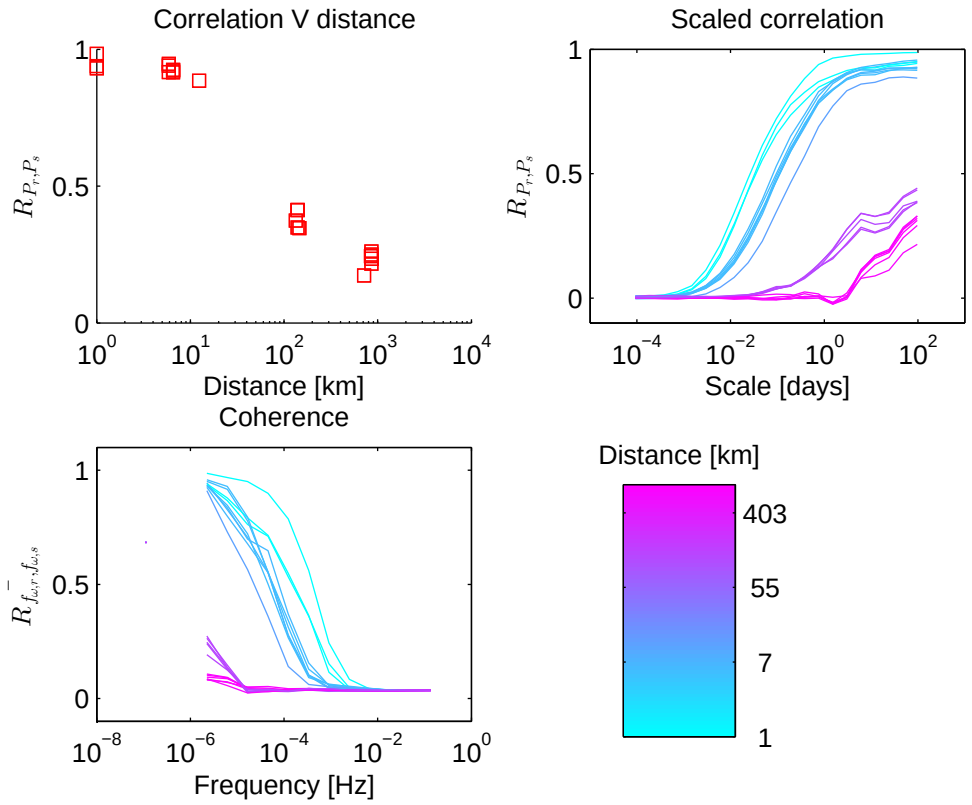

Figure 4.4 Wind power correlations; the top left graph show the correlation between pairs of wind power time-series as a function of distance. The top right graph shows the scaled correlation for pairs of power time-series coloured according to the separation distance. The lower left graph shows the coherence between pairs of power time series coloured according to the separation distance.

$$P(j,k) = \mu(P(t \geq t - \frac{dk}{2} \,\&\, t < t + \frac{dk}{2}) \tag{4.20}$$

Where $P(j,k)$ is the scaled power at scale j at translation k, and $P(t = k - \frac{dk}{2} : k + \frac{dk}{2})$ is the power time-series between time times $k - \frac{dk}{2}$ and $k + \frac{dk}{2}$.

$$\overline{R(P_r, P_s)(j)} = \frac{1}{K} \sum_{k=1}^{K} R(P_r(j,k), P_s(j,k)) \tag{4.21}$$

Where $\overline{R(P_r, P_s)(j)}$ is the scaled correlation between power time-series s and r at a scale of j.

While it is possible to determine the scaled correlation for any scale, between half the sampling period and the length of the time-series, it is unnecessary to derive the correlations for scales that are very close together as this results in redundant information. For pragmatic reasons the scaled correlation is calculated using segments of length $j = 2^N$ samples.

The scaled correlations for the wind power time-series are presented in the top right graph of 4.4. Each line represents the scaled correlation between two WPPs; as there are seven WPPs there are a corresponding 21 pairs. The lines are coloured according to the distance between the pairs of WPPs. It is seen that for scales less than 1×10^{-3} days or 1.4 minutes the correlation between all WPPs regardless of how close they are located equals zero. As the scale increases the correlation between WPPs increases such that for WPPs separated by less than 10 km the scaled correlation is greater than 0.9 at scales greater than one day.

4.3.3 Coherence

The dependence of correlation on distance and period is clearly seen using the scaled correlation. This relationship can also be illustrated using the magnitude squared cross Power Spectral Density or coherence. To calculate the coherence requires windowing or segmenting the time-series, so that a sufficient number of samples are created from which co-variances can be determined. The Fourier series expansion is found for each time-series segment, and the coherence at each frequency found; the coherence equals the ratio of the magnitude squared co-variance to the product of auto-variances (standard deviations). Thus for each pair of WPPs a coherence series can be found. To aid in graphical illustration the method of bins is applied to each coherence series and these plotted in the lower left graph of Figure 4.4.

$$R(f_{\omega,r}, f_{\omega,s}) = \frac{|\sigma(f_{\omega,r}, f_{\omega,s})|^2}{\sigma(f_{\omega,r}, f_{\omega,r}) \cdot \sigma(f_{\omega,s}, f_{\omega,s})} \tag{4.22}$$

Where $R(f_{\omega,r}, f_{\omega,s})$ is the coherence between sites s and r.

The time-series have been windowed into 32 non-overlapping segments, thus the lowest frequency (omitting the bias or zero frequency) for which the coherence function is valid is 2.01×10^{-6} Hz (a period of 5.47 d), equaling the reciprocal of the length of the time-series divided by the number of windows. Hence there is a trade off between the accuracy of the coherence and the lowest resultant non-zero frequency; the coherence misses some of the character evident in the scaled correlation analysis.

The windowing applied in this example uses simple rectangular windows. The discrete Fourier transform makes an implicit assumption that the windowed time-series is repetitive, and as the start and end points of the time-series segment may not be equal complementary frequencies are added to "fill-out" the periodic step, this is referred to as spectral leakage. It is usual in the

analysis signals to use weighted windowing functions, such as a Hamming window, to minimize the effect of the spectral leakage.

4.4 BENEFIT OF SPATIAL DIVERSIFICATION

The EA data can be used to demonstrate the benefits of spatial diversification by aggregating subsets of the data. The first is the centralised subset, which comprises all the WPPs in the Manawatu (Tararua 1,2, and 3, Te Apiti, and Te Rere Hau) aggregated to form a single power time-series with a capacity of 300 MW. The second, diversified subset, is constructed by aggregating the time-series for Te Apiti, White Hill, and West Wind with a capacity of 291 MW, which is then scaled by a factor of $\frac{300}{293}$ to be comparable to the centralised subset.

Time-series of the centralised (blue) and diversified (red) subsets are presented in the top left graph of Figure 4.5. The entirety of the EA datasets are used - stretching six months with a 4 s resolution results in nearly 4 million samples. Note the common pattern seen in both time-series, evidence that the two subsets are not independent.

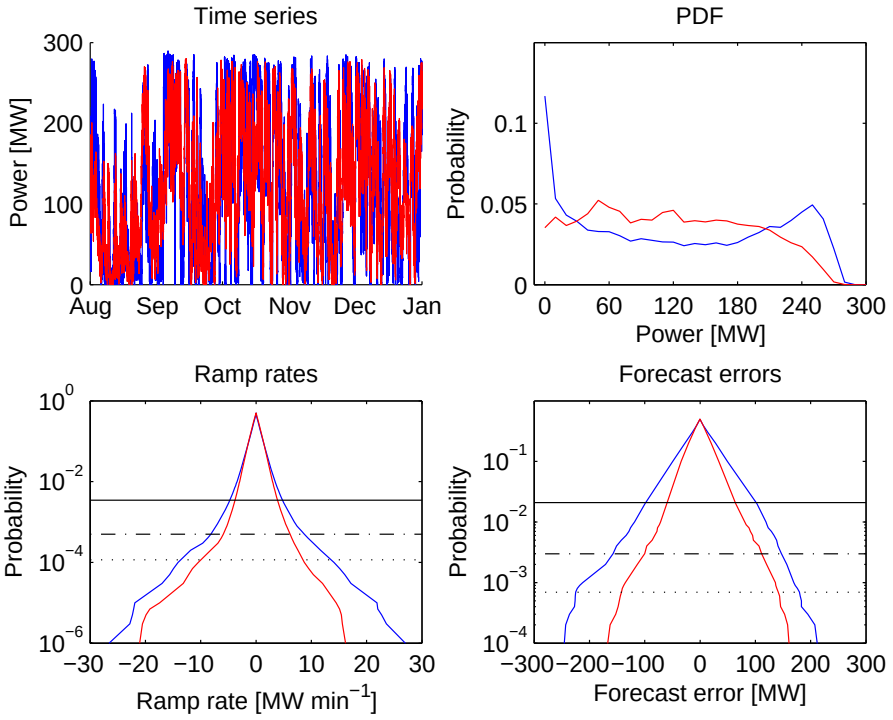

Figure 4.5 Statistics derived for Centralised (blue) and Diversified (red) wind energy scenarios

To assess the benefit of diversity of WPPs it is useful to introduce three metrics; reliability, variability, and predictability.

4.4.1 Reliability

Reliability describes the degree to which the power system can depend on power being available from a fleet of WPPs, thus it is related to the variance of the power. For instance if a WPP produces power at rated capacity for 30% of the time, and zero power for 70% of the time then it is less reliable than a WPP that produces 30% of its rated power 100% of the time even though the same amount of energy is produced by either WPP. The reliability can be assessed using the probability distribution function.

The mean power produced by the WPPs in the centralised subset was 122.7 MW, and for the diversified subset 121.02 MW, representing capacity factors of 40.9% and 40.34% respectively. There is little to differentiate the subsets based on energy production. However, the standard deviation of power for the centralised subset is 92.7 MW, and 72.0 MW for the diversified subset, showing the greater reliability inherent in the diversified subset.

The greater reliability of the diversified subset is seen by comparing PDFs for the centralised and diversified subsets in the top right graph of Figure 4.5. It can be seen that the centralised subset has a higher chance of producing zero power and also a higher chance of achieving power output of 200 MW and higher. It is more likely that the diversified subset will produce power in the range between 30 MW and 200 MW.

4.4.2 Variability

The variability of a set of WPPs can be illustrated by examining the distribution of ramp rates. The ramp rate is defined as the change in power per unit time and is presented in Equation 4.23. While ramp rates are defined as per unit time the magnitude is dependent on the sampling interval. If a WPP changes from rated power to zero over a period of 5 min and remains at zero output for a further 10 min then its maximum ramp rate will be 20% of rated power per minute using a 5 min sampling, however if the sampling interval increases to 10 min then the ramp rate will be 10% of rated power. Here the variability is calculated as the difference across a 5 min time difference using 4 s samples, 5 min is used because it is the present scheduling window used by the system operator in New Zealand.

$$\lambda(t) = \frac{P_{t+\tau} - P_t}{\tau} \tag{4.23}$$

Where λ is the ramp rate.

Ramp rates for a 5 min period are presented in the lower left graph of Figure 4.5. Also shown are probabilities indicative of events with recurrence periods of once per day (solid black line), once per week (dash-dotted black line), and once per month (dotted black line). The results show that ramp rates are very similar between the two subsets for events with recurrence intervals less than one day. For less common events ramp rates are lower for the diversified subset. For events that occur weekly the centralised subset has negative ramp rates of 8.1 MW min^{-1} and the diversified subset 5.8 MW min^{-1} equating to a difference of 40%. The ramp rate functions are nearly symmetric, although increases in power are generally slightly faster than decreases. This is particularly the case for the diversified subset.

4.4.3 Predictability

Predictability is important to enable the efficient scheduling of generation and allowing participants in the electricity market to make definite generation offers. If generation is unpredictable then it is not possible not make accurate forecasts and thus offers will not be definite. In New Zealand the 2 h forecast horizon is the closing time for bids and offers prior to a trading period, referred to as "gate closure", and thus is the most crucial horizon for efficient operation of the electricity market.

As seen in Figure 4.1 there is a high degree of persistence. Thus the wind power output is well characterised using a persistence forecast, i.e. using the present power output to forecast future power, for short forecast horizons. However as the forecast horizon increases the accuracy of a persistence forecast falls, so that for horizons greater than 1.3 d a persistence forecast has near zero accuracy. The accuracy of forecasts may be increased using tools such as wind speed and direction forecasts generated using Numerical Weather Prediction (NWP) models which can be converted to power using a power performance matrix. Time-series forecasting tools

can also be used to improve accuracy of predictions however these are not considered here. The improvement in the accuracy of these models over a persistence forecast depends on the forecast horizon. For horizons of less than 2.5 h persistence forecasts usually outperform forecasts generated using the output of NWPs [53]. Hence for the 2 h forecast horizon using persistence forecasts is appropriate.

The predictability of the centralised and diversified power time-series can be expressed as a single numeric using the root mean square (RMS) forecast error as presented in Equation 4.24. The RMS forecast error for the centralised subset is 43.2 MW and for the diversified subset 29.1 MW a difference of nearly 50%.

$$FE_s = \sqrt{\frac{1}{T-2}\sum_{t=1}^{T-2}(P_{t+2} - P_t)^2} \tag{4.24}$$

Where FE is the root mean squared forecast error, and t has units of hours.

Probability distributions of forecast errors are presented in the lower right graph of Figure 4.5. A black solid line is added to show the probability of a once per day event, a black dash dotted line to show once per week events, and a black dotted line to show events with a recurrence interval of once per month. The analysis shows that forecast errors for the distributed subset are less than for the centralised subset for all recurrence intervals. Also, forecasts are equally underestimates or overestimates, and the absolute magnitude of the underestimates is greater than for overestimates.

4.5 SUMMARY

The benefits of the diversification of WPPs has been demonstrated using measurements made at WPPs. However, the time-series used are limited in their temporal span, and do not necessarily cover periods when the power system has been placed under stress or periods when wind power output might have been extreme (such as during dry years, stormy periods, or during periods of prolonged calmness). Further, the number of WPPs constructed in New Zealand is insufficient to provide time-series to enable differences in the scenarios to be assessed. To determine the benefits of the spatial diversification of wind energy in New Zealand it is necessary to simulate power output time-series for WPPs.

Chapter 5

WIND

Wind power time-series can be simulated using many approaches such as re-sampling measured data (boot strapping), or extrapolating upon measured properties using statistical tools. However, it is desirable that the simulated time-series are temporally coincident and spatially consistent with other sources of generation and demand; such that combined effects on the power system can be determined. Hence, it is preferable to develop a method that uses historic or hindcast time-series. Hindcasts for wind power are not readily available, but they are for wind speed which can then be converted to power.

5.1 WIND

The wind is the movement of air across the surface of the Earth. The air moves because of pressure differentials in the atmosphere. The pressure differentials are caused by convective motion, induced by temperature differentials, and by tidal forces. The temperature of the air is dependent on heating from the sun, radiation to space, the heat capacity of the surface (ground or water), and the albedo of the surface. The heat derived from the sun, or solar flux, is dependent upon the angle subtended between the ground surface and the sun, the cloud cover, and atmospheric composition (primarily dependent on the amount of water vapour, or humidity, and also dependent on other aerosols and dust). The heating of the Earth causes air to become buoyant and rise forming convective currents. Non-uniformity in these currents results in areas of higher and lower pressure.

The heating of the Earth's surface not only causes convection but also causes water to evaporate. The water vapour is convected with the movement of the air parcel into which it evaporates. As the air parcel changes in altitude and location so will the pressure and temperature. The quantity of water vapour the air can dissolve is dependent on the temperature and pressure. If the temperature and pressure of the air parcel fall sufficiently, the air parcel will becomes saturated, and the water vapour will condense to form clouds and eventually rain will fall. Clouds change the amount of sunlight that reaches the Earth's surface, and also reduces the amount of infrared radiation escaping from the Earth back to space thus changing the heat flux. Clouds may not form in uniform sheets, around the edges of the clouds there will be rapid changes in heat flux and the resulting changes in convection may in turn generate more clouds, and thus constitute a feedback loop.

The rate of evaporation is dependent on the surface, over oceans water will evaporate readily, while over desert there is less water to evaporate. The surface type also affects the rate of heat absorption; the sea has a large heat capacity (as heat is conducted into the water) whereas the ground has poor heat conductivity and thus the surface heats rapidly in the sun. This difference in heat capacities leads to heat flux differentials at the coast, differences in convection currents, and surface pressures, which force winds referred to as sea and land breezes.

The albedo and hence heat flux is dependent on the coverage of the Earth's surface. Areas that are covered by snow and ice have the highest albedo and reflect a large amount of the solar flux back into space. By contrast, the ocean has a low albedo and absorbs most of the solar irradiance. Albedo is also affected by vegetation, plants that cover a large portion of the Earth's surface impact convection and the atmosphere. These plants may have seasonal growth patterns leading to a regular annual cyclic pattern of albedo. The albedo of the ocean is also altered by living creatures. Life on Earth is an intrinsic part of the dynamic atmospheric system.

The topography affects the atmosphere and wind; funneling wind through valleys and over mountain passes and stagnating air masses over continents in summer. The topography not only directs the movement of air but also affects the composition of the air. If air masses are forced over mountains, the pressure in the air mass drops and the air may become saturated. Thus clouds will form over the mountains and precipitation occurs. Once the air descends from altitude after crossing a mountain range, the air will warm up as the air has gained the latent heat of evaporation due to the loss of the water vapour. This effect produces a Foehn wind commonly referred to as the Nor'wester on the east coast of both the North and South Islands.

Tidal forces are imparted on the Earth by both the moon and the sun. As the Earth rotates within the gravitational fields, fluid (the oceans) and gas (the atmosphere) are pulled and released generating pressure differentials. Air from regions of higher pressure attempts to move toward the regions of lower pressure to restore a state of equilibrium. However, at non-polar and non-equatorial locations as the Earth rotates underneath the air its path toward the low pressure is deflected. This deflection is the Coriolis effect.

While the solar flux provides the energy to the atmosphere, the lack of solar flux at night has a large influence on the atmosphere. At night the Earth's surface is relatively warm compared with the depth of space, and hence radiates heat. The atmosphere insulates the Earth (particularly if there are clouds), however the heat loss causes temperatures to fall. The rate at which temperatures drop is dependent on the heat capacity of the surface, so that land surfaces temperatures will fall more rapidly than the sea surface, thus the sea breeze convection that forms during the day will reverse at night.

The interaction between the land, sea, and air is complex and dynamic. The dynamic character of the atmosphere is observed everywhere from the smallest fluttering of a blade of grass to the progression of cyclones over the southern ocean and is referred to as the weather, and the long term tendency of the weather as the climate.

5.2 WEATHER AND CLIMATE

Readily observable weather phenomena are commonly classified by their scale of influence; three scales are typically applied. The largest scale encompasses weather systems that have influence over 1000 km or more and are typified by cyclones and anti-cyclones. These features are referred to as *synoptic* or *Macro-scale* systems. Weather phenomena that have spatial extents between tens and hundreds of kilometres and are broadly referred to as *Meso-scale* systems. Such phenomena include sea-breezes and mountain winds. Weather phenomena affecting areas approximately one kilometre in extent are classified as *Micro-scale*. Micro-scale weather phenomena include small cloud features and dust devils or willy willys.

The physical size of weather phenomena has an intrinsic relationship to the time during which the system evolves and progresses over the surface of the Earth. Synoptic scale events such as cyclones in the roaring forties have a typical span of influence at individual locations of between 2 and 7 days. Meso-scale phenomena typically have temporal scales of a day, such as sea breezes which are generated by diurnal changes in convection. Micro-scale events such as Valley winds may have the same diurnal pattern as sea-breezes, however their peak intensity is usually a brief period such as a few hours after sunset.

The climate describes the pattern of weather over a long term period at a particular location. Beside the fact the climate norm may change over time, there are annual patterns of changes in the weather due to the rotation of the Earth around the sun on its tilted axis. The progression of the Earth changes the local solar flux, while this results in seasons, the seasonal pattern of weather is also observed as seasonal patterns in wind speed. Typically wind speeds in NZ peak during Spring. Longer term changes in wind speeds can also occur because of alternating large scale climate modes such as the El Nino, La Nina Southern Oscillation (ENSO). Further oscillations that may affect the NZ climate include the Interdecadal Pacific Oscillation and Antarctic Oscillation; these events have decadal or longer time scales.

The climate norm is known to change dramaticaly over time; 18,000 years ago ice sheets covered large tracts of NZ, whereas presently the climate is in a relatively warm period. The present warm period is exacerbated by high concentrations of greenhouse gases (carbon dioxide and methane) caused by the burning of fossil fuels [89]. The reaction of the atmosphere to anthropogenic changes to the global environment will lead to changes in climate and wind patterns will likewise change.

The weather and climate system is complex involving many forcings and feedbacks. The complexity results in a chaotic system, whereby the smallest changes in present conditions may grossly effect the future state of the weather and climate. Chaos is prevalent at all scales of weather and climate.

5.3 THE BOUNDARY LAYER

The boundary layer, when referring to the atmospheric, is that part of the atmosphere where flow properties are dominated by the influence of the ground. The flow structure in the boundary layer is dependent upon atmospheric forcing (geostrophic wind), topography, ground cover, and heat flux. Due to friction the wind velocity at ground level is zero and increases with altitude. The description of the increase is termed the wind shear profile. Wind turbines, as installed in NZ, are mounted on the ground and are of a height such that they can be considered to always be within the boundary layer.

The geostrophic wind is a theoretical wind velocity derived from surface pressures (i.e. it is the wind speed that would be inferred using a physical model and measurements of atmospheric pressure from meteorological stations). The geostrophic wind is representative of the wind speed at an altitude where the wind speed is not influenced by micro-scale factors such as local topography and can be reconciled with the wind speed expected at the top of the boundary layer.

$$\overline{v(z)} = \frac{u^*}{\kappa}\left[\ln\left(\frac{z}{z_0}\right) + \phi(z, z_0, MO)\right] \tag{5.1}$$

Where $\overline{v(z)}$ is the mean wind speed at height z, u^* is the friction velocity, κ is the Von Karman constant, ϕ is a stability term, z_0 is the surface roughness length, and MO is the Monin-Obukov stability parameter.

The degree to which the ground places drag on the atmosphere is represented by the log law as shown in Equation 5.1, where the drag or momentum deficit is characterised by the surface roughness length (z_0). The surface roughness length is dependent upon the type of ground cover. For terrain that is very smooth, such as sand flats, the surface roughness length is typically very small (in the order of 0.005m). In areas where there is forestry on a flat plane the effective surface roughness length may be as large as 1m. In NZ WPPs are typically located on farmland where the surface roughness length will be in the order of 0.1m.

The surface roughness is not constant throughout the year. Plants have an annual growth pattern and increase their height and vegetative matter during spring and summer. Deciduous

trees lose all their leaves in winter and hence there is a very large change in their effective surface roughness. While in NZ the dominant native vegetation is evergreen the seasonal change in surface roughness length is still important.

The atmospheric log law profile is representative of flow conditions over flat planes. However, most WPPs in NZ are constructed in areas with more complex topography. Wind velocities increase over ridge lines and decrease in deep gullies. The topography guides the flow of air and generates turbulence and eddies where the velocities are high and terrain steep.

Boundary layer velocity profiles that are representative of the log-law shear profile require adiabatic conditions, where there is zero heat flux from the ground to the air. In this case the boundary layer is said to be neutral. If the ground is warmer than the overlying air then there will be a positive heat flux from the ground, the air at the ground surface becomes warmer and hence buoyant. The buoyant air introduces convective currents and increases the turbulence and mixing within the boundary layer. This turbulent mixing increases the effective drag on the atmosphere and increases the effective height of the boundary layer. If the air is warmer than the ground then there will be a negative heat flux, mixing and turbulence will decrease, the boundary layer will thin, and wind speed profiles become steeper.

The stability of the boundary layer changes according to a diurnal cycle. As the ground is warmed by the sun during the day and the boundary layer becomes unstable, this lasts into the night. During the night the ground radiates heat back to space and cools. In the early hours of the morning the ground will have lost sufficient heat so that its surface temperature is less than the temperature of the overlying air and a stable boundary layer develops. Thus it is usual for wind speeds near to the ground to be higher in the early hours of the morning and lower in the afternoon and evening. Heating during the day and heat loss at night is reduced if there is cloud cover, and the cloud cover is itself affected by the heat flux.

Adding complexity; effects such as cloud cover, seasonal changes in solar flux, and advection of the air over different terrains modify the boundary layer velocity and turbulence profiles.

5.4 TURBULENCE

The convection and mixing of air causes eddies to form that are advected in the bulk flow of the air. The collective of these eddies is termed the turbulence. Mathematically the wind velocity at a point in the air can be described as the sum of the mean or bulk flow velocity and the departure from the mean or the turbulent component.

While the turbulent component of wind speed has a complex spectral composition it is usual to describe the magnitude of turbulence using a single metric; the turbulence intensity. The turbulence intensity is defined as the ratio of the standard deviation of wind speed to the mean wind speed measured in a 10 minute interval with a 3 second sampling period.

$$v(t) = \overline{v(T)} + v'(t) \tag{5.2}$$

Where $\overline{v(T)}$ is the mean or bulk velocity across time interval T, and $v'(t)$ is the turbulent component.

Turbulence is induced by convective currents particularly within unstable boundary layers, by air flowing over and around hills, trees, and other obstacles. The magnitude and scale of the turbulence depends upon the size of the obstacles, the heat flux and forcing conditions. The characteristic size of the eddies formed is described using a length scale.

In cyclones the motion of the bulk flow is largely planar or confined to two dimensions. Note that not all chaotic flows are turbulent, and that the propagation of cyclones and weather systems is a chaotic process. However the convective cells that form within cyclones are turbulent motion. The largest of these convective cells can have length scales as great as several kilometres and are

defined as mesocyclones. Some large scale turbulent motion can be readily observed in clouds, as formation of breaking waves in the lee of mountain ranges. These waves are referred to as atmospheric inertial gravity waves.

The terms eddy and vortex are very similar and often used interchangeably. An eddy occurs where localised flow is counter to the bulk flow. A vortex is a region in a flow where there is spinning motion about an axis. The subtle differences lead to the terms being used to describe phenomena that are not necessarily comprehensively described by either term.

To describe generation and dissipation of turbulence it is useful to consider an object placed in a wind tunnel. Upstream of the object the flow, in a well constructed wind tunnel, should be laminar. There are no eddies in the flow and no mixing occurs. As the flow interacts with the object particles are forced to diverge from their straight streamlined path and speed up as they flow around the obstacle. Behind the obstacle an area of low pressure is generated and the particles are accelerated toward the low pressure. However, due to the conservation of momentum and viscous forces, particles can not immediately alter their velocity. Instead the particles track toward the area of low pressure along a circular path changing some of their momentum to angular momentum. Due to the viscosity of the air, the particles move in a somewhat organised manner and form vortices that have a maximum diameter approximately equal to the diameter of the object. These vortices have an axis of rotation that is not necessarily a straight line. As the vortices propagate they elongate along the direction of their axis of rotation in a process known as *vortex stretching*. The elongation of the vortices and the requirement for conservation of angular momentum results in the diameter of the vortices decreasing in the manner that a pirouetting ballerina increases speed when raising her arms into a spike above her head. This process leads to a decrease in the diameter of the vortices, which also represents a reduction in wavelength and increase in frequency.

As vortices are stretched they become exposed to interaction with other vortices in the air. The interactions with (or interference from) other turbulent structures leads to vortices separating into smaller component vortices. The components that result then stretch and separate leading to a cascade of vortices. As the cascade of vortices progresses the characteristic diameter of vortices reduces, thus the characteristic length scale decreases, and the frequency of fluctuations from the mean flow increases. The terminal result due to the cascading of vortices is the dissipation of turbulence as heat. This cascade is termed Richardson's cascade, and the transfer of kinetic energy to heat is termed eddy dissipation.

In circumstances where the rotational direction and size of vortices are near synchronous the interference between vortices can lead to the vortices reinforcing their common rotational direction and merging. The cascade is not necessarily uni directional but rather describes the overall tendency for vortices to dissipate.

The overriding chaotic nature of the Richardsons cascade means that structures within the initial vortex formation are quickly eroded. The result is that the nature of turbulent motion is dependent not on initial conditions or locality but rather on the properties of the air itself. This property was first conjectured by Kolmogorov and is termed similarity. The amount of energy contained at each frequency, or scale, is described using Kolmogorov's theorem as shown in Equation 5.3, and is dependent upon the rate of energy dissipation which in turn depends on the viscosity of the air. The characteristic size of vortices (or length scale) at which dissipation from kinetic energy to heat occurs is dependent upon the molecular viscosity. The cascade of the eddies can also be described as an increase in the entropy of the flow.

$$E(j) = c\nu^{\frac{2}{3}} j^{\frac{-5}{3}} \tag{5.3}$$

Where E is energy, c is a constant, ν is the rate of energy dissipation, and j is the scale.

In turbulent flow there is continual formation, propagation, separation, and dispersion of vortices.

Thus within the turbulent flow there is a distribution of vortices with differing diameters or length scales. And, this distribution of vortices with different length scales is evident in the frequency spectra.

The distribution of frequencies forming the Power Spectral Density was measured in an oft cited experiment conducted by Van der Hoven [90]. The Van der Hoven spectrum as shown in Figure 5.1 is particularly useful in illustrating the energy contained in wind at varying time-scales. The spectrum, at the left hand side, shows a peak at the synoptic scale, due to the progression of weather systems across the site and has a periodicity of approximately a week. Another peak occurs at a frequency equivalent to a day due to diurnal changes in heat flux. There is a gap in the energy spectrum for frequencies between the daily peak and higher frequencies where the turbulent peak occurs.

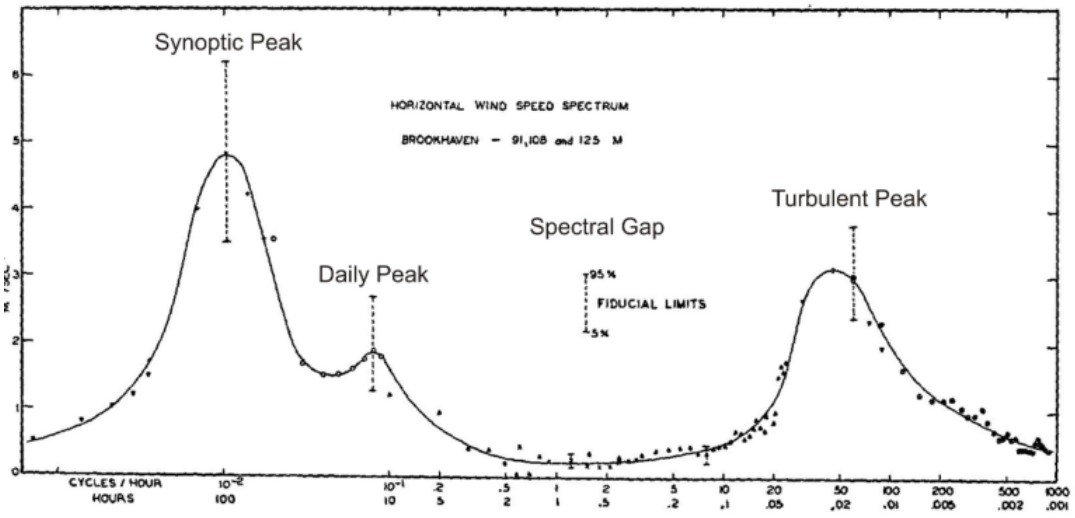

FIG. 1. Horizontal wind-speed spectrum at Brookhaven National Laboratory at about 100-m height. (See table 1 for date and time.)

Figure 5.1 Van der Hoven spectrum of wind speed (reproduced from [9]). Note that the scaling of the y-axis is not consistent with the scaling used in other periodograms.

5.5 WIND SPEED MEASUREMENT

The atmosphere has three spatial dimensions and wind is three dimensional. However near the ground the vertical component of wind velocity is relatively small and is typically ignored. It is usual to describe the bulk wind using a wind speed scalar and a wind direction. Wind turbines yaw to the wind direction so (neglecting yaw error) react only to the wind speed. To describe the wind resource it is common to apply a wind speed and direction frequency distribution, which can be graphically illustrated using a wind rose.

Wind speed measurements are best made using meteorological equipment that has been designed to measure the free stream wind speed. This means that the equipment needs to have as little interference to the flow of air as practical. Standards for meteorological measurements made for the purpose of power output calibration for wind turbines are covered in IEC61400-12 [35].

Measurements made at prospective WPP sites in NZ generally conform to IEC61400-12. The

exact configuration of masts depends upon the developer's intended development envelope. In NZ a guyed tubular or lattice mast is commonly used with cup anemometers and wind vanes mounted on cross arms with up-stands. The highest anemometer is usually mounted to be at least $\frac{2}{3}$ of a proposed turbine hub height and range from 30 m to 80 m. The masts are located in areas that have been identified as suitable for construction of a WPP, are in well exposed locations, and free from interference from obstacles such as trees. Due to the expense of erecting masts as tall as 80 metre, it is common for measurements to be made at 10 m when prospecting wind resources.

The IEC 61400-12 standard prescribes a 10 min period for the measurement of wind speeds with statistics calculated using 3 s samples. The turbulence intensity is calculated as the ratio of standard deviation of the 3 seconds samples to the mean recorded in a 10 minute period. The gust wind speed is maximum recorded 3 s sample in a 10 min period. While the measurement of wind speeds for the purposes of developing WPPs is well prescribed, the majority of wind measurements are made without the purpose of developing WPPs. As such the quality of measurements is not necessarily equal to that specified in the IEC standard.

The National Institute of Weather and Atmospheric research (NIWA) operates a network of meteorological stations located throughout NZ. The records from these stations are held in the Cliflo database. These meteorological stations have been sited to measure environmental conditions representative of those experienced by activities undertaken in the local area. Stations sited near towns will be located in a position that is generally representative of the town. A station located near a major forest may be sited to give the best representation of fire danger in the local area. Thus meteorological stations are not often located in exposed locations and thus wind speed measurements can be compromised. Measurements made at meteorological stations are typically at a 10m height using cup anemometers that have historically been developed for robust operation, although nowadays the anemometers employed are typically identical to those used in wind energy prospecting.

All wind measurements are subject to changes in exposure that occur over long periods as vegetation grows and is cleared, buildings constructed, and land usage around masts changed. This is particularly relevant for measurements made in locations that are not chosen for their exposure. Further changes in measurements may result from degradation of the anemometry either from bearings seizing or damage to the anemometers caused by the build up of ice.

While wind speed can be measured directly using anemometers it is also possible to infer wind speed using remote measurements. Localised remote sensing equipment such as Lidar (Light Detection and Ranging) and Sodar (SOnic Detection and Ranging) are typically mounted on the ground directly below the point at which the wind speed measurement is being made. Rather than making a single point measurement Lidar and Sodar infer wind speed from a volume of air, complicating inference of second order quantities such as turbulence [91]. Rawinsonde are used to infer wind speeds by radio tracking a balloon let aloft and are useful in measuring wind speed at altitudes above what is practical with meteorological masts. Remote wind speed measurements are also made using satellite based instrumentation such as Synthetic Aperture Radar (SAR) which measures back-scatter from the sea surface, and may be useful for inferring wind speeds at offshore WPP locations [92]. Satellites are also used to track clouds and infer high altitude wind speeds from their movement. A less direct measurement of wind speeds is possible using measurements of surface pressure; measurements made at meteorological stations can be combined to define a pressure surface and from this the geostrophic wind inferred.

Changes in types of wind speed measurements in a data set has a significant effect on long term wind time series [93]. Changes in the types of anemometers used by the United Kingdom meteorological office have affected the long term average wind speeds recorded at meteorological stations with significant over estimation of wind speeds resulting from the use of pressure tubes in the 1960's and Munro Mk4 type anemometers in the 1970's.

Most wind measurements made in NZ are in units of meters per second, however it is common for measurements derived from historic or marine sources to recorded in knots. The conversion of units and subsequent rounding can introduce errors in to the recorded wind speeds. Further, the digital measurement of wind speed by data loggers results in discretisation both in time and in scale. Dependent upon the manner in which data loggers have been programmed the discretisation can be relatively coarse; this can be particularly problematic when examining turbulence.

5.6 WIND SPEED TIME-SERIES

As there is no set of measured wind speed time-series suitable for supporting the analysis here, it is necessary to find alternative sources of wind speed time-series. "State of the art" integration studies, such as the Hawaiian integration study use hindcasts from Numerical Weather Prediction (NWP) models to provide wind speed time-series. There are many NWP models run by weather forecast providers world wide and in NZ. NWP models differ in their physics, data assimilation, temporal span, and spatial resolution.

NWP models use physical models of the atmosphere incorporating the principles of conservation of mass (continuity), conservation of momentum, and conservation of energy. The principles are modeled using the Navier-Stokes equations and are coupled with equations that describe the first and second laws of thermodynamics (conservation of energy and conservation of entropy). These equations are used to control the evolution of a simulated atmosphere of which the domain can cover either the entire globe or some smaller region. A model with a domain covering a smaller region is referred to as a Limited Area Model (LAM). Typically NWP models use a domain delineated using cells defined by latitude, longitude, and a vertical coordinate. The vertical coordinate is defined by constant pressure surfaces (the altitude coordinate is variable) and the models are solved using finite differencing. Another common computational fluid dynamic model type is the finite volume method where cell volumes are held constant and pressure varied. The models may use sub-models or parametrisations to allow greater accuracy in simulating the physics of particular atmospheric processes such as those that occur in the boundary layer or in clouds. This type of computational model is termed a deterministic model.

NWP model solutions are intrinsically dependent upon their initial state, thus it is critical that the data used to initiate a model run is representative of the atmospheric state. To define the initial state, data is assimilated from varying sources, including surface pressure, temperature, and humidity measurements. Data may also be assimilated from rawinsondes, SARs, and surface wind speed and direction measurements from select meteorological towers. Although many different NWP models are run throughout the world, the initialization data is usually common, collated through the World Meteorological Organisation (WMO). Data assimilated into a NWP help define a model initiation state, however this state may be very heterogeneous, as individual measurements may reflect local extremes. Thus it may take several model iterations to evolve an atmospheric state that is closer to a true norm.

NWP models are usually run to produce weather forecasts with horizons of several weeks. Models may also be run to assess future or historic climates. NWP models themselves evolve as increases in computational power allow greater resolution, and better physical parametrizations. Thus their solutions may not be temporally consistent. The use of a stable NWP model for simulation of historic weather patterns is termed re-analysis and produces hindcasts of the atmospheric state. It is this type of model that is useful for supporting integration studies.

The extent of the NWP domain is a trade-off between spatial coverage and resolution. Global models require a very large number of cells, and typically have limited resolution, as each cell is large. Within the area of each cell the weather patterns may diverge significantly from the cell mean; to achieve better correlation with local weather observations LAMs (LAM), or meso-scale

models, are used. LAMs are often nested within a global model, such that their initiation state is defined by the global model and evolved Model Output Statistics (MOS) may feed back to the global model.

LAMs are used to increase the resolution of wind flow analyses, as used in the Hawaiian Wind Study in Section 2.4.1. Primarily the mesoscale models have been applied so that the effects of topography on wind resources are well characterised. The process uses nested meso-scale models in order that the final resolution covering only the areas of interest is sufficiently high to allow diversity in wind speeds between parts of the WPPs to be resolved. Other methods commonly used for wind flow modeling include finite volume codes such as Windstation, and linear flow solvers such as WAsP (which employs the European Wind Atlas methodology [94]) and MS-Micro [95].

The temporal resolution of NWP models is limited, not only by the processing power, but also due to deterministic assumptions. The deterministic approach does not explicitly resolve turbulence at scales smaller than the models spatial resolution. And, the association between spatial and temporal spans of vortices means there is a limit to the temporal resolution. Further, the atmosphere does not evolve its bulk properties faster than a certain rate and it is not particularly useful to derive MOS at high temporal resolutions. Typically NWP produce MOS at 6 h intervals.

While there are many NWPs, MOS are not always readily and freely available. A search of web-based re-analyses has found the European Centre for Medium range Weather Forecasting (ECMWF) ERA-interim product is the most suitable for supporting integration studies in NZ [96]. The ERA-interim product has a long temporal span (January 1979 through present, data through to 01 May 2013 are used here), a relatively high spatial resolution for a global model (the model uses the T255 grid which has a spatial resolution of approximately 80 km or 0.7° x 0.7°), and a temporal resolution (6 hour). Grid points for the ERA-40 analysis are shown as magenta dots in Figure 5.2. The MOS derived from the ERA-interim product for this study are the 10 m latitudinal and longitudinal wind speeds. The 10 m level winds are representative of the wind speed at a height of 10 m across a surface that is topographically smoothed across a region equal to the cell size.

As the time-series from the ERA-interim have coarse spatial resolution, are not representative of turbine hub height, and have a temporal resolution insufficient for UCED studies, it is necesssary to interpolate, scale, and impute the time-series such that wind speed time-series representative of the wind incident on a WPP, with a temporal resolution of 5 min, can be derived.

State of the art integration studies such as the Oahu study have applied mesoscale models to increase the spatial resolution from NWPs. This approach has also been adopted in NZ. For instance, the NZ synthetic wind speed time-series were developed using MOS from the New Zealand Limited Area Model (NZLAM) run by the National Institute of Water and Atmosphere (NIWA) [97]. However, the resolution of the NZLAM is not sufficient to characterise the effect on wind flow from topography local to meteorological mast measurements. In developing the NZ synthetic wind dataset a scaling function was applied based on forming a type of sine function regression between MOS and measurements from the meteorological masts. It is possible to accomplish mesoscale modelling of sufficient resolution such that interpolation and scaling is unnecessary, as applied in the Oahu study. However, some adjustment is generally still necessary to remove model biases.

It is not practical within the course of this thesis to run a mesoscale model, as this in itself is a substantial task. Instead interpolation, scaling, and imputation schemes are implemented using numeric tools.

5.7 WIND SPEED DATA

For the ERA-interim derived wind speed time-series to be appropriately interpolated, scaled, and imputed it is necessary to correlate MOS with measured data. The measured wind speed time-series must be representative of the wind speed incident across an entire WPP. WPPs in NZ have been constructed in locations that are exposed to winds deriving from the passage of synoptic weather systems, hence the measurements need to have been made in well exposed locations using suitable anemometry. To ensure measurements are from suitable locations, data from meteorological masts that have been erected for the express purpose of prospecting wind resources for WPPs have been used.

A set of wind speed time series from 22 meterological masts spread throughout NZ has been collated. The location of the masts is shown in Figure 5.2. The data set has been collated to be as similar as possible to that collated for the Wind Generation Integration Project [67] and permissions were sought from data providers for use in this study. This data set is referred to as the WGIP dataset. The wind speed time series are from sites investigated for potential WPP development and are in exposed locations typically with high mean wind speeds and low turbulence intensities. The wind speed time series have been measured using cup anemometers, with a sampling period of 10 minutes, mounted at the top of each the masts at heights ranging from 10 m to 80 m above ground level. As the data are commercially sensitive, they have been normalised to have a mean of $8\,\mathrm{m\,s^{-1}}$, and the exact locations and heights of the masts cannot be released. However, proxy co-ordinates for each mast have been assumed so that spatial relationships can be explored. The proxy co-ordinates are within 3 km of the actual locations. The data have been cleaned so that erroneous or missing values have been identified and marked with error values. Details and data coverage is presented in Table 5.1.

Mast	**Start Date**	**End Date**	**Data coverage**	**Used**	**Imputed**
Auckland 1	13/02/2004	31/08/2005	0.99	Yes	0.3%
Central Otago 1a	01/07/2004	01/07/2005	0.99	Yes	0.4%
Central Otago 1b	01/07/2004	01/07/2005	0.99	Yes	0.2%
Marlborough 1	01/01/2004	09/10/2005	0.99	Yes	1.8%
Northland 1	01/01/2004	31/08/2005	1.00	Yes	0.0%
Northland 2	24/06/2004	21/07/2005	1.00	Yes	0.0%
Northland 3a	01/07/2004	28/04/2005	0.95	Yes	27.2%
Northland 3b	21/10/2004	01/07/2005	0.99	Yes	0.6%
Southland 1	26/01/2004	05/03/2005	0.99	No	46.8%
Southland 2	01/07/2004	01/07/2005	0.88	Yes	7.4%
Southland 3	01/07/2004	01/07/2005	0.95	Yes	4.7%
Tararua 1	01/01/2004	30/06/2005	0.92	Yes	12.1%
Tararua 2	11/05/2004	10/07/2005	0.90	Yes	14.2%
Tararua 3a	05/10/2004	01/07/2005	0.99	Yes	0.4%
Tararua 3b	24/09/2004	01/07/2005	0.98	Yes	0.6%
Waikato 1	05/03/2004	31/08/2005	1.00	Yes	0.0%
Waikato 2	10/09/2004	31/08/2005	0.99	Yes	0.7%
Waikato 3	15/12/2004	31/08/2005	0.99	Yes	21.7%
Wairarapa 1	07/04/2005	01/07/2005	1.00	No	66.3%
Wellington 1	01/01/2004	01/10/2005	1.00	Yes	0.1%
Wellington 2	01/01/2004	31/08/2005	1.00	Yes	0.3%
Wellington 3	01/07/2004	01/07/2005	1.00	Yes	0.1%

Table 5.1 Wind Generation Integration Project data set

As some numerical analyses performed using the data-set requires that that the data are coinci-

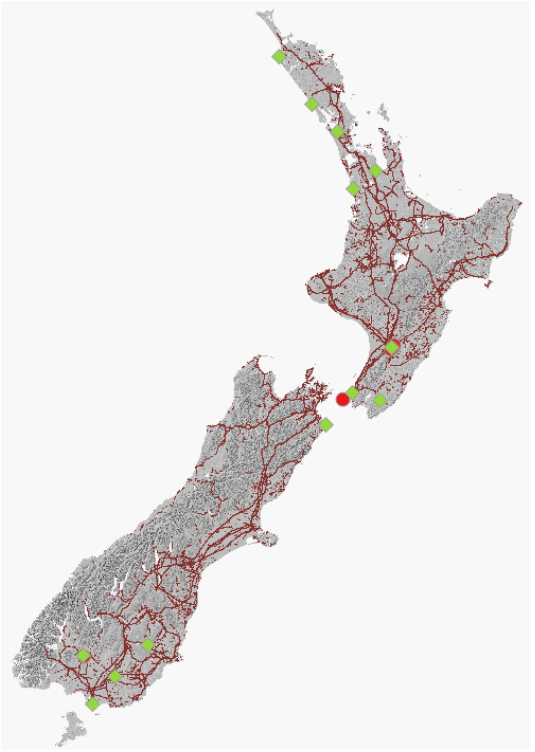

Figure 5.2 Location of WGIP masts (green diamonds) and EA WPPs (red circles)

dent and continuous, some manipulation has been performed. A period from 25^{th} October 2004 through 29^{th} June 2005 has been selected, two time series have been omitted, and missing values have been *imputed* using multiple linear regression based upon as many other coincident time series as possible. The resultant data-set consists of wind speed time series from 20 meteorological masts distributed throughout NZ with 35,712 samples (248 days).

The effect on the data of imputation using multiple linear regression is to reinforce correlations and not implicitly replicate auto-correlations. However, auto-correlations are replicated to some degree as the time series used to generate the approximations have their own auto-correlation structure.

Statistics from the WGIP dataset are presented in Figure 5.3. The top left graph presents probability distribution functions for each site, note that there are too many sites to assign individual colours and hence many have identical coding. A thick black line describing a Weibull PDF with shape 1.8 and scale 9.8 is also shown (wind speed probability distributions are often well approximated by a Weibull). The top right graph presents correlograms; these show that (as seen for the power data) the wind speed time-series have a high degree of persistence and the auto-correlation declines in an exponential manner to near zero after one day. The bottom left graph shows the Power Spectral Density of the wind speed time-series. This shows the periodograms are similar for all wind speed time-series with a slope close to that of the Kolmogorov law ($\frac{-5}{3}$) as referenced by the thick black line.

The relationships between wind speed time-series are presented in Figure 5.4 using scaled correlations. Each line represents the scaled correlation function between pairs of masts (there are a total of 190 pairs) and the lines are coloured according to the separation distance between the masts. The wind speed time-series correlations are a function of the averaging period, and even for masts that are very close together correlations are negligible at scales less than one hour and gradually increase as the scale increases. Note that correlations are sometimes negative for masts separated by more than 1000 km around scales of 1 day.

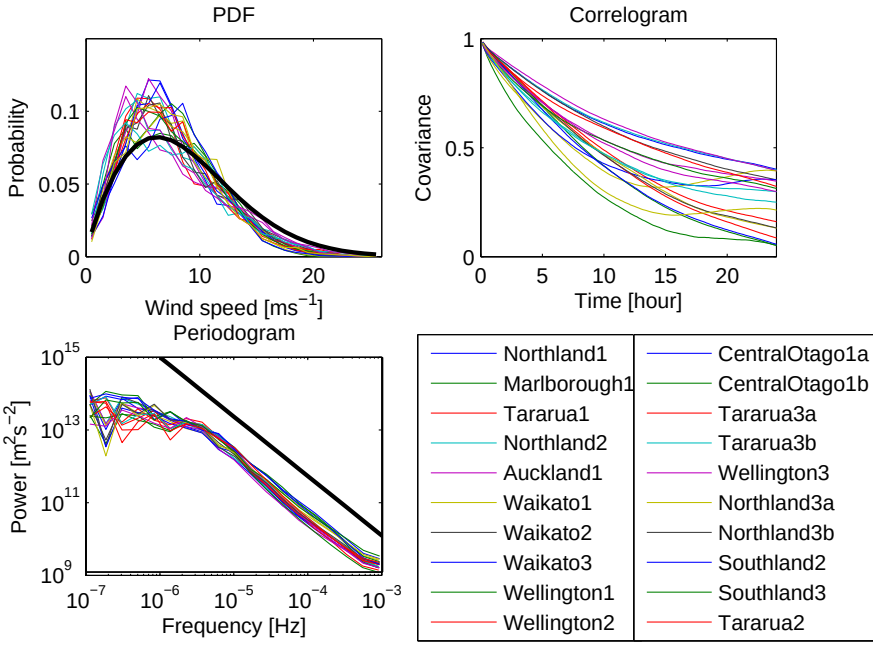

Figure 5.3 Statistics of WGIP data. The top left graph shows probability density functions with the black line showing a representative Weibull curve. The top right presents correlograms for each site. The lower left graph shows periodograms with the black line providing the slope of the Kolmogorov spectrum is offset from the measured spectra for comparison.

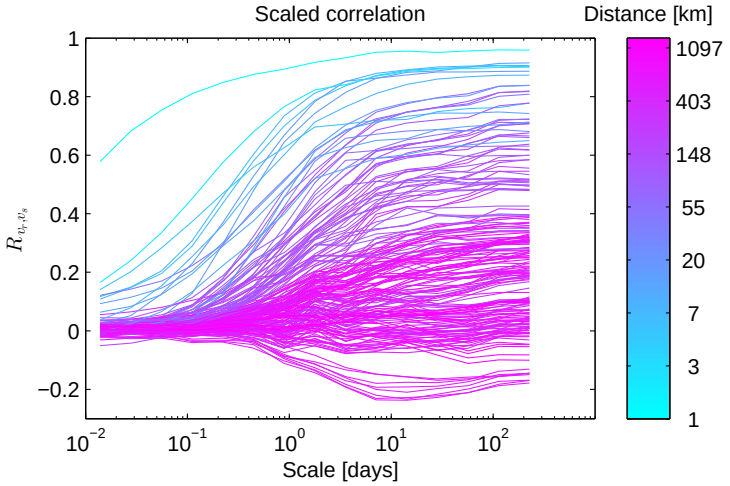

Figure 5.4 Scaled correlations of WGIP data

5.7.1 Wind direction

Wind turbines yaw into the wind and hence power output is somewhat independent of direction. However, topography and obstacles in the direction of fetch will impact on the turbulence and wind shear profiles, thus wind direction has a minor effect on power at individual turbines. Conversely, WPPs' turbines are located so that they produce the greatest amount of energy, thus turbines are usually positioned such that the greatest topographic speed ups occur in the prevailing wind direction. Further, sites in close proximity have similar topography and thus have some similarities in WPP design; hence power production from WPPs is not entirely independent of wind direction.

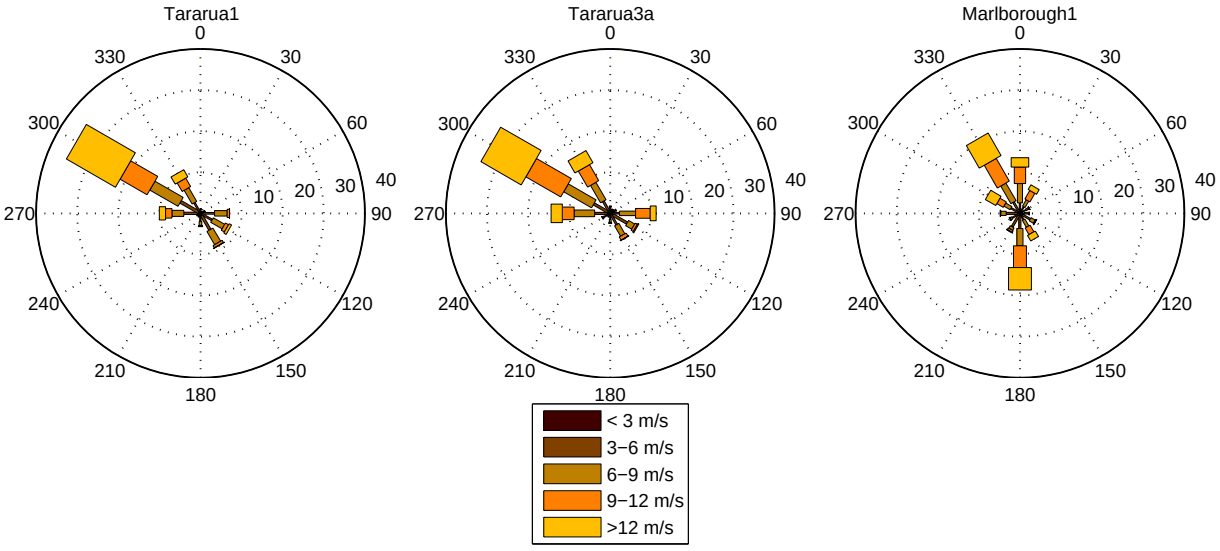

Figure 5.5 Selected wind roses from WGIP data

To illustrate similarities in wind resources for sites that are located in close proximity, three wind roses are presented in Figure 5.5. Each wind rose presents a wind speed and direction time-series binned by wind direction, using 30 degree sectors. These are subsequently binned by wind speed, and presented as a stacked bar radiating in the associated direction. The roses show that the sites in the Manawatu (Tararua1 and Taraura3a) have similar prevailing North-Westerly wind directions with little wind fetched from other directions, unsurprising given the masts are 7.5 km apart. The wind rose for Marlborough is quite different, with two predominant wind directions, one North-Westerly through Northerly and the other a Southerly. Marlborough mast is 200 km away from the Manawatu and located on the opposite side of Cook Strait.

5.7.2 Interpolation

The ECMWF Numerical Weather Prediction model produces wind speed and wind direction hindcasts on a $0.7^\circ \times 0.7^\circ$ grid, equating to a spatial resolution of approximately 70 kilometers. To infer the wind speed and direction at a specific location not co-incident with the grid requires two dimensional spatial interpolation.

There are many interpolation schemes, the simplest being nearest neighbour; where for each interpolant the closest grid vertex is found and variables from this used as predictors. A particular problem with the nearest neighbour approach occurs where two sites of interest are located nearby is that they may derive identical wind speed and wind direction predictions; thus correlation between the pair will equal to one. Using data from meterological stations across the

United Kingdom, Luo in 2008, assessed the performance of seven interpolation schemes, including trend surface analysis, inverse distance weighting, thin plate splines, and Kriging. Of these methods Kriging was found to be the best interpolation scheme [98]. Further methods of spatial interpolation were explored by Gorman, charcterising wind speeds near tropical cyclones. The interpolation schemes assessed included Fourier smoothing and Empirical Orthogonal Functions [99].

An exhaustive comparison of interpolation methodologies is not undertaken here, however comparison of a small number of the schemes is presented to illustrate the relative accuracy of the schemes and aid in the selection of the appropriate scheme. The methods explored here include nearest neighbour, bilinear interpolation, and cubic spline. All methods are as provided in the Matlab R2013a interp2 function [100].

The interpolation methods are applied by converting the wind speed and wind direction vectors derived from the ECMWF 10m product to Cartesian co-ordinates (easterly and northerly winds). The interpolation scheme is applied to find the vector components of wind at each meteorological mast location. The Cartesian components are then converted to wind speed and direction.

Bilinear interpolation requires that the input is a regular grid. Hence the longitude and latitude co-ordinate system from the ERA-interim model is assumed to be flat. For each Cartesian wind component linear interpolation is performed longitudinally, and then latitudinally to find a planar tilted surface. The Cartesian wind components for each mast location can then be inferred from the surface, and the wind speed and direction calculated. Cubic spline interpolation fits piecewise third order polynominals to the points surrounding each sample that is to be interpolated.

The performance of the spline interpolation scheme is illustrated in Figure 5.6. Wind speed time-series from the WGIP dataset have been averaged to a 6 hourly resolution, and coincident ERA-interim MOS have been extracted and interpolated such that values are predictors coincident and scaled to have a mean wind speed of $8\,\mathrm{m\,s^{-1}}$.

The top left axes presents a quantile-quantile plot (each line represents a meteorological mast), and it is seen that the probability distributions are generally well characterised with the exception that the simulations tend to over-estimate high wind speeds. The top right axes presents the periodogram. The PSD of the ECMWF interpolated time-series (red) generally agree with the measured time-series (blue), however the simulated wind speeds have higher PSDs frequencies around $2 \times 10^{-5}\,\mathrm{Hz}$ or 12 hours.

The lower left axes presents the correlation between pairs of sites with the measured correlation on the x-axis and the simulated correlation on the y-axis. It is seen that the simulated correlations are nearly always greater than those measured and that there is often large discrepancy between the measured and simulated. Note that as the interpolation uses nearest neighbour for sites that are very close together they may have identical predictions thus have correlation coefficient equal to one, where as the measured value is less than one.

The lower right axes shows the scaled correlations. The blue lines present the set of measured scaled correlations, and the red lines the set of scaled correlation derived from the ERA-interim data. Again, note the scaled correlations equal one for all scales resulting from sites that are close together. A green line presents the mean bias of scaled correlation errors, and the yellow line the root mean square of the scaled correlation errors. These show that the correlations between sites are on average over estimated by a uniform amount irrespective of the scale.

While inspection of analyses through graphic presentations may highlight gross deviations it is not easy to discern differences in interpolation methods. Statistics are presented in Table 5.2. The first column lists the mean of the root mean squared errors (for each site the root mean square error is calculated and then the mean taken of these RMS errors), resulting in an error of approximately 2.5 meters per second for all schemes. While the ERA-interim MOS provide hindcasts, and comparison with historic measurements is possible, this is not necessarily the

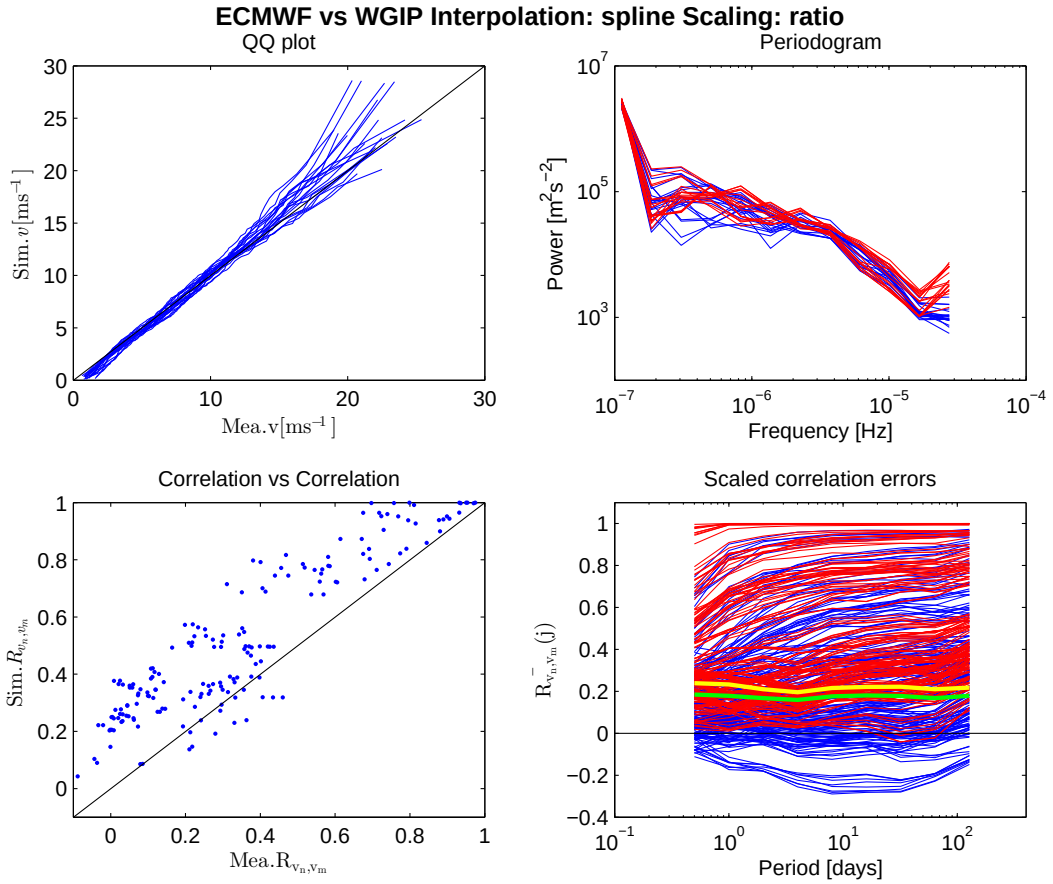

Figure 5.6 Comparison of WGIP wind speeds with ECMWF wind speeds interpolated using cubic splines

most important aspect of the simulated time-series. It is more important that the simulated time-series resolve the static and dynamic characteristics and the coherency of the measured data.

Interpolation	**Scaling**	$\bar{RMSE}$	$\bar{CvM}$	**Mean correlation bias**	**RMSE correlation**
near	ratio	2.565	0.056	0.169	0.215
linear	ratio	2.55	0.055	0.171	0.218
spline	ratio	2.575	0.057	0.168	0.214
spline	linear	2.32	0.103	0.176	0.219
spline	mcp	2.81	0.087	0.053	0.107

Table 5.2 Wind speed results from interpolation and scaling schemes

To aid in resolving static differences in interpolation schemes the the normalised Cramér von Mises (CvM) statistic is applied [101]. The CvM is presented in Equation 5.4, is the integral of absolute differences in CDFs, and has no units. The mean value of the CvMs is presented in the second results column of Table 5.2 and shows that there is very little difference between interpolation methods.

$$CvM = \int_{-\infty}^{\infty} (q(v) - q(v))^2 dq(v) \tag{5.4}$$

Where CvM is the Cramér von Mises statistic, and q is probability.

While it is important for individual wind speed time-series to be accurately simulated, of more concern for assessing statistics pertaining to the aggregation of wind power time-series is how the individual time-series relate to one another. Column four presents the mean correlation bias with all schemes significantly over estimating the correlation between sites. The final column presents the mean RMS correlation error, and shows that all interpolation schemes over estimate coherence, with little to separate the interpolation schemes.

While the power produced by a WPP is primarily related to the wind speed, the performance of a WPP is also related to the wind direction. If the terrain surrounding a WPP is not planar then as the wind direction changes the exposure of wind turbines to the free wind changes and thus the power produced also changes. This effect can be magnified as WPPs are designed using wind flow software so that the exposure of wind turbines to the wind in prevailing directions is maximised. Further WPPs that are in a similar location may be constructed to maximise their efficiencies in similar wind directions, such as in the Manawatu region where Te Apiti, Tararua 1,2, and 3, and Te Rere Hau are aligned along a single ridge and designed to maximise energy production in westerly winds.

The ability of the Numerical Weather Prediction model to hindcast wind directions is presented in the left axes of Figure 5.7 for the Northland1 site. This shows there is general agreement in wind direction. However there can be significant error in individual estimates. The right graph shows the ability of the ECMWF derived wind directions to reproduce the measured correlations between sites. This shows that there is a greater than 0.5 correlation in wind direction between all sites, and that the simulated wind directions nearly always are better correlated than the measured values.

To assess how well the different interpolation schemes perform, with respect to inferring wind direction, analyses are presented in Table 5.3. The first column presents the mean correlation coefficient, which can be seen to be high for all interpolation schemes. The second column presents the mean of the CvM statistics, showing the spline interpolation method performs best. The third column presents the RMSE for all sites, this shows that typically there is

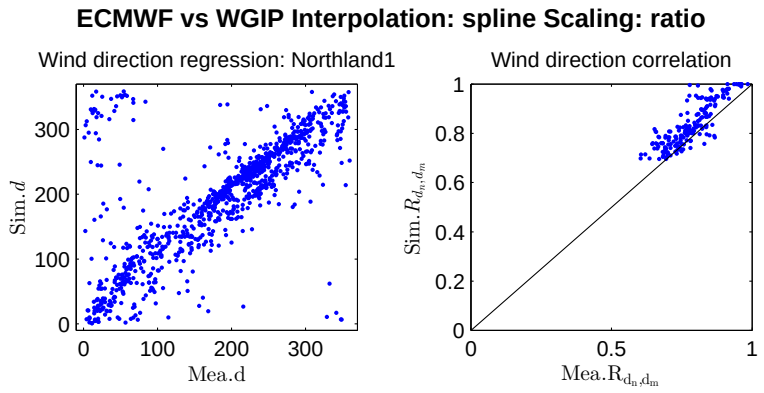

Figure 5.7 Comparison of WGIP wind direction with ECMWF wind direction derived using cubic splines

a disagreement of more than 40° between the simulated and measured wind directions. The fourth column presents the mean correlation bias, reflecting as observed in the right axes that the set of simulated wind directions is more coherent than that measured. The final column presents the mean error in correlations and shows the wind directions are, as a set, simulated reasonably well.

Interpolation	**Scaling**	$R_{\boldsymbol{d},d}$	**CvM**	**RSME [deg.]**	**Mean correlation bias**	**RMSE correlation**
near	ratio	0.91	0.067	44	0.052	0.070
linear	ratio	0.91	0.064	43	0.053	0.071
spline	ratio	0.91	0.063	42	0.052	0.070
spline	linear	0.91	0.063	42	0.052	0.070
spline	mcp	0.91	0.093	38	0.024	0.042

Table 5.3 Wind direction results from interpolation and scaling schemes

As there is little difference between the interpolation schemes applied, it is unlikely that any great benefit will result from using alternative schemes. Thus the spline interpolation scheme is adopted and will be applied to following analyses.

5.7.3 Scaling

The wind speed and wind direction time-series resulting from the spatial interpolation of the ERA-interim data are representative of a 10m wind speed measured over a locally flat plane. The wind speed measurements with which they are compared are from anemometers at various heights on meteorological masts that have surrounding complex terrain that will affect the measured wind speeds. It is desired that the wind speed time series should be representative of the wind field incident across a WPP. Thus it is necessary to apply a scaling function.

The most basic scaling function, applied in assessing scaling schemes is ratio scaling, where the time-series is scaled using a multiplier to obtain a desired mean wind speed. A further extension on this is to apply linear regression, allowing an offset in wind speed to occur.

A commonly applied scheme used to extend the effective period of measurement at a WPP site is the Measure Correlate Predict methodology (MCP) [102]. MCP uses the correlations in wind speed and direction time-series, between measurements made at the site of interest and those made at meteorological station, to scale the long term wind speed and direction time-series

measured at the meteorological station such that they are representative of the site. The MCP method is presented in Equation 5.5.

$$v_s(t) = S_{(s,r)}(d) \cdot v_r(t) \tag{5.5}$$

Where v is the wind speed, s is the predicted site, t is time, d is the wind direction sector, S is the speed up, and r is the predictor or reference site.

MCP requires solving a linear regression, forced through the origin, between coincident values of the NWP interpolated wind speed and the measured wind speeds in each of 12 wind direction sectors. The wind direction is based on the wind direction at the site of interest, hence wind directions from the NWP have to be transformed to be representative of the site, this is achieved by calculating the average directional offset between the NWP and site wind directions, in 10° sector bins. The offsets are calculated using samples when the wind speed is greater than $5\,\mathrm{m\,s^{-1}}$. The offsets are subtracted from the long term reference wind direction time-series. The effect of the transformation on wind direction time-series is presented in Table 5.3, showing that the simulated wind direction time series are improved, resulting in 10% lower RMSEs. The transformation also improves the simulated wind directions as a set with the mean correlation bias improving by 50% and RMSE correlation errors falling falling by 40%.

Using the reference wind direction time-series transformed to be representative of the site, wind speed regressions are formed in each of 12 (30°) sectors. Low wind speeds, less than $3\,\mathrm{ms^{-1}}$, are excluded. The resulting "speed ups" are applied to the wind speed time-series derived from the NWP model, as presented in Equation 5.5. The MCP method is used to scale the interpolated wind speed time-series, and the method is assessed alongside the ratio scaling and linear interpolation schemes with results presented in Table 5.2. The results of scaling using MCP are shown in Figure 5.8.

The application of the MCP methodology provides a wide range of results. RMSE errors are increased by 20%, but the probability distributions are on average better matched with CvM statistics improved by 15%. The Quantile-Qunatile plots show that the probability distributions for some sites are grossly affected and often do not match the empirical counterparts (particularly for high wind speeds). The application of MCP also changes the PSD of some sites which in turn will impact auto-correlations and thus inferred ramp rates. While MCP adversely impacts some individual wind speed time-series it does greatly improve the replication of correlations with the mean correlation error falling by 50%. The improvement in correlations is greater for larger scales; the improvement in scaled correlation at a period of 6 h is approximately 20%.

5.7.4 Imputation

Imputation is the act of replacing missing data with substituted values. Interpolation is a type of imputation whereby the missing values are derived from some function of the surrounding values. However, when deriving missing wind speed values, to increase the temporal resolution, it is turbulence that is being simulated and there is no deterministic function that can be resolved. The imputation problem is complex and is the subject of Chapter 6.

5.8 SUMMARY

To be able to produce sufficient wind power time-series to support integration studies it is necessary to use the MOS from a NWP. The ECMWF ERA-interim model provides relatively good spatial resolution and is freely available. It is necessary to interpolate, scale, and impute the grid point data from the ERA-interim model. A data-set of wind speed and direction measurements from meteorological masts located at prospective WPP sites has been collated to aid in this process. It is shown that the cubic spline interpolation scheme offers benefit

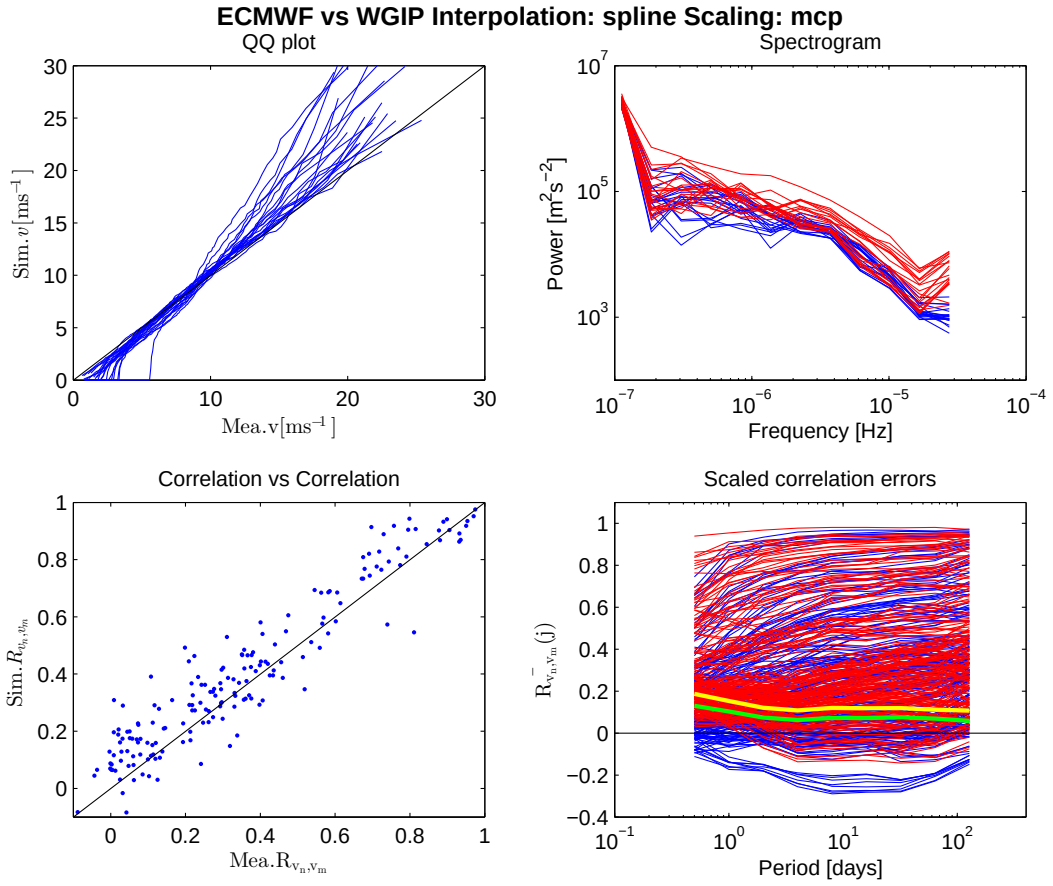

Figure 5.8 Comparison of WGIP wind speeds with ECMWF wind speeds interpolated using cubic splines and scaled using MCP

over the simplest nearest neighbour approach. The benefit is not so outstanding as to warrant further investigation into which of a multitude of schemes may be the best. In the absence of a meso-scale model the MCP methodology has been applied to scale ERA-interim MOS. The MCP scheme is shown to greatly improve simulated correlations; however the statistics of some individual wind speed time-series are maladjusted. The imputation of the wind speed time-series is a complex task and is addressed in the following chapter.

Chapter 6

TIME-SERIES SIMULATION

Time-series derived from the ECMWF ERA-interim MOS have a temporal resolution of 6 h which is insufficient for supporting Unit Commitment and Economic Dispatch (UCED) studies. Perhaps not coincidentally the 6 hourly period falls in the spectral gap of the Van Der Hoven spectrum. It may be reconciled that processes with characteristic time spans greater than 6 h are well described by deterministic processes, whereas processes with characteristic time spans less than 6 h are best characterised as stochastic processes. A deterministic process is one where the evolution of the process can be well described by the present state and its physics. A stochastic process is one that is inherently random, cannot be precisely predicted using a physical model, and must be modeled using statistical methods. While a stochastic process may include a contribution that is deterministic crucially it must also include some random process.

A useful approximation is to equate those components of wind speed that have temporal spans less than 6 h with turbulence and those components that have longer temporal spans to be representative of the bulk flow, weather, or geostrophic wind. Hence imputation of the ERA-interim data requires a model of turbulence, which is a stochastic process and must be formulated using a statistical model. The bulk flow velocity can be defined using Equation 6.1 and the turbulent component defined using Equation 5.2.

$$\overline{v(t)} = \frac{1}{T}\sum_{t-3}^{t+3} v(t) \tag{6.1}$$

Where there are T samples between times $t-3$ and $t+3$, and t having units of hours.

The model used for imputation should preserve the characteristics of the measured time series. The characteristics include statistics intrinsic to individual series such as the mean, variance, and dynamic variation and also those describing the manner in which the group of time series vary together or the covariance.

There are many methods that can be used for stochastic time-series simulation such as Auto Regressive Moving Average models (ARMA), Markov Chains, and spectral based models. Selection of the method depends on which characteristics of the time-series are deemed the most important, the data requirements for constructing the model, the degree to which the models represent some physical generalisation, and the ease with which the model can be manipulated to achieve a desired result. Further, methods developed using quite different numerical tools may be equivalent.

For instance if the crucial property of the simulated time-series is deemed to be the probability distribution, and the data set used to establish the model is comprehensive, then an appropriate choice of model will be a Markov Chain. A Markov Chain uses transition matrices to describe the evolution of the time-series from one instant to the next. The matrices are derived from the data and if a sufficient resolution matrix is used, then the complete probability distribution is

described. The use of Markov Chains in simulating WSTS has a long history; being described by McNerney in 1985 [103], Shamshad in 2005 [104], and Liang in 2013 [105]. However, a Markov Chain model can not be easily manipulated to increase the temporal resolution, or increase the number of time-series simulated in parallel. As it is necessary to perform both of these tasks, a Markov Chain model is rejected. This decision is reinforced by Brokish who noted the pitfalls when synthesizing wind data using Markov Chains [106].

Wind speed time-series have a strong spectral conformity as described by the Kolmogorov spectrum exhibited in Section ‘5.3. A model based on a spectral method, capable of replicating the coherence, may be suitable. Indeed this approach has been developed by Davenport in 1961 [107], where the coherence is described as a function of frequency. However, spectral methods are not easily adapted to the simulation of non-stationary time-series. It is shown in this chapter that the turbulence time-series are heteroskedastic and thus non-stationary.

In the creation of synthetic wind speed time series for 15 New Zealand wind farms, Turner et al. applied an ARMA approach [97]. The methods used in the creation of these synthetic wind speed time-series are used as the starting point for developing imputation methods in this chapter.

6.1 AUTO-REGRESSIVE MOVING AVERAGE MODELS

The ARMA methodology for univariate time series simulation was described by Box and Jenkins in the 1970's and their names are often afforded to a simple set of methods for model selection [108]. The Box-Jenkins methodology uses a combination of auto-regressive and moving average functions to approximate the dynamics of a time series. The auto-regressive component describes how a value in a time series is dependent upon preceding values, thus it reflects the degree of persistence. The moving-average component describes how fast the time series fluctuates, thus it characterises damping effects. The general equation for an ARMA model is presented in Equation 6.2.

$$v'(t) = c + \sum_{l=1}^{L} A(l)v'(t-l) + \sum_{l=1}^{O} B(l)\varepsilon(t-l) + \varepsilon(t) \tag{6.2}$$

Where c is a constant term, L is the order of the auto regressive components, $A(l)$ is the auto-regression coefficient for lag l, O is the moving average model order, $B(l)$ is the moving average coefficient for lag l, and ε is the innovation coefficient.

The ARMA model was derived primarily as a forecasting and control tool. As such the model uses values from the evolution of the time series so that subsequent values can be predicted or forecast. The degree to which the model is dependent on historic values in the time series is reflected by the model order, and typically the innovation coefficient is modelled as a white noise process.

The ARMA model can be fitted to a time-series using the Yule-Walker equations. As will be shown the turbulence time-series can be approximated as a purely Auto-Regressive (AR) process (see Section 6.1.2), with Moving Average components excluded. The pure AR model equation takes the form shown in Equation 6.3. AR models have been used to simulate WSTS by Brown et al. in 1984 [109], and applied to simulate multi-area wind power output by Papavasiliou and Oren in 2012 [110].

$$v'(t) = c + \sum_{l=1}^{L} A(l) \cdot v'(t-l) + \varepsilon(t) \tag{6.3}$$

Where c is constant, $A(l)$ is the regression coefficient for lag l, L is the maximum lag used in the auto-regression equal to the model order.

The AR model can be rewritten in expanded notation as shown in Equation 6.4, and expressed in matrix notation in Equation 6.5. The matrix form can then be expanded and written in the form of a linear regression, as shown in Equation 6.6, thus the model may be solved using ordinary least squares as shown in Equation 6.7

$$v'(t) = c + A(t-1)\cdot v'(t-1) + A(t-2)\cdot v'(t-2) + \cdots + A(t-L)\cdot v'(t-L) + \varepsilon(t) \quad (6.4)$$

$$\begin{bmatrix} v'(1) \\ v'(2) \\ v'(3) \\ \vdots \\ v'(T) \end{bmatrix} = \begin{bmatrix} v'(0) & v'(-1) & v'(-2) & \cdots & v'(-L) \\ v'(1) & v'(0) & v'(-1) & \cdots & v'(1-L) \\ v'(2) & v'(1) & v'(0) & \cdots & v'(2-L) \\ \vdots & \vdots & \vdots & \vdots & \vdots \\ v'(T-1) & v'(T-2) & v'(T-3) & \cdots & v'(T-L) \end{bmatrix} \begin{bmatrix} A(1) \\ A(2) \\ A(3) \\ \vdots \\ A(L) \end{bmatrix}^{\mathsf{T}} + \begin{bmatrix} \varepsilon(1) \\ \varepsilon(2) \\ \varepsilon(3) \\ \vdots \\ \varepsilon(T) \end{bmatrix} \quad (6.5)$$

Where T is the transpose operator.

$$v' = \Lambda A + \epsilon \quad (6.6)$$

Where $\Lambda = \begin{bmatrix} v'(0) & v'(-1) & v'(-2) & \cdots & v'(-L) \\ v'(1) & v'(0) & v'(-1) & \cdots & v'(1-L) \\ v'(2) & v'(1) & v'(0) & \cdots & v'(2-L) \\ \vdots & \vdots & \vdots & \vdots & \vdots \\ v'(T-1) & v'(T-2) & v'(T-3) & \cdots & v'(T-L) \end{bmatrix}$ is the lag operator.

$$A = \left(\Lambda^{\mathsf{T}}\Lambda\right)^{-1}\Lambda^{\mathsf{T}}v' \quad (6.7)$$

To apply the AR model to a time-series, that time-series must be a stationary Gaussian process. A stationary process is one which is statistically invariant. A Gaussian process is one whose probability distribution conforms to a Gaussian distribution.

6.1.1 Stationarity

A time series is strictly stationary if its probability distribution is time invariant as presented in Equation 6.8.

$$Q(v'_{1+\tau}, \cdots, v'_{T+\tau}) = Q(v'_1, \cdots, v'_T) \quad (6.8)$$

Where Q is the cumulative probability distribution function, τ is a temporal offset, and T is the time over which the probability distribution is assessed, which must be sufficiently large such that the probability distribution is well defined.

The strict definition of stationarity infers that all properties of the time-series are independent of time, thus there can be no trends or cyclical processes that affect the time-series. A process that is stationary in this manner is also ergodic. However, is difficult to test for strict stationarity as all moments of the time series must be independent of time.

Rather than applying a condition of strict stationarity it is sufficient to require the process to have time invariant first and second order derivatives. That is the process has time invariant mean, variance, and auto-covariances [111]. A time series that has these properties is said to have stationarity of order 2, or have wide sense stationarity, and it is this definition that is applied here. If a time-series has variance independent of time then it is homoskedastic.

There are many tests for stationarity, many of which rely on detecting the existence of a unit root in the characteristic equation of the auto-regressive process. A commonly applied test for

unit roots is the augmented Dicky Fuller (aDF) test. However, confirming that the measured turbulence time-series has wide sense stationarity is not necessary; the necessary condition is that the turbulence time-series is well approximated by a stationary process. Further, for the turbulence time-series to be non-stationary requires either some progressive change in a physical process manifest in the time-series, such as seasonality, or that the time-series is the result of some measurement that changes. The wind speed measurements may change through time as the result of changes in exposure, due to vegetation growth, or due to changes in measurement equipment, such as the degradation of anemometers. Here we desire consistency, hence it is a necessity that the simulated process be largely stationary. This is achieved by conditioning and fitting as described in Section 6.1.2.

6.1.2 Model conditioning and fitting

To develop an ARMA model for turbulence, it is necessary to identify the transformations required to obtain a process representative of turbulence from a stationary Gaussian process. While the bulk flow component of wind speed is removed from the measured wind speed time-series to obtain the turbulence, and hence the turbulence time-series are by definition first order stationary, it is reasonable to expect that the magnitude of turbulence should be dependent on the mean wind speed. The wind consists of the advection of eddies and higher wind speeds are the manifestation of increased bulk flow velocities and eddies with greater magnitudes. Hence it is expected that turbulence is greater at higher wind speeds. To assess whether this assumption is correct, the relationship between the mean wind speed and the absolute value of the turbulence is presented in the top left graph of Figure 6.1. For each time series the turbulence is binned by each integer value of the bulk flow wind speed, and the average for each bin calculated as shown in Equation 6.9. The relation between turbulence and the wind speed magnitude is quantified using the Pearson's correlation statistic ($R(\bar{(}v), v')$) for each time-series in Table 6.1.

$$\overline{v'(V)} = \frac{1}{T}\sum_{1}^{T} v'(t) \left\{ v(t) >= V - 0.5 \;\&\; v(t) < V + 0.5 \right. \tag{6.9}$$

Where V is the wind speed bin center.

One way of stating that the turbulence is dependent on the bulk wind speed is to say that the variance of the wind speed is dependent on the magnitude of the wind speed, thus the variance of the wind speed time-series changes with time; hence the turbulence time-series is heteroskedastic. Note that while the mean of the turbulence time-series equals zero by definition, the dependence of the magnitude of the turbulence on the mean wind speed ensures the mean of the turbulence for the sets binned by wind speed magnitude is not equal to zero.

The dependence of turbulence on the bulk wind speed can be removed from the time-series using Taylor's power law transform as shown in Equation 6.10 [112]. The Taylor exponent a is solved using an optimisation search formed such that the Pearson's correlation coefficient between v'_T and $\overline{v(t)}$ is minimised. The resulting Taylor exponents are presented in Table 6.1.

$$v'_T(t) = \frac{v'(t)}{\overline{v(t)}^a} \tag{6.10}$$

Where a is the Taylor exponent, and T represents the Taylor transformed variable.

The transformation of a stationary process to represent turbulence also requires the simulation of cyclic oscillations resulting from atmospheric processes. It is expected that turbulence varies with changes atmospheric stability and thus will exhibit diurnal and seasonal patterns. It is seen that the bulk wind speed time-series has definite diurnal patterns, shown in the top right graph of Figure 6.1. The lower left graph shows the turbulence as a function of the time of

day, calculated by binning the normalised variance of the turbulence by hour of the day for each mast. The average diurnal turbulence cycle is shown by the solid blue line; the range of values across the sites is indicated using the maximum (dashed dotted line) and minimum (dotted line) values. The diurnal turbulence profile subsequent to the application of the Taylor's power transform is shown as a red line; showing a minor impact on the shape of the diurnal turbulence cycle.

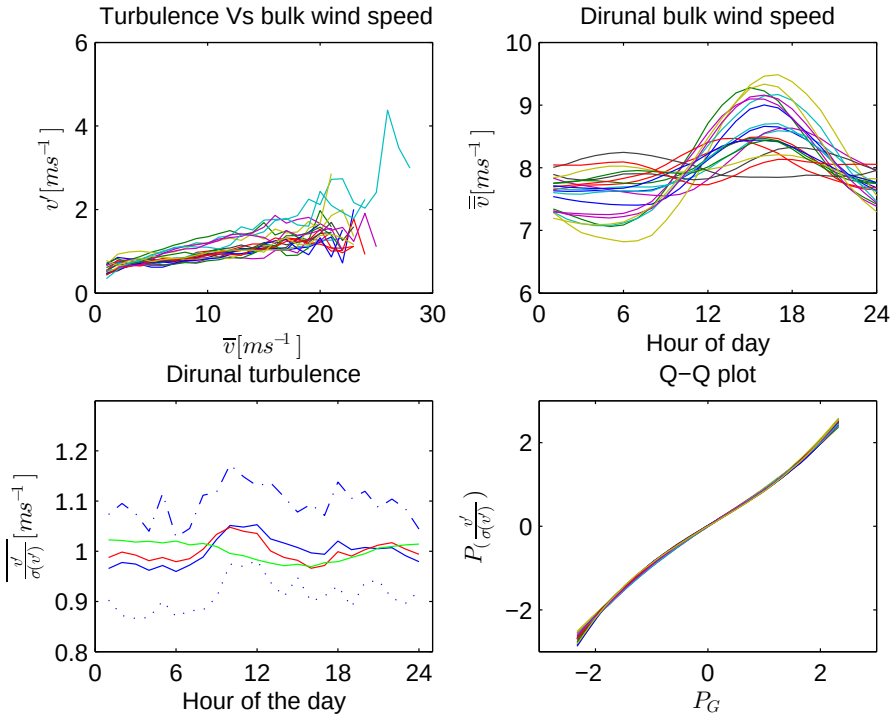

Figure 6.1 Dependence of turbulence on the bulk wind speed (top left), dependence of bulk wind speed on the time of day (top right), dependence of turbulence on time of day (bottom left), and Quantile-Quantile plot showing that turbulence is well characterised by an AR model with Gaussian innovations. Each line in the top left, top right, and bottom right graphs represent measurements from different masts. In the bottom left graph the blue line shows the mean diurnal turbulence profile with dotted lines shows the range diurnal turbulence profiles. The green line shows the mean diurnal turbulence after correction, and the red line shows the mean error resulting after the correction is applied.

It is possible to add a diurnal pattern to the turbulence time-series. One method is to add a correction, which is a function of the time of day, as shown in Equation 6.11. The mean wind speed in each hour being given by Equation 6.12. The magnitude of the correction is calculated by finding the mean turbulence in each hour for each of the measured time-series. The effect of the correction can be resolved by removing the diurnal correction from the measured turbulence time-series and examining the resulting mean daily profile of the corrected turbulence time-series, as shown in the lower left graph of Figure 6.1 by the green line. While this transform works well for some of the time-series it also introduces an inverted diurnal signal. A successful generic transform has not been found and hence no correction for the diurnal cycle is made to the turbulence time-series

$$v'_D(t) = v'(t) + \overline{v'(H)} \tag{6.11}$$

Where D denotes the diurnal correction.

$$\overline{v'(H)} = \frac{1}{T}\sum_{1}^{T} v'(t) \left\{ t >= H - 0.5 \,\&\, t < H + 0.5 \right. \tag{6.12}$$

Where H is the hour of the day.

Just as there is a diurnal cycle of atmospheric stability there is also a seasonal pattern. However, it is not possible to detect a significant seasonal pattern in the turbulence time-series as the WGIP data-set has an insufficient temporal span, so no detection or adjustment for seasonality is possible.

For an AR process to approximate turbulence, it not only needs to be second order stationary but must also be Gaussian. To illustrate that the turbulence time-series are approximately Gaussian, a Quantile-Quantile (QQ) plot, where quantiles are evaluated from 0.01 at steps of 0.01 through 0.99, is presented in the lower right graph of Figure 6.1. Gaussianity is further confirmed by observing that the normalised Cramer von Mises coefficients are all less than 0.05, as presented in Table 6.1.

Mast	$\sigma(v')$	$R(\overline{v}, v')$	**Taylor exp.**	A_1	A_2	A_3	$R(v_t, v_{t+1})$	**CvM**
Northland1	0.56	0.16	0.29	0.79	-0.07	0.03	0.85	0.05
Marlborough1	0.43	0.21	0.41	0.99	-0.18	0	0.69	0.05
Tararua1	0.45	0.22	0.39	0.84	-0.04	-0.01	0.75	0.04
Northland2	0.55	0.17	0.3	0.82	-0.08	0.02	0.78	0.04
Auckland1	0.64	0.13	0.22	0.69	0.03	0.02	0.82	0.04
Waikato1	0.57	0.17	0.28	0.83	-0.05	-0.01	0.77	0.03
Waikato2	0.56	0.17	0.29	0.84	-0.09	0.02	0.84	0.05
Waikato3	0.63	0.13	0.23	0.74	-0.03	0.03	0.82	0.04
Wellington1	0.63	0.13	0.23	0.8	-0.01	-0.01	0.74	0.04
Wellington2	0.56	0.17	0.29	0.77	-0.03	0.01	0.64	0.04
CentralOtago1a	0.3	0.35	0.58	0.87	-0.1	0	0.78	0.03
CentralOtago1b	0.35	0.32	0.51	0.89	-0.1	-0.01	0.79	0.03
Tararua3a	0.73	0.09	0.16	0.8	-0.02	0	0.69	0.04
Tararua3b	0.45	0.22	0.39	0.8	-0.02	-0.01	0.66	0.04
Wellington3	0.56	0.16	0.29	0.83	-0.03	-0.01	0.82	0.05
Northland3a	0.58	0.15	0.27	0.77	-0.04	0.01	0.74	0.04
Northland3b	0.54	0.16	0.3	0.81	-0.06	0.02	0.8	0.04
Southland2	0.39	0.28	0.46	0.9	-0.12	0.01	0.77	0.03
Southland3	0.37	0.26	0.48	0.78	-0.06	0.02	0.81	0.04
Tararua2	0.59	0.13	0.26	0.78	0.02	-0.01	0.67	0.05
Average	0.52	0.19	0.33	0.82	-0.05	0.01	0.76	0.04

Table 6.1 Turbulence time-series parameters

6.1.3 Autocorrelation and partial-autocorrelation

The Box Jenkins method for resolving the order of the AR model relies on observation of the auto-correlation and partial auto-correlation functions and their standard errors. The auto-correlation is defined in Equation 4.7; in a similar form the auto-correlation for turbulence is presented in Equation 6.13. Note the absence of the mean as this is by definition zero. The significance of the auto-correlation is given by the standard error of the estimate as shown in Equation 6.14.

$$R_{s,s}(l) = \sum_{t=1}^{T} (v'_s(t+l))(v'_s(t)) \tag{6.13}$$

$$\varsigma_{s,s}(l) = \sqrt{\frac{1}{T}(1 + 2\sum_{t=1}^{T} R_{s,s}(l))} \tag{6.14}$$

Where ς is the standard error.

The partial auto-correlation function describes how well a time series matches itself given a time shift or lag and given that the auto-correlation, modeled using the linear regression in Equation 6.7, for lesser lags had been removed. The partial auto-correlations indicate the presence of long memory, or low frequency, components within the time series. The partial auto-correlation can be determined using multiple linear regression based upon the lag operator, and is expressed in Equation 6.15.

$$R'_{s,s}(l) = \sum_{t=1}^{T}(v'_s(t+l) - \widehat{v'_s(t+l)})(v'_s(t) - \widehat{v'_s(t)}) \tag{6.15}$$

Where $R'_{s,s}(l)$ is the partial auto-correlation, and $\widehat{v'}$ is the regressed turbulence found by applying the AR model.

The shape of the auto-correlogram can be used to identify the appropriate type of ARMA model for the time series and Table 6.2 provides a guide for model selection.

Partial Auto-Correlation Shape	**Indicated ARMA model**
Exponetial, decay to zero	Autoregressive model. Partial autocorrelogram used to identify model order
Alternating positive and negative decaying to zero	Autoregressive model (over differenced). Partial autocorrelogram used to identify model order
One or more spikes rest are zero	Moving average model, order identified where autocorrelation is zero
Decay, starting after a few lags	Mixed autoregressive moving average model
All zero or close to zero	Data have no persistence, so no ARMA model
High values at fixed intervals	Data have a periodic function and are not stationary
No decay to zero	Data are not stationary

Table 6.2 Auto-regressive moving-average model selection criteria

The method used in this thesis for finding the model order is prescriptive. However, it is possible to define the model order using information criteria, such as the Bayesian Information Criteria (BIC) or Akaike Information Criteria (AIC); these seek to determine the quality of the model based on the quantity of data used to construct the model. Hence a model based on these criteria will seek to increase the model order to the point where the increased complexity of the model is not justified given the quantity of data. Given the time-series here are very long the use of an information criteria will force a higher model order than necessary, and over fitting may result which is not be helpful when generalising the models.

To aid in model fitting, correlograms for turbulence are presented in the top graph of Figure 6.2, and partial correlograms in the lower graph. Each line represents an individual turbulence time-series. The standard errors, represented by the solid horizontal black line near zero, are very small, and do not limit the model order.

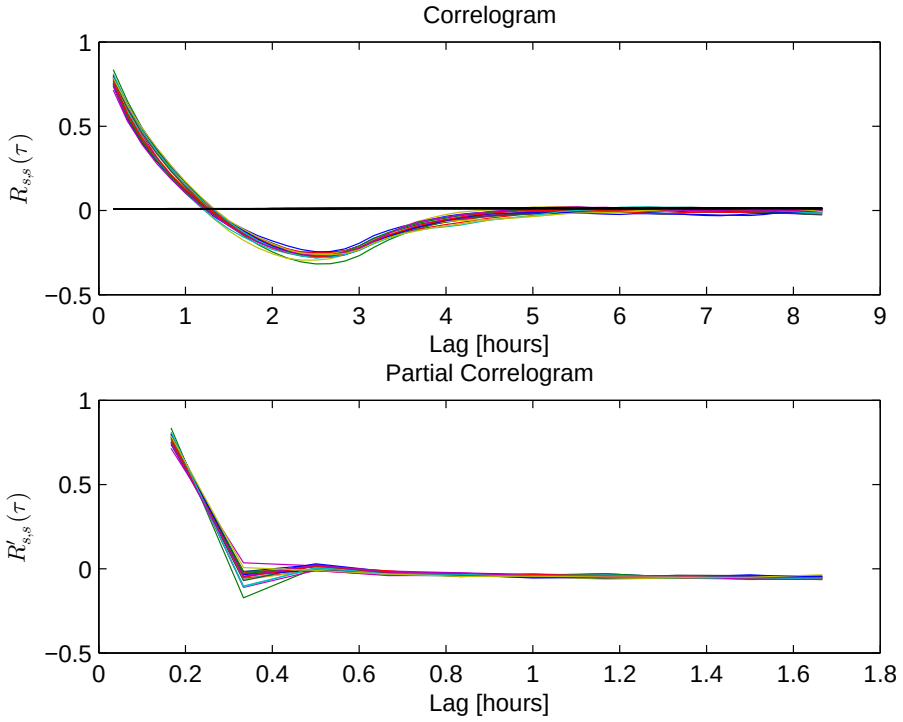

Figure 6.2 Correlograms and partial-correlograms for turbulence time-series. Each line represents analysis of turbulence measurements from a meteorological mast in the WGIP data-set.

It is seen that the correlograms and partial-correlograms are very similar for all time series. The auto-correlations exhibit exponential decay with no spikes or delay in the start of the exponential decay, hence use of a pure AR model is appropriate (as indicated by row 1 of Table 6.2). Note that the auto-correlation for lags greater than 1.5 hours becomes negative; this is the result of the generation of the time-series (removal of the bulk wind speed). As the partial-autocorrelation quickly decays a model of order 3 is selected. As all correlograms and partial-correlograms are very similar it is appropriate to generalise a single model for turbulence based on averages of the parameters derived from all the time-series. The resulting AR model parameters (A_1, A_2, A_3) are presented in Table 6.1.

6.1.4 vector Auto-Regression

The AR model is used for characterising the dynamic variability of an individual time series. However, we know that the set of wind time series are related; the time series measured at sites that are in close proximity to one another exhibit similar characteristics and are co-variant. Typically the further removed sites are the less well correlated they are. It is necessary to extend the AR model to include not only the dynamic variation of an individual time series but also its dependence on other time-series in the set of data. A comprehensive method for achieving this is vector Auto-Regression (vAR). The governing Equation for a vAR model is presented in Equation 6.16. Application of vAR models to the simulation of WSTS was presented by Mur-Amada in 2007 [113]. Mur-Amada then applied the WSTS model in the simulation of wind power and subsequent calculation of wind power variability [114], and validation thereof [115].

$$v' = A_{(1,2,\cdots,s)}(1)V'(1) + A_{(1,2,\cdots,s)}(2)V'(2) + \cdots + A_{(1,2,\cdots,s)}(L)V'_{(1,2,\cdots,s)}(L) + \epsilon \tag{6.16}$$

Where $V'(l)$ is the lagged matrix of turbulence time-series as shown in Equation 6.17.

$$V'(l) = \begin{bmatrix} v'_1(-l) & v'_2(-l) & \cdots & v'_s(-l) \\ v'_1(1-l) & v'_2(1-l) & \cdots & v'_s(1-l) \\ \vdots & \vdots & \ddots & \vdots \\ v'_1(T-1) & v'_2(T-2) & \cdots & v'_s(T-l) \end{bmatrix} \tag{6.17}$$

The vAR approach has been used by Miranda for the simulation of the wind data in Great Britain [116]. Miranda simulated wind speed time-series, as opposed to turbulence, and selected a 4th order vector Auto-Regressive model from wind speed measurements, with an hourly temporal resolution, made at 20 meteorological stations spread across Great Britain.

The vAR equation can be rewritten in matrix notation, as is presented for a single time series in Equation 6.5, except the lag operator here is formed from the time series from the site of interest concatenated to the lag operators from all other sites in the data-set. The lag operator for a vAR process is described in Equation 6.18, and the multiple linear regression is solved using least squares regression using the relationship in 6.7.

$$\Lambda = \left[V'(1)V'(2)\cdots V'(L)\right] \tag{6.18}$$

The vAR approach introduces significant numerical requirements, as in this study the data set contains 20 sites and a model order of three is selected. This results in the lag operator having 35,712 rows and 60 columns. While this is not particularly problematic for computing, it does present problems for generalisation. It is desired that a single model be developed that can replicate both the dynamic character and the coherence, based on as few parameters as possible.

6.1.5 Correlated Innovation Matrix

As noted the Correlated Innovation Matrix (CIM) approach has been used by Turner et al. and is presented in Equation 6.19. The CIM method has also been applied by Karki et al. and by Morales et al. for simulating wind power time-series by first simulating wind speed time-series and transforming these to power [117] [118]. Both Karki and Morales faced difficulties when applying the CIM model as wind speed time-series are positive and asymmetric, hence transformations are required. This is not encountered here as the turbulence time-series are approximately Gaussian and easily transformed to stationarity.

$$v'_s(t) = c + \sum_{l=1}^{L} A_s(l) \cdot v'_s(t-l) + \gamma \cdot \varepsilon(t) \tag{6.19}$$

Where γ is the CIM correlation matrix.

The innovation matrix coefficients are found by calculating a matrix of the correlation coefficients and then calculating the Cholesky decomposition of the correlation matrix. The cross correlation matrix is presented in Equation 6.20.

$$C = \begin{bmatrix} R_{1,1} & R_{1,2} & R_{1,3} & \cdots & R_{1,S} \\ R_{2,1} & R_{2,2} & R_{2,3} & \cdots & R_{2,S} \\ R_{3,1} & R_{3,2} & R_{3,3} & \cdots & R_{3,S} \\ \vdots & \vdots & \vdots & \ddots & \vdots \\ R_{S,1} & R_{S,2} & R_{S,3} & \cdots & R_{S,S} \end{bmatrix} \tag{6.20}$$

The Cholesky decomposition splits a matrix into a product of an upper triangular matrix and its complex conjugate as shown in Equation 6.21. This ensures that the innovation $\varepsilon(t)$ adds an appropriately correlated change to all the individual time-series. The upper triangular matrix is of a form that when applied to a set of independent variables or time-series the resultant time-series will have a dependence relationship equal to the cross-correlation matrix.

$$\gamma^{\mathsf{T}}\gamma = C \tag{6.21}$$

Where γ is the Cholesky decomposed correlation matrix.

For the Cholesky decomposition to be applied, the matrix C must be Hermitian and positive definite. A Hermitian matrix is one that is square (has equal numbers of rows as columns) and is equal to its own conjugate transpose (the element in the i-th row and j-th column is equal to the complex conjugate of the element in the j-th row and i-th column. The Hermitian requirement is presented in Equation 6.22.

$$\gamma = \gamma^{\mathsf{T}} \tag{6.22}$$

Where T is the complex conjugate transpose.

To be positive definite, the matrix must satisfy the relationship shown in Equation 6.23. For multi-variate time series this condition is equivalent to stating that no individual time-series can be derived as an exact linear combination of the other time-series. The Cholesky decomposition is calculated using the Cholesky algorithm, as applied in the Matlab function chol.m, which is a recursive algorithm, and the number of operations required to compute is approximately $\frac{n^3}{3}$. The correlation matrix may not always be positive definite and Hermitian; the algorithm nearestSPD.m is applied to find the nearest correlation matrix that is semi positive definite [119].

$$A^{\mathsf{T}}\gamma A > 0 \tag{6.23}$$

Where A is any non-zero column vector.

The CIM model developed from the WGIP data set allows the wind speed time-series derived from the ERA-interim model to be imputed. The ERA-interim time-series have been interpolated using cubic splines and scaled using MCP. Model parameters and results are presented in Table 6.3 and Figure 6.3.

The top left graph, of Figure 6.3, presents a quantile-quantile plot and shows minor differences compared with the equivalent plot for the unimputed data. Some changes are seen at the extremes of the probability distributions; the result of adding a normally distributed variable to the skewed distribution derived from the ERA-interim data. The top right graph presents the periodogram and the imputation is evident with the spectra extending to 10×10^{-3} Hz; the left hand side of the periodogram frequencies lower than 4.6×10^{-5} Hz derive from the ERA-interim data and those above derive from the CIM model (note the dip in the PSD at approximately 5×10^{-4} Hz).

The lower left graph of Figure 6.3, presents the correlations between site pairs from the measured data versus those simulated; this does not materially change with the imputation. The lower right graph presents the scaled correlations with blue line representing the measured values and red the simulated values. The green line presents the bias error and the yellow line presents the RMS error. As for the spectrogram the scaled correlations cover a greater range of periods than the ERA-interim data alone. The CIM model reproduces the measured scaled correlations with a higher degree of accuracy than the ERA-interim data; unsurprising given the model parameters are extracted from the data-set against which simulations are being compared.

The results for the imputation presented here are from one run of the CIM model and thus represent one possible outcome. The imputation model could be run many times using a Monte Carlo procedure to ensure the properties of the time-series are stable. However, the length of the time-series imputed is such that a single run of the model is sufficient for characterising the dynamic variation of the wind.

The results presented here are for simulations with model parameters derived from the WGIP data set, thus the results are specific to this data set. To enable the simulation of wind speed

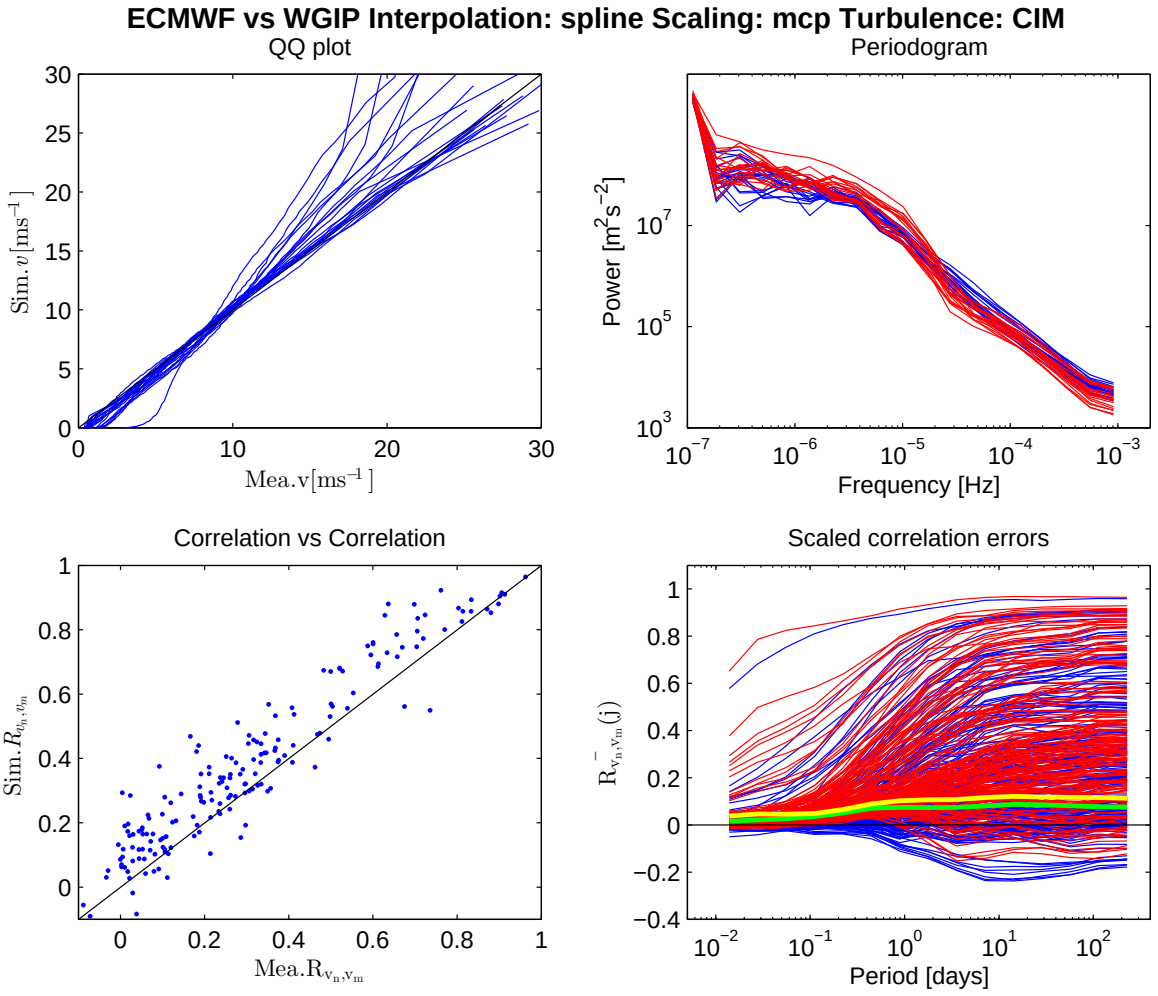

Figure 6.3 Statistics comparing wind speed time-series, derived from the ECMWF-interim Model Output statistics which have been interpolated using cubic splines, scaled using measure Correlate Predict, and imputed using the CIM turbulence model, with time-series from the WGIP data-set. Top left graph show a Quantile-Quantile plot with each line representing results from a different meteorological mast. The top right graph presents a periodogram with PSDs from measured WSTS shown as blue lines, and from simulated time-series as red lines. The bottom left graph presents simulated correlations versus measured correlations. The bottom right graph shows scaled correlations between pairs of sites (blue lines represent measured time-series, and red line simulated time-series). The green line presents the mean bias in the difference between simulated and measured scaled correlations, and the yellow line shows the associated RMS difference.

Mast	$\sigma(v')$	$R(\overline{v}, v')$	**Taylor exp.**	A_1	A_2	A_3	$R(v_t, v_{t+1})$	**CvM**
Northland1	0.56	0.16	0.29	0.79	-0.07	0.03	0.85	0.05
Marlborough1	0.43	0.21	0.41	0.99	-0.18	0	0.69	0.05
Tararua1	0.45	0.22	0.39	0.84	-0.04	-0.01	0.75	0.04
Northland2	0.55	0.17	0.3	0.82	-0.08	0.02	0.78	0.04
Auckland1	0.64	0.13	0.22	0.69	0.03	0.02	0.82	0.04
Waikato1	0.57	0.17	0.28	0.83	-0.05	-0.01	0.77	0.03
Waikato2	0.56	0.17	0.29	0.84	-0.09	0.02	0.84	0.05
Waikato3	0.63	0.13	0.23	0.74	-0.03	0.03	0.82	0.04
Wellington1	0.63	0.13	0.23	0.8	-0.01	-0.01	0.74	0.04
Wellington2	0.56	0.17	0.29	0.77	-0.03	0.01	0.64	0.04
CentralOtago1a	0.3	0.35	0.58	0.87	-0.1	0	0.78	0.03
CentralOtago1b	0.35	0.32	0.51	0.89	-0.1	-0.01	0.79	0.03
Tararua3a	0.73	0.09	0.16	0.8	-0.02	0	0.69	0.04
Tararua3b	0.45	0.22	0.39	0.8	-0.02	-0.01	0.66	0.04
Wellington3	0.56	0.16	0.29	0.83	-0.03	-0.01	0.82	0.05
Northland3a	0.58	0.15	0.27	0.77	-0.04	0.01	0.74	0.04
Northland3b	0.54	0.16	0.3	0.81	-0.06	0.02	0.8	0.04
Southland2	0.39	0.28	0.46	0.9	-0.12	0.01	0.77	0.03
Southland3	0.37	0.26	0.48	0.78	-0.06	0.02	0.81	0.04
Tararua2	0.59	0.13	0.26	0.78	0.02	-0.01	0.67	0.05
Average	0.52	0.19	0.33	0.82	-0.05	0.01	0.76	0.04

Table 6.3 Model parameters and results for the CIM imputed ERA-interim time-series

time-series that are representative of different meteorological masts requires generalisation of the model. As seen in Figure 6.2, the correlograms and partial-correlograms are very similar and hence a generic model using the average of the Auto-Regression coefficients, as presented in the final row of Table 6.3, is justifiable. The generic model can be further constructed using the average of the Taylor's power law exponents and turbulence time-series standard deviations. A generalisation also requires a model for the correlation between turbulence time-series; the correlation is a function of the distance between sites as shown in Figure 6.4, which can be generalised as a log-linear function for distances less than 30 km, and zero for greater distances.

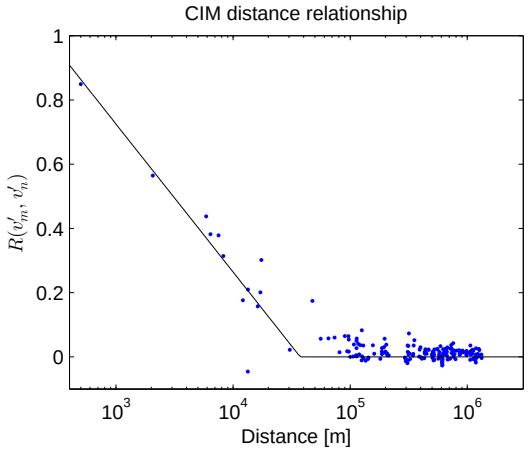

Figure 6.4 Correlation of turbulence versus distance

The CIM approach can be used to impute wind speed time-series, however the method cannot be directly extended to simulate time-series with shorter temporal resolution than that of the

data-set used in its derivation. The desired temporal resolution for the power time-series is 5 min, greater than the 10 min resolution of the WGIP data. A generic CIM model can be developed by applying a correlation versus distance relationship, however it is seen using the scaled correlation analysis that the correlations are also a function of the period, see Figure 4.4. Thus it is desirable to seek a method for simulating turbulence that can replicate the scaled correlations with a temporal resolution of 5 min.

6.2 SPECTRAL REPRESENTATION

As a vortex is advected past the measurement point, the wind speed will deviate from the mean velocity in a manner that reflects the size of the vortex, both in terms of the magnitude of the deviation and the time span of the deviation. Further, vortices do not exist in isolation, they spawn from the interaction of the bulk air movement over a landscape that is complex topographically and thermally. As the landscape is unchanging, and the rate of change of atmospheric stability slow, compared with the wind speed, chains of vortices with similar dimensions are generated and advected in the bulk flow. As this chain of vortices passes the measurement point, there will be a recurrent pattern in the deviation of the wind speed from its mean value. The conservation of angular momentum results in the ideal vortex being cylindrical, and as a chain of cylindrical emanations is advected past a point, the deviations in wind speed will tend to an oscillatory pattern. This is illustrated by Karman vortex sheets which are not only observed in the laboratory but also in satellite imagery [120]. The physical characteristics of idealised turbulence suggest that a representation of the time series using sets of sinusoidal functions should be useful.

The Fourier series expansion (as expressed in Equation 4.9) allows the representation of a time series in the frequency domain, whereby the time series is defined as a set of sinusoids of differing magnitudes, frequencies, and phases. As noted, the vortices have a spatial structure and as they are advected past the point of measurement, the wind speed will vary in a manner corresponding to the spatial size of the vortex. This deviation will be represented in the frequency domain as a spike at the frequency corresponding to the duration that the vortex influences the wind flow at the point of measurement. This is the fundamental component of the Fourier series expansion. However, as the world is not ideal and vortices are not perfect cylinders, the wind speed does not deviate from the mean in a manner that is precisely sinusoidal. To generate the actual shape of the wind speed deviations, further complementary sinusoids are added to the fundamental, and thus the turbulence is represented by a spectrum of frequency components.

The sinusoidal functions derived using the Fourier series expansion are unbounded, that is they exist throughout the entirety of the time series. Thus the fundamental frequency component that results from the advection of an individual eddy past the measurement point will exist equally throughout the length of the time series, and complementary frequencies are added to cancel the oscillation at all other instances in the time series when this fundamental component is not present. Fundamental components will change with time as vortices do not have predetermined properties (they are the result of chaotic processes) and a vortex chain will include a range of vortex magnitudes. Furthermore, vortex chains themselves are not continuous as the speed of the bulk flow varies.

To enable the representation of a time series using sinusoidal functions and to accommodate the non-stationary nature of the turbulence time series, a windowed Fourier series expansion can be applied. Windowing segments the time-series into small temporal spans, and a Fourier series expansion is applied to each of these segments. Thus magnitude and phases for sinusoidal components are found for each segment and vary throughout the entire time-series. The windowed Fourier series expansion has been applied by Woods et al. in the synthesis of wind speed time series in Australia [121].

While the windowed Fourier series expansion addresses some of the issues of non-stationarity it is compromised by the selection of a window size. If a small window is chosen, low frequencies are eliminated, but if large window is used, high frequency oscillations with short temporal spans may not be revealed. The windowed Fourier series expansion is also compromised as it is not a continuous function; the edges of the windows cause a sharp discontinuity which introduces a set of frequency components that are not natural to the time-series (known as spectral leakage). Spectral leakage can be addressed by weighting the window such that the time-series at the edges is graduated to zero; there are many such weighting functions such as Bartlett (triangular), Welch, and Hamming windows, each having its own pattern of spectral leakage.

6.3 MULTI-RESOLUTION ANALYSIS

The transformation of the turbulence time-series into the frequency domain is attractive given that turbulence is the product of oscillatory motions. However, turbulence is non-stationary, making a representation of the turbulence time-series in the frequency domain less useful. It is therefore desirable to seek a method that separates the time-frequency plane such that the temporal span is related to the frequency. This is termed Multi-Resolution Analysis (MRA).

An example of the division of the time frequency plane is presented in Figure 6.5. A short time series is generated using a damped sinusoidal oscillation, with a period of 8 s, and is represented as a function of time in the top left graph. The division of the time-frequency plane for the time-series is illustrated in the bottom left graph.

A discrete Fourier series expansion of the time-series is presented in the middle top graph of Figure 6.5, where the blue bars show the magnitudes, and the red line represents the phases, of the frequency components. While, there is a peak in the power spectra at the fundamental frequency (0.125 Hz), complementary components are necessary for constructing the time-series shape (if the oscillation was not damped the frequency spectra would consist of a single component at the fundamental frequency). The bottom middle graph shows the division of the time frequency plane for the Fourier series expansion.

The top right graph of Figure 6.5 presents a Multi-Resolution decomposition of the time series using the Beylkin wavelet. Wavelets as the name suggests are small wave-like functions that can be used to decompose a time-series. Wavelets are discussed in the following sections. This results in a spike in the time frequency atom centered at a frequency of 0.2 Hz and translation of 2.5 s. As for the Fourier series expansion, the Beylkin wavelet does not exactly match the shape of the damped sinusoidal. Hence, complementary time-frequency atoms are required to construct the time-series. The segmentation of the time frequency plane for the MRA is presented in the bottom right graph, here a dyadic decomposition has been applied.

The segmentation of the time frequency plane for a discrete time series is limited by the resolution of the time series. As shown in the bottom right graph of Figure 6.5 the time-frequency plane corresponding to the time series is segmented such that the number of atoms, or segments, is equal to the number of samples. For the Fourier series expansion the time-frequency plane is segmented such that the the number of atoms is equal to half the number of samples, as each frequency component requires two pieces of information; the magnitude and phase. The frequency components extend from the Nyquist frequency (equal to half the sampling frequency) to the fundamental circular frequency. Here the width of the atoms in the time domain are equal to the length of the time-series and localisation of oscillations in the time domain is not possible. The trade-off between the localisation in frequency and localisation in time of an oscillation is a manifestation of Heisenberg's uncertainty principle [8].

There are many methods that enable a MRA approach, each differentiated by the basis function that they employ. A basis function is a numerical element that can be used to generate a

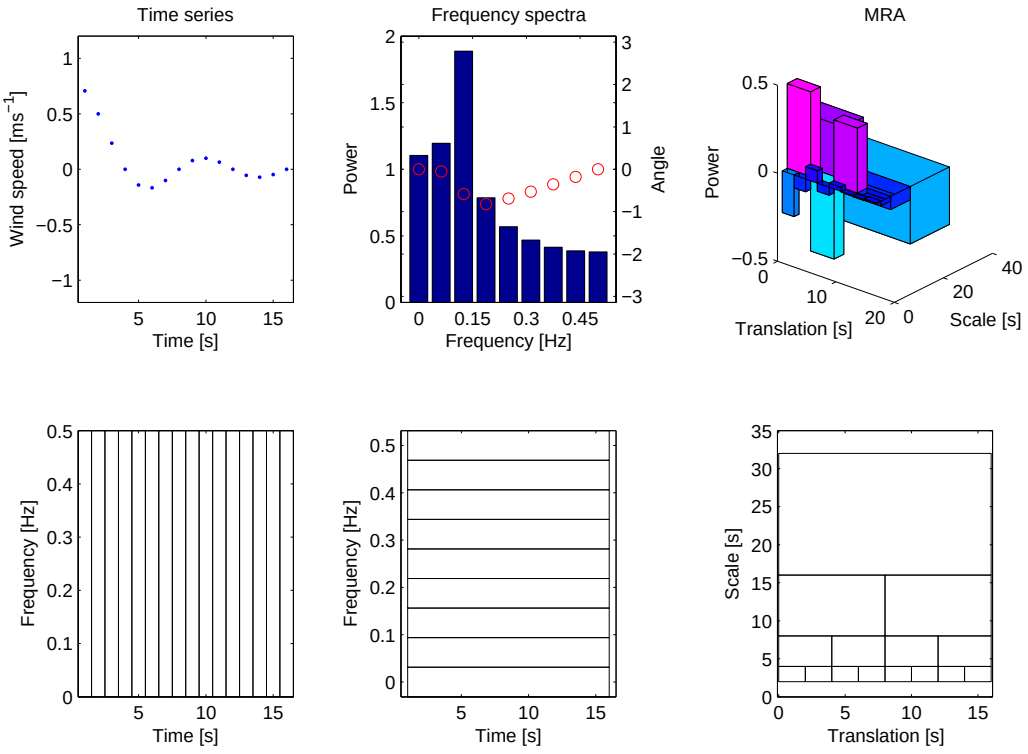

Figure 6.5 Time-Frequency (TF) partitioning example. The top left graph presents a time-series with the partitioning of the TF plane below. The centre top graph shows the Fourier expansion of the time series with magnitudes presented using bars and phases using red circles, the partitioning of the TF plane is shown below. The top right graph shows a Multi-Resolution Analysis representation of the time-series, with the TF plane partitioning below.

numerical sequence by scaling its magnitude and expanding its temporal span (dilation). For example the basis functions for the Fourier series expansion are the sine and cosine functions.

If a wind speed time-series is continuous, i.e. not discretely sampled, then the passage of each vortex past the point of measurement will scribe a fluctuation in the wind speed that can be described by a shape with a unique magnitude, position in time (translation), and temporal span (scale). If all vortices scribe the same shape and this shape, or basis function, is used to decompose the time-series, a precise decomposition of the time-series can be obtained, as each vortex will be described independently. This basis function is referred to as the natural basis and can be used to define a Hilbert space. The function of decomposition forms a projection from the time-domain onto the Hilbert space.

If a basis function other than the natural basis is applied, then the space defined by the basis functions will not perfectly align, or be parallel to the natural space, and a representation with non-minimal entropy will result. Each vortex will not be described as a unique atom, but rather as a fundamental atom and a set of complementary atoms that are the result of the transformation from the natural space to the applied space. As the space described using the applied basis functions is not parallel to the time-frequency plane, it is useful to differentiate its dimensions and apply the terms translation and scale. Further, patterns that are exhibited in the natural space will be distorted when viewed in the applied space, and the effect of the transformation can be construed as distortion of the natural signal much like a lens distorts an image.

There are many methods available to transform a time-series into an MRA, such as the aforementioned windowed Fourier series expansion (and more complex relations such as Gabor function), Smooth Localized Complex Exponentials (SLEX), radial basis functions, extended modulating function (applied to WSTS simulation by Jinhua [122]), and Weinerstrasse functions. The MRA method applied in this thesis uses wavelets. The use of wavelets for modeling WSTS is has been researched with contributions by Hunt in 2001 [123], Kitigawa in 2003 [124], and Siddiqi et al in 2005 [125].

6.3.1 Wavelet decomposition

A wavelet is, as the name suggests, an element that is like a small wave. Numerically a wavelet is a compactly supported oscillatory function (localised and zero outside of a finite range) that is square integrable (a complex function where the integral of the square of absolute values is finite). The wavelet function is presented in Equation 6.24, with its conditions given in Equation 6.25. A time-series can be constructed using a set of wavelets with differing magnitudes that are dilated and translated.

$$\{\psi_{j,k} = \frac{1}{\sqrt{2^j}}\psi\left(\frac{t-2^j k}{2^j}\right)\}_{(j,k)inZ^2} \tag{6.24}$$

Where j is the scale, k is the translation, and Z denotes integers.

$$\begin{gathered}\int_{-\infty}^{\infty}\psi(t)dt = 0,\\ \psi\left(|t|\right) = 0\ for\ t > \iota\end{gathered} \tag{6.25}$$

Where ι is an iota or small value.

The process of decomposition using wavelets is best explained using an example construction of a short time series. For the example the Haar wavelet is used. The Haar wavelet can be considered the primary or most basic wavelet, proposed by Alfrd Haar in 1909, and is equivalent to a single period of a square wave. The Haar wavelet is described in Equation 6.26.

$$\psi(t) = \begin{cases} 1 & if\, 0 \leq t < 1/2 \\ -1 & if\, 1/2 \leq t < 1 \\ 0 & otherwise \end{cases} \tag{6.26}$$

Where ψ denotes the wavelet.

The translation (moving along the time axis) and dilation (extension along the time axis) of the Haar wavelet can be used to generate an ortho-normal basis. An ortho-normal basis is a basis that is both orthogonal and normalised. Orthogonality allows wavelets of differing dilations, or scales, to be added together without interference. The translation k and dilation j are denoted in Equation 6.24. Note that as j can only take integer values and that as j incrementally increases the wavelet is dilated by a power of 2 resulting in the dyadic structure as seen in the bottom right graph of Figure 6.5.

The construction of a time series using the translation and dilation of wavelets is akin to the popular computer game Tetris. However, unlike Tetris the building blocks are all the same shape and come in different sizes. Also, unlike Tetris the building blocks can only be placed in certain positions, and the number of positions available depends on the size of the piece. An example time series constructed using the Haar wavelet is presented in Figure 6.6.

The time-series constructed is a single period of a sine wave. Starting at the top left graph of Figure 6.6, the wavelet structure is arranged into a vector, with coefficients grouped by scale (shown numerically across the top of the graph). The first element in the vector is the "residual time series term" (which can be reconciled as a bias term) having a scale of 8 and a translation of 4. The second element is the wavelet coefficient for a Haar wavelet with scale of 8 and a translation of 4. The remaining wavelet coefficients are zero. The time-series formed using the inverse wavelet transform of this wavelet structure is presented in the middle top graph. It reflects the Haar wavelet shape, and has samples centered at 0.5 through 7.5 with increments of one. The top right graph shows the portion of the translation-scale plane covered by non-zero atoms in this wavelet series.

The middle row of Figure 6.6 shows the construction of the sine wave using wavelet series with scales of 8 and 4, the centre graph shows the time-series partly exhibiting the sine shape. The bottom row shows the construction of the sine wave using scales of 8, 4, and 2. Using scales of 8, 4, and 2 the time-series is recognisable as a sine wave, although discretised. To obtain a smoother sine function, further wavelet series with scales of one and lower would need to be added to the wavelet structure.

Although Haar applied his basis function to decompose time-series as early as 1909 it was not until 1984 that the word wavelet was posited by Morlet and Grossmann. Thereafter, contributions by Yves Meyer, Stephane Mallat, Ingrid Daubechies, David Donoho, and Iain Johnstone helped cement the field of wavelet analysis, such that by 1999 wavelets had become intrinsic to processes such as the denoising that underlies the JPEG-2000 compression standard [126]. Some examples of wavelets that have been discovered are presented in Figure 6.7. The wavelets are typically named after the discoverer; Ingrid Daubechies is a prolific discoverer of wavelets and defined a sequence of wavelets. The Daubechies wavelets are characterised by having a maximal number of vanishing moments for the given support. In effect the Haar wavelet could be referred to as a Daubechies 2 wavelet. Note that while solid lines are used to illustrate the wavelet shape the wavelet only exists at integer values of translation as these are discrete wavelets used for decomposition of discrete time-series. The wavelet analysis used here is performed using the WaveLab toolbox for Matlab [8], hence the selection of wavelets is limited.

The example of the construction of a time-series is useful as an illustration. However, the usefulness of wavelets is not limited to their constructive utility, but also their ability to deconstruct or decompose a time series, and it is this process that is termed the wavelet transform. The wavelet

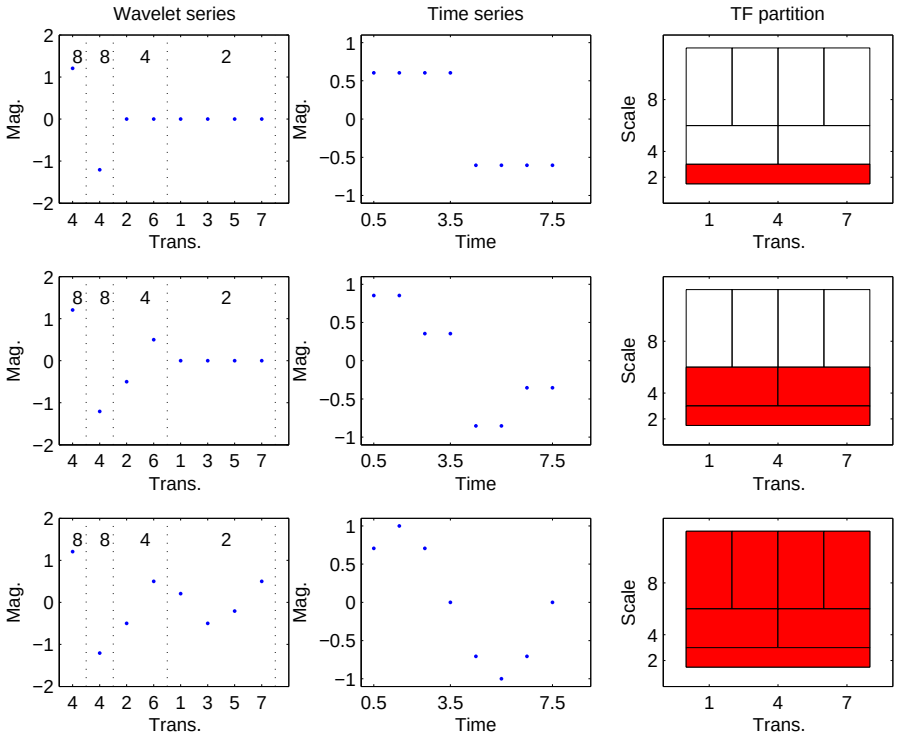

Figure 6.6 Time series construction using Haar wavelet. Wavelet structures are presented in the left column of graph, with scales denoted by the integer values, the left most atom is the residual component, the second atom from the left is the wavelet series with a scale of 8. The center column of graphs present the time-series resolved through the inverse wavelet transform given the wavelet structure on the left. The right most column of graphs shows the portion of the time-frequency plane covered by non-zero atoms in the wavelet structure.

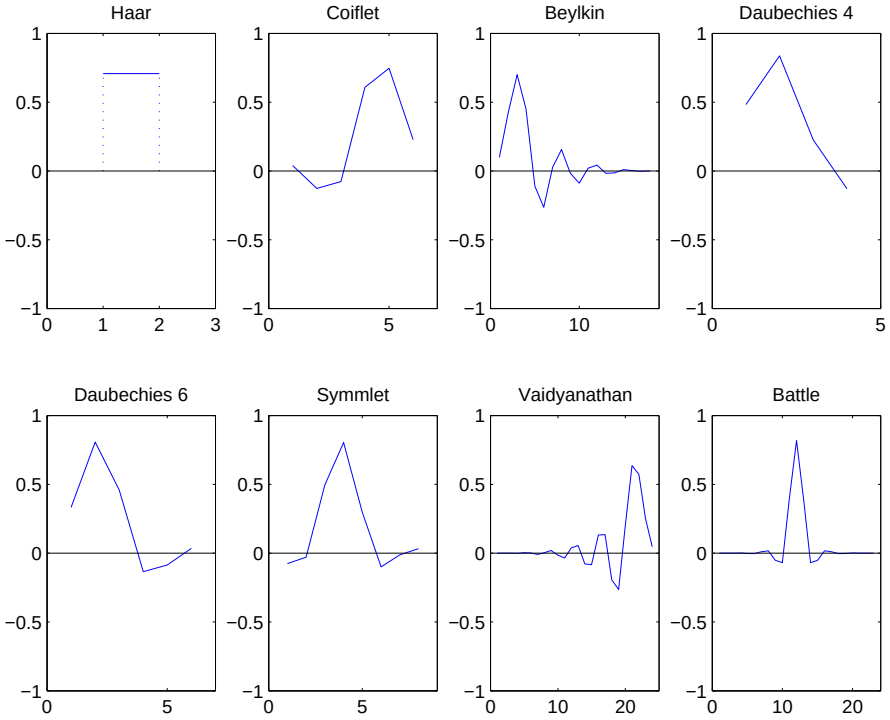

Figure 6.7 Example wavelets. Note that solid lines have been used to scribe the shape of the wavelet. Wavelets are integer functions.

transform is the convolution of the wavelet over the time series and is presented in Equation 6.27.

$$\langle u(k, 2^j), \Psi(j, k)\rangle = \int_{-\infty}^{\infty} v(t)\frac{1}{\sqrt{j}}\psi^*\left(\frac{t-k}{j}\right)dt \qquad (6.27)$$

Where Ψ is the wavelet coefficient series, t is time, and * denotes the complex conjugate.

The popularity of the Fourier transform, aside from the mathematical and natural importance of sine waves, is largely due to the existence of the Fast Fourier Transform (FFT). The FFT allows the numerically efficient computation of the Fourier series expansion. Likewise the existence of the Fast Wavelet Transform (FWT) and its inverse transform for discrete time-series encourages the application of wavelets as a method to decompose time-series. While it is possible to decompose a time-series using MRA in a manner that does not result in a dyadic decomposition, and this may be attractive for analytic purposes, the existence of the Fast Wavelet Transform (FWT), and its availability, incentivises analyses that make use of the FWT.

The wavelet decomposition of a time-series is often presented graphically as a spectrogram. The spectrogram for the Northland 1 wind speed time series for the period from 1 January 2005 through 7 January 2005 is presented in Figure 6.8. Spectrograms can be useful for identifying structures within the time-series. Of note in the example are the vertical stripes that indicate correlation between wavelets of different magnitudes; this is a manifestation of the heteroskedasticity of turbulence.

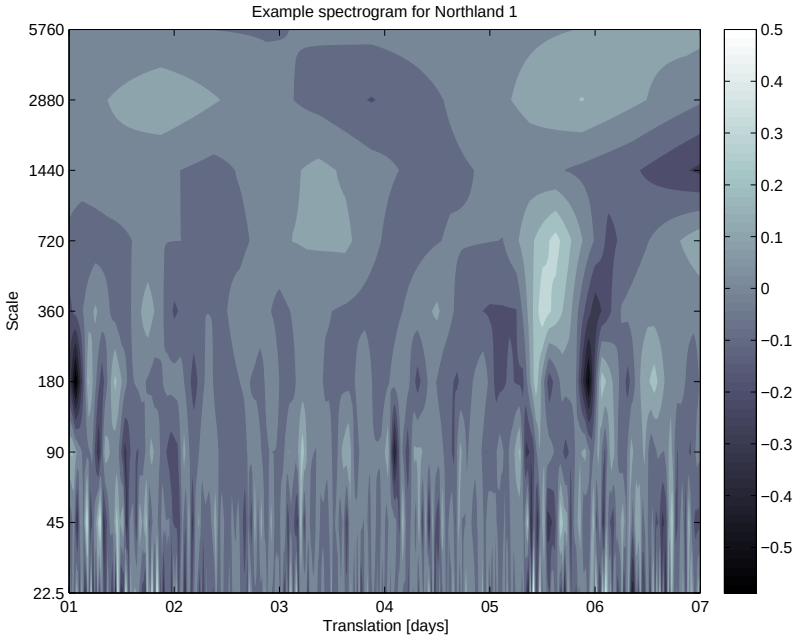

Figure 6.8 Spectrogram of Northland 1 wind data for period from 1 January 2005 through 7 January 2005, shaded according to normalised magnitudes

It could be advantageous to use a non-dyadic decomposition for time-series where regular cycles are expected; a dyadic decomposition of a time-series with 10 min sample period results in scales centered on 20, 40, 80, 160, 320, 640, 1280, and 2560 min. This does not mesh with the daily period of 1440 min, thus oscillatory motions with a diurnal cycle will not be decomposed as a regular pattern at a discrete scale and hence decomposition will not be straightforward. Further, the resolution of the NWP model is 6 h (360 min), which does not equal a scale resulting from the dyadic decomposition of the 10 min sampled time-series. Hence, coupling of the turbulence time-series to the interpolated and scaled ECMWF-interim time series is not straightforward.

In order that the FWT can be applied the wind time-series is re-sampled using cubic spline interpolation at a resolution of $\frac{1}{128}$ days or 11.25 min.

The process of wavelet decomposition of a time-series, using the Beylkin wavelet, is presented in Figure 6.9. A small time-series is presented in the graph at the top left with a sampling period of 22.5 min. Each operation or level of decomposition is shown by the arrows, and corresponds to the application of a pair of high and low pass filters. The high pass filter results in a series of coefficients for wavelets with a scale of 45 min. The low pass filter results in a residual time-series also with a temporal resolution of 45 min. Note that the number of samples in the time-series is halved with each stage of decomposition, and that the magnitude increases by $\sqrt{2}$.

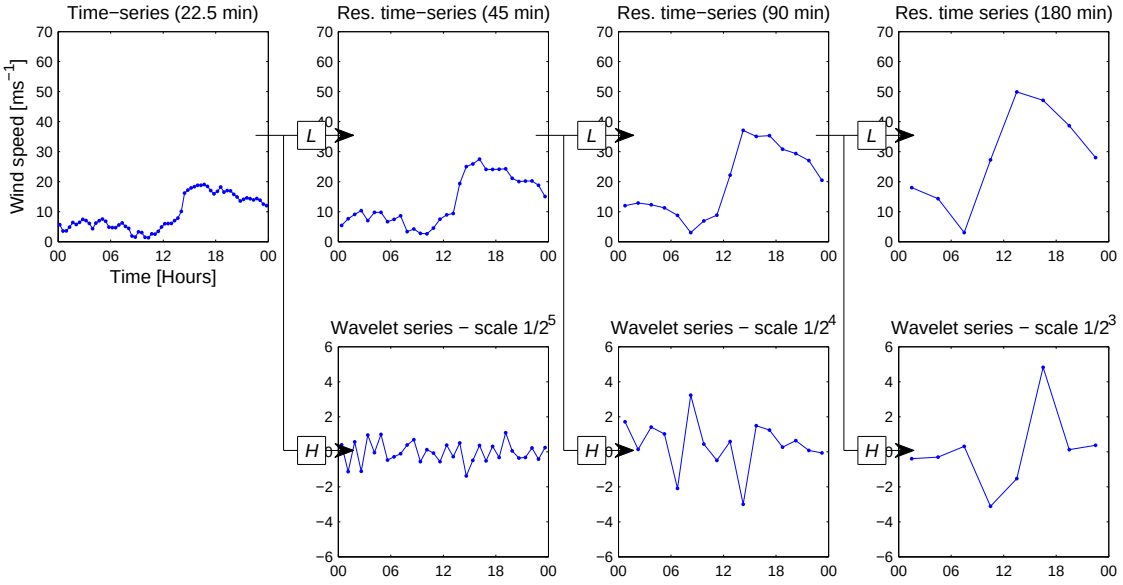

Figure 6.9 Example of wavelet decomposition. A time-series is presented in the top left graph. Each stage of wavelet decomposition involves the application of a pair of low pass and high pass filters resulting in a residual time-series and a wavelet series.

6.3.2 Wavelet Multi-resolution Analysis model fitting

The decomposition of the time-series in this example results in three wavelet series and a residual time series. Each of the wavelet series can be treated as a time-series and modelled using an ARMA approach. The residual time-series is a smoothed and scaled replica of the original time-series. For a time-series with an 11.25 min resolution, if 5 stages of decomposition are applied, 5 wavelet series (with scales 22.5, 45, 90, 180, and 360 min) and a residual time series with a resolution of 360 min result.

As shown in 6.7 there are many wavelets; the selection of the wavelet depends on the process that is being modeled and the desired result. Selection criteria may weight certain properties, i.e. if the process is time critical then a compact wavelet may be selected. A wavelet that has compact support, such as the Haar, has very good time-resolution. That is the timing of an event is well known, but the shape or frequency of the event is not well known. As the wavelet support is increased the shape of the wavelet becomes more complicated. If the wavelet shape matches an oscillatory motion, the scale of the event will be well captured but the accuracy of the temporal position (translation) compromised. Another selection criteria, often applied for 'de-noising' processes, is minimisation of entropy.

Here the selection of the wavelet is made to simplify the model structure. The wavelet transform increases the dimensionality of the time-series by projecting it onto a translation-scale plane; the set of wavelet series, as for the time-series, have not only auto-correlations and correlations (as shown in Equations 6.28 and 6.29), but also have cross correlations as shown in Equation 6.30. The cross correlation is defined as the correlation between wavelets of different scales resulting from the same time-series. Note the translation increment in Equation 6.30; in the dyadic decomposition each time frequency atom at a certain scale and translation has two neighbouring time-frequency atoms in the incrementally lower scale, nominally these atoms are centered at translations plus and minus quarter the width of the atom.

$$R(\Psi_s(j), \Psi_s(j)) = \sum_{k=1}^{K} \{(\Psi_s(j,k) - \overline{\Psi_s(j)}) \cdot (\Psi_s(j,k+1) - \overline{\Psi_s(j)})\} \tag{6.28}$$

Where $R(\Psi_s(j,k), \Psi_s(j,k+\delta))$ is the wavelet series auto correlation at scale j, s is a site, k is the translation, and $\overline{\Psi_s(j)}$ is the average of the wavelet coefficients with scale j.

$$R(\Psi_s(j), \Psi_r(j)) = \sum_{k=1}^{K} \{(\Psi_s(j,k) - \overline{\Psi_s(j)}) \cdot (\Psi_r(j,k) - \overline{\Psi_r(j)})\} \tag{6.29}$$

Where $R(\Psi_s(j), \Psi_r(j))$ is the correlation between wavelet series of scale j from sites s and r.

$$R(\Psi_s(j), \Psi_s(j+1)) = \sum_{\delta=[-\frac{1}{4},\frac{1}{4}]} \sum_{k=1}^{K} \{(\Psi_s(j,k) - \overline{\Psi_s(j)}) \cdot (\Psi_s(j+1,k+\delta) - \overline{\Psi_s(j+1)})\} \tag{6.30}$$

Where $R(\Psi_s(j), \Psi_s(j+1))$ is the cross correlation between wavelet series with scale j and $j+1$ from site s.

The wavelet is selected such that the cross-correlation is minimised, and can be assumed zero so that wavelet series from the same time-series can be treated as independent AR series. To be treated as an AR model the wavelet series must be able to be represented by stationary Gaussian processes and, as for the CIM model, some conditioning is required. The wavelet series are found to be heteroskedastic, the dependence od wavelet magnitude on the mean or bulk wind speed is seen in the top left graph of Figure 6.10. A Taylor's power transform, shown in Equation 6.31, is applied to remove the dependence on the bulk wind speed. The mean wind speed is derived from the residual time-series with a scale of 6 h. Full results for Taylor's exponents are presented in Appendix B.

$$\Psi^{(T)}(j,k) = \frac{\Psi(j,k)}{\overline{v(t)}^{a}} \tag{6.31}$$

Where a is the Taylor exponent, T represents the Taylor transformed variable, and $\overline{v(t)}$ is the mean or residual wind speed.

The Taylor transformed wavelet-series (adjusted to account for the magnitude of the wind speed) are found to be non-Gaussian. The shapes of the probability distributions, for wavelet series at all scales and from all sites, are very similar, but not closely related to any commonly applied probability distribution. The probability distributions are found to be leptokurtic (having kurtosis greater than that of the best fit Gaussian distribution) and to have some consistent relationship to the Gaussian distribution. It is found that a Johnson transform, as presented in

Equation 6.32, can be used to transform the measured distribution to the Gaussian distribution; the fitting and application of which is achieved using the Johnson Curve Toolbox for Matlab [127]. Full results for fitting Johnson curves are presented in Appendix B. The Gaussianity of the conditioned wavelet-series is confirmed by normalised Cramer von Mises statistics less than 0.03 for all sites at all scales.

$$\Psi s^{(TJ)}(j,k) = \gamma_J + \eta_J \, sinh^{-1}(\frac{\Psi_s^{(T)}(j,k) - \epsilon_J}{\lambda_J}) \tag{6.32}$$

Where J represents the Johnson transformed variable, γ_J and η_J are Johnson shape parameters, ϵ_J is the Johnson location parameter, and λ_J is the Johnson scale parameter.

The selection of the wavelet shape is made by minimising the cross correlation of the set of Taylor-Johnson transformed wavelet series. The average (across all sites) cross correlation for each scale for each of the wavelets is presented in Table 6.4. This shows the Haar wavelet is particularly poor at minimising cross-correlations and the Beylkin and Vaidyanathan wavelets perform very well, with very little to separate them. The Beylkin wavelet is selected as it is more compact.

Scale [min]	**Low**	22.5	45	90	180
	High	45	90	180	360
Wavelet	Haar	0.44	0.39	0.44	0.47
	Coiflet	0.13	0.13	0.12	0.13
	Beylkin	-0.01	-0.01	0	0.01
	Daubechies 4	0.24	0.16	0.2	0.23
	Daubechies 6	0.14	0.08	0.11	0.13
	Symmlet	0.09	0.1	0.1	0.11
	Vaidyanathan	0.01	0.01	0	-0.01
	Battle	0.1	0.11	0.1	0.11

Table 6.4 Wavelet selection - cross correlations

The conditioning of the wavelet series derived from the WGIP data set is illustrated for a scale of 22.5 min in Figure 6.10. The top left graph presents the magnitude of wavelet coefficients binned by wind speed with the blue lines representing the raw data and the red line showing the Taylor's power law transformed wavelet coefficients. The top right graph presents a quantile-quantile (QQ) plot with blue lines representing the Taylor's power law transformed wavelet coefficients and the red lines show the Taylor-Johnson transformed coefficients conforming to a Gaussian distribution. The lower left graph presents the PSD of the wavelet coefficients, each line representing a different mast. The lower right graph shows the scaled correlation of wavelet series showing the correlation in wavelet series is independent of the period.

Once the Taylor and Johnson transforms have been applied the conditioned wavelet series are found to be well approximated by stationary Gaussian processes. As for the CIM model, correlograms and partial-correlograms are used to derive the model order, these are shown for a scale of 22.5 min in Figure 6.11, with each line representing a wavelet series derived from a meteorological mast. These show the wavelet series to all have similar characteristics; being over-differenced and able to be approximated using a pure AR model of order two. The CIM method, as used for the turbulence model, is applied to the wavelet series.

A set of time-series can be simulated using wavelet decomposition using the following procedure:

- Wavelet structures are formed, for each time-series, and the coarse resolution wind speed time-series (interpolated and scaled from the ERA-interim data) placed into the residual time-series partition.

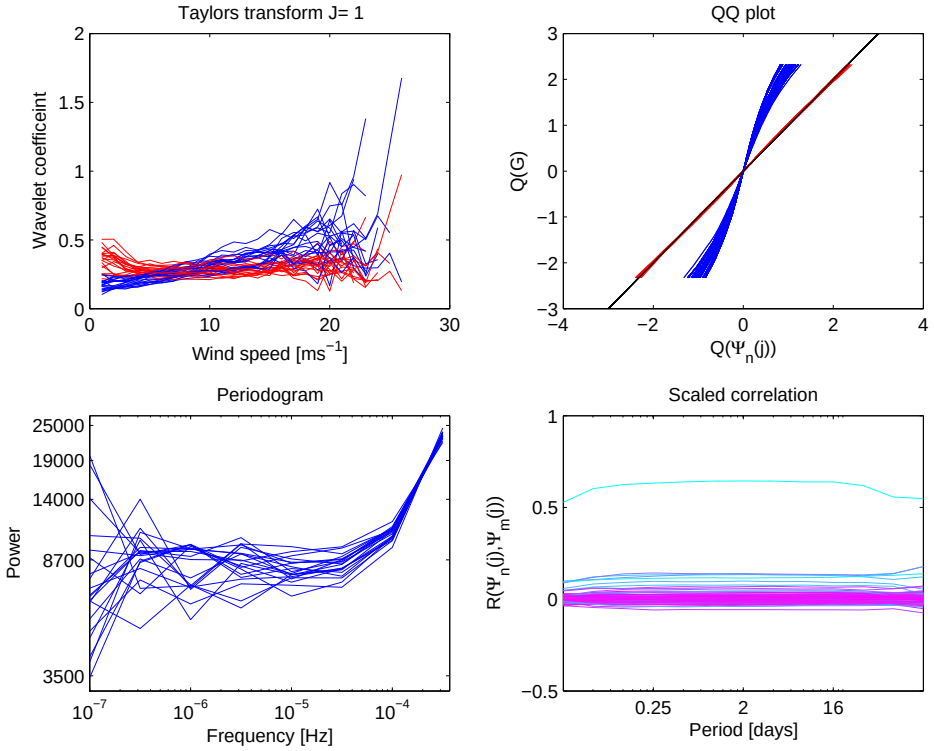

Figure 6.10 Statistics for wavelet series, scale 22.5 min. The top left graph shows the relationshipo between the wavelet magnitude and the bulk wind speed using the blue lines (each line representing measurements from a different meteorological mast). The removal of the dependence on bulk wind speed using the Taylor's transform is shown using the red lines. The top right graph shows a Quantile-Quantile plot. The unconditioned wavelet series, shown using blue lines, have probability distributions that do not resemble a Gaussian distribution. The wavelet series conditioned using a Johnson transform are shown as red lines and are well matched to a Gaussian distribution. The lower right graph shown a periodogram for the wavelet series, and the lower right graph presents scaled correlations for the wavelet series.

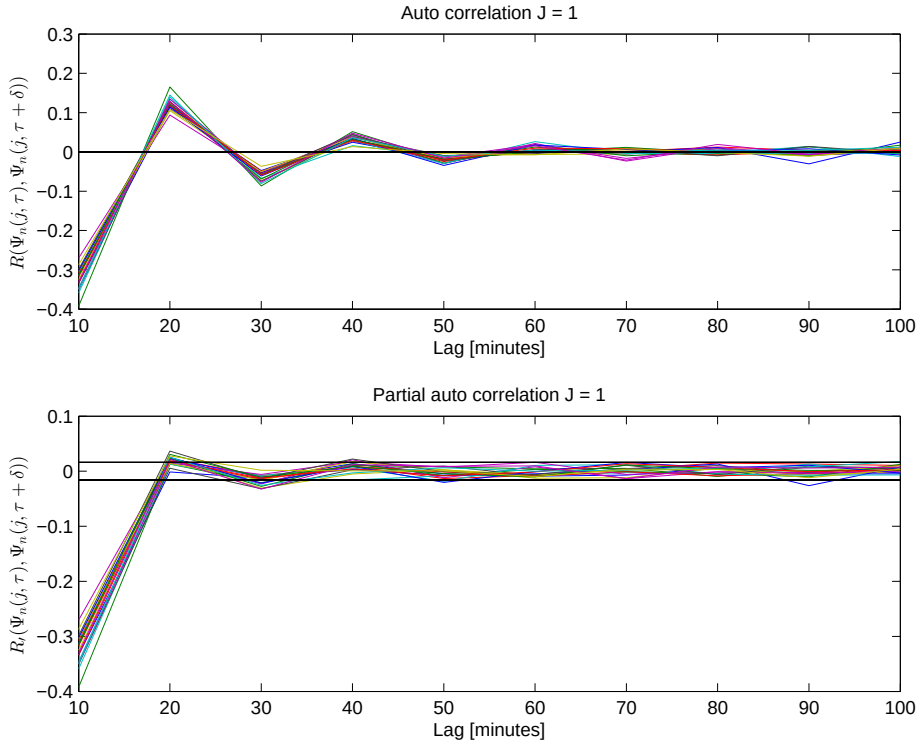

Figure 6.11 Correlogram and partial-correlogram for wavelet series, scale = 22.5 minutes. Each line represents the analyses of wavelet series from a meteorological mast.

- Wavelet series are simulated using the CIM approach, and placed into their respective partitions.
- The inverse wavelet transform is applied to the wavelet structures to obtain coherent sets of wind speed time-series.

The set of time-series simulated using the WMA method is compared with the measured data in Figure 6.12. The top left graph presents the quantile-quantile plot showing little change from the distribution inherited from the ERA-interim interpolated and scaled data. The top right graph presents a periodogram showing that the WMA model has better adherence to the measured spectra than the CIM model, illustrating the advantage of the MRA approach. The lower left graph presents the simulated correlations versus those from the measured data again showing little change from the properties of the inherited ERA-interim data. The lower right graph presents scaled correlations and shows the WMA model performs very well, and performs better than the CIM model. The CIM model has a tendency to over predict correlations at low scales.

6.3.3 A generic Wavelet Multi-resolution Analysis model

The motivation for applying the WMA model is not only to increase the accuracy of the correlation structure, but also to enable the time-series to be imputed to a higher temporal resolution than that of the measured data. Assuming a Kolmogorov spectrum enables a log-linear extrapolation of the measured power spectra obtained using a Fourier series expansion. However, extrapolation using the Kolmogorov spectrum does not enable the heteroskedasticity of turbulence to be replicated. The WMA method can be extended to accommodate the increased temporal resolution while ensuring the spatial correlation structure and heteroskedasticity are replicated.

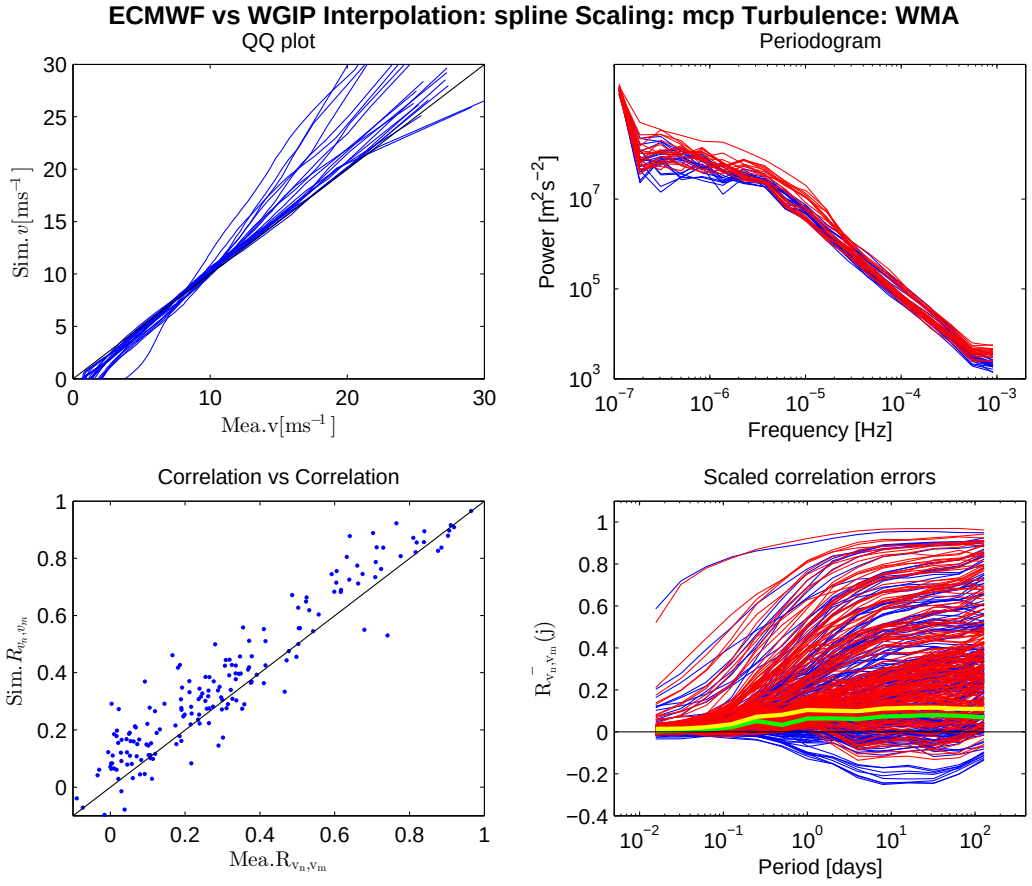

Figure 6.12 Statistics comparing wind speed time-series from WGIP data-set with those simulated using Model Output Statistics from the ECMWF-interim reanalyses which have been interpolated using cubic splines, scaled using Measure Correlate Predict, and imputed using the WMA turbulence model. Top left graph shows a Quantile-Quantile plot with each line representing results from a different meteorological mast. The top right graph presents a periodogram with PSDs from measured WSTS shown as blue lines, and from simulated time-series as red lines. The bottom left graph presents simulated correlations versus measured correlations. The bottom right graph shows scaled correlations between pairs of sites (blue lines represent measured time-series, and red line simulated time-series). The green line presents the mean bias in the difference between simulated and measured scaled correlations, and the yellow line shows the associated RMS difference.

While the Kolmogorov spectrum may hold for the power spectra obtained using the Fourier series expansion, and the magnitude of the wavelet series observed to possess a near power law relationship with the scale, it is not axiomatic that the Kolmogorov spectral relationship should be applied to wavelet decomposition. Hence, wind speed time-series at higher temporal resolution are required to extend the wavelet model. Data from the Mt Stuart WPP have been obtained and are used for this purpose, they are also used later to derive WPP power curves.

The Mt Stuart WPP comprises nine 850 kW Gamesa G52 wind turbines (total 7.65 MW) with a hub height of 45 m, stretching north to south in a single line across the top of Mt Stuart in South Otago, NZ. The wind turbine power curve for the Gamesa G52 turbine has been obtained from sales documentation [128]. Mt Stuart is elevated above the rolling hill country, well exposed to the prevailing westerly winds. Each wind turbine has a cup anemometer mounted on the rear of the nacelle. The WPP also has a 30 m meteorological mast, sited between turbines, near the middle of the WPP. Power, wind speed, and nacelle orientation for each turbine, total WPP power, and meteorological mast wind speed and direction data have been extracted from the SCADA, at a resolution of 1 min, for a period of one year. There are few missing values, and as for the WGIP data-set these are imputed using multiple linear regression based on the set of coincident valid wind speed measurements.

The wind speed time-series from the nacelle anemometers have a high pass filter applied to assist in turbine fault diagnostics. Further, the nacelle anemometers are located behind the turbine rotor and are affected by the rotor wake and the nacelle bulk. It is necessary to scale the nacelle WSTS such that they are representative of the free stream wind speed. Kolmogorov's theory for the spectral energy density, as presented in Equation 5.3, is used as a target to scale the nacelle WSTS [6]. The effect of the scaling is illustrated in Figure 6.13.

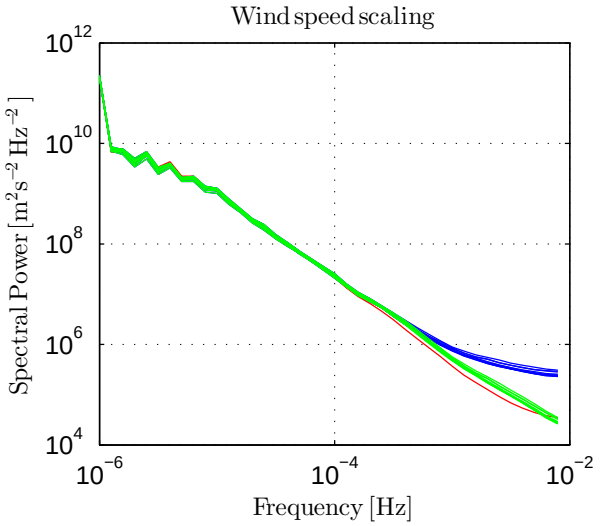

Figure 6.13 Kolmogorov scaling: nacelle wind speed power spectra shown by blue lines, scaled power spectra shown by green lines, and power spectra from meteorological mast shown by red line.

The nacelle anemometers from the Mt Stuart WPP can be used to define wavelet series for scales of 11.25 min and 5.625 min. The time-series resulting from the extended WMA model has a temporal resolution of 2.8125 min which is interpolated to obtain a time-series with the desired 5 min resolution. To achieve this the 1 min data from Mt Stuart are interpolated using cubic splines to 2.8125 min, and a wavelet decomposition using the Beylkin wavelet applied. Results from the wavelet decomposition of the Mt Stuart nacelle anemometer data are presented in Appendix B.

The WMA model results presented in Figure 6.12 are developed using the WGIP data and are

specific to that data-set. For the WMA model to be extended using parameters derived from a different data-set, generalisation of the model is required. The WMA model is generalised by applying the average values for each parameter as shown in Table 6.5. Note that the values for standard deviation derived from the WGIP data are multiplied by a factor of 2^2 as the level of decomposition has two more steps. The model is extended to scales of 2.8125 min and 5.625 min using parameter values equaling the average values calculated from the Mt Stuart data. The WGIP data is used in preference to the Mt Stuart data, as the veracity of wind speed measurements made at Mt Stuart are compromised by the application of the filter and mounting of anemometers on the nacelle behind the rotor.

Scale [min]	**5.63**	**11.25**	**22.5**	**45**	**90**	**180**	**360**
$R(\Psi n^{(TJ)}(j,\tau), \Psi n^{(TJ)}(j,\tau+1)$	-0.15	-0.25	-0.31	-0.28	-0.24	-0.27	-0.29
Taylor exp.	0.68	0.62	0.47	0.39	0.32	0.26	0.17
Johnson coefficient (γ)	-0.01	-0.01	0	0.01	-0.02	0	0.02
Johnson coefficient (η)	1.57	1.63	1.43	1.53	1.69	1.88	2.13
Johnson coefficient (ϵ)	-0.01	-0.01	0	0.01	-0.02	0	0.13
Johnson coefficient (λ)	1.26	1.33	0.43	0.97	2	4.1	9.05
$\sigma(\Psi n^{(TJ)}(j)$	0.5	0.8	1.57	3.2	5.73	10.17	19.17

Table 6.5 Generic wavelet model parameters. Parameters with scales of 5.63 and 11.25 min are derived from the Mt Stuart data, all other parameters are derived from the WGIP data.

The model parameters presented in Table 6.5 exclude correlations. It is hypothesised that the correlation is a function of distance and scale and this is confirmed in Figure 6.14. The correlations are presented for both data sets; samples marked with a dot come from the Mt Stuart data set and those marked with a circle derive from the WGIP data set. It is found that the distance relationship is well described using a log-linear relationship, fitted using least squares, and presented as the solid lines. Both data sets are used in conjunction to form the distance relationships as the separation distances between masts in the WGIP data set are too great to ensure correlations at scales less than 180 min are well defined.

6.4 SUMMARY

The wind speed time-series derived from the ERA-interim model have insufficient temporal resolution for supporting UCED integration studies and must be imputed. The wind is inherently variable and imputation requires a model of turbulence. A turbulence time-series can be modelled as a pure Auto-Regressive process with model order and type identified using the Box-Jenkin method. A set of coherent turbulence time-series can be simulated by weighting the innovations in the AR process using the Cholesky decomposition of the correlation matrix. This method is termed the Correlated Innovation Matrix method and is shown to accurately replicate the set of turbulence time-series. However, the wind speed time-series used to form the CIM model are of insufficient temporal resolution for supporting UCED studies and the correlation term is independent of the scale of the turbulence, hence a method using Wavelet Multi-resolution Aanalysis is developed. The WMA method requires careful selection of the wavelet shape to ensure cross-correlations are mininsed and the dimensionality of the set of wavelet series is effectively reduced. The WMA method also requires application of Taylor's power law and Johnson transforms to ensure the wavelet series can be represented by stationary Gaussian processes and can be simulated using an AR model. It is shown that the WMA model can accurately replicate the statistics of the set of wind speed time-series and the model can be generalised to enable augmentation using additional data-sets to obtain higher temporal resolutions. The generalised WMA model allows sets of coherent wind speed time-series, that are

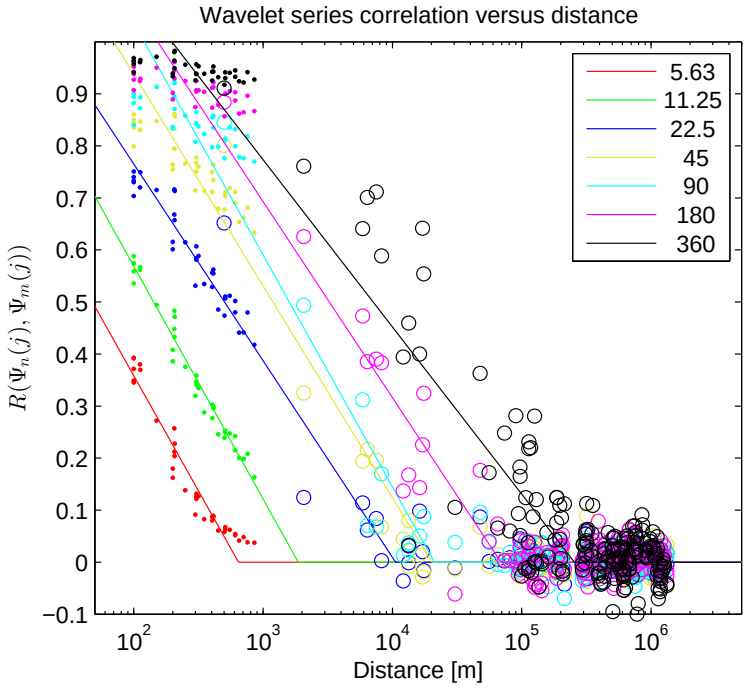

Figure 6.14 Correlation versus distance for WMA model. Scales are represented using different colours. Correlations derived from the Mt Stuart nacelle anemometers are presented as dots, and correlations derived from the WGIP data-set are shown using circles.

representative of notional wind power plants, to be simulated and these can then be converted to wind power time-series as described in the following chapter.

Chapter 7

WIND POWER SIMULATION

Coarse Wind Speed Time-Series (WSTS) that can be used to represent the wind incident on notional WPPs, are obtained from the ERA-interim NWP model. These coarse WSTS are interpolated, scaled, and imputed to obtain statistically coherent sets suitable for supporting UCED studies. UCED studies require power time-series, hence it is necessary to transform the WSTS to power.

As shown in Section 2.2 the transformation of wind speed to power by an individual wind turbine is well defined by the wind turbine power curve. The wind turbine power curve is a steady state function; a transformation from wind speed to power that is independent of the dynamic character of the wind (the turbulence). Likewise the WPP power curve, as shown in Equation 2.4, constitutes a steady state transform. However, WPPs comprise wind turbines distributed over an area and diversity in the wind incident on individual turbines results in smoothing of the power [129]. Further, wind turbines have a rotor (over which the wind is integrated), and control systems to regulate and smooth the power. Hence it is necessary to add a dynamic component such that the transformation from WSTS to power correctly captures variability.

7.1 WIND SPEED TO POWER TRANSFORM

To procedure for transforming a wind speed time-series to power is complicated and a flow chart is presented in Figure 7.1.

The power from a WPP can be referenced to a wind speed and direction measurement made at a meteorological mast to form a power performance matrix, see Equation 2.3. While there is extensive information available to aid in simulating wind speed time-series, and wind turbines are marketed using published wind turbine power curves, there is less information pertaining to the performance of WPPs (as such information is usually proprietary). To help develop a model for the transformation of WSTS to power, data have been obtained from the Mt Stuart Wind Farm. A view of the Mt Stuart Wind Farm is shown in Figure 7.2.

7.1.1 Steady state transform

A WPP comprises wind turbines spread across a landscape, as such the wind speed incident on each turbine is different. As stated in Section 5.7.3 the average difference in wind speed between two points, for a given wind direction, in close proximity is well described using a linear regression and this gives rise to the MCP method [102]. The MCP method is a steady state transformation and is applied to the Mt Stuart Wind Farm using the following procedure.

The WSTS at the meteorological mast is binned into twelve 30° sectors (with periods when the wind speed is less than $3ms^{-1}$ excluded). For each turbine, in each direction sector, a linear

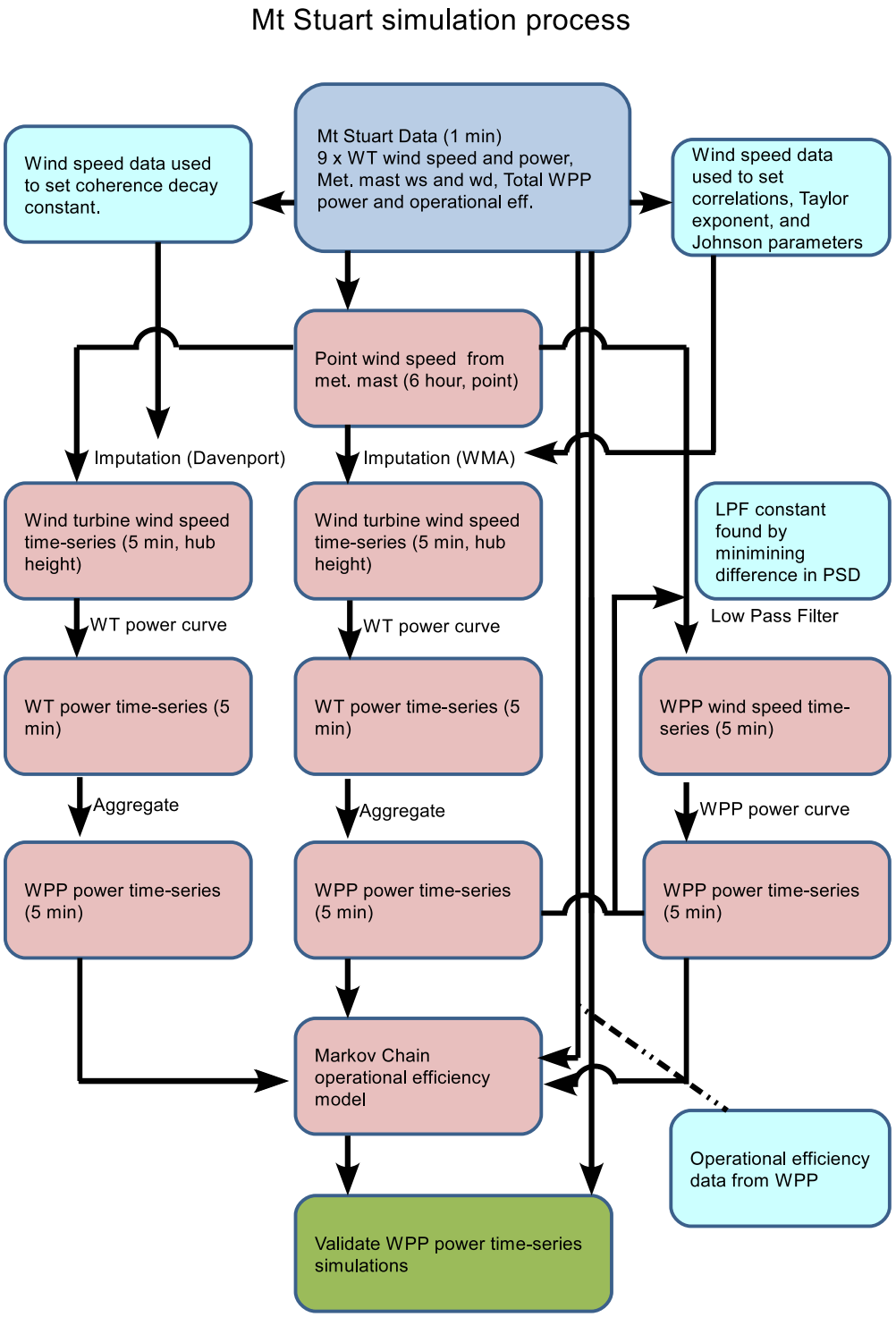

Figure 7.1 Flow chart for process of simulating the power from Mt Stuart.

Figure 7.2 Mt Stuart WPP: 8 Gamesa G52 WTs, the meteorological mast is located between turbines 5 and 6 numbered left to right.

regression is formed between the meteorological mast and the nacelle anemometer WSTS. The best fit linear regression is solved using least squares forced through the origin, resulting in a slope parameter which is termed the "speed-up". The speed-ups are applied to the WSTS measured at the meteorological mast to obtain WSTS for each turbine as shown in Equation 5.5. Parameters resulting from the MCP method applied to Mt Stuart are presented in Appendix B.

The WSTS, calculated using the MCP method for each wind turbine, are smoothed so that as a set they can be considered concomitant. Concomitance is a function of the temporal resolution, being the temporal equivalent of coherence. It can be seen in Figure 6.14, for the Mt Stuart data, that all WSTS pairs have a correlation greater than 0.9 for a scale of 360 min and thus are assumed concomitant for scales of 360 min and higher.

The MCP method applies speed-ups, calculated for each direction sector, between the meteorological mast and each wind turbine. It is reasonable to expect that the speed-ups for each direction sector can be approximated using a Gaussian distribution, and this is confirmed by the data. While the location of the notional WPPs to be assessed in the scenarios is known and it may be possible through extensive effort to design representative WPPs, apply wind flow modeling software (such as WAsP which applies methodologies defined in the European Wind Atlas [94]), and obtain an entire collection of speed-ups for each WPP, this would require extensive resource and is not practical. Rather, a statistical model for speed-ups is constructed using the results from Mt Stuart.

As shown in Equation 7.1 the power produced by the WPP is a function of the wind direction and it is assumed that the speed-ups, in each of the direction sectors have a Gaussian distribution. If the moments of the distribution of speed-ups are assumed identical in all direction sectors and that the speed-ups of individual turbines are independent, then the MCP equation can be collapsed such that the WPP power curve is independent of the wind direction. The resulting Gaussian WPP power curve is shown in Equation 7.2. The Gaussian power curve method has been applied in the WGIP study [1] and by Norgard [130] among others.

$$P(t) = P(\sum_{n=1}^{N} S(n, d(t)) \cdot v(t)) \tag{7.1}$$

Where P is power, n is a wind turbine with a total of N turbines, S is the speed-up, d is the wind direction, and v is the wind speed.

$$P_{WPP}(v) = \int_{q=0}^{1} P_{WT}(v \cdot S_{\mu_g,\sigma_g}(q))dq \tag{7.2}$$

Where P is power, S_{μ_g,σ_g} are the speed-ups conforming to a Gaussian distribution with mean μ_g and standard deviation σ_g, d is wind direction sector, and q is probability.

It is found for Mt Stuart that the mean speed-up is 1.08, and the frequency weighted standard deviation of the speed-ups is 0.065. The frequency weighted standard deviation is presented in Equation 7.3.

$$\sigma_w(S) = \sqrt{\frac{\sum_{d=1}^{D} q_d(S_d - \mu(S))}{\frac{(D-1)}{D}\sum_{d=1}^{D} q_d}} \tag{7.3}$$

Where D is the total number of direction sectors.

An alternative method for deriving a WPP power curve was proposed by De Tommasi. This method uses the convolution of a Gaussian filter with the wind turbine power curve as shown in Equation 7.4 [131]. De Tommasi recommends that σ_G should equal the standard deviation of the wind speed. In practice values of approximately $2\,\mathrm{ms}^{-1}$ are obtained for wind farms varying in size from 10 to 100 wind turbines.

$$PC_{WPP}(v) = PC_{WT} * \frac{1}{\sqrt{2\pi}\sigma_G} e^{-\frac{S \cdot v^2}{2\sigma_G^2}} \tag{7.4}$$

Where σ_G is the standard deviation or width of the Gaussian filter.

7.1.2 Dynamic transform

The MCP method models speed-ups as a steady state function, dependent on the topography not on time; however the actual speed-ups change dynamically as a result of the propagation of eddies across the landscape. In the application of the MCP algorithm the WSTS are averaged to 6 h to ensure concomitance and hence approximate a steady state function, however, a higher temporal resolution is required for UCED studies. Hence, a dynamic model of turbulence is also required.

Although this study requires a temporal resolution of 5 min, which is much coarser than that required for dynamic power quality or turbine load studies, which can require temporal resolutions as fine as milli-seconds, it is useful to look to methods used for these purposes to inform the dynamic transform.

Turbulence models for simulating wind vector fields are used for turbine load calculations. Turbine components, such as towers and blades, have resonant frequencies and accurate reproduction of the frequency spectrum is requisite. Frequency based wind speed simulations are also used to assess the impacts on the electrical network (dynamic power quality studies). The loading and dynamic studies require WSTS that accurately reproduce the frequency spectrum, have high temporal resolution, and can have short temporal spans, thus an assumption that turbulence is homoskedastic is reasonable. The Davenport relationship describes the coherence between spatially separate points; the coherence being a function of separation distance, frequency, and mean wind speed, as presented in Equation 7.5 [107]. Davenport's relationship is applied to the simulation of wind incident on wind turbines in a WPP in the Sandia method [129] where the steady state transform is modeled using MCP.

$$\Gamma(f, x, \bar{u}) = e^{-y\frac{x}{\bar{v}}f} \tag{7.5}$$

Where Γ is the coherence, f is frequency, x is separation distance, y is the decay constant, and $\overline{v}$ is the mean wind speed.

The coherence is dependent on the decay constant and this reflects the complexity of the terrain. The decay constant has been investigated by Nanahara et al. who suggested a range for values with 7 being representative of low coherence, or complex terrain, and 3 being suggested for smooth terrain [132]. The coherence functions derived for pairs of wind speed time-series (the definition of coherence is presented in Equation 4.22), measured using the nacelle anemometers at Mt Stuart is presented in Figure 7.3. The coherence between turbine pairs is presented using the solid lines, with the lines coloured according to the separation distance. A decay constant can be found by minimising the RMS difference between the coherence estimated using Davenport's relationship and those measured, resulting in a decay constant of 3.31 when applying the mean wind speed of $6.54\,\mathrm{m\,s^{-1}}$. The dotted lines represent the coherence for turbine pairs calculated given the separation distance, the derived decay constant, and the mean wind speed. It is seen that the the Davenport relationship replicates the pattern of coherence observed in the Mt Stuart data, however the measured coherence has slightly less dependence on distance than that predicted using the Davenport relationship. There are many alternatives to Davenport's relationship for characterising the coherence; a good summary of coherence relationships is presented by Martin et al. [133].

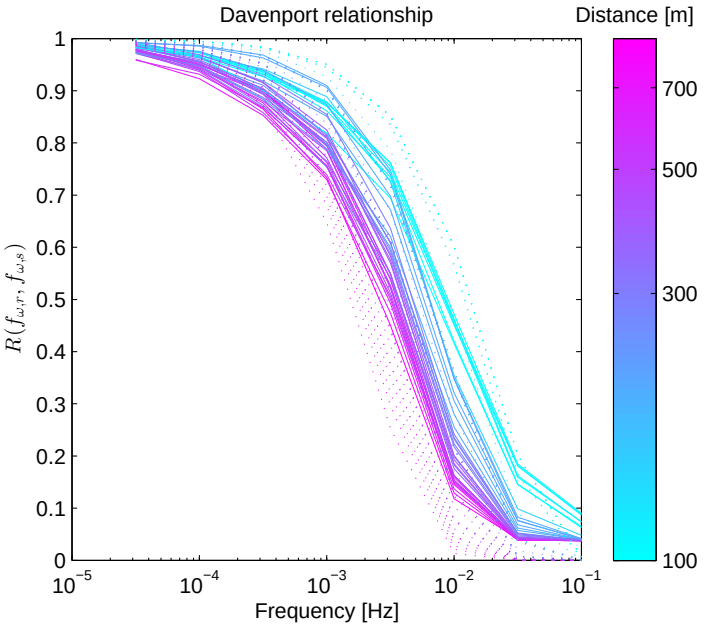

Figure 7.3 Coherence for Mt Stuart nacelle anemometers. Coloured according to separation distance in meters. Solid lines represent measured coherence and dotted estimates found using Davenport's relationship.

The Sandia method, as applied by Rose and Apt [134], can be used to simulate wind speed time-series for each wind turbine using the following procedure:

1. For each turbine white noise time-series are generated. Fourier series expansions are found and the spectra coloured to approximate Kolmogorov's relationship (as defined in Equation 5.3).

2. Coherence matrices are defined for each frequency using Davenport's relationship and the distance between each turbine pair. The set of complex power spectra are multiplied by the Cholesky decompositions of the coherence matrices to obtain a set of correlated power spectra.

3. The low frequency components of the power spectra are substituted with power spectra obtained from the MCP scaled WSTS from the meteorological mast.

4. Inverse Fourier series expansions are applied to the resultant spectra to find time-series representative of the wind speed incident at each wind turbine.

5. The WSTS are transformed to power by applying the wind turbine power curve, and the WPP power time-series is found as the aggregate.

The MCP / Sandia method characterises the spatial integration over a WPP. However, the spatial integration of a wind turbine is not accounted for. The averaging of a wind turbine should be evident as differences in power spectral densities (PSD) of the measured wind turbine power and that simulated. However, the use of the Kolmogorov spectrum as a target in filtering nacelle wind speeds removes veracity of the measured spectra and there is no substantial difference between simulated and measured spectra, see the top right graph in Figure 7.5. While it is expected that the wind turbine PSD should differ from that measured using an anemometer it should be noted that wind turbines are mechanically complex, experiencing phenomena such as blade / tower interactions, and are not representative of free stream measurements.

7.1.3 Mt Stuart efficiency

The WPP power output is lower than that calculated using the Sandia method due to electrical losses, turbine wakes, and operational efficiency. Electrical and wake losses for the Mt Stuart WPP are small and thus omitted. The wake losses are small as the turbines are aligned in a single line perpendicular to the prevailing wind, so no turbine is in the wake of another for the majority of the time. The operational efficiency describes the ratio of power produced to that which would be produced if all turbines were operating in an unrestricted manner. The operational efficiency has been calculated using data from the Mt Stuart SCADA; the average operational efficiency for the period is found to be 97%. A Markov Chain (MC) model, as described by Sulaeman [135], is applied to simulate the operational efficiency. The transition matrix is constructed assuming wind turbines can only be either on or off, thus a total of 10 operational states are possible (note that the status of the individual turbines is not important, rather it is the number of turbines that are on or off that is of interest). The MC model is used to generate operational efficiency time-series and these are used to adjust the simulated WPP power time series.

To enable the simulated power time-series to be comparable with the measured power time-series, it is necessary to adjust the mean MCP speed-up applied to the wind speed time-series, such that the total energy in the simulated power time-series adjusted for operational efficiency equals that measured.

7.1.4 WMA model

In the Davenport relationship the coherence is dependent on the mean wind speed. It may be possible to window the time-series so that the coherence changes through time as the bulk wind speed varies; however, this would have significant computational burden. The Sandia method applies the Davenport relationship by assuming a constant mean wind speed across the entire time-series; hence the WSTS simulated using the Davenport relationship are homoskedastic. Turbulence is heteroskedastic and the correlation is scale dependent, thus a Wavelet Multi-resolution Analysis (WMA) approach is more appropriate.

The WMA model is constructed in the same manner as used for imputing the ERA-interim WSTS. However, the model is derived solely using data from the nacelle anemometers at Mt Stuart, as detailed in Section 6.3.2. Rather than deriving the residual time-series from the ERA-interim data, the residual time-series is derived from the MCP model applied to the WSTS, with a 6 hour temporal resolution, measured at the meteorological mast.

The WMA model is combined with the MCP model to simulate power time-series using the following procedure:

1. The MCP scaled WSTS, with a temporal resolution of 6 hours, is scaled appropriately (by a factor of $\sqrt{2^7}$) and placed into the residual time-series portion of the wavelet structure.

2. For each scale 2^1 through 2^7 minutes wavelet series are simulated. These series are generated using the Correlated Innovation Matrix (CIM) approach, where the CIM loci (γ) are defined using the Cholesky decomposition of the matrix formed using the turbine separation distances and log-linear relationships (as presented in Figure 6.14). The CIM series are inverse Johnson and inverse Taylor transformed and the resultant wavelet series placed into the wavelet structure. The parameters for the Johnson and Taylor transformations are derived for each scale from the mean values found using the Mt Stuart data.

3. The inverse wavelet transformation is applied to the simulated wavelet structures to find WSTS representative of each wind turbine.

4. The WSTS are transformed to power using the wind turbine power curve, and the WPP power time-series calculated as the aggregate of the wind turbine power time-series.

5. The WPP power time-series is multiplied by the operational efficiency time-series simulated using the MC model.

6. An iterative procedure is followed altering the mean speed up applied in the MCP model so that the total energy of the simulated power time-series equals that of the measured power time-series.

The effect of including heteroskedasticity is illustrated in Figure 7.4. The top graph shows the RMS wind speed differential as a function of the wind speed. To ensure comparability the measured wind speed time-series is multiplied by 1.08, the mean MCP speed up. The measured values, derived from the meteorological mast, show definite increase in variability with increasing wind speed and this is replicated by the WMA model (although the the WMA model generally overestimates variability). As expected the Sandia method shows no increase in variability with increasing wind speed.

The effect of the heteroskedasticity on power is shown in the lower graph of Figure 7.4; it is seen that the WMA model closely replicates the measured power variability. While the Sandia method replicates the measured power relationship to an extent it is notable that the variability in power for wind speeds between 15 and 22 $\mathrm{m\,s^{-1}}$ is less than that measured.

Differences in measured and simulated wind speed time-series are also evident in the scaled correlations as shown in the lower left graph of Figure 7.5. The scaled correlations derived from the turbine power measurements are presented as black lines. The scaled correlations derived for WSTS using the Sandia method are presented using the blue lines and show much higher correlations than measured, and those derived from the WMA model are closer to the measured values but also overestimate the scaled correlations. The overestimates at scales greater than 0.25 d are the result of assuming concomitance in application of the MCP model.

7.1.5 Low pass filter

The Sandia and WMA methods are numerically complex and require turbine separation distances to be known; hence they are unsuitable for transforming WSTS to power for fleets of notional WPPs. The power produced by a WPP equals the sum of the WT power time-series. Further to this, the manner in which the WT power time-series aggregate depends on the frequency. At

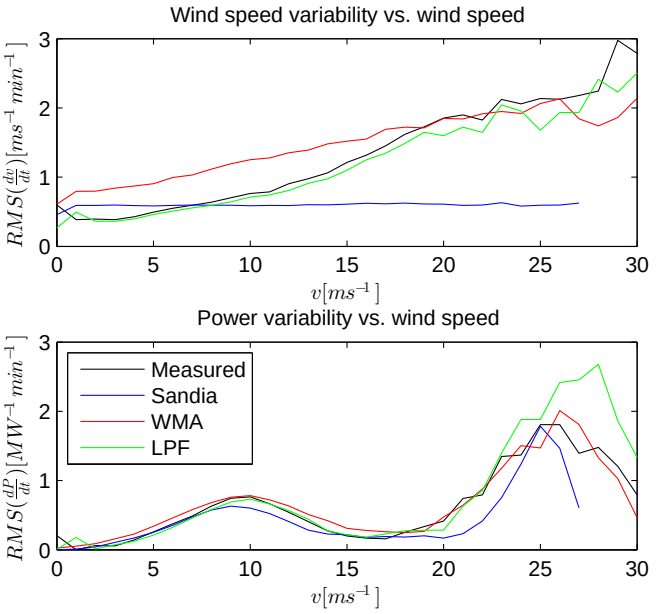

Figure 7.4 Effect of heteroskedasticity on simulated power. Top graph shows wind speed variability versus wind speed, with the Sandia method showing homoskedasticity. The bottom graph shows the effect of assuming homoskedasticity in underestimating the variability in power output.

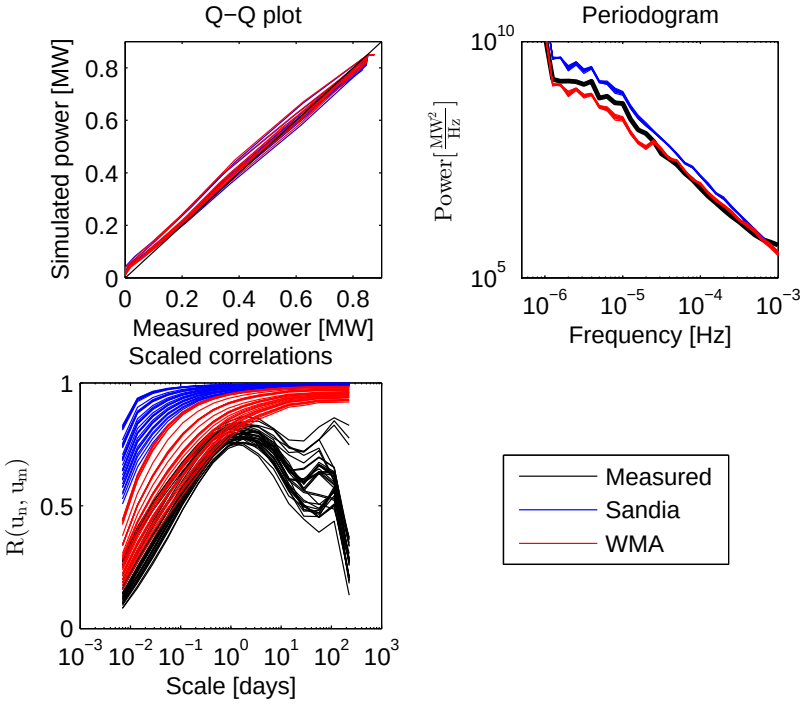

Figure 7.5 Results for wind turbine power simulation at Mt Stuart. The top left graph shows a QQ-plot. The top right graph shows a periodogram. The bottom left graph presents scaled correlations.

low frequencies, the wind speeds incident on wind turbines are well correlated, and the WPP power time-series scales in proportion to the number of turbines (N). At high frequencies, the wind incident on wind turbines is uncorrelated, and the power time-series from the WTs add as independent components, scaling in proportion to the square root of the number of turbines ($\frac{1}{\sqrt{N}}$).

The WPP power time-series can be found by applying a WPP power curve to a WSTS made by an anemometer. However, the WSTS must be transformed such that it is representative of the wind incident over the entire WPP. The transformation of the WSTS should not alter the low frequency components, and should scale high frequency components in proportion to $\frac{1}{\sqrt{N}}$. This transformation can be accomplished using a Low Pass Filter (LPF). An appropriate LPF has been derived by Welfonder and is presented in Equation 7.6 [136].

$$v_f = \mathcal{F}'\{\mathcal{F}(v)\frac{1+\frac{2\pi f \cdot M}{\sqrt{N}}^2}{1+2\pi f M^2}\} \tag{7.6}$$

Where v_f is the filtered wind speed time-series, f is frequency (with units being Hertz), $\mathcal{F}$ denotes the Fourier expansion, $\mathcal{F}'$ the inverse Fourier expansion, M is the low pass filter constant, and N is the number of turbines.

Welfonder's filter displays the desired behaviour; as the frequency increases the filter's power tends to the square root of the number of turbines multiplied by the time constant, and at low frequencies the scaling function tends to the number of turbines. However, in the application here the filter is applied to frequencies less than 0.0033 Hz (5 min), hence the behaviour of the filter at higher frequencies is not necessarily important. Further, Welfonder applies his filter to the power time-series from a WT, hence the smoothing by individual WTs does not need to be considered. Here the filter is applied to the WSTS hence the smoothing by individual WTs should be included. Welfonder's LPF has a relatively complicated form and it is found a simple LPF allows a better fit to the measured WPP power time-series.

Madsen proposed the use of a first order LPF to transform the power time-series from a WT to be representative of a WPP in 1984 [42]. While not a true first order LPF, the LPF as presented in Equation 7.7 has the correct form for the desired transformation, and is found to perform well. The LPF requires a time constant M, which for Mt Stuart is 195 s, found by minimising the RMS difference in measured and simulated PSDs of the WPP power time-series. The effect of the filter is shown in the top right graph of Figure 7.6, where the cyan line represents the spectrum of the wind speed measured by an anemometer, and the green line shows the spectrum obtained after applying the LPF with time constant optimised to match the spectra derived using the WMA model (red).

$$v_f = \mathcal{F}''\{\mathcal{F}(v)\frac{1}{1+Mf}\} \tag{7.7}$$

The wind power time-series is found by applying the low pass filter to the WSTS from the meteorological mast, and subsequently applying the WPP power curve. In this case the WPP power curve is found by applying a Gaussian distribution of speed-ups to the wind turbine power curve as shown in Equation 7.2. The mean and standard deviation for the speed-ups are taken from the frequency weighted average of all speed-ups as applied in the Mt Stuart MCP model.

The wind speed variability as a function of wind speed for the Low Pass Filtered WSTS is nearly identical to the unfiltered values, see Figure 7.4, and the variability of power is likewise nearly identical to that measured.

7.1.6 Results - Mt Stuart power simulation

Analyses of the simulated and measured power time-series are presented in Figure 7.6. The power time-series have been simulated using the Sandia, WMA ,and LPF methods and these have been adjusted using the operational efficiency time-series calculated using the MC model.

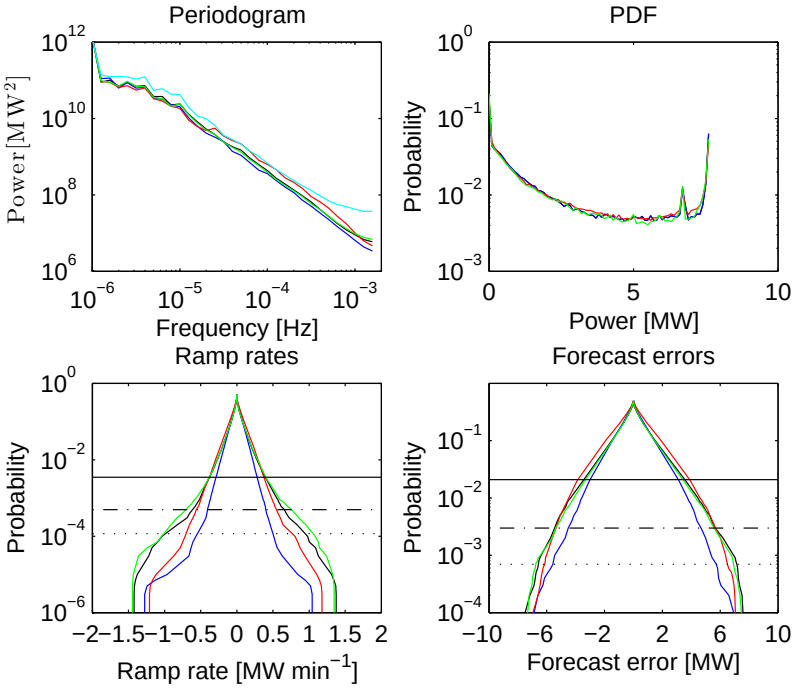

Figure 7.6 Power simulation results for Mt Stuart. Measured: black, Sandia: blue, WMA: red, LPF: green, Scaled from single turbine: cyan. The horizontal solid black line shows events with a probability of occurring once per day, the dash-dotted line corresponds to once per week, and the dotted line corresponds to once per month.

The top left graph of Figure 7.6 presents periodograms for WPP power. The periodogram resulting from the power time-series from a single turbine multiplied by the number of turbines is shown as a cyan line, this is included so that the effect of the spatial integration across the WPP can be illustrated; integration is evident for frequencies greater than 5×10^{-3} Hz or periods of approximately 3 h, otherwise the periodograms are all similar. The top right graph presents Probability Density Functions (PDFs), and shows all methods accurately replicate the power time-series character; this is especially important as the MC operational efficiency model is shown to accurately capture the peak at 6.8 MW, caused by occasions when a single turbine is out of operation but the WPP would otherwise achieve rated power. The lower left graph presents ramp rates and here differences in the models becomes evident. The Sandia model underestimate ramp rates (by 40 % at the once per week probability), the WMA model underestimates ramp rates to a lesser extent (cf. 17 %), and the LPF model over estimates ramp rates (cf. 18 %). The lower right graph presents forecast errors and it is seen that the Sandia method underestimates errors whereas the WMA and LPF models are more accurate.

7.2 SIMULATION OF EA DATA-SET POWER TIME-SERIES

The EA data-set, as described in Section 4.1, is used to validate the simulation of wind power time-series. The wind power time-series are grouped into two subsets, with the first subset representing a centralised portfolio of WPPs (consisting of Te Apiti, Tararua 1, 2, & 3, and Te Rere Hau) and the second subset representing a diversified portfolio (Te Apiti, West Wind,

and White Hill). A flow chart showing the process used for simulating power time-series for the WPPs in the EA data-set is presented in Figure 7.7.

Power times-series for a WPP can be simulated by assuming the WSTS measured by a proxy mast is representative of the wind speed incident on a WPP. Proxy masts for each of the WPPs in the EA dataset are sourced from the WGIP data set. The association between proxy masts and WPPs is shown in Table 4.1. Note that there are insufficient masts to associate each WPP with a unique mast hence TWF1 and TWF2 are associated with the same proxy mast (this is acceptable as the two WPPs are co-located).

A WSTS is simulated for a proxy mast by interpolating and scaling the ERA-interim MOS, see Sections 5.7.2 and 5.7.3. The MOS are interpolated using cubic splines and scaled using MCP; with the MCP speed-ups derived empirically (as explained in the following paragraph). The proxy mast WSTS are transformed to power using the Gaussian WPP power curve - LPF model and the results compared with the measured power. While we are primarily interested in the statistics of the power time-series the period coincident with the EA dataset is simulated as this ensures the samples are directly comparable.

The Gaussian WPP power curve requires the mean speed-up and the standard deviation of the speed-ups to be known. The mean speed up is found by optimisation, such that mean of the simulated power time-series equals the mean measured power (over the entire time-series). It is not known what an appropriate standard deviation of speed-ups for each WPP is. It is possible to derive speed-ups using a wind flow model; however, this is beyond the scope of this thesis. It is assumed the standard deviation of speed-ups measured at Mt Stuart, 0.065, is representative of all WPPs.

The LPF model requires a LPF time constant and this is related to WPP size. To identify a LPF constant for each WPP, power time-series are simulated using the MCP-WMA model and the Gaussian WPP power curve-LPF models. The LPF constant is found by optimisation so that the RMS difference in PSDs between the two simulated power time-series is minimised.

Similar to the Gaussian WPP power curve model, the MCP model requires the mean speed-up and standard deviation of speed-ups to be assigned. As for the Gaussian WPP power curve model the mean speed-up is found by optimisation, and the standard deviation is taken to be 0.065.

The WMA model for a WPP requires the separation distance between wind turbines as an input. The location of all wind turbines in each WPP has been identified using Google Earth and distances between turbine pairs calculated. The accuracy of positions is not high (10 m); however, the WMA model is not particularly sensitive to the separation distance. In an ideal model the parameterisation of the distance should be dependent not only on the distance between turbines but also on the relative exposure of the turbines.

To transform the representative WSTS to power the Gaussian-LPF and MCP-WMA models require wind turbine power curves. The wind turbine power curves are presented in Appendix A and shown in the top graph of Figure 7.8. The power curves are taken from sales documents [128] [137] [138] [139] [140] [141], and an on-line power curve database [142]. The Te Rere Hau WPP, at the time the EA dataset was collated, exported power from 5 turbines through the Tararua 1 point of supply. The Tararua 1 WPP power time-series consists of 55 V47 machines and 5 WF500 machines, and the Te Rere Hau WPP of 92 WF500 turbines. The WPP power curves for each of the WPPs in the EA data set and for Mt Stuart are shown in the lower graph of Figure 7.8.

The power time-series simulated for the WPPs, using the MCP-WMA and Gaussian-LPF models, span the same period of time as the EA data set. This is a relatively short period of time (7 months), so a Monte Carlo procedure is followed and the LPF constant for each WPP taken as the average of the LPF constants derived from each of the trials. The resultant LPF constants

Figure 7.7 Flow chart showing the process of simulating power time-series for specific WPPs.

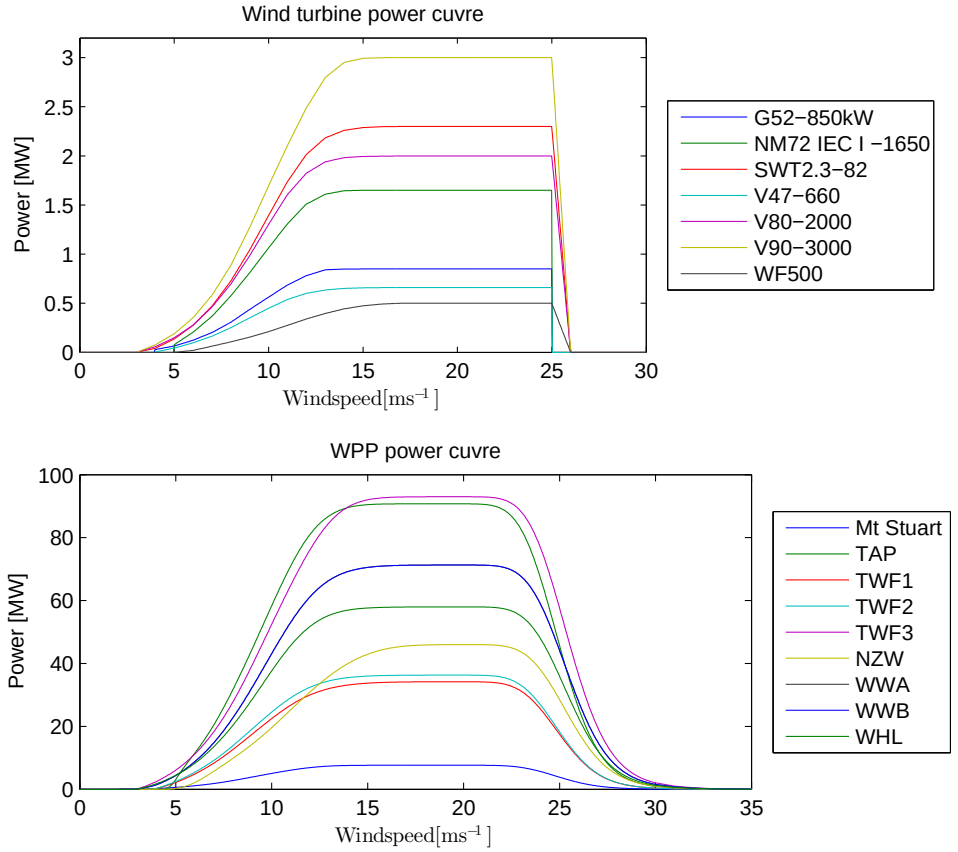

Figure 7.8 Wind turbine and WPP power curves

are presented in Table 7.1, and in Figure 7.12. The Cramer von Mises statistics, a measure of the difference between probability distributions, are all greater than 0.05, indicating that the Gaussian-LPF model does not accurately simulate the measured power time-series.

WPP	LPF constant (M) [s]	Mean speed up (μ_g)	CvM
Te Apiti	1790	1.39	0.14
Tararua 1	1458	1.17	0.15
Tararua 2	1624	1.15	0.1
Tararua 3	2008	1.48	0.15
Te Rere Hau	1522	1.22	0.21
West Wind A	1497	1.07	0.11
West Wind B	1906	1.2	0.1
White Hill	1647	1.16	0.07

Table 7.1 Results from simulation of EA data set

7.2.1 Efficiency model for WPPs in the EA data-set

To be compared with measured data the power time-series simulated using the Gaussian-LPF model need to be modified to account for losses. Electrical losses are related to the power output, hence they are also related to wind speed. As the mean speed up applied in the Gaussian model is optimised such that the mean power of the simulated power time-series equals that measured, the electrical losses are combined within this parameter. Turbine wakes affect downwind turbines reducing in the wind speed incident on the downwind turbine, and this is embedded within the Gaussian power curve model as a change to the speed-up. The standard deviation of speed-ups could be manipulated to account for wakes losses due to WPP design, however the exact value is unknown and it is left unchanged. Losses due to operational efficiency are not directly proportional to the wind speed and cannot be incorporated into any other model parameter. As for the Mt Stuart power simulation; operational efficiency is simulated using a Markov Chain (MC) model.

Data for the operational efficiency of each of the WPPs in the EA data set have been provided by the WPP operators; this data was gathered independently of the Electricity Authority. Mean operational efficiency statistics are presented in Table 7.2. Some of the operators provided time-series of individual turbine availability whereas other provided time-series of WPP availability. The time-series have a temporal resolution of 10 min and have been interpolated to a 5 min resolution using nearest neighbour interpolation. As the number of turbines in each WPP is different the operational availability has been defined using integer percentile values hence the transition matrix has 101 rows and 101 columns. For each power time-series an operational efficiency time-series is simulated and multiplied by the simulated power from the Gaussian-LPF model to obtain a power time-series representative of the exported power.

7.2.2 Results - EA data-set simulation using a specific model

Power time-series simulated using the Gaussian-LPF model that are coincident with the measured power time-series, and statistics deriving from these are presented in Figure 7.9 and Table 7.1. The probability distributions are compared in the top left graph of Figure 7.9 using a QQ plot, as the WPPs all have different capacities the power time-series have been normalised and quantiles calculated from these. Each line relates to a different WPP; it is seen that the simulated power is consistently under-predicted when the power output less than half the WPP capacity, and over-predicted when the power output is greater than half the WPP capacity.

WPP	Mean operational efficiency [%]
Te Apiti	94.4
Tararua 1	94.9
Tararua 2	96.8
Tararua 3	94.8
Te Rere Hau	96.2
West Wind A	94.1
West Wind B	94.1
White Hill	94.6
All	95.0

Table 7.2 Operational efficiency statistics for EA WPPs

Power Spectral Densities are presented in the top right graph of Figure 7.9, measured (blue) and simulated (red), and it is seen that the simulated values generally mirror the measured except they are lower at frequencies greater than 5×10^{-4} Hz (scales lower than 30 min).

The lower left graph of Figure 7.9 presents the simulated versus measured correlation between pairs of WPPs. It is seen that for WPP pairs that are highly correlated, or close together, the correlations are under predicted; and vice versa for WPP pairs that are separated by more than 50 km.

The lower right graph of Figure 7.9 presents scaled correlations for turbine pairs. Scaled correlations from measured values are shown using blue lines and simulated scaled correlations shown using red lines. The green line presents the mean error between measured and simulated scaled correlations. The cyan line presents the RMS of scaled correlation differences. It is seen that there is very little bias in scaled correlation errors, and that the model replicates the pattern of scaled correlations reasonably well.

The simulated power time-series can be grouped according to the scenarios presented in Section 4.4, with subsets representing centralised (Cen.) and diversified (Div.) paradigms. The simulated WPP power time-series are aggregated into the appropriate sets and compared with the measure power time-series in Figure 7.10. The reliability is assessed using PDFs (top left), the variability is assessed using ramp rates (top right), and the predictability is assessed using forecast errors (lower left). The horizontal black lines in the ramp rates and forecast errors graphs relate to the probability of once per day (solid), one per week (dash-dotted) and once per month (dotted) events.

The reliability results (PDF) mirror those for the individual power time-series, with the centralised subset showing a greater probability of producing high power and a lesser probability of producing mean power. The differences between the centralised and diversified subsets observed in the measured data are generally replicated by the simulations with the diverisified subset producing power more reliably.

The simulated ramp rates for the diversified subset match the measured values very well, however the ramp rates simulated for the centralised subset are marginally greater than the diversified subset, whereas those measured for the diversified subset are significantly greater.

The forecast errors for the power simulations of diversified subset match the measured values reasonably well, however the simulated forecast errors for the centralised subset are generally over-estimated when compared with the measured.

Periodograms for the simulated and measured power time-series are presented in the lower right graph of Figure 7.10; these show the simulated PSDs match those measured. Ramp rates and forecast errors for horizons other than those assessed are likely to have similar margins of error to those presented here.

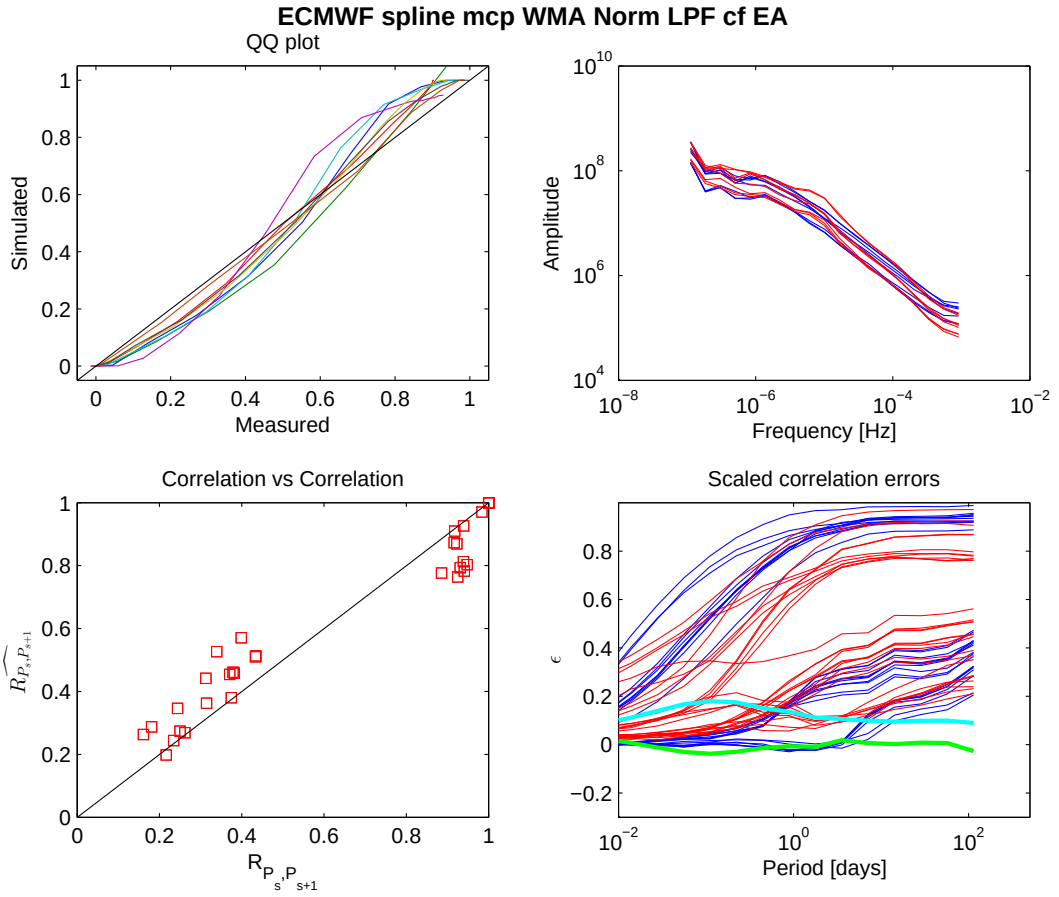

Figure 7.9 Wind power simulation results for EA data set. Top left graph shows QQ-plot, each line represents a different wind power plant. The right presents periodograms with blue measured spectra and red simulated. Bottom left graph presents simulated correlations versus measured. The bottom right presents scaled correlations, red are from simulations and blue from measured power time-series. The green line presents the mean error and the cyan line the RMS error in scaled correlations.

	Mea. [MW]		**Sim. [MW]**		**Error [%]**	
	Cen.	**Dis.**	**Cen.**	**Div.**	**Cen.**	**Div.**
Mean	123	121	123	121	0	0
Standard deviation	93	72	106	84	14	17
+ve ramp rate	-22	-15	-17	-17	-24	11
-ve ramp rate	21	13	17	16	-20	20
+ve forecast error	-160	-99	-201	-118	25	19
-ve forecast error	147	110	184	113	25	3

Table 7.3 Results for simulation of Centralised (Cen.) and Diversified (Div.) subsets from the EA dataset using specific model. Results represent values with a probability of occurrence of once per week.

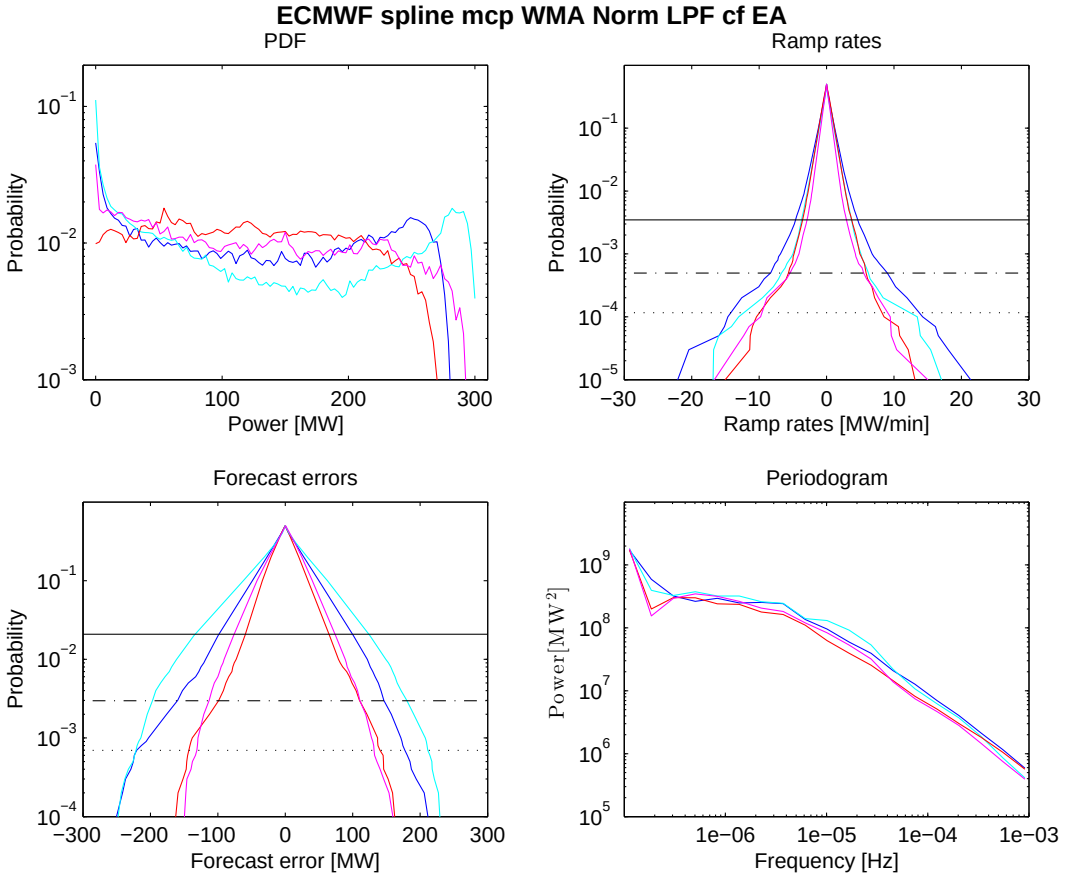

Figure 7.10 Scenario simulation results cf EA data set; blue: measured centralised, cyan: simulated centralised, red: measured diversified, magenta: simulated diversified. Top left graph shows PDFs, top right graph presents ramp rates, bottom left graph shows forecast errors, and bottom right graph presents periodograms.

7.3 GENERIC WIND POWER MODEL

It is unsurprising that the power time-series simulated (using proxy masts, ERA-interim MOS interpolated using cubic splines, scaled using MCP, converted to power using the Gaussian-LPF model, and modified using the MC operational efficiency model) do not exactly reproduce the statistics of the measured power time-series as many generalisations and assumptions have been made. It is encouraging that the power time-series have similar magnitudes of reliability, variability, and predictability. However, it is necessary to make further generalisations if the power from a fleet of notional WPPs, as defined in Section 3.4.1 is to be simulated. It is necessary to remove the dependence on proxy masts, approximations to a specific WPP design, and specific wind turbine types. The processes used for simulating generic power time-series is presented in Figure 7.11.

Proxy mast assumptions are removed by combining the MCP scaling function with the MCP algorithm, applied in transforming the WPP wind speed time-series to power, and collapsing the two into a single Gaussian power curve model (as explained in the following paragraph).

The dependence on specific design of the WPPs is removed by assuming WPPs comprise a number of Vestas V80 turbines such that the total capacity is as close to the actual capacity as possible, and the turbines are arranged in approximate square arrays.

The WSTS are imputed using the WMA method, with WPP center points used to define the separation distance matrix and wavelet series correlations defined using the linear approximations as shown in Figure 6.14. The LPF model is used to model the dynamic transform; the LPF filter constants are derived later in this section. Lastly, the wind power time-series are modified using the MC operational efficiency model to obtain generic power time-series.

The WPP power curve is characterised by the wind turbine power curve, a mean speed-up, and a standard deviation of speed-ups. The speed-ups applied to the MCP scaling of the ERA-interim wind speed time-series can likewise be described using a Gaussian distribution. The application of these two MCP algorithms can be compressed into a single scaling function applied to the WSTS derived from the NWP product as shown in Equation 7.2. The mean value of the generic speed-up model can be manipulated such that the power derived from the WPP equals a desired energy production. The energy production here it is equated with a capacity factor of 40%. The standard deviation of speed-ups is taken from that measured at Mt Stuart (0.065).

The LPF time constant is dependent on the WPP size and design, and a value must be assigned for each WPP. The generic WPPs comprise Vestas V80 turbines arranged to approximate square arrays. The WMA-MCP method is used in Section 7.2 to derive LPF constants given specific WPP layouts, and this method can be applied to simulate a power-time series for square arrays of wind turbines, from which a relationship between the number of turbines and the LPF constant can be defined. The WMA-MCP model is used to simulate power time-series for WPPs comprising 3, 9, 16, 36, 64, 144, and 256 wind turbines, and LPF constants found for each of these notional WPPs. The LPF as a function of the number of turbines is shown in Figure 7.12, with the squares representing the results of the simulations. It is seen that the LPF constant is a function of the number of turbines, which can be approximated using the relationship presented in Equation 7.8. The LPF model parameters are found using an optimisation algorithm with M_c equal to 151 s and M_e equal to 0.57.

The LPF time constant for a WPP comprising a single turbine should equal one. However, if the relationship in Equation 7.8 is applied the LPF constant M equals M_c. As this is inconsistent an exception is used to ensure no filtering occurs if the WPP has only one turbine.

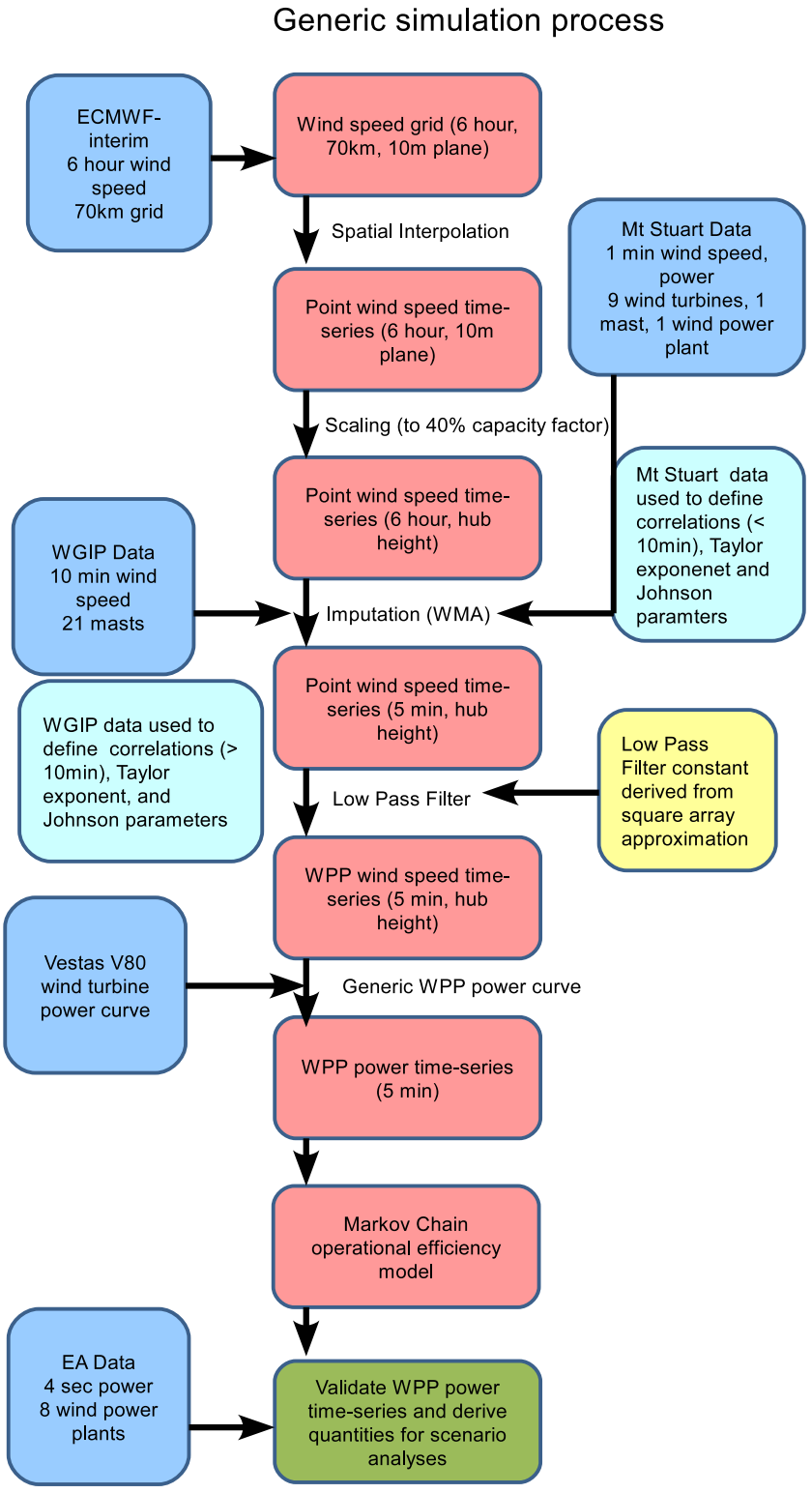

Figure 7.11 Flow chart showing the process of simulating power time-series for generic WPPs.

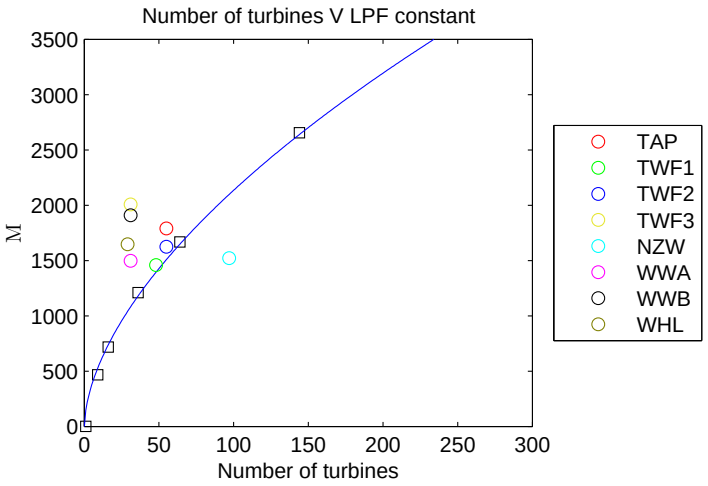

Figure 7.12 Low pass filter constant M as a function of WPP capacity. Results for EA WPPs shown using circles. Results for simulation of square arrays shown using squares. Best fit approximation to square arrays shown using blue line.

$$M = \begin{cases} M_c \cdot N^{M_e}, & \text{if } N \geq 2 \\ 1, & \text{otherwise} \end{cases} \tag{7.8}$$

Where N is the number of wind turbines, M_c is the time constant multiplier, and M_e is the exponent of N.

The effect of the LPF on the Power Spectral Density of the WSTS for WPPs of varying sizes is shown in the top graph of Figure 7.13. The solid lines represent the PSD derived from the WMA model. The dotted lines represent the PSD for power time-series derived using the Gaussian WPP power curve applied to an unfiltered WSTS. Dash-dotted lines represent the PSD for power time-series that derive from a WSTS that has been Low Pass Filtered and then modified using the Gaussian power curve. For the most part the dash-dotted lines are not visible as they are coincident with the PSD derived from the WMA model, i.e. the LPF filter performs as desired.

In lower graph of Figure 7.13 dotted lines shows the LPF scaling function ($\frac{1}{1+M\omega}$) for square array WPPs of differing sizes derived using Equation 7.8. The solid lines represent the target scaling functions. The target scaling functions are the ratio of the PSD calculated from the WMA model to the PSD found by applying the Gaussian WPP power curve to an unfiltered WSTS. Note that the x-axes of the top and bottom figure are the same, however the top graph is labelled with frequency and the bottom with scale allowing the reader comparison between the two measures.

The target scaling functions are complicated; components with scales greater than 6 hours are derived from the meteorological mast WSTS, components with scales of between 6 hours and 10 minutes derive from the WMA model with parameters set using the WGIP data, and components with scales less than 10 minutes derive from the WMA model with parameters set using the Mt Stuart data.

It is seen that the scaling functions derived using the LPF fit the target scaling functions very well for WPPs with large numbers of WTs, but the LPF does not perform very well at high frequencies for small WPPs. The target scaling function for a WPP comprising a single turbine is given by the blue line. This scaling function should equal one for all frequencies, however the application of the Gaussian WPP power curve smooths the power time-series compared with the WMA model in which the WT power curve is used.

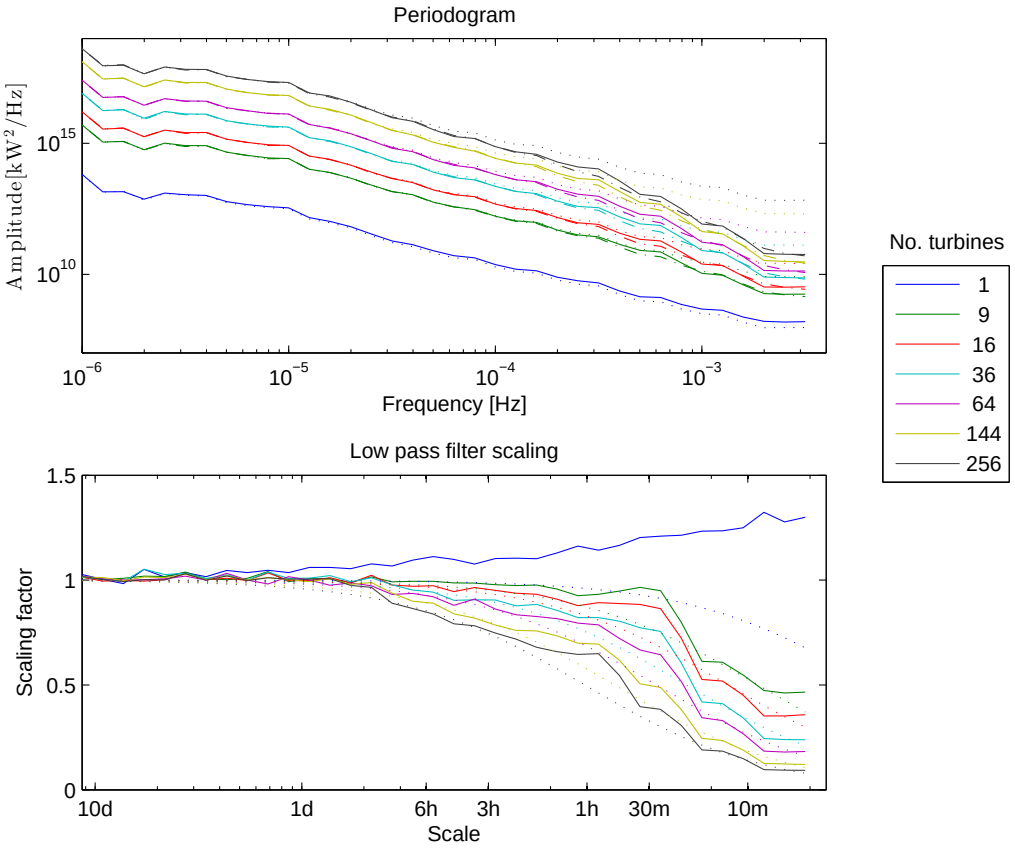

Figure 7.13 The top graph presents Power Spectral Densities for power time-series simulated using the WMA model (solid lines), PSDs found using a Gaussian power curve applied to an unfiltered WSTS (dotted lines), and PSDs from Gaussian WPP power curves applied to Low Pass Filtered WSTS. The bottom graph shows the target scaling functions (the ratio of the PSD derived using the WMA model to that found using the Gaussian power curve applied to an unfiltered WSTS) using solid lines, and the scaling functions derived using the Low Pass Filter with time constant dependent on the number of turbines as dotted lines.

7.3.1 Results - EA data-set simulation using a generic model

The power time-series simulated for each of the WPPs in the EA dataset using the generic WPP model are compared with the measured time-series in Figure 7.14. The quantile - quantile plot at the top left shows little change from that resulting from the specific model. The periodogram, top right, shows some change with the simulated spectra resulting from the generic model having lower magnitudes at high frequencies than that measured or that simulated using the specific model. The correlation between WPP pairs, lower left, is higher for the generic model than for the specific model resulting in better replication of the correlations for WPPs in close proximity and even greater over estimation of the correlation between WPPs that are separated by distances greater than 50 km. Scaled correlations, lower right, show the generic model generally performs better than the specific at low scales (<1 d), but worse at higher scales.

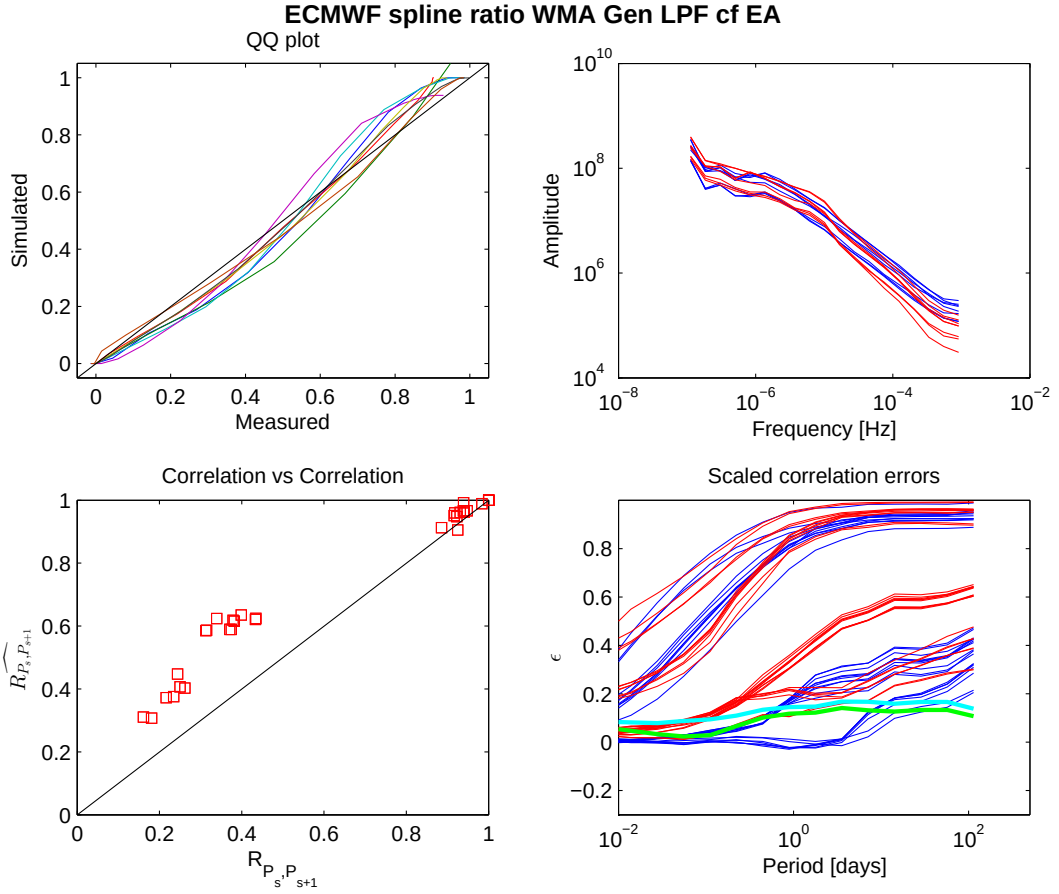

Figure 7.14 Generic wind power simulation results for EA data-set. Top right graph presents a Quantile-Quantile plot with each line representing a different wind power plant. The top right graph is a periodogram with blue lines derived from measured power time-series and red line from simulations. The bottom left graph presents simulated correlations versus measured correlations. The bottom right graph shows scaled correlations, with blue lines representing measured values and red lines simulated value. The green line presents the mean error in scaled correlations and the cyan line the RMS error.

The power time-series developed using the generic model are aggregated into the centralised and diversified sets and the results presented in Figure 7.15. The probability distributions, top right, of the power time-series simulated using the generic model are slightly different to those found using the specific model; generally the differences between the scenarios is replicated by the generic model. The ramp rates, top right, simulated using the generic model are generally slightly lower than those simulated using the specific model, and the inability of the model to reproduce the significant difference in ramp rates between scenarios is not improved. As for the

specific model the differences in forecast errors, lower left, between the scenarios are replicated quite well, with the generic model matching the measured data better than the specific model. The PSDs resulting from the simulated power time-series using the generic model have lower magnitudes at high frequencies ($>1 \times 10^{-4}$ Hz) than those measured or those resulting from the specific model.

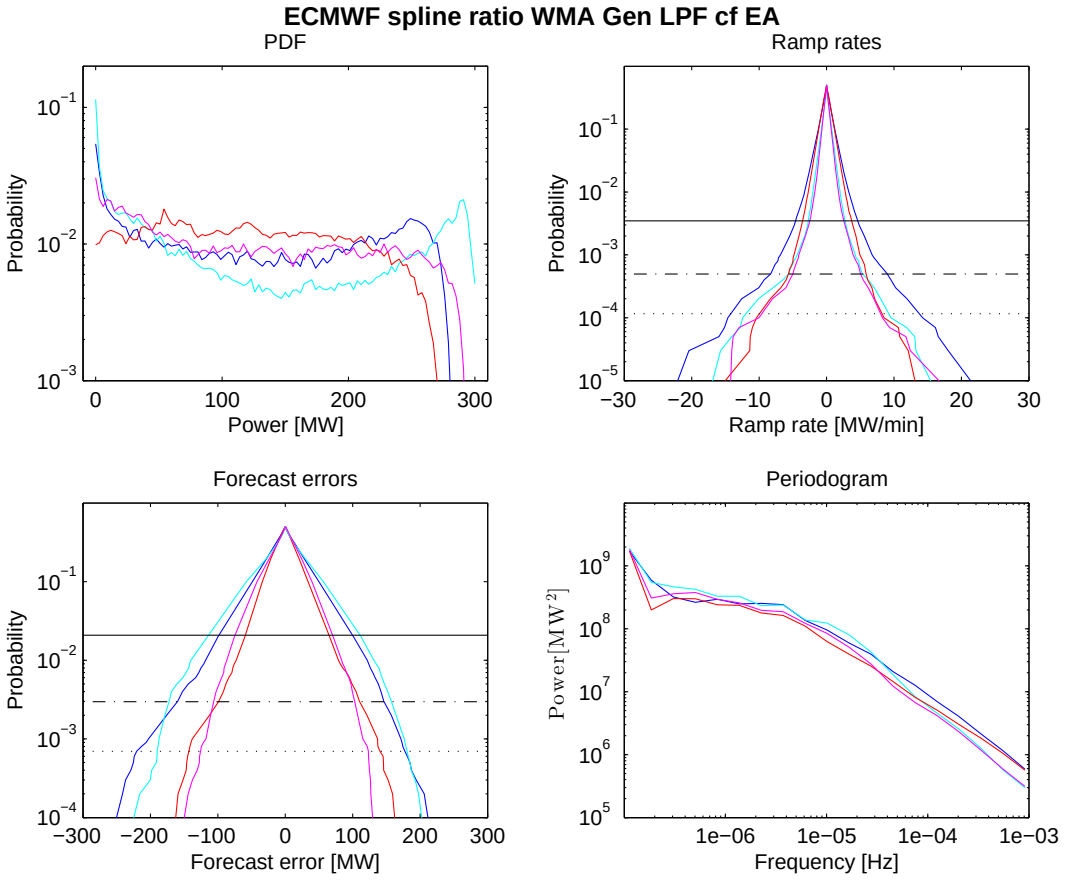

Figure 7.15 Generic simulation results cf EA data set; blue: measured centralised, cyan: simulated centralised, red: measured diversified, magenta: simulated diversified. Top left graph shows PDFs, top right graph presents ramp rates, bottom left graph shows forecast errors, and bottom right graph presents periodograms.

7.4 POWER SIMULATION FOR SCENARIOS

The generic wind power model is shown to replicate the measured wind power time-series with some accuracy. The shape of the probability distributions, magnitude of ramp rates, and forecast errors are close to those measured, hence it is acceptable to use the generic model to simulated power time-series for the scenarios developed in Section 3.4.1. The scenarios for testing the benefit of the spatial diversification of wind power in New Zealand include compact, disperse, diverse, and Business As Usual (BAU) cases. The year 1998 is used for analysis as this is the year that Cyclone Bola crossed NZ. Cyclone Bola produced damaging winds across much of the North Island which would most certainly have disrupted the power from WPPs if they had existed at the time[143]. While it is possible to simulate power time-series covering the entire 40 year period of the ERA-interim data-set this is unnecessary for demonstrating differences between the scenarios.

Power time-series for each WPP are simulated using the generic power model which comprises the following procedure:

	Mea. [MW]		Sim. [MW]		Error [%]	
	Cen.	**Div.**	**Cen.**	**Div.**	**Cen.**	**Div.**
Mean	123	121	123	121	0	0
Standard deviation	93	72	107	86	16	20
+ve ramp rate	-22	-15	-17	-15	-23	0
-ve ramp rate	21	13	15	17	-29	29
+ve forecast error	-160	-99	-182	-113	14	14
-ve forecast error	147	110	169	110	15	0

Table 7.4 Results from simulation of EA dataset using generic model. Results represent values with a probability of occurrence of once per week.

- ERA-interim MOS are extracted and interpolated using cubic splines to find a representative Wind Speed Time-Series (WSTS),
- the WSTS are scaled using a multiplier such that the energy output from the WPP equals a capacity factor of 40%,
- imputation is achieved using the WMA model,
- the WSTS are smoothed by applying a first order low pass filter with the filter constant derived using the MCP-WMA WPP model,
- transformation to power is performed using the Gaussian power curve,
- the power time-series are modified using the MC operational efficiency model.

7.4.1 Results - scenario simulation using a generic model

The WPP power time-series are aggregated according to the scenarios and the results presented in Figure 7.16 and Table 7.5. The top left graph presents time-series for each scenario covering only the period when Cyclone Bola crossed NZ (note that the simulations cover the entire year of 1998 and this graphs shows only the period from 7 March through 14 March). The cyclone began to affect northern NZ on the 6 March 1998 and continued to batter the country until 12 March 1998. It can be seen that the fluctuations in power for the compact scenario are much greater than the other scenarios with the diverse scenario producing the smoothest power. The compact scenario is seen to rise by 84% of the total capacity within 6 h on the 7 March whereas the disperse scenario rises little more than 50% of the total capacity within the same period of time.

The top right graph presents PDFs for the scenarios; it is seen all scenarios have similar distribution shapes except the compact scenario which has heavier tails (higher probabilities of generating power above 1800 MW and of producing near zero power). The standard deviation of power for the compact scenario is 25% higher than the diverse scenario.

The lower left graph presents ramp rates and it is seen that the compact and disperse scenarios have near identical variability, whereas the diverse scenario results in ramp rates 25% of the compact scenario. The distribution of ramp rates has a slight positive bias; the magnitude of ramp rate increases, with a probability of occurrence equating to once per week, is 10% greater for the disperse and BAU scenarios than the equivalent ramp down.

The lower right graph presents forecast errors for the scenarios; the once per week forecast errors for the compact scenario are 45% greater than for the other scenarios (which all exhibit similar magnitudes of forecast errors). It is seen that the distribution of forecast errors is skewed in

favour of negative errors with once per week forecast errors having a 20% greater magnitude of under-prediction than the equivalent over prediction.

The conclusion is made that a compact wind generation portfolio will exhibit lower reliability, a diverse portfolio will exhibit less variability, and a disperse portfolio will exhibit greater predictability.

To assess the benefit from spatial diversification that the current portfolio of WPPs in NZ realises the Business As Usual (BAU) scenario is assessed. The BAU scenario exhibits a balance between the diverse and compact scenarios with:

- variance 83% of the compact scenario but 6% higher than the diverse scenario,
- ramp rates half those for the compact scenario but twice the diverse scenario,
- forecast errors 75% of the compact scenario but 15% greater than the diverse scenario.

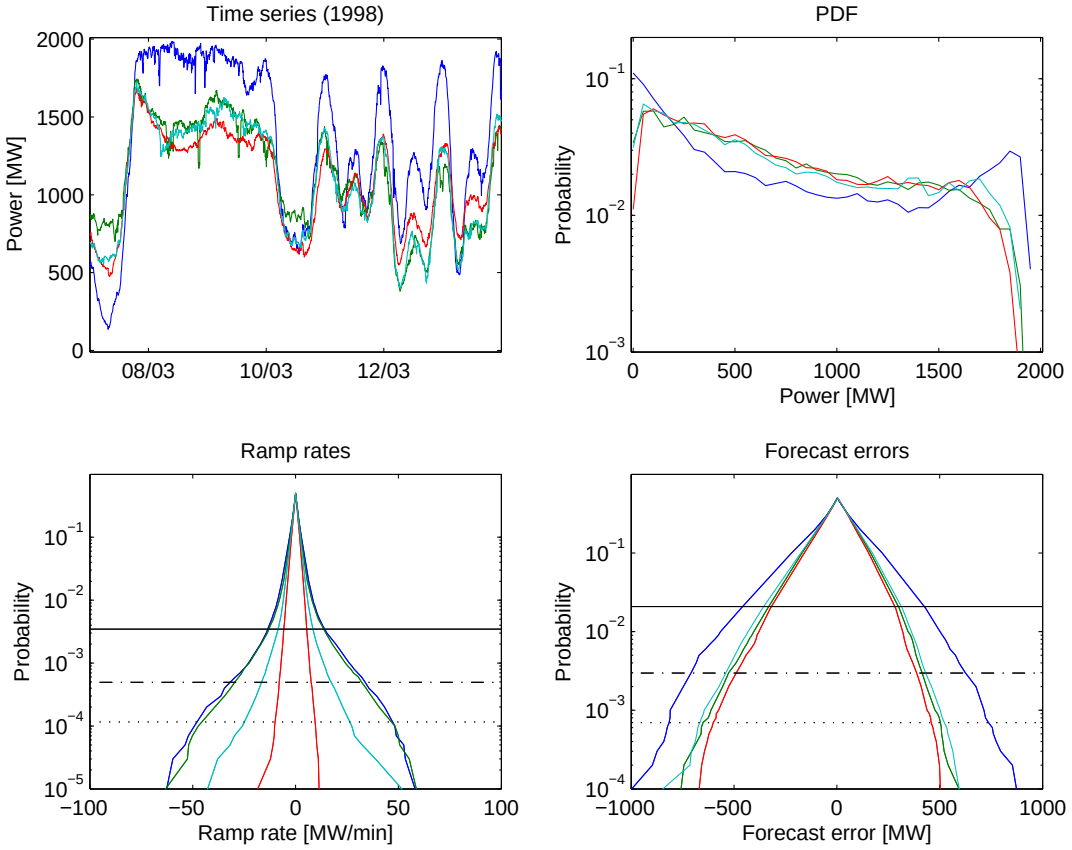

Figure 7.16 Power simulation results for scenarios: blue (compact), green (disperse), red (diverse), cyan (BAU). The top left graph presents a time-series for the period during which Cyclone Bola effected NZ. The top right graph presents Probability Density Functions being a measure of reliability. The bottom left graph presents ramp rates, over a 5 minute period, which are a measure of the variability. the bottom right graph presents forecast errors, assuming persistence over a 2 hour horizon, which are a measure of predictability.

7.5 SUMMARY

Coherent sets of WSTS, with sufficient temporal resolution, that are representative of WPPs can be derived from the ERA-interim MOS imputed using a WMA turbulence model. These WSTS must be transformed to power time-series using a method that captures the spatial integration

Results [MW]	Compact	Disperse	Diverse	BAU
Mean	799	799	799	799
Standard deviation	664	534	519	551
+ve ramp rate	-33	-32	-8	-18
-ve ramp rate	35	37	8	20
+ve forecast error	-758	-514	-487	-563
-ve forecast error	636	438	397	457

Table 7.5 Results from simulation of scenarios. Results represent values with a probability of occurrence of once per week.

intrinsic to WPPs. The transformation from wind speed to power can be constructed assuming two components; a steady state transform and a dynamic transform. The steady state transform can be modeled using a Gaussian WPP power curve and the dynamic transform can be modeled using a LPF.

Measurements made at the Mt Stuart WPP are used to derive a WPP power curve and model parameters for the Sandia and WMA methods. It is shown that the assumption of homoskedasticity inherent in the Sandia method results in underestimation of power variability, whereas the WMA model characterises the heteroskedasticity and is shown to provide a better match with the measured power variability. The WMA model is used to define LPF model parameters for the WPPs in the EA data-set. The derived model parameters are specific to the WPPs and are used to simulate power time-series for the WPPs in the EA dataset. The power time-series simulated using the specific model are shown to match the measured with some accuracy.

A generic model is constructed using the Gaussian-LPF model and used to simulate power time-series for each of the WPPs in the EA data-set. The generic model is formed by collapsing the speed-ups applied in the scaling of the WSTS with the speed-ups applied in the Gaussian WPP power curve, and deriving a relationship between the WPP size and the LPF time-constant. The power time-series simulated using the generic model are compared with measured power time-series and shown to have good agreement.

Scenarios have been created to assess the benefits of spatial diversification and the generic wind power model has been applied to simulate power time-series for 1988, the year Cyclone Bola crossed New Zealand. The conclusion is made that a compact wind generation portfolio will exhibit lower reliability, a diverse portfolio will exhibit less variability, and a disperse portfolio will exhibit greater predictability. It is shown that the present portfolio of WPPs in NZ realises significant benefit from spatial diversification although greater benefit could be gained if the future development of WPPs is driven toward greater diversity and dispersion.

Chapter 8

CONCLUSION

The electric power system in New Zealand has been built incrementally over the course of 115 years. The power system is a portfolio of assets that reflects the technological and political evolution of New Zealand. Resources and demand have shaped a power system that must continue to evolve to ensure future requirements are met. There will be an increase in the requirement for electricity generated from renewable resources, if climate obligations are to be met through replacing fossil fuels. Thus it is likely that the wind power portfolio in New Zealand will expand. Changes to the generation mix will impact the operation of the electric power system, and studies are required to determine what actions are required to ensure the reliability and quality of the power are maintained.

This thesis comprises part of Research Aim 1.1 of the GREEN Grid programme, which seeks to help New Zealand grow its renewable energy generation, and transition to new technologies connecting to the grid. Specifically this thesis provides methods to determine the benefit from the spatial diversification of wind power in New Zealand. This research contributes to the GREEN Grid programme, in particular Research Aim 1.3, by providing wind power time series for different scenarios of spatial diversification of wind power plants in New Zealand.

The New Zealand power system can be separated into generation, transmission, and distribution components. It is operated through a regulatory regime that includes the New Zealand Electricity Market (NZEM). The NZEM, a secondary control mechanism, keeps the power system in balance, taking bids to cover demand and ensuring the least cost generation is dispatched from a stack of offers. The NZEM uses 30 minute trading periods, and has a gate closure of 2 hours. However, demand and generation can vary faster than this so a reserves market is also operated using a windows of 5 minutes to ensure power quality is kept within acceptable limits. These time frames define the requirements for power time-series models and shape the variability and predictability metrics.

Although a relatively recent addition to the electricity generation mix, Wind Power Plants (WPP) are one of the most cost effective forms of electricity generation. The variable and unpredictable nature of wind means that wind power output can lead to large ramp rates and significant uncertainty in power forecasts, thereby placing added stress on the power system. Wind power integration studies are undertaken to ensure the addition of WPPs into the power system does not place unacceptable levels of risk on the power system. Integration studies can be classified into steady-state, dynamic, Unit Commitment and Economic Dispatch (UCED), and capacity studies. These studies address different aspects of the power system design and operation and have their own requirements. Increases in the penetration of wind power may lead to specific issues, mostly related to secondary and tertiary control, that are addressed in UCED and capacity studies. Many UCED studies conducted throughout the world conclude that the impacts of increased wind power penetration may be alleviated through the spatial diversification of WPPs.

Located in the roaring forties New Zealand has excellent wind resources. The geography of New Zealand means that exceptional wind resources are located in the Manawatu and Wellington regions. Wind Power Plants have been constructed to take advantage of these wind resources, with 72 % of NZ's 697 MW located in these regions. The concentration of WPPs in the Manawatu caused the system operator to have significant concerns relating to large ramp rates observed in the power from these WPPs. The Electricity Commission conducted the Wind Generation Investigation Project (WGIP) that addressed these concerns and found that some of the impacts of increasing wind power penetration could be alleviated through the spatial diversification of New Zealand's wind generation assets. The WGIP was limited in its scope and methods, and a more rigorous approach has been developed in this thesis. To demonstrate the varying benefits of spatial diversification of wind power, four scenarios have been developed representing 2 GW wind power portfolios. The scenarios are Compact, Disperse, Diverse, and Business As Usual (BAU). The locations of the notional WPPs are obtained from media releases in which WPPs are either operational, consented, notified, or have been withdrawn. The design of the WPPs is chosen as square arrays of Vestas V80 2 MW turbines, with a spacing of 4 rotor diameters, and capacity factors of 40 %.

The benefit of spatial diversification can be illustrated using measured power time-series in the Electricity Authority (EA) data-set. Statistical measures such as scaled correlation can be used to quantify the spatial and temporal dependence of the correlation between the power produced by pairs of WPPs. The measured power time-series from a set of WPPs have been grouped in two ways, one representing a centralised subset, and the other a diversified subset. These subsets have been used to show that the diversified subset has greater reliability, lower variability, and greater predictability than the centralised subset.

As there is insufficient measured data to determine the impact of the wind generation scenarios it is necessary to simulate power time-series. The best way to produce power time-series for fleets of WPPs is to simulate Wind Speed Time-Series (WSTS), with the appropriate temporal and spatial resolutions, and convert these to power. The ECMWF ERA-interim reanalysis model provides wind speed time-series with relatively good spatial (70 km) and temporal (6 hour) resolutions and is freely available. The Model Output Statistics from the ERA-interim reanalyses require interpolation, scaling, and imputation. The cubic spline method is found to be the preferred method for interpolation, and the Measure Correlate Predict method the most appropriate for scaling the WSTS.

The imputation of the WSTS is the research topic that has received the greatest focus in this thesis. To impute the WSTS a turbulence model is required that is spatially and temporally consistent. The New Zealand synthetic wind speed data-set applied the Correlated Innovation Matrix (CIM) approach and this has been used to simulate a set of WSTS which have been validated using a data-set consisting of wind speed measurements made at 21 proposed WPPs located throughout New Zealand (the WGIP data-set). However, the correlations enforced in the CIM method are independent of the temporal scale. To address this concern a Multi-Resolution Analysis approach using wavelets has been developed. The Wavelet Multi-Resolution Analysis approach requires selection of a wavelet such that cross correlations (across scales in the same time-series) are minimised allowing wavelet series of different scales to be treated independently. To obtain a wavelet series with the correct statistical properties from simulated stationary Gaussian processes, it is necessary to define and apply Taylor and Johnson transforms. It is shown that WSTS simulated using the WMA more accurately reproduce the statistical character seen in the WGIP data-set. As integration studies require greater temporal resolution than the WSTS in the WGIP data-set it is necessary to derive model parameters using supplementary data. This is obtained from the Mt Stuart Wind Farm.

The transformation of WSTS to power requires a transform that captures the spatial integration intrinsic to WPPs. The transform can be constructed assuming steady-state and dynamic

component models. The steady-state transform can be modelled using a WPP power curve (which removes the need for scaling the WSTS), and the dynamic component using Davenport's coherence relationship. This method is termed the Sandia method. However, the Sandia method assumes homoskedasticity and it is shown that this leads to underestimation of the variability of power measured at the Mt Stuart Wind Farm. The WMA method is applied, at WPP scale, and is shown to accurately reproduce the variability. The numerical requirements of the WMA method make it impractical for simulating power time-series for fleets of WPPs, however it is shown that a simple Low Pass Filter (LPF) can be usefully applied. The WMA model is used to set the LPF time-constant for WPPs in the EA data-set and power time-series simulated to be coincident with the measured power time-series. The simulated power time-series are shown to replicate the statistics of the measured power, giving confidence in the methods. A generic wind power model can be formed by relating the LPF time-constant to the WPP size. Power time-series simulated using the generic model are shown to also match the measured power time-series with good agreement.

The generic wind power model is used to simulate power time-series for each of the WPPs in the Compact, Disperse, Diverse, and Business As Usual (BAU) scenarios. The year of 1988 is selected for demonstrating the use of the generic wind power model as in this year Cyclone Bola crossed the North Island. The extreme winds during Cyclone Bola would have caused many of the WPPs that are currently operating in New Zealand to shut down, if they had been operating at the time, potentially resulting in large ramp rates and forecast errors. It is shown that during the period that Cyclone Bola crossed the North Island the fluctuation in wind power output would have been much greater for a compact scenario than for the other scenarios, with the diverse scenario providing the smoothest power delivery.

Metrics for reliability, variability, and predictability are used to quantify the differences between the scenarios. Reliability being measured using the standard deviation of power, the variability measured using ramp rates over a 5 minute period, and the predictability measured using the forecast error over a 2 hour horizon, assuming persistence, for power time-series with temporal resolutions of 30 minutes. It is found that:

- the standard deviation of power for the compact scenario is 25% higher than the diverse scenario,
- the compact and disperse scenarios have near identical variability, whereas the diverse scenario results in ramp rates 25% of the compact scenario's,
- the once per week forecast errors for the compact scenario are 45% greater than for the other scenarios (which all exhibit similar magnitudes of forecast errors).

The BAU scenario is used to determine how much benefit from spatial diversification the current paradigm of wind power development would achieve if expanded to a 2 GW portfolio. It is found that the BAU scenario will result in:

- variance 83% of the compact scenario but 6% higher than the diverse scenario,
- ramp rates half those for the compact scenario but twice the diverse scenario,
- forecast errors 75% of the compact scenario but 15% greater than the diverse scenario.

8.1 LIMITATIONS

This thesis has sought to develop a specific methodology to determine the benefits of spatial diversification of wind power in New Zealand. The method has been constructed using the available data. As with any work there are limitations some of which are presented here.

The data-sets used in the analyses are limited. Many of the models developed, such as the imputation and power curve models, would have increased accuracy if more data-sets were available. In particular the WMA wind speed imputation model would benefit from additional wind speed measurements made by anemometers at temporal resolutions greater than 10 minutes, and from masts that are separated by less than 1 km. The WPP power curve model could be defined more accurately given measurements from further WPPs. In particular the standard deviation of speed-ups has been defined using only measurements made at the Mt Stuart Wind Farm. The validation wind power data-set, EA data, has a relatively short temporal span and covers a limited number of WPPs. Addition of more WPPs and measurements of longer duration would help identify seasonal patterns and provide stronger validation of the simulated wind power time-series.

The scenarios have been developed from media releases, and while this is a good way of ensuring a realistic distribution of WPPs, the proposals do not necessarily represent the best wind resources. WPP developers may keep information secret for proprietary reasons and speculators may hype proposals.

The wind speed time-series derived from the Numerical Weather Prediction (NWP) model represent measurements made by anemometers at a height of 10 m on a locally flat plane, thus they require scaling to be representative of the wind incident on a WPP. The scaling in this thesis is accomplished firstly using Measure-Correlate-Predict, and later this algorithm is discarded as the scaling is combined with the WPP power curve within the speed-up parameter. Thereby assuming the scaling is independent of wind direction; however there is some correlation in the pattern of speed-ups between sites that are in close proximity. For instance it is expected that speed-ups in prevailing wind directions are higher, as WPPs are constructed to maximise their exposure, and WPPs that are in close proximity share wind resources.

The simulation of turbulence requires transformations that take Gaussian process white noise processes and produce coherent sets of time-series that are similar to those measured. In other words the methods convert a process that is stationary to one that is heteroskedastic. Observed probability distributions have been replicated by applying a Johnson transform to the Gaussian process, and the dependence of turbulence on the mean value of the wind speed has been enforced using a Taylor transform. However, no transformations have been applied to simulate expected cyclical behaviours, such as diurnal and seasonal patterns resulting from changes in atmospheric stability.

The Vestas V80 WT has been used in wind power simulations. This turbine has a high wind speed cut-out and associated hysteresis loop, and this in turn affects the WPP power curve. There is a trend by WT manufacturers to change the high wind speed control systems toward a gentle ramping down of power at high wind speeds (patented as storm control) and this will affect WPP power curves and thus modify the variability of the resulting power time-series.

The WPP operational efficiency is simulated using a Markov Chain (MC) model based on the EA data-set. While the MC model replicates the mean operational efficiency, the model has been applied at a higher temporal resolution than that of the data from which it has been derived. The operational efficiency model has not been the focus of this thesis and a more complex model could better simulate the dynamic character of the WPP operation.

The transform from wind speed time-series to power has been modeled assuming steady state and dynamic components. The dynamic component captures the integration, or smoothing, due to the Wind Turbines (WTs) and the design of the WPP (separation between WTs). Due to limitations in the data, it is assumed that individual WTs do not contribute to the power smoothing. Although WTs are mechanically and electrically complex it is likely that WTs, particularly of larger sizes, will provide significant power smoothing.

The WPP designs used in simulations assume approximate square arrays with 4 diameter turbine separation distances. In reality, as seen in Figure 7.12, the LPF time constants derived from the

WMA model with actual turbine co-ordinates differ significantly from those calculated using the generic model. Hence the power time-series simulated using the generic model will underestimate the smoothing of power produced by a single WPP and this will impact on the final results. Further, data from the Mt Stuart WPP has been used to define the coherence relationships, with WTs aligned perpendicular to the prevailing wind. However, the coherence parallel to the wind direction is greater hence the WMA model as applied will underestimate power smoothing for WPPs where their design is different to Mt Stuart's.

8.2 RECOMMENDATIONS

Further studies will be conducted in Research Aim 1.3, using the results from this thesis, including dynamic, economic dispatch, and load flow modelling.

The results presented in this thesis relate to the reliability, variability, and predictability of power derived from WPPs. These need conversion to a cost metric if the actual value of spatial diversification is to be calculated. To calculate a cost metric with the simulated wind power time-series as an input requires modelling the electricity market. This is possible through the application of market models, such as SPD, that can find the costs associated with various wind power development scenarios. This work is planned for latter stages of GREEN Grid in Research Aim 1.3.

While the Business As Usual scenario represents a realistic development case, the other scenarios are specified to demonstrate the possible benefit from spatial diversification. The models can now be applied to assess the possible benefit from different probable development scenarios. The application of the models to test alternate scenarios may require redefining assumptions related to WPP design. This will require adjustment of model parameters, such as the LPF time constant, capacity factor, and the standard deviation of speed-ups.

The WSTS incident on WPPs have been scaled such that the simulated power achieves a 40 % capacity factor. However, capacity factors for WPPs in New Zealand may be anywhere from 33 % [64] to 50 % [61] depending on the wind resource, WT type, and WPP design. As the capacity factor of the WPP changes so will the reliability, variability, and predictability of the power time-series. Wind resource maps such as that published by the National Institute of Water and Atmosphere [144] may be used to assign capacity factors for each WPP; however, the WPPs would also need to pass some economic threshold if they were to be constructed.

While the Numerical Weather Prediction (NWP) model used in this thesis (ECMWF ERA-interim reanalysis) is freely available, it has a limited spatial resolution. It would be beneficial to increase the spatial resolution by taking Model Output Statistics (MOS) from a NWP model with higher resolution, such as the New Zealand Limited Area Model, or incorporate meso-scale models.

The construction of the Wavelet Multi-resolution Analysis (WMA) model for turbulence is the major contribution of this thesis. As it is a novel application there are many avenues of research that could add to its accuracy and extend its usefulness. For instance the WMA model does not simulate expected diurnal and seasonal patterns of turbulence, and the WMA model assumes the correlation between sites is related solely to the separation distance. Applying a roughness index, or other parameters that describe topographic and climatic variations in wind resources, could improve the accuracy of the simulated correlations.

The WMA models, both intra-WPP and inter-WPPs, characterise the correlation versus distance relationships using log-linear regressions. Observation of the data, and other models (e.g. Davenport) suggest a regression based on an exponential function would be more appropriate. Greater understanding of the wavelet correlation through application to larger data-sets or through further theoretical derivations could be pursued.

The combination of the WMA model with the NWP derived time-series uses a harsh temporal join. i.e the characteristics of wind speed time-series with scales greater than 6 hours are derived from the NWP (deterministic) model and those for shorter time frames use the WMA (stochastic) model. A more gradual meshing of the two models could provide better simulation of the actual processes.

The simulation of power time-series in this thesis requires assumptions pertaining to wind turbine types, and WPP designs. The methods developed in this thesis make it possible to test what effect different turbine types and WPP designs will have on the aggregate power produced by wind power portfolios.

8.3 SUMMARY

The benefit of the spatial diversification of wind power in New Zealand has been quantified in this thesis through the identification of metrics, construction of scenarios, and simulation of power time-series. This has accomplished part of the GREEN Grid project aims and provides data critical for further GREEN Grid research. A methodology has been developed using Wind Speed Time-Series (WSTS) from a Numerical Weather Prediction model, which are interpolated and scaled. It is necessary to impute the WSTS in a way that is spatially and temporally congruent. An imputation method Multi-Resolution Analysis using wavelet decomposition has been developed and validated against a set of measured wind speed time-series. The WSTS require transformation to power and this transform is constructed using component steady-state and dynamic models. The steady-state component has been modeled using Gaussian Wind Power Plant power curves, and the dynamic component modeled using Wavelet Multi-resolution Analysis (WMA). The WMA model has large numerical requirements and the equivalence to a Low Pass Filter (LPF) has been demonstrated; the WMA model is subsequently used to define LPF time constants for WPPs of varying sizes. Power time-series have been simulated for a set of WPPs and compared with measured power time-series. Subsets representing centralised and diversified portfolios have been made, and the simulations are shown to acceptably replicate the observed reliability, variability, and predictability metrics. Power time-series have been simulated for sets of WPPs representing Compact, Disperse, Diverse, and Business As Usual portfolios. It is concluded that a compact wind generation portfolio will exhibit lower reliability, a diverse portfolio will exhibit less variability, and a disperse portfolio will exhibit greater predictability. The BAU portfolio will achieve some of the benefits of spatial diversification, however greater benefit could be achieved through careful planning.

Appendices

Appendix A

POWER CURVES

Wind Speed $[ms^{-1}]$	**NM72**	**Siemens 2.3-82**	**Vestas V47**	**Vestas V52**	**Vestas V80**	**Vestas V90**	**Wind flow 500**
0-3	0	0	0	0	0	0	0
4		42	2.9	25.5	58	77	0
5.0	2	136	43.8	67.4	149	190	0
6.0	79	276	96.7	125	277	353	20
7.0	204	470	166	203	461	581	63
8.0	370	727	252	304	696	886	107
9.0	576	1043.00	350	425	985	1272	155
10.0	808	1394.00	450	554	1303	1696	211
11.0	1067	1738.00	538	671	1607	2106	275
12.0	1308	2015.00	600	759	1824	2489	340
13.0	1507	2183.00	635	811	1939	2797	396
14.0	1610	2260.00	651	836	1982	2951	443
15.0	1645	2288.00	657	846	1994	2993	474
16.0	1650	2297.00	659	849	1997	2999	492
17.0	1650	2299.00	660	850	1999	3000	500
18.0	1650	2300.00	660	850	2000	3000	500
19.0	1650	2300.00	660	850	2000	3000	500
20-24	1650	2300.00	660	850	2000	3000	500
25.0	1650	2300.00	660	850	2000	3000	500
26+	0	0.00	0	0	0	0	0

Table A.1 Wind turbine power curves

Appendix B

ADDITIONAL RESULTS

Scale	22.5	45	90	180	360
Northland1	-0.34	-0.23	-0.26	-0.27	-0.36
Marlborough1	-0.38	-0.35	-0.25	-0.3	-0.24
Tararua1	-0.3	-0.31	-0.25	-0.28	-0.3
Northland2	-0.33	-0.28	-0.22	-0.27	-0.3
Auckland1	-0.26	-0.25	-0.22	-0.27	-0.32
Waikato1	-0.29	-0.29	-0.24	-0.25	-0.19
Waikato2	-0.33	-0.26	-0.23	-0.27	-0.31
Waikato3	-0.31	-0.26	-0.2	-0.3	-0.34
Wellington1	-0.29	-0.29	-0.27	-0.32	-0.29
Wellington2	-0.3	-0.27	-0.23	-0.23	-0.31
CentralOtago1a	-0.33	-0.31	-0.27	-0.27	-0.27
CentralOtago1b	-0.34	-0.33	-0.25	-0.25	-0.26
Tararua3a	-0.29	-0.28	-0.27	-0.22	-0.3
Tararua3b	-0.28	-0.27	-0.25	-0.26	-0.28
Wellington3	-0.29	-0.26	-0.24	-0.31	-0.33
Northland3a	-0.31	-0.28	-0.2	-0.23	-0.28
Northland3b	-0.33	-0.28	-0.22	-0.24	-0.3
Southland2	-0.34	-0.32	-0.25	-0.23	-0.28
Southland3	-0.32	-0.26	-0.21	-0.26	-0.22
Tararua2	-0.27	-0.28	-0.28	-0.27	-0.29
Average	-0.31	-0.28	-0.24	-0.27	-0.29

Table B.1 Autocorrelation coefficients for WMA model

Scale	22.5	45	90	180	360
Northland1	0.72	0.54	0.36	0.27	0.17
Marlborough1	0.31	0.33	0.34	0.24	0.18
Tararua1	0.33	0.28	0.29	0.3	0.28
Northland2	0.67	0.54	0.39	0.36	0.11
Auckland1	0.64	0.49	0.34	0.14	0.02
Waikato1	0.48	0.38	0.29	0.16	0.02
Waikato2	0.67	0.55	0.4	0.31	0.18
Waikato3	0.49	0.36	0.24	0.11	0.03
Wellington1	0.43	0.34	0.3	0.2	0.07
Wellington2	0.34	0.31	0.28	0.25	0
CentralOtago1a	0.45	0.5	0.43	0.42	0.33
CentralOtago1b	0.45	0.42	0.44	0.37	0.36
Tararua3a	0.28	0.15	0.06	0.1	0.06
Tararua3b	0.36	0.31	0.31	0.33	0.33
Wellington3	0.36	0.34	0.26	0.21	0.09
Northland3a	0.52	0.38	0.3	0.24	0.21
Northland3b	0.67	0.48	0.35	0.23	0.16
Southland2	0.42	0.42	0.43	0.35	0.23
Southland3	0.59	0.5	0.41	0.43	0.42
Tararua2	0.26	0.19	0.24	0.19	0.22
Average	0.47	0.39	0.32	0.26	0.17

Table B.2 Taylor exponents for WMA model

Scale	22.5	45	90	180	360
Northland1	-0.02	0.06	-0.06	0.15	0.06
Marlborough1	0.02	0.03	0.03	0.13	0.25
Tararua1	0.05	0.04	0	0.02	0.12
Northland2	-0.04	0.03	0.09	-0.05	-0.08
Auckland1	0.05	-0.04	-0.11	-0.07	-0.01
Waikato1	-0.03	-0.06	0.07	0.16	-0.28
Waikato2	-0.01	0.13	0.06	0.09	-0.07
Waikato3	-0.03	0.1	0	-0.12	-0.29
Wellington1	0	0.03	-0.06	-0.13	-0.21
Wellington2	0.05	-0.01	-0.05	-0.04	-0.1
CentralOtago1a	-0.06	-0.05	-0.05	-0.02	0.29
CentralOtago1b	0.02	-0.02	-0.02	-0.1	0.14
Tararua3a	-0.06	-0.01	-0.05	-0.07	0.07
Tararua3b	-0.02	0.03	0.05	-0.07	-0.04
Wellington3	0.03	0	0.05	-0.25	0.16
Northland3a	-0.04	-0.04	-0.08	0.12	-0.11
Northland3b	-0.03	-0.06	-0.05	0.1	0
Southland2	0.05	-0.01	-0.15	0.08	0.15
Southland3	-0.03	0.07	0.01	0.13	-0.1
Tararua2	0.04	0.02	-0.02	-0.08	0.4
Average	0	0.01	-0.02	0	0.02

Table B.3 Johnson γ_J coefficient for WMA model

Scale	22.5	45	90	180	360
Northland1	1.34	1.37	1.56	1.56	2.16
Marlborough1	1.48	1.54	1.76	1.71	1.77
Tararua1	1.56	1.61	1.9	2.19	1.93
Northland2	1.32	1.39	1.67	1.91	1.95
Auckland1	1.33	1.55	1.63	2.22	1.94
Waikato1	1.41	1.46	1.66	2.13	2.4
Waikato2	1.24	1.38	1.44	1.72	2.28
Waikato3	1.37	1.52	1.89	2	2.48
Wellington1	1.57	1.73	1.77	1.6	2.55
Wellington2	1.39	1.52	1.77	1.83	1.67
CentralOtago1a	1.35	1.42	1.47	1.71	1.98
CentralOtago1b	1.54	1.43	1.59	1.82	2.2
Tararua3a	1.54	1.71	1.89	2.47	2.32
Tararua3b	1.58	1.57	1.85	1.87	2.1
Wellington3	1.5	1.66	1.67	1.5	1.62
Northland3a	1.5	1.64	1.71	1.91	1.76
Northland3b	1.41	1.52	1.64	1.94	1.79
Southland2	1.39	1.6	1.61	1.98	2.53
Southland3	1.37	1.46	1.71	1.65	2.02
Tararua2	1.35	1.54	1.67	1.92	3.17
Average	1.43	1.53	1.69	1.88	2.13

Table B.4 Johnson η_J coefficient for WMA model

Scale	22.5	45	90	180	360
Northland1	-0.01	0.04	-0.1	0.26	0.24
Marlborough1	0.01	0.04	0.06	0.34	1.35
Tararua1	0.01	0.02	0	0.08	0.45
Northland2	-0.02	0.02	0.12	-0.15	-0.29
Auckland1	0.02	-0.03	-0.1	-0.13	-0.13
Waikato1	-0.02	-0.06	0.13	0.42	-1.5
Waikato2	-0.01	0.09	0.08	0.15	-0.37
Waikato3	-0.01	0.08	-0.01	-0.29	-1.23
Wellington1	0	0.02	-0.07	-0.25	-0.72
Wellington2	0.02	0	-0.06	-0.11	-0.43
CentralOtago1a	-0.03	-0.06	-0.07	-0.09	1.98
CentralOtago1b	0.01	-0.02	0.02	-0.31	0.75
Tararua3a	-0.02	-0.01	-0.08	-0.15	0.24
Tararua3b	-0.01	0.02	0.08	-0.14	-0.12
Wellington3	0.01	0.01	0.05	-0.51	0.6
Northland3a	-0.02	-0.04	-0.11	0.25	-0.41
Northland3b	-0.01	-0.04	-0.07	0.2	0.09
Southland2	0.02	0	-0.23	0.33	0.71
Southland3	-0.02	0.07	0	0.31	-0.47
Tararua2	0.01	0.02	-0.04	-0.18	1.93
Average	0	0.01	-0.02	0	0.13

Table B.5 Johnson ϵ_J coefficient for WMA model

Scale	22.5	45	90	180	360
Northland1	0.36	0.75	1.57	2.72	7.5
Marlborough1	0.48	1.21	2.77	5.05	9.84
Tararua1	0.41	0.9	2.1	4.64	7.71
Northland2	0.37	0.83	1.89	3.96	7.16
Auckland1	0.38	0.89	1.5	3.97	6.54
Waikato1	0.49	1.09	2.32	5.85	11.49
Waikato2	0.33	0.81	1.55	3.32	9.4
Waikato3	0.43	0.94	2.21	4.08	9.72
Wellington1	0.39	0.89	1.71	2.75	9.03
Wellington2	0.42	0.96	2.07	3.63	6.34
CentralOtago1a	0.45	1.08	2.15	4.62	10.02
CentralOtago1b	0.51	1	2.29	4.68	11.14
Tararua3a	0.43	1.01	2.09	5.2	9.54
Tararua3b	0.47	0.93	2.11	3.96	8.81
Wellington3	0.38	0.9	1.66	2.65	5.68
Northland3a	0.52	1.14	2.07	4.15	7.16
Northland3b	0.4	0.91	1.75	3.79	6.79
Southland2	0.42	1.15	2.14	5.08	13.51
Southland3	0.51	1.08	2.28	3.73	8.8
Tararua2	0.37	0.88	1.83	4.14	14.77
Average	0.43	0.97	2	4.1	9.05

Table B.6 Johnson λ_J coefficient for WMA model

Scale	22.5	45	90	180	360
Northland1	0.02	0.01	0.01	0.01	0.02
Marlborough1	0.01	0.01	0.02	0.03	0.01
Tararua1	0.01	0.01	0.01	0.01	0.02
Northland2	0.02	0.02	0.02	0.01	0.01
Auckland1	0.01	0.01	0.01	0.02	0.01
Waikato1	0.01	0.02	0.02	0.01	0.01
Waikato2	0.01	0.02	0.01	0.02	0.02
Waikato3	0.02	0.02	0.02	0.01	0.02
Wellington1	0.01	0.01	0.01	0.02	0.02
Wellington2	0.02	0.01	0.01	0.01	0.01
CentralOtago1a	0.01	0.01	0.01	0.01	0.02
CentralOtago1b	0.01	0.01	0.01	0.02	0.01
Tararua3a	0.01	0.01	0.01	0.02	0.01
Tararua3b	0.01	0.01	0.01	0.01	0.01
Wellington3	0.01	0.02	0.02	0.03	0.02
Northland3a	0.01	0.02	0.01	0.02	0.02
Northland3b	0.02	0.01	0.01	0.02	0.01
Southland2	0.01	0.02	0.01	0.02	0.02
Southland3	0.01	0.02	0.01	0.02	0.02
Tararua2	0.01	0.02	0.01	0.01	0.01
Average	0.01	0.01	0.01	0.02	0.02

Table B.7 Normalised Cramer von Mises statistics for Taylor and Johnson transformed wavelet series

Direction sector	T1	T2	T3	T4	T5	T6	T7	T8	T9
0	1.23	1.2	1.14	0.87	0.91	0.84	0.84	0.89	1.17
30	1.05	1.19	1.08	1.01	0.93	0.99	0.85	0.96	0.99
60	0.98	1.12	1.05	1.03	1.01	0.99	0.96	0.93	0.92
90	0.94	1.07	1.02	1.03	1.03	1.01	0.98	0.95	0.97
120	0.9	1.02	0.97	0.94	1.04	1.03	1.02	1.02	1.07
150	1.11	1	0.84	0.77	1.04	1.13	0.93	1.19	1.01
180	1.25	1.25	1.05	1.18	0.8	0.85	0.87	0.91	0.9
210	1.06	1.11	1.07	1.02	0.98	0.94	0.95	0.93	0.96
240	0.98	1.04	1.02	1.02	1.02	1	0.99	0.98	0.94
270	0.94	1.04	1.02	1.02	1.03	1.02	1	0.98	0.95
300	1	1.08	0.93	0.99	1.02	1.02	0.99	0.99	0.98
330	0.98	0.83	0.75	1.09	1.2	0.91	1.18	0.88	1.24
All	0.98	1.05	1.01	1.02	1.02	1	0.99	0.97	0.96

Table B.8 Speedups for MCP applied to Mt Stuart

Direction sector	T1	T2	T3	T4	T5	T6	T7	T8	T9
0	1378	1371	1389	1232	1270	1173	1062	1173	1399
30	1128	1145	1130	1118	1006	1078	839	1019	1030
60	3000	3052	3004	3028	3030	2965	2973	2891	2944
90	3478	3698	3592	3679	3711	3645	3699	3628	3689
120	1459	1550	1514	1481	1554	1528	1549	1541	1566
150	642	638	588	549	623	643	592	653	628
180	556	563	548	560	469	419	511	481	528
210	1650	1666	1663	1653	1629	1543	1623	1563	1637
240	16242	16326	16324	16327	16345	16288	16273	16323	16329
270	8097	8246	8182	8215	8260	8253	8191	8208	8201
300	5281	5363	4883	5316	5369	5362	5359	5336	5305
330	2284	2096	1575	2379	2463	1995	2452	1952	2456
All	45195	45714	44392	45537	45729	44892	45123	44768	45712

Table B.9 Counts for MCP applied to Mt Stuart

REFERENCES

[1] D McQueen, P Wong Too, and G White. Wind power variability and forecast accuracy in New Zealand, 2007. http://www.ea.govt.nz/our-work/programmes/pso-cq/wgip/.

[2] Electric Power Engineering Centre. GREEN Grid, 2016. http://www.epecentre.ac.nz/greengrid/index.shtml.

[3] L Evans and R Meade. *Alternating Currents or Counter-Revolution? Contemporary Electricity Reform in New Zealand*. VUW Press, 2005.

[4] P Gipe. *Wind Power*. Chelsea Green Publishing company, 2004.

[5] Megan J. Clark and John A. Randal. *A First Course in Applied Statistics*. Pearson New Zealand, 2010.

[6] R Stull. *An introduction to boundary layer meteorology*. Atmospheric sciences library. Kluwer Academic, repr. with errata. edition, 2003.

[7] H. Ltkepohl. *New Introduction to Multiple Time Series Analysis*. Springer, 2007.

[8] S Mallat. *A Wavelet Tour of Signal Processing, Third Edition: The Sparse Way*. Academic Press, 2008.

[9] Van der Hoven I. Power spectrum of horizontal wind speed in the frequency range from 0.0007 to 900 cycles per hour. *Journal of Meteorology*, 14, 1956.

[10] Electricity Authority. Electricity in New Zealand, 2011. https://www.ea.govt.nz/dmsdocument/12292.

[11] Editor. Mining notes. *Evening Star*, 9951(11 March), 1896. https://paperspast.natlib.govt.nz/newspapers/ESD18960311.2.46, accessed 2 August 2016.

[12] Editor. Special advertisement. *Otago Daily Times*, 12400(9 July), 1902. https://paperspast.natlib.govt.nz/newspapers/ODT19020709.2.19, accessed 2 August 2016.

[13] Editor. Waipori electric scheme. *Otago Daily Times*, 11731(12 May), 1900. https://paperspast.natlib.govt.nz/newspapers/ODT19000512.2.19, accessed 2 August 2016.

[14] R Lawson, P Thorsnes, and J Williams. Consumer response to time varying prices for electricity. *Economic discussion papers, University of Otago*, 1116, 2011.

[15] J Weir. Uncertain future for Tiwai Point Smelter, 2013. http://www.stuff.co.nz/business/industries/8483672/Uncertain-future-for-Tiwai-Point-Smelter, accessed 13 September 2016.

[16] N Watson, V Gosbell, S Pererra, S Elphick, and S Hardie. Power Quality (PQ) Guidelines, 2012. Technical report, Electricity Engineers Association, University of Canterbury, 2013.

[17] H Markiewicz and A Klajn. Standard EN 50160 - voltage characteristics in public distribution systems. *Standard EN 50160*, 2004.

[18] T. Ackermann. *Wind Power in Power Systems*. Wiley, 2005.

[19] R Strahan and A Miller. Systems to implement demand response in new zealand, 2014.

[20] Transpower. Load forecast methodology and processes, 2014. https://www.systemoperator.co.nz/sites/default/files/bulk-upload/documents/GL-SD-204\%20Load\%20Forecast\%20Methodology\%20and\%20Processes.pdf.

[21] Transpower. Aufls activation grid owner report, 12 Nov 2003. www.transpower.co.nz/sites/default/files/publications/resources/aufls-activation-12-11-13-grid-owner-report.pdf.

[22] Executive Office of the President. Economic benefits of increasing electric grid resilience to weather outages, 2013.

[23] Electricity Authority. Electricity industry participation code 2010; part 13 trading arrangements, 2010.

[24] Electricity Authority. Vectorised schedule, pricing and dispatch (vspd) - v1.2, 27 September 2013 2012.

[25] C. Samarasinghe and G. Ancell. Effects of large scale wind generation on transient stability of the new zealand power system. In *IEEE Power and Energy Society 2008 General Meeting: Conversion and Delivery of Electrical Energy in the 21st Century, PES, July 20, 2008 - July 24*, 2008.

[26] T Stevenson. Claimed undesirable trading situation, 26 march, 2011. https://www.ea.govt.nz/dmsdocument/10222.

[27] Transpower. Main transmission system planning guideline, 2005. https://ea.govt.nz/dmsdocument/3859.

[28] B Bull. Correlation between wind generation output and hydro inflows. Technical report, Electricity Authority, July 2010. https://www.ea.govt.nz/dmsdocument/7255.

[29] Transpower. Grid upgrade plan 2009 instalment 3, part v: Lower South Island renewables investment proposal, 2009.

[30] Commerce Commission. Transpower major capital proposal, 2016.

[31] International Renewable Energy Agency. Wind power, 25 November 2012.

[32] S. Yoshida. Storm control for horizontal axis wind turbine, 2006. http://www.google.com/patents/EP1612412A2?cl=en.

[33] J N Libii. Comparing the calculated coefficients of performance of a class of wind turbines that produce power between 330 kw and 7,500 kw. *World Transactions on Engineering and Technology Education*, 11(1):36–40, 2013.

[34] IEC. Iec 61400: Wind turbines part 1-2: Design requirements, 2001.

[35] IEC. Iec 61400: Wind turbines part 12-1: Power performance measurements of electricity producing wind turbines, 2005.

[36] R. Yan and T. K. Saha. Frequency response estimation method for high wind penetration considering wind turbine frequency support functions. *IET Renewable Power Generation*, 9(7):775–82, 2015.

[37] Standards New Zealand. NZS 6808:2010, acoustics - wind farm noise, 2010.

[38] K Thomsen and P Sorensen. Fatigue loads for wind turbines operating in wakes. *Journal of Wind Engineering and Industrial Aerodynamics*, 80(1-2):121–36, 1999.

[39] T Burton, N Jenkins, D Sharpe, and E Bossanyi. *Wind Energy Handbook*. Wind Energy Handbook. John Wiley & Sons, Ltd, 2011.

[40] A Graves, K Harman, M Wilkinson, and R Walker. Understanding availability trends of operating wind farms, 2008.

[41] C Bell. Great lengths to foil possums, 21 July 2012. `http://www.stuff.co.nz/marlborough-express/news/6969320/Great-lengths-to-foil-possums`.

[42] W Schlez. *Voltage fluctuations caused by groups of wind turbines*. Doctor of philiosophy, Loughborough University, 2000.

[43] H Holttinen. Expert group report on recommended practices; 16. wind integration studies, 2013. `https://www.ieawind.org/task_25.html`.

[44] J Dowds, P Hines, T Ryan, W Buchanan, E Kirby, J Apt, and P Jaramillo. A review of large-scale wind integration studies. *Renewable and Sustainable Energy Reviews*, 49:768–94, 2015.

[45] M Milligan, B Kirby, T Acker, M Ahlstrom, B Frew, M Goggin, W Lasher, M Marquis, and D Osborn. Review and status of wind integration and transmission in the united states: Key issues and lessons learned, 2015. `www.nrel.gov/docs/fy15osti/61911.pdf`.

[46] S Achilles, K Anaparthi, H Johal, G Hinkle, D Manz, S Meeran, N Miller, and W Ren. Oahu wind integration study, 9 February 2010. `www.hnei.hawaii.edu/sites/dev.hnei.hawaii.edu/files/Oahu_Wind_Integration_Study__Dec2010.pdf`.

[47] D Corbus, M Schuerger, L Roose, J Strickler, T Surles, D Manz, D Burlingame, and D Woodford. Oahu wind integration and transmission study: Summary report. Technical report, National Renewable Energy Laboratory, 2010. `http://www.nrel.gov/docs/fy11osti/50414.pdf`.

[48] J Manobianco, C Alonge, and J Frank. Development of regional wind resource and wind plant output datasets for the Hawaiian Islands, 2010. `http://www.nrel.gov/electricity/transmission/oahu_wind.html`.

[49] AWS Truepower. Wind resource maps and data, 2012. `https://www.awstruepower.com/assets/Wind-Resource-Maps-and-Data-Methods-and-Validation1.pdf`.

[50] Australian Electricity Market Operator. Wind integration in electricity grids work package 3: Simulation using historic data, 2012. `http://www.aemo.com.au/Electricity/Planning/Related-Information/Wind-Integration-Investigation`.

[51] Australian Electricity Market Operator. Wind integration in electricity grids work package 5: Market simulation studies, 2012. `http://www.aemo.com.au/Electricity/Planning/Related-Information/Wind-Integration-Investigation`.

[52] European Network of Transmission System Operators for Electricity. Entso-e at a glance, 2016. https://www.entsoe.eu/publications/general-publications/entso-e-at-a-glance/Pages/default.aspx, accessed 14 September 2016.

[53] Metservice. Response to consultation paper: Wind forecasting and integration options, 2010. https://www.ea.govt.nz/dmsdocument/6029.

[54] A Bossavy, R Girard, and G Kariniotakis. Forecasting ramps of wind power production with numerical weather prediction ensembles. *Wind Energy*, 16(1):51–63, 2013.

[55] N Cherry. Wind energy resource assessment of New Zealand. *Pacific Northwest Laboratory (Technical Report) PNL*, pages 261–71, 1979.

[56] P Edwards. Wind energy resource studies in New Zealand. *Solar & Wind Technology*, 7(1):9–14, 1990.

[57] Bowen A. Engineering aspects of the wind. *The Meteorological Society of New Zealand*, 1(1), 1981.

[58] P Edwards and K Dawber. Investigation of wind-energy prospects in the Otago region of New Zealand. *Journal of industrial aerodynamics*, 5(3-4):281–96, 1980.

[59] R Vos and S Fortuin. Energyscape summary of resource maps, 1 Feburary 2010.

[60] New Zealand Government. Te Ara The Encyclopedia of New Zealand, 2015. http://www.teara.govt.nz/en.

[61] New Zealand Wind Energy Association. Brooklyn wind turbine, 2016. http://www.windenergy.org.nz/brooklyn-wind-turbine, accessed 28 July 2016.

[62] R Brown. Te Uku Wind Farm - planning and operation of a deeply embedded power plant with advanced ancilliary services, 2012.

[63] Ministry Business Innovation and Employment. Energy in New Zealand 2015, 2015. http://www.mbie.govt.nz/info-services/sectors-industries/energy/energy-data-modelling/publications/energy-in-new-zealand.

[64] Parsons Brincherhoff. 2011 NZ generation data update, 2012.

[65] European Wind Energy Agency. *Wind Energy - The Facts: A Guide to the Technology, Economics and Future of Wind Power*. Earthscan, 2008.

[66] N Boccard. Capacity factor of wind power realized values vs. estimates. *Energy Policy*, 37(7):2679–88, 2009.

[67] P Wong Too, W Thorp, and G White. Wind - regional wind farm correlations, 2005. www.ea.govt.nz/our-work/programmes/pso-cq/wgip.

[68] A Oliver. The dark side of wind power, 17 November 2015 2008.

[69] Transpower. Effect of unpredictability of wind generation output on pre-dispatch processes, investigation 1- part a, 2007.

[70] Transpower. Effect of unpredictability of wind generation output on pre-dispatch processes, investigation 1 - part b, 2007.

[71] Transpower. Effect of variability of wind generation output on dispatch of generation, investigation 2, 2007.

[72] Transpower. Effect of variability of wind generation output on asset loading, investigation 3, 2007.

[73] Transpower. Effect of wind generation on ability to manage system voltages within voltage qualuity targets- investigation 4, 2007.

[74] Transpower. Effect of wind generation on management of frequency excursions, 2007.

[75] Transpower. Effect of wind generation on small distrurbance voltage stability, investigation 6, 2007.

[76] Transpower. Effect of wind generation on transient stability, investigation 7, 2008.

[77] DigSILENT. Wind generation impact studies, 2007.

[78] Transpower. Effect of wind generation on small signal stability, investigation 8, 2008.

[79] Transpower. Efefct of wind generation on reactive power contribution and dynamic voltage responses, investigation 9, 2008.

[80] B. W. McDonald. Prediction intervals for power generation from multiple wind farms. In *Proceedings of the 11th Biennial Engineering Mathematics and Applications Conference, EMAC-2013*, 2013. `http://journal.austms.org.au/ojs/index.php/ANZIAMJ/article/view/7804`.

[81] I Rasmussen and M Windolf. *Wind Power Integration in New Zealand : a scenario analysis of 15-25 % wind power in the electricity market in 2025.* Masters thesis, Technical University of Denmark, 2008.

[82] J Khazaei, G Zakeri, and G Pritchard. The effects of stochastic market clearing on the cost of wind integration: a case of New Zealand electricity market. *Energy Systems*, 5(4):657–75, 2014.

[83] H Alzaanin. *The potential of utilising residential demand reponse to balance the fluctuation of wind power in New Zealand.* PhD thesis, Victoria University, 2014.

[84] Energy Link and MWH NZ. Wind energy integration in New Zealand, 2005. `http://citeseerx.ist.psu.edu/viewdoc/download?doi=10.1.1.132.9261\&rep=rep1\&type=pdf`.

[85] G Strbac, D Pudjianto, A Shakoor, M Castro, and G Waipara. The system impacts and costs of integrating wind power in New Zealand, 2008. `http://www.epoc.org.nz/workshops/ww2008/NZWindIntegrationCostsPhase-IIReportFinal.pdf`.

[86] Parliamentary Commissioner for the Environment. Wind power, people, and place. Technical report, Parliamentary Commissioner for the Environment, 2006. `www.pce.parliament.nz/media/pdfs/Wind_power,_people,_and_place.pdf`.

[87] L Ott. *An introduction to statistical methods and data analysis.* PWS-Kent publishing, 3 edition, 1988.

[88] K Nan. *Wind power in the New Zealand Electricity Market.* PhD thesis, The University of Auckland, 2012.

[89] C Rosenzweig, D Karoly, M Vicarelli, P Neofotis, Q Wu, G Casassa, A M, T Root, N Estrella, B Seguin, P Tryjanowski, C Liu, S Rawlins, and A Imeson. Attributing physical and biological impacts to anthropogenic climate change. *Nature*, 453(7193):353–7, 2008.

[90] Isaac Van der Hoven. Power spectrum of horizontal wind speed in the frequency range from 0.0007 to 900 cycles per hour. *Journal of Meteorology*, 14(2):160–4, 1957.

[91] D McQueen. Simulation of turbulence measurements made by a zephir lidar, 2008.

[92] S Watson D McQueen. Validation of wind speed prediction methods at offshore sites. *Wind Energy*, 9:75–85, 2006.

[93] S. Watson and P Kritharas. Long term wind speed variability in the UK, 2012.

[94] I Troen and E L Petersen. *European Wind Atlas.* Riso National Laboratory, 1989.

[95] J Salmon. Ms-micro version 3, 2013. `http://www.zephyrnorth.com`.

[96] D Dee et al. The ERA-Interim reanalysis: configuration and performance of the data assimilation system. *Quarterly Journal of the Royal Meteorological Society*, 137(656):553–97, 2011.

[97] R Turner, X Zheng, N Gordon, M Uddstrom, G Pearson, R De Vos, and S Moore. Creating synthetic wind speed time series for 15 New Zealand wind farms. *Journal of Applied Meteorology and Climatology*, 50(12):2394–409, 2011.

[98] W Luo, M Taylor, and S Parker. A comparison of spatial interpolation methods to estimate continuous wind speed surfaces using irregularly distributed data from england and wales. *International Journal of Climatology*, 28(7):947–59, 2008.

[99] R Gorman. Intercomparison of methods for the temporal interpolation of synoptic wind fields. *Journal of Atmospheric and Oceanic Technology*, 26(4):828–37, 2009.

[100] The MathWorks Inc. Matlab, 2013. `www.mathworks.com`.

[101] J Williams. Evaluating user simulations with the cramervon mises divergence. *Speech Communication*, 50(10):829–46, 2008.

[102] A Derrick. Development of the Measure Correlate Predict strategy for site assessment. *Proceedings of the EWEC*, 1993.

[103] G McNerney and P Veers. Markov method for simulating non-gaussian wind speed time series. In *Fourth ASME Wind Energy Symposium. Presented at the Eighth Annual Energy Sources Technology Conference and Exhibition.* ASME, 1998.

[104] A Shamshad, M Bawadi, W Wan Hussin, T Majid, and S Sanusi. First and second order markov chain models for synthetic generation of wind speed time series. *Energy*, 30(5):693–708, 2005.

[105] L Liang, Z Jin, L Jianing, L Puming, Z Cailiang, and M Zijie. An implementation of synthetic generation of wind data series. In *Innovative Smart Grid Technologies (ISGT), IEEE PES*, 2013.

[106] K Brokish and J Kirtley. Pitfalls of modeling wind power using markov chains. In *2009 IEEE/PES Power Systems Conference and Exposition, PSCE 2009, March 15, 2009 - March 18, 2009.* IEEE Computer Society, 2009.

[107] A Davenport. The spectrum of horizontal gustiness near the ground in high winds. *Quarterly Journal of the Royal Meteorological Society*, 87(372):194–211, 1961.

[108] D Smith. Investigation of stationary and nonstationary wind data using classical Box-Jenkins models. *Journal of wind engineering and industrial aerodynamics*, 49(1):319–28, 1993.

[109] B Brown, R Katz, and A Murphy. Time series models to simulate and forecast wind speed and wind power. *Journal of Climate and Applied Meteorology*, 23(8):1184–95, 1984.

[110] Oren S Papavasiliou A. Stochastic modeling of multi-area wind power production, 2012. `http://perso.uclouvain.be/anthony.papavasiliou/public_html/PMAPS2012.pdf`.

[111] G Nason. Tests of stationarity, 2016.

[112] A Fronczak and P Fronczak. Origins of Taylor's power law for fluctuation scaling in complex systems. *Physical Review E - Statistical, Nonlinear, and Soft Matter Physics*, 81(6), 2010.

[113] J Mur-Amada and A Bayocl-Rujula. Characterization of spectral density of wind farm power output. In *9th International Conference on Electrical Power Quality and Utilisation*, 2007.

[114] J Mur-Amada and A Bayocl-Rujula. Wind power variability model part ii - probabilistic power flow. In *9th International Conference on Electrical Power Quality and Utilisation*, 2007.

[115] J Mur-Amada and A Bayocl-Rujula. Wind power variability model part iii - validation of the model. In *9th International Conference on Electrical Power Quality and Utilisation*, 2007.

[116] M Miranda and R Dunn. Spatially correlated wind speed modelling for generation adequacy studies in the UK. In *Power Engineering Society General Meeting, 2007. IEEE*, 2007.

[117] R Karki, H Po, and R Billinton. A simplified wind power generation model for reliability evaluation. *IEEE Transactions on Energy Conversion*, 21(2):533–40, 2006.

[118] J Morales, R Mnguez, and A Conejo. A methodology to generate statistically dependent wind speed scenarios. *Applied Energy*, 87(3):843–55, 2010.

[119] J D'Errico. nearestspd.m, 2013. `www.mathworks.com/matlabcentral/fileexchange/42885-nearestspd`.

[120] National Aeronautics and Space Administration. Science focus: Von karman vortices, 2016. `http://disc.sci.gsfc.nasa.gov/education-and-outreach/additional/science-focus/ocean-color/science_focus.shtml/vonKarman_vortices.shtml`.

[121] M Woods, C Russell, R Davy, and P Coppin. Simulation of wind power at several locations using a measured time-series of wind speed. *IEEE Transactions on Power Systems*, 28(1):219–26, 2013.

[122] J Li, C Li, L He, and J Shen. Extended modulating functions for simulation of wind velocities with weak and strong nonstationarity. *Renewable Energy*, 83:384–97, 2015.

[123] K Hunt and G Nason. Wind speed modelling and short-term prediction using wavelets. *Wind Engineering*, 25(1):55–61, 2001.

[124] T Kitagawa and T Nomura. A wavelet-based method to generate artificial wind fluctuation data. *Journal of Wind Engineering and Industrial Aerodynamics*, 91(7):943–64, 2003.

[125] Rehman S Siddiqi A, Khan S. Wind speed simulation using wavelets. *Americian Journal of Applied Sciences*, 2(2):557–64, 2005.

[126] National Academy of Sciences. Beyond discovery: wavelets - seeing the forest and the trees, 2001. `http://www.nasonline.org/publications/beyond-discovery/wavelets.pdf`.

[127] D Jones. The Johnson curve toolbox for matlab: analysis of non-normal data using the Johnson system of distributions, 2014. `http://www.marine.usf.edu/user/djones/`.

[128] Gamesa. Gamesa g52-850 kw, 2007. `http_myweb.tiscali.co.uk/eclecticaLibraryTurbine/20leafletsGamesaGamesa/20G52/20850kw.pdf`.

[129] P Veers. Three-dimensional wind simulation. In *Eighth ASME Wind Energy Symposium, January 22, 1989 - January 25, 1989*, volume 7 of *American Society of Mechanical Engineers, Solar Energy Division (Publication) SED*. Publ by American Soc of Mechanical Engineers (ASME), 1989.

[130] Norgard P and Holttinen H. A multi-turbine power curve. *Nordic Wind Power Conference, Gothenburg, Sweden*, page 5, 2004.

[131] L De Tommasi, M Gibescu, and A Brand. A dynamic wind farm aggregate model for the simulation of power fluctuations due to wind turbulence. *Journal of Computational Science*, 1(2):75–81, 2010.

[132] Toshiya Nanahara, Masahiro Asari, Takamitsu Sato, Koji Yamaguchi, Masaaki Shibata, and Tsutomu Maejima. Smoothing effects of distributed wind turbines. part 1. coherence and smoothing effects at a wind farm. *Wind Energy*, 7(2):61–74, 2004.

[133] C St. Martin, J Lundquist, and M Handschy. Variability of interconnected wind plants: Correlation length and its dependence on variability time scale. *Environmental Research Letters*, 10(4), 2015.

[134] S Rose and J Apt. Generating wind time series as a hybrid of measured and simulated data. *Wind Energy*, 15(5):699–715, 2012.

[135] S Sulaeman, M Benidris, and J Mitra. A method to model the output power of wind farms in composite system reliability assessment. In *North American Power Symposium (NAPS)*, 2014.

[136] E. Welfonder, R. Neifer, and M. Spanner. Development and experimental identification of dynamic models for wind turbines. volume 5 of *Control Engineering Practice*. Elsevier Science Ltd, 1997.

[137] Vestas. General Specification, 660 kW Variable Slip Wind Turbines, V47 - 660 kW. Technical report, 2001.

[138] Vestas. General Specification, Vestas V52 850 kW, 50/60 Hz, OptiSpeed Wind Turbine. Technical report, 2008.

[139] Vestas. General Specification,V80 2.0 MW 50 Hz VCS. 2010.

[140] Vestas. General Specification, V90 3.0 MW VCS 50 Hz. Technical report, 2010.

[141] Windflow. Windflow 500 kW Wind Turbine, S500 General Specification, Standard Scope of Supply and Options. Technical report, 2009.

[142] Windpower Programme. The wind turbine database, 2016. http://www.wind-power-program.com/download.htm.

[143] National Institute for Water and Atmosphere. NZ Historic Weather Events Catalogue - March 1988 North Island Ex-tropical Cyclone Bola, 2016. https://hwe.niwa.co.nz/event/March_1988_North_Island_Ex-tropical_Cyclone_Bola, accessed 19 September 2016.

[144] National Institute of Water and Atmosphere. New Zealand wind resource map. https://www.niwa.co.nz/sites/niwa.co.nz/files/imported/__data/assets/image/0004/50539/renewable3_large.gif, accessed 28 July 2016.